Dynamic Frequency Response of Wind Power Plants

Altin, Müfit

Publication date:
2012

Document Version
Publisher's PDF, also known as Version of record

Dynamic Frequency Response of Wind Power Plants

by

Mufit Altin

Dissertation submitted to Faculty of Engineering, Science, and Medicine
at Aalborg University in partial fulfillment of the requirements
for the degree of Doctor of Philosophy in Electrical Engineering

Aalborg University
Department of Energy Technology
Aalborg, Denmark
November 2012

Aalborg University
Department of Energy Technology
Pontoppidanstraede 101
9220 Aalborg East
Denmark
Phone: + 45 2137 1218
Fax: +45 9815 1411
Web: http://www.et.aau.dk

Printed in Denmark by UniPrint
ISBN

Resumé

Elproduktion fra vindkraft har hurtigt vokset i de seneste fem år på verdensplan. I mange lande har vind energimål sat i intervallet fra 20% til 50% af al elproduktion på grund af bekymringerne for CO_2-emissioner, fossile brændsler omkostninger og energieffektivitet. For at opretholde en bæredygtig og pålidelig drift af elsystemet for disse mål, har transmissionssystemoperatørerne (TSO) revideredes de forsyningsnetkodeks krav. Også, skal TSO'erne planlægger den fremtidige udvikling af elsystemet med forskellige vind indtrængen scenarier at integrere mere vindkraft i henhold til deres netkrav. I disse scenarier særligt med høje vindkraft penetration sager, konventionelle kraftværker (CPPs) sådanne som gamle termiske kraftværker planlægges at blive erstattet med vindkraftværker (WPPs). Derfor vil elsystemet stabilitet blive påvirket og kontrol evne WPPs ville blive undersøgt.

Formålet med dette projekt er at analysere og identificere elsystemet krav til synkroniserende strømforsyning og inerti svar kontrol af WPPs i høj vindkraft penetration scenarier. Den dynamiske frekvensrespons WPPs er realiseret som den synkroniserende strømforsyning og inerti svar kontrol i denne afhandling. Derfor er vurderingen af dynamiske frekvensrespons udførelse af WPPs udført. Et generisk elsystemet model og en generisk WPP model med flere forskellige vindkraftprojekter indtrængen scenarier gennemføres på en RMS værktøjskasse, som er udviklet til vinden integrationsstudier.

For den inerti respons undersøgelse bliver en ny kontrol foreslåede metode, som forbedrer de eksisterende kontrolbestemmelser begreber i forhold til at reducere den frigjorte energi og peak aktiv magt WPPs. Det er også vist, at når evnen til WPPs

betragtes foreslåede kontrol metode har mindre indflydelse på elsystemet frekvens i forhold til eksisterende styringskoncepter. En anden fordel ved den foreslåede inerti respons regulator tuning metode, som kan anvendes som en generisk fremgangsmåde til enhver power system med høj vindkraft penetrationen.

Desuden er en vurderingsmetode af synkroniseringssekvensen strømforsyning fra WPPs udviklet til synkroniserende strømforsyning. De simulering Resultaterne viser, at integration af WPPs har reduceret synkroniserende power flow mellem CPPs i høj vindkraft penetration scenarier. Desuden er kontrolmetoder til at støtte synkronisering magt foreslået og evalueret med den udviklede metode.

Abstract

Electricity generation from wind energy has rapidly increased for the last five years worldwide. In many countries, wind energy targets have been set in the range of 20% to 50% of all electricity generation due to the concerns of CO_2 emissions, fossil fuel costs, and energy efficiency. In order to maintain sustainable and reliable operation of the power system for these targets, transmission system operators (TSOs) have revised the grid code requirements. Also, the TSOs are planning the future development of the power system with various wind penetration scenarios to integrate more wind power according to their grid codes. In these scenarios particularly with high wind power penetration cases, conventional power plants (CPPs) such as old thermal power plants are planned to be replaced with wind power plants (WPPs). Consequently, the power system stability will be affected and the control capability of WPPs would be investigated.

The objective of this project is to analyze and identify the power system requirements for the synchronizing power support and inertial response control of WPPs in high wind power penetration scenarios. The dynamic frequency response of WPPs is realized as the synchronizing power support and inertial response control in this thesis. Accordingly, the assessment of dynamic frequency response performance of WPPs is carried out. A generic power system model and a generic WPP model with various wind power penetration scenarios are implemented in a RMS toolbox which is developed for the wind integration studies.

For the inertial response study, a new control method is proposed which improves the existing control concepts in terms of reducing the released energy and peak active power of WPPs. It is also shown that when the capability of WPPs considered proposed control method has less impact of the power system frequency compared to existing control concepts. Another advantage of the proposed inertial response control has the tuning methodology which can be utilized as a generic approach for any power system with high wind power penetration levels.

Additionally, an assessment methodology of the synchronizing power support from WPPs is developed for the synchronizing power support. The simulation results show that integration of WPPs have reduced the synchronizing power flow between CPPs in high wind power penetration scenarios. Moreover, the control methods to support synchronizing power are proposed and evaluated with the developed methodology.

Acknowledgements

I express my sincerest thanks to my main supervisors; Remus Teodorescu, co-supervisors; Birgitte Bak-Jensen from Aalborg University, Pedro Rodriguez from Technical University of Catalonia (October 2009-December 2011), and to Vestas Reference Group members; Florin Iov and Philip Carne Kjaer from Vestas Wind Systems for their guidance, support, encouragement, and valuable contributions throughout my doctorate study.

Special thanks to Tim C. Green in Control and Power Research Group Imperial College, London, UK, where I spent my four-month study abroad period with his kind hospitability.

I wish to thank gratefully to my family, my future spouse, and my housemates for their endless support, encouragement, and patience.

I would like to thank all my colleagues in Vestas Power Program and Department of Energy Technology for their friendship throughout my doctorate study. Also, I wish to thank to the staff of Department of Energy Technology and Doctoral School of Engineering, Science, and Medicine for their help throughout my doctorate study.

I acknowledge that this doctorate study was supported by the Aalborg University-Vestas Wind Systems partnership under Vestas Power Program.

Table of Contents

List of Abbreviations

CPP	Conventional Power Plant
WPP	Wind Power Plant
WT	Wind Turbine
VSWT	Variable Speed Wind Turbine
FC	Full Converter
DFIG	Doubly-fed Induction Generator
PCC	Point of Common Coupling
RMS	Root-mean-square
STATCOM	Static Reactive Power Compensator
TSO	Transmission System Operator
SG	Synchronous Generator
HPP	Hydro-Power Plant
TPP	Thermal Power Plant
SVC	Static VAR Compensator
WTG	Wind Turbine Generator

Chapter 1
Introduction

1.1 Background

As power systems have grown in size and complexity over the last century, power system stability is an important concern for the power system operators to maintain the equilibrium between generation and consumption. Since the power system is highly nonlinear and vast, the classification of the power system stability is required to understand the instability problems and to develop solutions to these problems regarding the physical nature of the instability, the size of the disturbance, and the time frame [1.1]. Frequency stability has been defined in this classification as the ability of the power system to maintain steady frequency within a nominal range following a major system upset [1.2].

From 1970s to 2000s, major frequency disturbances had been experienced resulting serious system upsets (e.g. islanding situations or blackouts) led to investigate the reasons of the frequency instability problems. For instance, following cases are selected among these frequency disturbances:

- In England, during 1981 summer, due to the inadequate clearance of a temporary line fault, there was an islanding condition for one part of the power system (South West and South Coast of England) where load shedding occurred following cascade tripping of lines. The islanded part of the power system experienced 47.3 Hz with a recovery as shown in Fig. 1.1 [1.3].

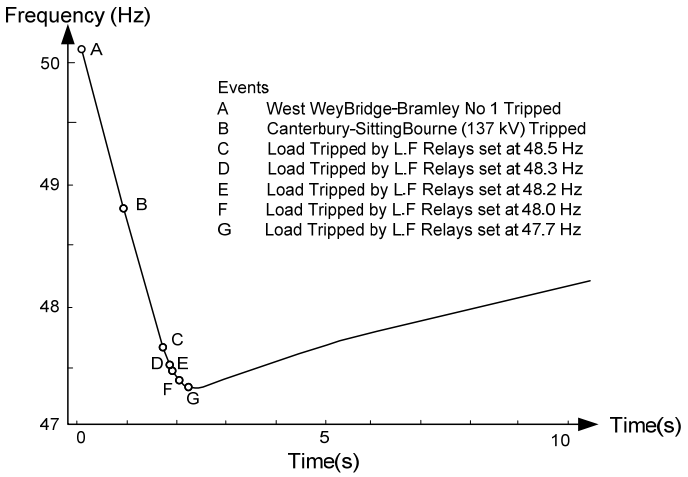

Fig. 1.1. Frequency deviation of isolated system in England after the cascade tripping of lines (1981) [1.3]

- In France, on February 1985 [1.3], an incident started with tripping of six HV transmission lines and caused twelve pole slips after the action of fast valving systems. At the same time the frequency of the European system dropped to 49.6 Hz due to the lack of generation (Fig. 1.2).

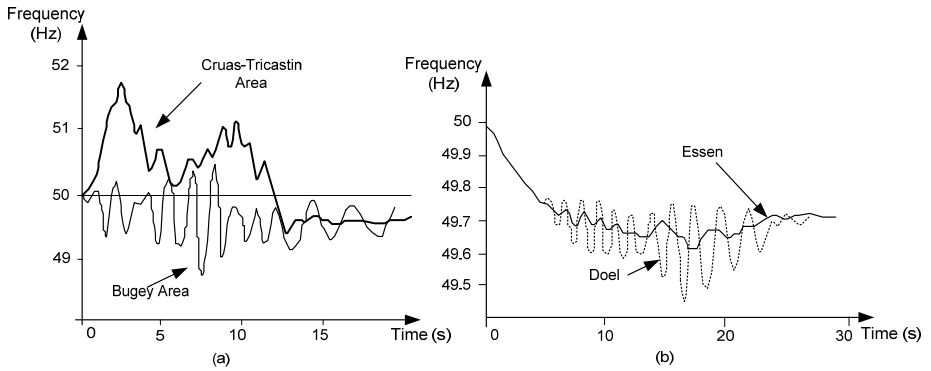

Fig. 1.2. System frequency of France (a) and Europe (b) after the major frequency disturbance in 1985 [1.3]

- In small island systems, the frequency deviations are more serious than the cases mentioned above due to low inertia of the power system. The Perth island frequency dropped at a rate of 3.5 Hz/s and stabilized at around 40 Hz for 30 to 40 seconds. After the load shedding occurred a 300 kV transmission line was tripped by flashover due to the overvoltage. The frequency declined further leading to blackout.
- In Malaysia, on August 1996, due to a stuck breaker and incorrect protection coordination 922 MW generation was lost. The frequency dropped to 49.1 Hz during 3 seconds. Gas turbines with primary frequency control picked up rapidly, however a number of them tripped out on either turbine temperature limit or "flame out" resulting in 2143 MW loss of generation. After loss of generation, load shedding was not sufficient hence, blackout occurred.

The major frequency disturbances were investigated by evaluating the ability of power plants to ride through these disturbances, analyzing behavior of different power system components, and proposing control and protection methods to improve the frequency stability. The extensive summary of related studies is presented in [1.3].

In addition to the frequency stability studies, the rotor angle stability has been also investigated in terms of synchronizing and damping power of synchronous generators (SG). Due to lack of these components, the rotor angle instability limits power transfers over long distances. Therefore, several methods have been developed such as fast fault clearing, fast exciters, power system stabilizers, and the generator tripping. These advanced angle stability control methods have been summarized extensively in [1.4].

Aforementioned power system stability problems are very complex in nature and require extensive analysis of the power systems regardless of the size and structure. Every power system component and controller should be modeled and simulated in detail. Furthermore, in the last decade the power system stability has started to be affected by the integration of wind power into power systems. Due to the low wind power penetration level accommodated so far, the impact is not significant. However,

for high wind power penetration levels, the analysis of the power system for the frequency stability and rotor angle stability analyses should be broadened considering the behavior and control capability of wind power.

Electricity generation from wind energy has rapidly increased for the last five years by 27.4% worldwide [1.5]. In many countries, wind energy targets have been set in the range of 20% to 50% of all electricity generation due to the concerns of CO_2 emissions, fossil fuel costs, and energy efficiency [1.6]-[1.8]. In order to maintain stable and reliable operation of the power system for these targets, TSOs have revised the grid code requirements [1.9]. Also, the transmission system operators (TSOs) are planning the future development of the power system to integrate more wind power according to the grid code requirements. In [1.6], the fundamental issue was defined as the frequency stability after largest infeed loss (i.e. N-1 contingency). Additionally, the impact of the severe network faults on the frequency and rotor angle stability was investigated the as the next key issue in the wind integration studies. Accordingly, various future wind penetration scenarios have been specified covering low level to high level of wind penetration with low and high level of load [1.5], [1.10]. In the scenarios with high wind power penetrations, conventional power plants (CPP) such as old thermal power plants (TPP) are planned to be replaced with wind power plants (WPP) [1.11].

The variable speed wind turbines (VSWT), which dominate the current wind industry market [1.12], with converter-based grid interface provide decoupled, fast, and flexible control of active and reactive power [1.13], [1.14]. However, due to this control strategy, a VSWT does not have characteristics of a SG in terms of contributing to the power system inertia and synchronizing power between CPPs. With integration of WPPs employing VSWTs, the power system inertia becomes reduced for high wind power penetration scenarios which include replacement of CPPs. Therefore, in the future the frequency stability of power systems with high wind power penetration will be affected adversely and the control capability of WPPs should be investigated to enhance the frequency stability of the power system. Accordingly, the synchronizing

power support from WPPs has not been addressed in detail by TSOs. Since there are no mandatory requirements for both of the research areas, the power system requirements should be addressed first for a given generic power system with appropriate representation of WPPs.

1.2 Problem Formulation

In this thesis, two problems are addressed and investigated in accordance with the power system stability studies mentioned above. The first problem is how to enable the inertial response control of WPPs which may be a future code requirement for high wind power penetration scenarios. The second problem is the investigation of the synchronizing power change between remaining CPPs when some of the CPPs are replaced with WPPs in high wind power penetration scenarios.

In order to solve the first problem, several control concepts have been proposed related to the inertial response of VSWTs in the previous studies [1.15]-[1.25]. The derivative control, which estimates the rate of change of frequency (ROCOF) with a low-pass filter, is implemented to emulate the inherent inertial response of a SG [1.15]-[1.21]. The impact of the derivative control on the power system is studied without considering the converter limitations of the VSWT in [1.15]. In [1.16], the influence of the derivative control on the converter and generator limitations of the VSWT is addressed and a novel control algorithm, which extracts the maximum energy from the turbine, is proposed. However, the proposed control algorithm provides a pre-defined temporary active power which is independent from the frequency deviation. In [1.17]-[1.19], the inertial response control of the VSWT is improved by implementing primary frequency control as an additional control loop. Further improvement for the DFIG based VSWT is achieved by employing the generator slip control [1.20], and coordinating WPPs with the CPPs' frequency response [1.21]. Besides the derivative control, the temporary frequency control, which is provision of an additional active power for a certain time period after detection of the frequency deviation, has been introduced [1.22]-[1.23]. The temporary frequency control response is determined with respect to the frequency deviation in [1.22] or a predefined active power pulse in

[1.23]-[1.25]. Similar to the derivative control studies, the capability of VSWTs is evaluated for the temporary frequency control in [1.24], and evaluation results are utilized to tune the parameters of the temporary frequency control in [1.23]. Briefly, the previous inertial response control studies are focused on either capability of VSWTs or simulation of the control concepts, however, without considering the power system requirements for the inertial response. Additionally, the description of the methodology for tuning the control parameters has not been mentioned in the previous studies. In fact, the inertial response control should consider power system requirements and the tuning methodology of the control concept should be developed according to power system characteristics. Furthermore, in future grid code revision studies, a generic inertial response control with the tuning methodology should be able to be used for power systems with high wind power penetration.

About second problem addressed in this thesis, there are a few publications available in the literature [1.26]-[1.28]. In [1.26], the rotor angle stability of the 39-bus test system with high wind penetration (22%) was investigated for different active and reactive power operating conditions of WPPs. The aim of the study was to determine the interaction between the rotor angle stability and the active and reactive power control strategies. Another study proposed a new control strategy to provide VSWTs the synchronizing power capability similar to synchronous generators [1.27]. Finally, the small signal stability and transient stability assessment were performed to analyze the impact of increased DFIG-based wind turbines in [1.28]. The primary basis of the method is to converted DFIG machines to round rotor SGs, then evaluate the sensitivity of the eigenvalues with respect to inertia. However, the previous studies have not mentioned directly the impact of the wind power on the synchronizing power between CPPs.

1.3 Objectives

According to the reviewed discussions about the impact of the wind power on the frequency stability and synchronizing power of CPPs, the main objective of this thesis is to analyze the impact of high wind power penetration on the frequency stability and

the synchronizing power between CPPs for identifying the power system requirements; accordingly, to develop methods for WPPs' contribution considering these power system requirements.

The main objective can be divided into two sub-objectives; the first sub-objective is to analyze the inertial response control requirements of a generic power system taking into account the WPP capability and then to develop a control method which satisfies these requirements. In order to reach this sub-objective, the previous inertial response control concepts are analyzed to comprehend requirements for a generic power system. The investigation results are employed to propose a new control concept with a tuning methodology for the generic power system. Eventually, the aim of the proposed control is to quantify the inertial response requirements from WPPs considering the VSWT capability for a given power system. The proposed control concept determines the inertial response profile, and the tuning methodology specifies the parameters of the profile according to the power system characteristics.

The second sub-objective is to analyze the impact of WPPs on the synchronizing power between remaining CPPs where the old CPPs are replaced by the WPPs. For the analysis, a small generic power system is required to understand the synchronizing power phenomena and a methodology is developed to assess the impact of WPPs and also the contribution of the WPPs' control methods to support the synchronizing power.

In summary, to achieve the main objective the following objectives should be reached:

- to establish a generic power system model which accommodates various wind power penetration scenarios to have the analysis platform with related operational metrics;
- to derive appropriate models of wind turbines and WPPs is required for the wind power integration studies particularly inertial response control;
- to develop and open source and flexible RMS toolbox for wind integration studies;

- to assess the existing control concepts for the inertial response using the generic power system and additionally to propose a new control method with a tuning methodology that can be utilized to any power system with high wind power penetration;
- to develop an assessment methodology for the impact of WPPs on the synchronizing power between CPPs also the contribution of WPPs for the synchronizing power support.

1.4 Scope and Limitations

The scope of this thesis is the analysis of the inertial response control and synchronizing power support of WPPs consist of FC-VSWTs. The simulations performed for the wind integration studies cover only symmetrical stead-state dynamics of the power system (i.e. RMS simulations). The developed models are in the frequency range of the RMS simulations. Additionally, the power electronic components and their fast inner current controllers are not included in the modeling.

For the frequency stability studies voltage dynamics of the CPPs (i.e. AVR) and WPPs are also included to have realistic scenarios in the generic power system. WPPs are operated at constant power factor control mode. In the analysis, the largest infeed loss is considered as an N-1 contingency to observe a major frequency disturbance. Moreover, to specify the power system requirements for the inertial response of WPPs the simplified WPP model is employed without the aerodynamic and mechanical dynamics of wind turbines. Later, with the aggregated WPP model the inertial response control methods are assessed considering both the wind turbine capability and its impact on the generic power system. WPPs consist of FC-VSWTs are modeled and investigated. In the aggregated WPP model, the effects of WPP collector system and different wind turbine conditions are not included.

Finally, in the synchronizing power analysis the severe faults (e.g. three-phase short circuit fault) are not included and the control of wind turbines during these transient

events is not modeled. Instead of the severe faults, the load increase is determined as the disturbance to observe rotor angle deviations.

1.5 List of publications

P1. M. Altin, R. Teodorescu, B. Bak-Jensen, P. Rodriguez and P. C. Kjær, "Aspects of Wind Power Plant Collector Network Layout and Control Architecture," The Danish PhD Seminar on Detailed Modeling and Validation of Electrical Components and Systems 2010.

P2. M. Altın, Ö. Göksu, R. Teodorescu, P. Rodriguez, B. Bak-Jensen, L. Helle, "Overview of Recent Grid Codes for Wind Power Integration," 12th International Conference on Optimization of Electrical and Electronic Equipment (OPTIM), 2010.

P3. M. Altin, R. Teodorescu, B. Bak-Jensen, P. Rodriguez, F. Iov, P. C. Kjær, "Wind Power Plant Control - An Overview," 9th International Workshop on Large-Scale Integration of Wind Power into Power Systems, pp. 581-588, 2010 Proceedings ISBN 978-3-9813870-2-5.

P4. M. Altin, R. Teodorescu, B. Bak-Jensen, U. D. Annakage, F. Iov, P. C. Kjaer, "Methodology for Assessment of Inertial Response from Wind Power Plants," IEEE Power and Energy Society General Meeting 2012.

P5. A. Adamczyk, M. Altin, O. Goksu, R. Teodorescu, F. Iov, "Generic 12-Bus Test System for Wind Power Integration Studies," EPE Joint Wind Energy and T&D Chapters Seminar, Aalborg, Denmark, Jun. 2012.

P6. M. Altin, A. Adamczyk, R. Teodorescu, B. Bak-Jensen, U. D. Annakage, F. Iov, P. C. Kjaer, "Improved Inertial Response Control for Wind Power Plants," submitted to *IEEE Transactions on Power Systems*.

1.6 Outline of the thesis

The introduction chapter is followed by the main body of the thesis which is organized as follows:

In the second chapter, a brief overview regarding synchronizing power support and inertial response control is presented for wind turbines and WPPs, which will be the basis for the proposed control methods [P2], [P3].

In the third chapter, a generic power system model with various wind power penetration scenarios [P5] are developed with generic WPP models [P6] including a simplified and aggregated representation for wind power integration studies. The developed models are utilized in the simulations of Chapter 4 and Chapter 5.

In the fourth chapter, the existing control concepts, which are summarized in Chapter 2, are analyzed according to the defined operational metrics for the generic power systems [P4]. Using the results of the analysis, a new control method is proposed considering the power system requirements and the capability of the WPP. Consequently, the proposed control method is compared with the existing control methods in terms of the peak active power and released energy during the inertial response control [P6].

In the fifth chapter, the assessment of the WPPs' impact on the synchronizing power between CPPs is analyzed for high wind power penetration scenarios where CPPs are replaced with WPPs. The analysis results are demonstrated by simulations and a methodology which is based on the piecewise linear approximation of current injections of WPPs and load flow equations. Furthermore, various control methods of the synchronizing power support are proposed and assessed with this methodology.

The final chapter summarizes the conclusions of this thesis with discussions and the recommendations for future work.

1.7 References

[1.1] L. Grigsby, *Power System Stability and Control*, 2007, CRC Press.

[1.2] IEEE/CIGRE Joint Task Force, "Definition and Classification of Power System Stability," Jun. 2003.

[1.3] CIGRE TF 38.02.14, "Analysis and modeling needs of power systems under major frequency disturbances," December 1997.

[1.4] CIGRE, "Advanced Angle Stability Controls," Technical Brochure, TF 38.02.17, Dec. 1999.

[1.5] BTM Consult ApS, "International Wind Energy Development, World Market Update 2010," Mar. 2010.

[1.6] Ecofys Final Report for Work Package-3 prepared for EirGrid, "All Island TSO Facilitation of Renewables Studies," June 2010.

[1.7] EcoGrid Phase 1 Work Package 3, "Step toward a Danish Power System with 50% Wind Energy", Jan. 2007.

[1.8] IEA Wind Task 25 Final Report Phase 1, "Design and Operation of Power Systems with Large Amounts of Wind Power," 2009.

[1.9] M. Altın, O. Gőksu, R. Teodorescu, P. Rodriguez, B.-Bak Jensen, L. Helle, "Overview of recent grid codes for wind power integration," in *Optimization of Electrical and Electronic Equipment (OPTIM), 2010 12th International Conf.*, pp.1152-1160.

[1.10] National Grid UK, "Frequency Response Technical Sub Group Meeting Summary," Mar. 2011.

[1.11] National Grid UK, "National Electricity Transmission System Seven Year Statement," May 2011.

[1.12] Z. Chen, J. M. Guerrero, and F. Blaabjerg, "A review of the state of the art of power electronics for wind turbines," IEEE Trans. Power Electron.,vol. 24, no. 8, pp. 1859–1875, Aug. 2009.

[1.13] J. B. Ekanayake, L. Holdsworth, Wu XueGuang , N. Jenkins, "Dynamic Modeling of Doubly Fed Induction Generator Wind Turbines," *IEEE Transactions on Power Systems*, vol.18, no.2, pp. 803- 809, May 2003.

[1.14] A.D. Hansen, G. Michalke, "Multi-pole permanent magnet synchronous generator wind turbines' grid support capability in uninterrupted operation during grid faults," *Renewable Power Generation, IET*, vol.3, no.3, pp.333-348, Sept. 2009.

[1.15] G. Lalor, A. Mullane, and M. O'Malley, "Frequency Control and Wind Turbine Technologies," *IEEE Trans. Power Systems,* vol. 20, no. 4, pp. 1905-1913, Nov. 2005.

[1.16] M. Kayikci and J. V. Milanovic, "Dynamic Contribution of DFIG-Based Wind Plants to System Frequency Disturbances," *IEEE Trans. Power Systems,* vol. 24, no. 2, pp. 859-867, May. 2009.

[1.17] J. Morren, S. W. H. de Haan, W L. Kling, and J. A. Ferreira, "Wind turbine emulating inertia and supporting primary frequency control," *IEEE Trans. Power Systems,* vol. 21, no. 1, pp. 433-434, Feb. 2006.

[1.18] J. F. Conroy and R. Watson, "Frequency response capability of full converter Wind turbine generators in comparison to conventional generation," *IEEE Trans. Power Systems,* vol. 23, no. 2, pp. 649-656, May 2008.

[1.19] J. Morren, J. Pierik, and S. W. H. de Haan, "Inertial response of variable speed wind turbines," *Electric Power Systems Research,* vol. 76, no. 11, pp. 980-987, Jul. 2006.

[1.20] O. Anaya-Lara, F. Hughes, N. Jenkins, and G. Strbac, "Contribution of DFIG-based wind farms to power system short-term frequency regulation," in *Proc. IEE Generation, Transmission and Distribution,* vol. 153, no. 2, pp. 164-170, Mar. 2006.

[1.21] J. M. Mauricio, A. Marano, A. Gomez-Exposito, and J. L. Martinez Ramos, "Frequency Regulation Contribution Through Variable-Speed Wind Energy Conversion Systems," *IEEE Trans. Power Systems*, vol. 24, no. 1, pp. 173–180, Feb. 2009.

[1.22] S. Wachtel and A. Beekmann, "Contribution of wind energy converters with inertia emulation to frequency control and frequency stability in power systems," in *Proc. 8th Workshop on Large-Scale Integration of Wind Power into Power Systems,* pp. 460-465, Oct 2009.

[1.23] N. R. Ullah and T. Thiringer, "Temporary primary frequency control support by variable speed wind turbines-potential and applications," *IEEE Trans. Power Systems,* vol.23, no.2, pp.601-612, May 2008.

[1.24] K. Ping-Kwan, L. Pei, H, Banakar, B. T. Ooi, "Kinetic Energy of Wind-Turbine Generators for System Frequency Support," *IEEE Trans. Power Systems,* vo1.24, no.1 , pp.279-287, Feb. 2009.

[1.25] G. C. Tarnowski, P C. Kjaer, P. E. Sorensen, and J. Ostergaard, "Variable speed wind turbines capability for temporary over-production," in *IEEE Power & Energy Society General Meeting,* pp. 1-7, Calgary, USA, July 2009.

[1.26] E. Vittal, M. O'Malley, and A. Keane, "Rotor angle stability with high penetrations of wind generation," *IEEE Trans. Power Systems,* vol. 27, no. 1, pp. 353-362, Feb. 2012.

[1.27] O. Anaya-Lara and F. Hughes, "Provision of a synchronising power characteristic on DFIG-based wind farms, " *IET Generation, Transmission & Distribution, IET*, vol. 1, no. 1, pp. 162-169, Jan. 2007.

[1.28] G. Gautam, V. Vittal, and T. Harbour, "Impact of Increased Penetration of DFIG-Based Wind Turbine Generators on Transient and Small Signal Stability of Power Systems," IEEE Trans. on Power Systems, vol. 24, no. 3, pp. 1426-1434, August 2009.

Chapter 2
Synchronizing Power Support and Inertial Response Control of WPPs, an Overview

2.1 Introduction

With the integration of the wind power plants (WPP), the power system stability is going to be affected in the future for high wind power penetration scenarios [2.1], [2.2]. The stability analysis of conventional power plants (CPP) is defined in [2.3] and consists of the following steps:

1. Modeling assumptions and formulation of appropriate mathematical models for the time scales and phenomena under analysis
2. Appropriate stability definition
3. Simulations to determine the stability using a scenario of events

However, WPPs due to the wind turbine technology do not behave like CPPs, and classical control methods to enhance the power system stability should be revised considering the dynamics of WPPs. First, the impact of WPPs on the power system stability should be investigated, accordingly the control methods of WPPs should be proposed considering these impact studies for the stable and reliable operation of power systems with high wind power penetration. Therefore, in this chapter, the rotor angle and frequency stability studies regarding WTs and WPPs are summarized.

2.2 Synchronizing Power Support, Overview

There are a few publications directly related to the synchronizing power support from WTs and WPPs in the literature [2.4], [2.5]. Furthermore, flexible AC transmission systems (FACTs) control [2.6], [2.7], excitation control of CPPs, prime mover control with fast valving, control of load and generator tripping [2.8] are investigated for the rotor angle stability of power systems. In this section, starting with the definition of the rotor angle stability, the impact studies of wind power penetration on the rotor angle stability, and the control solutions of WTs and other power system equipments to the rotor angle instability are reviewed.

Rotor angle stability refers to the ability of synchronous generators (SG) of an interconnected power system to remain in synchronism after being subjected to a disturbance [2.9]. It depends on the ability to maintain equilibrium between electromagnetic torque (T_e) and mechanical torque (T_m) of each SG in the system which is represented in (1). This equation describes the source of the acceleration and deceleration of SGs due to the imbalance between T_e and T_m. Fig. 2.1 briefly illustrates (2.1) and (2.2) for a SG with generator and power system dynamics.

$$2H\frac{d\omega}{dt}=T_m-T_e \tag{2.1}$$

$$\frac{d\delta}{dt}=\Delta\omega \tag{2.2}$$

where H is the inertia constant, δ is the rotor angle and Δω is the speed deviation.

Instability that may result occurs in the form of increasing angular swings of some generators (δ) leading to their loss of synchronism with other generators. Subjecting a disturbance the equilibrium between T_m and T_e is upset. SGs start to decelerate or accelerate according to (1). If a SG rotates faster than another generator, the angular position of its rotor relative to the slower generator will increase. This increase results in change of the generators' loading, and if the power system is stable, the speed and the angular difference between the generators tend to reduce. Otherwise, the excess

kinetic energy due to the rotor speed difference cause loss of synchronism that can occur for one generators or a group of generators in a power system.

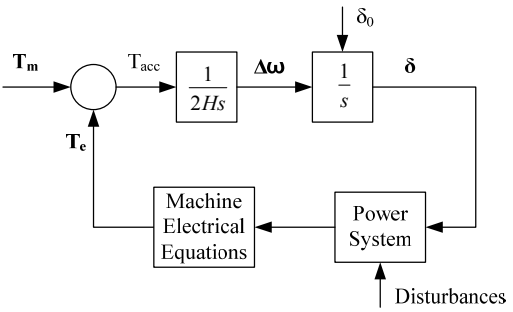

Fig. 0.1. Block diagram of synchronous generator electromechanical dynamics [2.2]

Following a disturbance, T_e can be characterized by two components according to rotor angle and speed deviation; synchronizing torque and damping torque, respectively. Since the rotor speed deviation is considered within a small range the terms can be referred as synchronizing and damping power which are the components of electrical power (P_e) [2.8]. Since the damping power is outside the scope of the study, the studies related to the damping power is not reviewed in this section.

In [2.4], the rotor angle stability of the 39-bus test system with high wind penetration (22%) was investigated for different active and reactive power operating conditions of WPPs. The aim of the study was to determine the interaction between the rotor angle stability and the active and reactive power control strategies. First, the impact of active power control for WPPs based on doubly-fed induction generator (DFIG) on the rotor angle stability was presented using prony analysis for loss of generation contingency. In the active power analysis, the case of WPPs with DFIGs operated at a fixed 0.95 capacitive power factor was compared to another case where WPPs are replaced by equivalently rated SGs with exciter systems. As a result, in the capacitive DFIG operated case, the burden on the CPPs increased in terms of providing large active power output and increasing damping support. Second, the reactive power control

strategies of the WPPs were varied to assess the impact on the rotor angle stability. The cases varied in the simulations were the unity power factor control and terminal voltage control of the WPPs. According to simulation results, the voltage control is better able to damp power system oscillations that may lead to the rotor angle stability.

Another study proposed a control strategy to provide variable speed wind turbines (VSWT) the synchronizing power capability similar to synchronous generators [2.5]. The auxiliary control loop was developed on the 'flux magnitude and angle control' (FMAC) which controls the position and magnitude of the rotor-flux vector to enable the synchronizing power-angle characteristics of a synchronous generator. The simulation results showed that providing the synchronizing power-angle characteristic with the proposed control was possible, however it eliminated the beneficial transient-power characteristics of the FMAC control such as better voltage recovery and damping of the post-fault oscillations.

In addition to above mentioned studies, synchronizing power/torque analysis of synchronous generators with FACTS are available in the literature [2.6], [2.7]. FACTs have the capability of providing reactive power for rotor angle stability and also voltage stability of the power system. While increasing the transient stability, FACTs may decrease the damping of the power oscillations in power systems. Regarding the synchronizing power analysis, the effect of the static VAR compensator (SVC) was analytically explained in [2.6] for a simplified power system. The simplified power system and the derived equation for the synchronizing torque are given as follows:

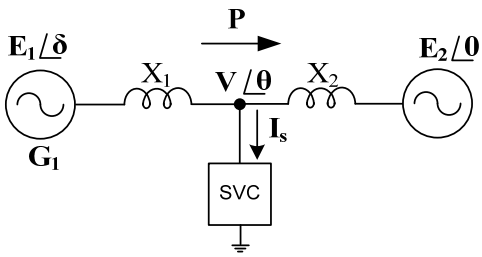

Fig. 0.2. Simplified Power System Model [2.6]

Current equation at the connection point of the SVC:

$$I_s = \frac{E_1 e^{i\delta}}{jX_1} + \frac{E_2 e^{i0}}{jX_2} - Ve^{i\theta}\left(\frac{1}{jX_1} + \frac{1}{jX_2}\right) \tag{2.3}$$

Current injection of the SVC:

$$I_s = \left(\frac{\alpha_i}{jX_i} - \frac{\alpha_c}{jX_c} - \frac{1}{jX_t}\right)Ve^{i\theta} + \frac{Ve^{i\theta}}{jX_t} \tag{2.4}$$

$$Ve^{i\theta} = \left(X_1 E_2 e^{i0} + X_2 E_1 e^{i\delta}\right) \Big/ X_e \tag{2.5}$$

Effective reactance of the power system with SVC:

$$X_e = \left(X_1 + X_2\right) + X_1 X_2 \left(\alpha_i / X_i - \alpha_c / X_c\right) \tag{2.6}$$

With a constant voltage (V_0) control of SVC the effective reactance is:

$$X_e = \frac{1}{V_0}\sqrt{\left(X_1 E_2\right)^2 + \left(X_2 E_1\right)^2 + 2E_1 E_2 X_1 X_2 \cos\delta} \tag{2.7}$$

The power transfer from G1:

$$P = E_1 E_2 \sin\delta / X_e \tag{2.8}$$

Synchronizing torque coefficient is defined as:

$$K_s = \frac{\partial P}{\partial \delta} \tag{2.9}$$

Increase in the synchronizing torque considering SVC effect:

$$\Delta K_s = \frac{X_1 X_2}{X_e}\left(\frac{P}{V_0}\right)^2 + E_1 E_2 \cos\delta\left(\frac{1}{X_e} - \frac{1}{X_1 + X_2}\right) \tag{2.10}$$

Both steady-state and transient stability limits for the synchronous generator was increased by modifying the effective reactance (X_e) of the power system with SVC. As a result, implementing a fast voltage control with a SVC increased the synchronizing power of the synchronous generator connected via long transmission lines.

Similar to the analysis summarized above, [2.7] also investigated the SVC effect on the synchronizing and damping torque and the power system steady-state stability. The following equations were employed to analyze the synchronizing torque.

$$\Delta\omega_r(j\omega) = j\omega.\Delta\delta(j\omega) \tag{2.11}$$

$$\Delta T_e(s) = K_e(s).\Delta\delta(s) \tag{2.12}$$

Replacing s with $j\omega$ and substituting (12) in (11), it was obtained:

$$\Delta T_e(s) = K_e(s).\Delta\delta(s) \tag{2.13}$$

$$\Delta T_e(j\omega) = \Delta T_s(j\omega).\Delta\delta(s) + \Delta T_d(j\omega).\Delta\omega_r(s) \tag{2.14}$$

$$\Delta T_s(j\omega) = real(K_e(j\omega)) \tag{2.15}$$

The contribution was the sensitivity analysis with varied operating conditions of the synchronous generator and reactive power support from the SVC for different power system oscillation frequencies. Consequently, SVC reactive power contribution through the voltage control enhances the synchronizing torque coefficient. Better enhancement can be achieved if the SVC is applied to the electric center of the power system.

An extensive summary was presented in [2.8] about the advanced angle stability control. Feedback and feedforward controls for the rotor angle stability were reviewed. Accordingly, examples of the stability controls are of many types including:

- Generator excitation control (e.g. automatic voltage regulator, power system stabilizer)
- Prime mover controls including fast valving
- Generator tripping
- Fast fault clearing
- High speed reclosing, and single-pole switching
- Dynamic braking

- Load tripping and modulation
- Reactive power compensation switching or modulation (series and shunt)
- Current and voltage injections by voltage source inverter devices (e.g. STATCOM, UPFC, SMES, battery storage)
- Fast voltage phase angle control
- HVDC link supplementary controls
- Adjustable-speed (doubly-fed) generation
- Controlled separation and under-frequency load shedding

One of the statements in [2.8] is that for the rotor angle stability control, injection of real power is more effective than reactive power regarding the energy storage (e.g. superconducting magnetic energy storage or battery storage). The applications of energy storage systems for damping of the power oscillations were also presented in this study.

As a result of the overview, the impact of FACTs on the rotor angle stability are addressed and quantified by the derived equations for the synchronizing power analysis. The control solutions proposed and implemented for FACTs mainly focused on voltage control. Consequently, the reactive power injection by the voltage control enhances both steady-state and transient stability. However, the impact of the wind power penetration on the power system in terms of synchronizing power flow between CPPs was only studied by time domain simulations. For a given power system how the penetration level changes the synchronizing power flows between CPPs and the angular separation is affected with the integration of WPPs need extensive analysis and simulations.

2.3 Inertial Response Control, Overview

Similar to rotor angle stability definition, frequency stability is defined as the ability of a power system to maintain steady frequency after a disturbance resulting in a significant imbalance between generation and consumption. It depends on the control performance at the generation side and the protection settings at the consumption side.

Generally, frequency stability problems are associated with inadequacies in power system component responses, poor coordination of control and protection equipment, or insufficient generation reserve [2.3].

In frequency stability studies, the system frequency response's stages following a disturbance are investigated. The power system progresses through the frequency response stages which are described in Table 2.1. The frequency response stages represent the response of SGs to frequency deviations without and with a control. The first two stages in Table 2.1 describe the natural response of SGs (i.e. without control). The last two stages on the contrary, describe the control responses by governor controller in CPPs and automatic generation controller in power system dispatch center.

Table 2.1. Frequency Response Stages Following a Generation Loss [2.10]

	Stage	**Impact**	**Origin**
1	Electromagnetic energy release	Maintain synchronism (synchronizing power release)	Magnetic field of synchronous generator
2	Inertial response	Slow down ROCOF (providing time for primary frequency control)	Kinetic energy from rotor
3	Primary frequency control	Bring frequency to a steady-state level	Frequency responsive reserve
4	Automatic generation control	Bring frequency back to its nominal value	Contingency reserve

The first stage is described in the previous section. After this stage, the inertial response stage has started immediately according to (2.1). During the inertial response stage, the additional power comes primarily from the stored rotational energy in SGs. The change of the active power depends on the H and $d\omega/dt$. The inertial response of a SG is illustrated in Fig. 2.3. The dashed curve is the active power delivered from the rotational stored energy and the dotted curve shows the active power given by the primary frequency control after a generation loss. As an overall response the solid line represents the active power output.

The total inertial response of each SG determines the power system inertia. Accordingly, the power system inertia determines the sensitivity of the system frequency which indicates how fast and deep the system frequency deviates after a disturbance. It is the resistance of power system with respect to the frequency deviations after a disturbance (e.g. loss of generation or load). For instance, lower system inertia (e.g. in isolated power systems) causes higher frequency deviation after a generation loss.

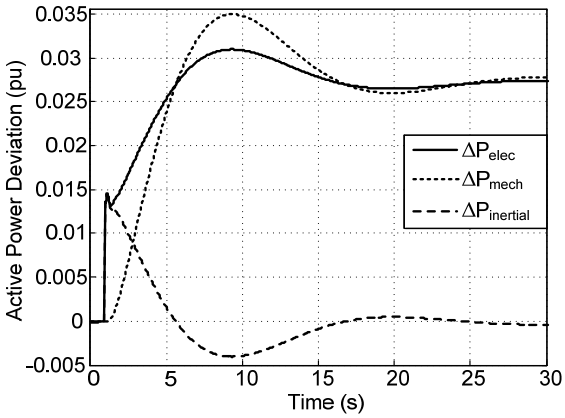

Fig. 0.3. Frequency response of a synchronous generator after a generator loss or load increase

On the contrary, variable speed wind turbines (VSWT) with power electronic grid interface are insensitive to frequency deviations and therefore do not behave like CPPs following a disturbance. The speed of the wind turbine is decoupled from the system frequency due to the control strategy of VSWTs [2.11], [2.12]. Without any supplementary control, WPPs based on VSWTs only control their active power output according to the set value such as available or curtailed active power reference. Therefore, WPPs can be realized as constant active and reactive power sources. With integration of WPPs employing VSWTs, the power system inertia becomes reduced for high wind power penetration scenarios which include replacement of CPPs. Therefore, in the future, the frequency stability of power systems with high wind power

penetration will be affected adversely and the control capability of WPPs should be reconsidered to enhance the frequency stability [2.1], [2.2].

The wind power industry has focused on the inertial response capability of VSWTs in the last five years [2.13]. Transmission system operators (TSO) have been working on grid code requirements for implementation of a generic inertial response from WPPs [2.14]. Although some reports and recommendations for future grid codes have been published [2.15], there are no mandatory requirements at present. National Grid in UK, ENTSO-E in EU, Red Electrica in Spain, and Hydro-Quebec in Canada have been working on grid code requirements for the implementation of an inertial response from WTGs mainly and WPPs. Table 2.2 summarizes the recent requirements and studies from TSOs with the illustration in Fig. 2.4.

Table 2.2. Summary of the requirements and studies for inertial response from WPPs

TSO	**Requirements**
Red Electrica	df/dt control (future requirement)
Hydro Quebec	emulating a synchronous generator with H=3.5s (draft grid code requirement)
National Grid	similar to inertial response of a synchronous generator (discussion and recommendation)
ENTSO-E	similar to inertial response of a synchronous generator (pilot grid code draft)

In this section, previous studies for the inertial response control of VSWTs and WPPs are reviewed in terms of control approach and procurement of additional active power [2.16]-[2.32]. The inertial response has introduced with different phrases such as *synthetic inertial response* [2.14], [2.15], *inertial response* [2.16]-[2.18], *inertia emulation* [2.19], [2.20], *frequency control/response* [2.21]-[2.26], *short-term frequency regulation* [2.27], and *temporary frequency* control [2.28]-[2.31]. These studies are reviewed in two parts; the first part discusses how to provide the additional

active power from VSWTs regardless of the control approach. In the second part the control methods are investigated.

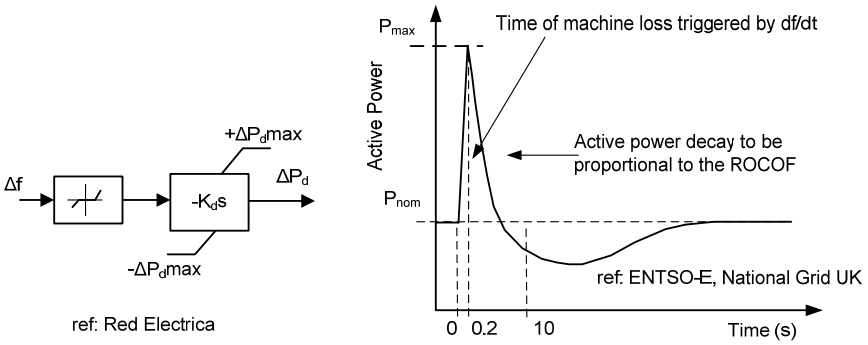

Fig. 2.4. Recommendations and studies regarding inertial response of WPPs

When the inertial response is activated for a VSWT, the additional active power can be released from:

1. Reserve active power (i.e. de-rated operation) [2.16], [2.18], [2.22], [2.25]
2. Kinetic energy of the wind turbine where the VSWT is operating at available power, low wind speed [2.17], [2.19]-[2.21], [2.25], [2.26], [2.28]-[2.31]
3. Excess wind power where the VSWT is operating at high wind speed [2.21], [2.23], [2.24], [2.27]-[2.31]
4. Energy storage employed in the VSWT [2.32]

If the reserve active power is used for the inertial response control, the operating point should be different than the optimum operating point (i.e. maximum available power at given wind speed). This can be done by setting a different pitch angle reference for the pitch control (Fig. 2.5) or different rotor speed reference for torque/active power control (Fig. 2.6). The drawback of this approach is that the mechanical dynamics of the pitch control determines the inertial response performance. In Fig. 2.6, there are two ways depending on the end point of the inertial response control (i.e. from A to B or A to C). Furthermore, during the inertial response control implemented in Fig. 2.6, the kinetic energy of the rotor has been also used. This approach is faster than the

previous approach, also efficient by using kinetic energy. The VSWT is operated less than the available power for both of the approaches thus spilling wind power.

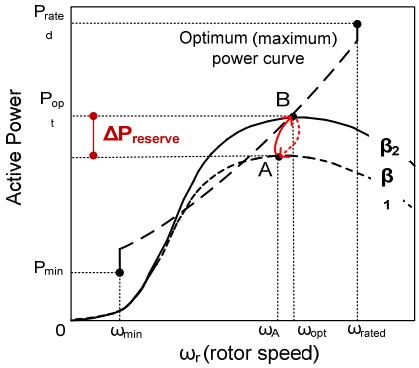

Fig. 2.5. Illustration of active power reserve by setting different pitch angle reference

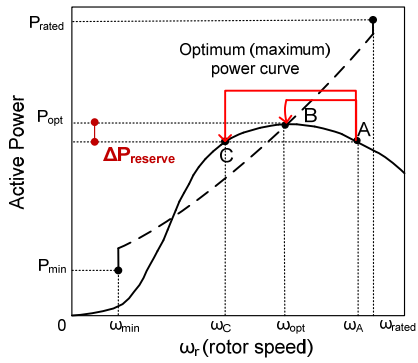

Fig. 2.6. Illustration of active power reserve usage by setting different rotor speed reference (e.g. A to B or A to C)

Kinetic energy stored in the wind turbine is hidden due to VSWT control strategy. Therefore, with a supplementary control, the additional active power can be released to the power system as illustrated in Fig. 2.7. In this approach, the advantage is the fast performance of the inertial response control, however there will be a 'recovery period' after releasing the additional active power. The recovery period can be described as the duration to recover its previous operating condition after releasing the additional power when it is operating at available power due to deceleration of the wind turbine rotor (Fig. 2.7). During this period, the active power output is reduced below the available power (i.e. optimum power).

When the VSWT operates at high wind speed conditions (above rated wind speed), the additional active power can be provided from the excess wind by overloading the VSWT. This approach is illustrated in Fig. 2.8 where straight line represents the available active power, dashed line is optimum rotor speed, and pitch angle is the

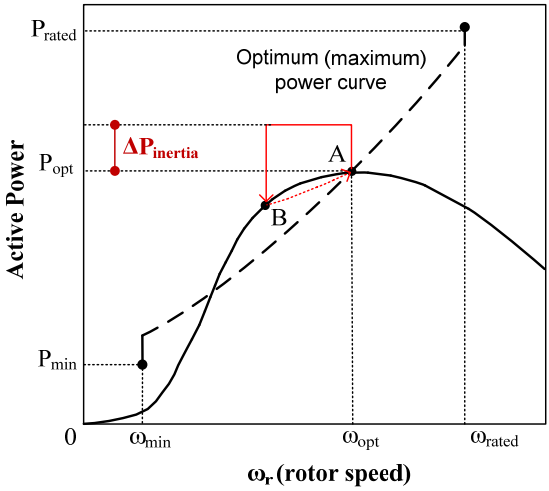

Fig. 2.7. Illustration of releasing additional active power from kinetic energy of the wind turbine

dashed line with dots with respect to different wind speeds. In this case, the recovery period will not be observed due to high wind speed. The pitch angle is controlled to capture the excess active power from wind.

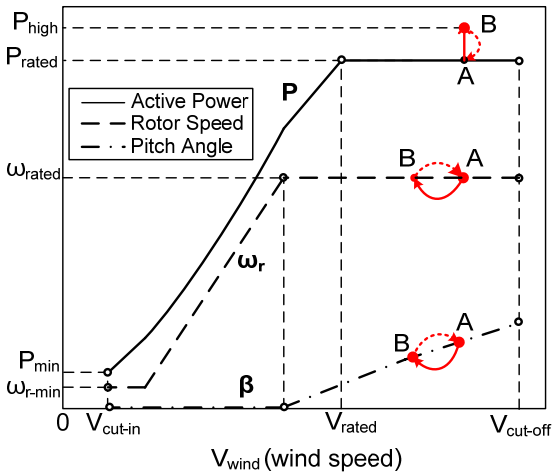

Fig. 2.8. Illustration of providing additional active power from excess wind power at high wind speed

Finally, the energy storage is another option to enable the inertial response control [2.32]. In this option, there can be several approaches such as energy storage control with VSWTs at turbine level or control at the WPP level without including wind turbine control. However, energy storage option is very expensive approach with respect to previously mentioned approaches.

After reviewing the procurement approaches of the additional active power for the inertial response control, the control methods are summarized in the rest of the section. In the literature, several control methods are proposed to enable the inertial response of WPPs [2.11]-[2.31]. These control methods can be grouped generally into two categories according to response profiles [2.33]. The first method is the derivative control based on rate of change of frequency (i.e. ROCOF or *df/dt*). Accordingly, the second method is temporary frequency control which is triggered by ROCOF or frequency deviation (*Δf*).

The derivative control method based on ROCOF was proposed to emulate the inertial response of a synchronous generator [2.16], [2.18], [2.20], [2.21], [2.23]-[2.25], [2.27]. The control modifies the active power or torque set point by an additional active or torque value based on (2.1). However, the derivative control is sensitive to the noise in the frequency measurements. To solve this problem, a low-pass filter is added to the control as shown in Fig. 2.9. However, the derivative control should be fast (order of milliseconds) and it should not be affected by non-generation loss events (e.g. switching incidents) that makes the appropriate filtering becomes challenging [2.13].

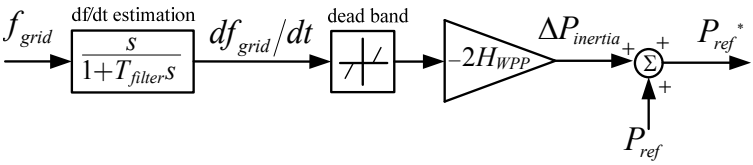

Fig. 2.9. Block diagram of the derivative control

The derivative control method can be modified by adding a droop control similar to CPPs' governor control. The droop control given in Fig. 2.10 improves the inertial response behavior, but active power reserve is required in order to sustain the frequency support. Another frequency support control was developed in Fig. 2.11 to extract the stored kinetic energy from wind turbine when the operating point is higher the optimum rotor speed (i.e. Fig. 2.6 from A to B) [2.18].

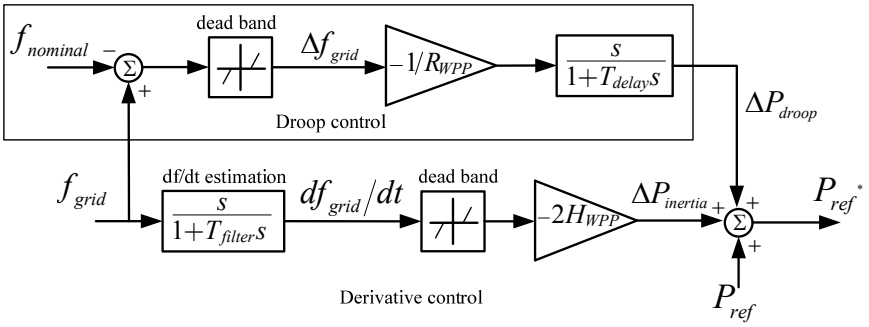

Fig. 2.10. Block diagram of the derivative control with the droop control

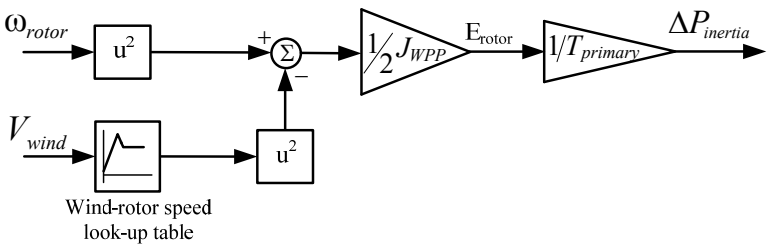

Fig. 2.11. Block diagram of the frequency support control to extract stored kinetic energy [2.17]

In temporary frequency control, an additional active power is released temporarily after detecting the frequency disturbance [2.19], [2.22],[2.24], [2.26], [2.28]-[2.31]. The magnitude of the additional active power is determined in two ways; proportional to the frequency deviation [2.19] or a predefined value (e.g. an active power pulse) [2.26], [2.28]-[2.31]. The control provides additional active for a certain period of time faster than the CPPs' frequency response. The temporary frequency control with a ROCOF

triggering is illustrated in Fig. 2.12. Moreover, it is mainly developed to test the capability of VSWTs for the frequency support. When the disturbance or the operating conditions of the power system has changed, the magnitude and duration of the temporary frequency response should be changed by the WPP operator or TSO. Otherwise, it may destabilize the power system providing less or more active power without considering the frequency deviation and CPPs' frequency response.

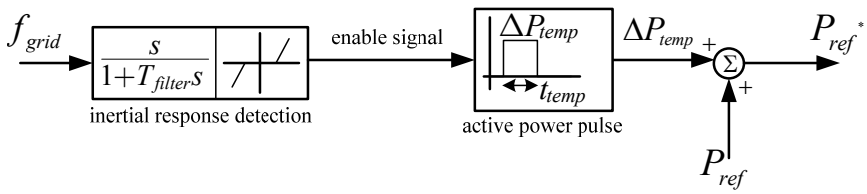

Fig. 2.12. Temporary frequency control with ROCOF triggering

2.4 Summary

To sum up, various inertial response control methods and procurement of the active power for these control methods have been reviewed in this chapter. The previous studies investigated either capability of VSWTs or simulation of the control methods' performance; however without considering the power system requirements of the inertial response control from WPPs. Additionally, the description of the methodology for tuning the control parameters has not been mentioned in the previous studies. Only, sensitivity analyses for the parameters of control methods have been conducted. In fact, the inertial response control should consider power system requirements and the tuning methodology of the control method should be developed according to power system characteristics. Furthermore, in future grid code revision studies, a generic inertial response control with the tuning methodology will be able to be used for power systems with high wind power penetration.

2.5 References

[2.1] National Grid UK, "National Electricity Transmission System Seven Year Statement," May 2011.

[2.2] J. Bömer, K. Burges, C. Nabe, and M. Pöller, "All Island TSO Facilitation of Renewables Studies", Final Report for Work Package 3, [Online]. Available: http://www.uwig.org/Faciltiation_of_Renwables_WP3_Final_Report.pdf

[2.3] IEEE/CIGRE Joint Task Force, "Definition and Classification of Power System Stability," Jun. 2003.

[2.4] E. Vittal, M. O'Malley, and A. Keane, "Rotor angle stability with high penetrations of wind generation," *IEEE Trans. Power Systems,* vol. 27, no. 1, pp. 353-362, Feb. 2012.

[2.5] O. Anaya-Lara and F. Hughes, "Provision of a synchronising power characteristic on DFIG-based wind farms," *IET Generation, Transmission & Distribution, IET*, vol. 1, no. 1, pp. 162-169, Jan. 2007.

[2.6] A. E. Hammad, "Analysis of Power System Stability Enhancement by Static VAR Compensators," *IEEE Trans. Power Systems,* vol. 1, no. 4, pp. 222-227, Nov. 1986.

[2.7] S. E. M. De Oliveira, "Synchronizing and damping torque coefficients and power system steady-state stability as affected by static VAR compensators," *IEEE Trans. Power Systems,* vol. 9, no. 1, pp. 109-119, Feb. 1994.

[2.8] CIGRE, "Advanced Angle Stability Controls," Technical Brochure, TF 38.02.17, Dec. 1999.

[2.9] P. Kundur, *Power System Stability and Control*, 1993, McGraw-Hill.

[2.10] EPRI, "Power System Dynamics Tutorial," July 2009.

[2.11] J. B. Ekanayake, L. Holdsworth, Wu XueGuang , N. Jenkins, "Dynamic Modeling of Doubly Fed Induction Generator Wind Turbines," *IEEE Transactions on Power Systems*, vol.18, no.2, pp. 803- 809, May 2003.

[2.12] A.D. Hansen, G. Michalke, "Multi-pole permanent magnet synchronous generator wind turbines' grid support capability in uninterrupted operation during grid faults," *IET Renewable Power Generation*, vol.3, no.3, pp.333-348, Sept. 2009.

[2.13] P. W. Christensen, G. C. Tarnowski, "Inertia for Wind Power Plants-State of the Art Review Year – 2011," in Proc. *10th International Workshop on Large-Scale Integration of Wind Power into Power Systems as well as on Transmission Networks for Offshore Wind Power Plants,* pp. 457-463, Oct. 2011.

[2.14] ENTSO-E, "Draft Network Code for Requirements for Grid Connection applicable to all Generators, European Network for Transmission System Operators for Electricity," Jan. 2012.

[2.15] National Grid Code Frequency Response Working Group, "Requirements for System Inertia," UK, July 2010.

[2.16] J. Morren, J. Pierik, and S. Dehaan, "Inertial response of variable speed wind turbines," *Electric Power Systems Research*, vol. 76, no. 11, pp. 980-987, Jul. 2006.

[2.17] A. Mullane and M. O'Malley, "The Inertial Response of Induction-Machine-Based Wind Turbines," *IEEE Trans. Power Systems*, vol. 20, no. 3, pp. 1496-1503, Aug. 2005.

[2.18] D. Banham-Hall, C. A. Smith, G. A. Taylor, and M. R. Irving, " Grid connection oriented modeling for simulation of frequency response and inertial behaviour of full converter wind turbines," in *Proc. 2009 8th Workshop on Large-Scale Integration of Wind Power into Power Systems*, pp. 605-610.

[2.19] S. Wachtel and A. Beekmann, "Contribution of wind energy converters with inertia emulation to frequency control and frequency stability in power systems," in *Proc. 8th Workshop on Large-Scale Integration of Wind Power into Power Systems*, pp. 460-465, 2009.

[2.20] J. Morren, S. W.H. de Haan, W L. Kling, and J. A. Ferreira, "Wind turbine emulating inertia and supporting primary frequency control," *IEEE Trans. Power Systems*, vol. 21, no. 1, pp. 433-434, 2006.

[2.21] L. Holdsworth, J. B. Ekanayake, and N. Jenkins, "Power system frequency response from fixed speed and doubly fed induction generator-based wind turbines," *Wind Energy*, vol. 7, no. 1, pp. 21-35, Jan. 2004.

[2.22] C. Jecu, A. Teninge, D. Roye, S. Bacha, R. Belhomme, and P.Bousseau, "Contribution to frequency control through wind turbine inertial energy storage," *IET Renewable Power Generation*, vol. 3, no.3, pp. 358-370, Sep. 2009.

[2.23] G. Lalor, A. Mullane, and M. O'Malley, "Frequency Control and Wind Turbine Technologies," *IEEE Trans. Power Systems*, vol. 20, no. 4, pp. 1905-1913, Nov. 2005.

[2.24] J. F. Conroy and R. Watson, "Frequency response capability of full converter Wind turbine generators in comparison to conventional generation," *IEEE Trans. Power Systems,* vol. 23, no. 2, pp. 649-656, May 2008.

[2.25] M. Kayikci and J. V. Milanovic, "Dynamic Contribution of DFIG-Based Wind Plants to System Frequency Disturbances, " IEEE Trans. Power Systems, vol. 24, no. 2, pp. 859-867, May. 2009.

[2.26] K. Ping-Kwan, L. Pei, H, Banakar, B. T. Ooi, "Kinetic Energy of Wind¬Turbine Generators for System Frequency Support," *IEEE Trans. Power Systems*, vo1.24, no.1 , pp.279-287, Feb. 2009.

[2.27] O. Anaya-Lara, F. Hughes, N. Jenkins, and G. Strbac, "Contribution of DFIG-based wind farms to power system short-term frequency regulation," in *IEE Proceedings Generation, Transmission and Distribution*, 2006, vol. 153, no. 2, pp. 164-170.

[2.28] N. R. Ullah and T. Thiringer, "Temporary primary frequency control support by variable speed wind turbines-potential and applications," *IEEE Trans. Power Systems*, vol.23, no.2, pp.601-612, May 2008.

[2.29] G C. Tarnowski, P C. Kjaer, P. E. Sorensen, J. Ostergaard, "Study on variable speed wind turbines capability for frequency response" in *Proceedings of the European Wind Energy Conference (EWEC)*, p. 16-19, 2009.

[2.30] G. C. Tarnowski, P C. Kjaer, P. E. Sorensen, and J. Ostergaard, "Variable speed wind turbines capability for temporary over-production," in *IEEE Power & Energy Society General Meeting*, 2009, pp. 1-7.

[2.31] G. C. Tarnowski, P. C. Kjaer, S. Dalsgaard, and A. Nyborg, "Regulation and frequency response service capability of modem wind power plants," in *IEEE Power & Energy Society General Meeting*, pp. 1-8, 2010.

[2.32] J. Driesen, K. Visscher, "Virtual synchronous generators," *IEEE PES General Meeting*, Pittsburgh, USA, July 2008.

[2.33] M. Altin, R. Teodorescu, B.-Bak Jensen, U. D. Annakage, F. Iov, P.C. Kjaer, "Methodology for Assessment of Inertial Response from Wind Power Plants", *IEEE Power & Energy Society General Meeting,* San Diego, USA, July 2012.

Chapter 3
Modeling for Inertial Response Control and Synchronizing Power Support

3.1 Introduction

Beyond a certain level a wind power penetration into a power system poses challenges regarding wind power control and stable power system operation. With the advancements in wind turbine technology, wind power can offer capabilities for ancillary services that can contribute to the power system stability (Chapter 2). It is expected that these control capabilities will expand in the future with new functionalities such as inertial response, power system damping, secondary voltage control, etc. Thus, grid connection requirements of wind power are revised considering the new functionalities. The ancillary services may play an important role especially in power systems with high wind power penetration levels.

In order to identify power system requirements and investigate the impact of this control capability on power systems, simulation studies must be performed on a generic power system model including a WPP model with various power penetration scenarios. Therefore, the generic power system model is developed with various wind power penetration scenarios [3.1], accordingly WPP models (i.e. simplified and aggregated WPP models) are developed and implemented in the generic power system model. This section describes the details of the generic power system model and the WPP models

used in this thesis. Moreover, an RMS toolbox is introduced which is used to simulate the generic power system and WPP models for the wind integration studies.

3.2 Power System Model [3.1]

Various power system models were proposed in the literature [3.2]-[3.4]. A simple test system represented by a voltage source behind an impedance is proposed in Danish grid code [3.2] to assess the stability of a wind turbine for symmetric three-phase faults. However, this simple power system does not include the dynamics regarding the frequency response, voltage control, and electromechanical oscillations. Furthermore, for the inertial response and frequency control studies the average system frequency (i.e. single mass) model is implemented in the literature [3.3]. The rotating masses of all synchronous generators in CPPs are lumped as a single-mass; and governor controls act on this single-mass. The single-mass model represents the frequency control dynamics however neglecting the voltage variations and electromechanical oscillations. Another simplified model comprising these two models' behavior is implemented as a single-bus model in the literature [3.4], where all the generating units are connected to a single bus with their voltage and frequency controllers. In the single-bus model, the voltage dynamics are limited due to the small electrical distances between the synchronous generators. However, in order to cover the wind integration studies, which comprise inertial response, power system damping control, and reactive power/voltage control analyses, thoroughly, a multi-machine multi-bus power system model is required with appropriate voltage and frequency controls.

A multi-machine multi-bus power system represents a HV transmission system. It has the generation side modeled as CPPs and the consumption side modeled as lumped loads at HV level. Different multi-machine multi-bus power system models that can exhibit particular phenomena exist in the available literature, e.g. 9-bus system [3.5], 2-area 4-machine system [3.6], 12-bus system [3.7], [3.8], and 68-bus 16-generator system [3.8]. There are other power system models also available in the literature however the aim is to develop a generic power system model, which should be generic and adequate enough for the wind integration studies, among the reviewed models. It

can be realized that the developed power system model should represent the fundamental theory related to analysis without complex grid and test cases.

The 9-bus system [3.5] is not adequate to create various generation mixes, voltage profiles and electromechanical oscillation modes. The 2-area 4-machine system [3.6] has been developed for studying the theory of the small signal stability; however it is not representing a realistic power system layout. The voltage profile of the 2-area 4-machine system is relatively stiff due to small electrical distances between the system buses and the radial and symmetrical system structure does not allow flexibility in mode creation. The original 12-bus system [3.7], [3.8] was developed to test FACTS devices and it is supporting small signal stability analysis. However, it does not include a wide range of parameters and settings for CPPs. The 68-bus 16-generator system [3.9] gives great flexibility in formulating system dynamics and enables approaching realistic system behavior. However, due to the system size it is too complex to handle it analytically in small-signal stability analysis or other wind integration studies.

The existing power system models described briefly are not able to accommodate wind integration studies when they are used in their current form. For wind integration studies, the wind power locations in the power system and different wind penetration scenarios should be specified in detail. Moreover, the frequency stability studies require a power system model with different conventional generation mix including settings for governors as well as load variations. Inertial response control studies have the similar requirements additionally with different wind power penetration scenarios. Considering these model requirements, number of test cases can be defined in order to impose disturbances such as line/generating tripping, step load change etc. and excite different types of instabilities. By modifying the original 12-bus system, the generic 12-bus system model is developed for the wind integration studies. The details regarding the power system layout, CPPs, and loads are described in the following subsections.

3.2.1 Generic 12-bus System Description

The layout (i.e. single-line diagram) of the generic 12-bus system is given in Fig. 3.1. To demonstrate a realistic power system with the symmetrical stead-state dynamics (i.e. RMS simulation), the following modifications are made to the original 12-bus system:

- Generator step-up transformers were sized accordingly to plants MVA capacities; ratings for the autotransformers were matched with 345kV line rating. Also per-unit values of impedances were slightly increased.
- Reactive power consumption at the load buses was reduced in order to maintain adequate voltage profile within the limits for HV networks.
- Voltage set point of the AVR in generator 1 was lowered to the more reasonable level of 1pu and for the rest of the generators, it was 1.01pu.
- Line parameters were adjusted to make a consistent set for the system. Length of lines between Bus 2-5 and Bus 4-5 were adjusted to diversify the impact of a WPP on the areas 1 and 3.
- Active power dispatch between the areas was adjusted to improve voltage profile and to meet the N-1 contingency criterion. For the inertial response control studies, N-1 contingency is defined as the largest infeed loss which is the trip of 200 MW from G2 (connected to Bus 10 in Fig. 3.1).
- Loads were shifted from Area2 to Area1 in order to balance power flow.
- Previous generation profile was re-defined. First, the infinite bus (Bus 1) was replaced by a slack bus. A reference CPP, which is the biggest plant in the generic 12-bus system, was connected to the slack bus. Second, it was also decided to change the generation mix from hydro dominated to thermal dominated as can be found in most of European countries and US. Therefore, HPPs, which are connected to Bus 9 and Bus 10, were replaced by TPPs.
- The detailed CPP's model was implemented which includes the 5^{th} and 6^{th} order of the SG models (i.e. for steam and hydro units respectively), the prime mover, governor control, AVR, exciter, and PSS.

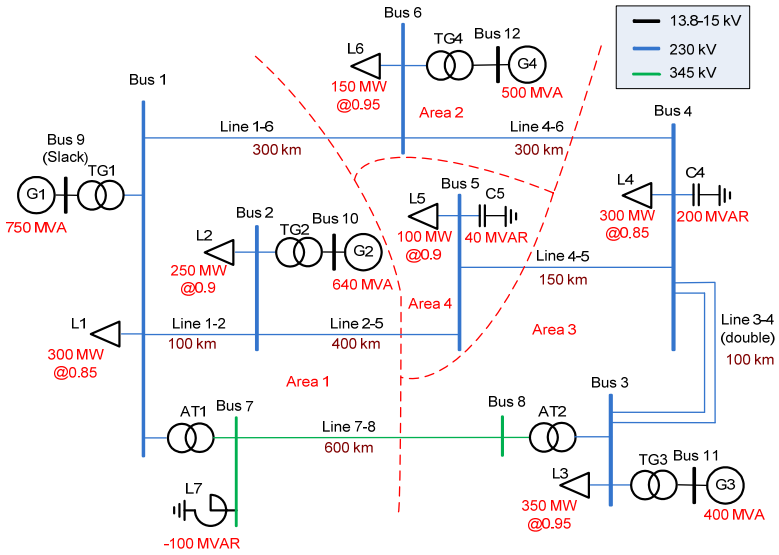

Fig. 3.1. Single-line diagram of generic 12-bus system for wind integration studies [3.1]

As a result of the above adjustments the generic 12-bus system has four areas; Area1 is the biggest thermal generation area with industrial and residential loads, Area2 is rich hydro power generation with small amount of rural load, Area 3 is heavily industrial load centre with thermal generation with possible wind power installation, finally Area 4 is very rich in wind resources but no other generation connected to Bus 5. With this representation, the generic power system can also be linked to some countries like US, UK and Germany as small scale power system. For example, in UK, area 4 is representing offshore WPPs, area 2 is Wales, finally area 1 and 3 are the congested, north-south generation regions of the country as shown in Fig. 3.2.

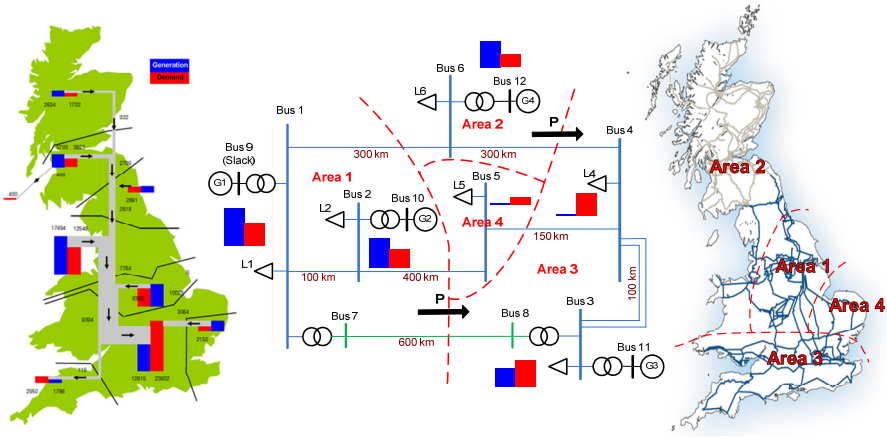

Fig. 3.2. Single-line diagram of generic 12-bus system for wind integration studies [3.1]

3.2.2 Generic 12-bus System Base Case

Before proposing the wind power penetration scenarios, the base case scenario is defined for the generic 12-bus system (Fig. 3.1). In the base case, voltage profiles and load flows are balanced in order to represent steady-state operating conditions of the generic 12-bus system with proper reactive power compensation. Bus voltages are within the specified limits as ±5% of the nominal value, and accordingly the generator loadings (around 70%) and line loadings (around 50%) are within the acceptable limits. N-1 contingency criterion is achieved except the tripping of the longest line between Bus 7 and Bus 8. As a result of these considerations, the load flow results are illustrated in Fig. 3.3. The parameters of the lines, transformers, shunt reactors, shunt capacitor banks, and set points of CPPs and loads are given in [3.1].

From the load flow results the voltage profiles of the base case is shown in Fig. 3.4. In addition to the load flow analysis, the stiffness of the system buses is evaluated by the short circuit calculation, and presented in Fig. 3.5.

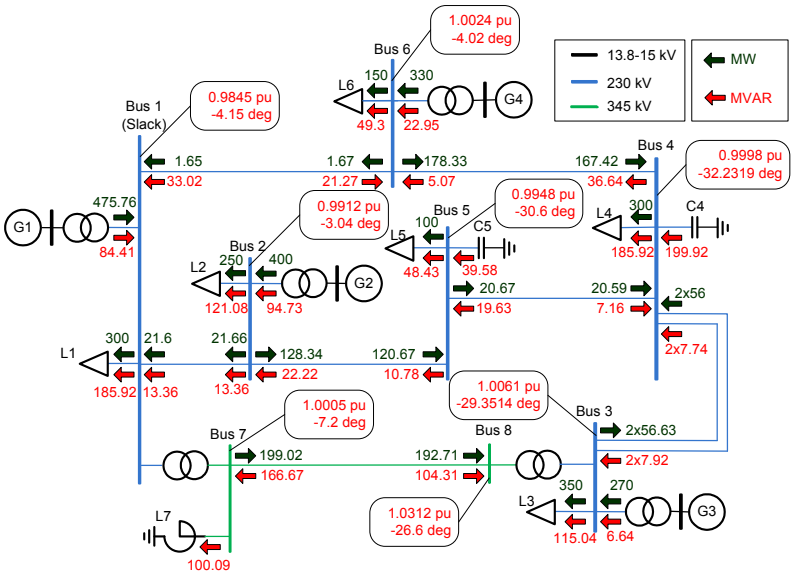

Fig. 3.3. Base case load flow results of generic 12-bus system [3.1]

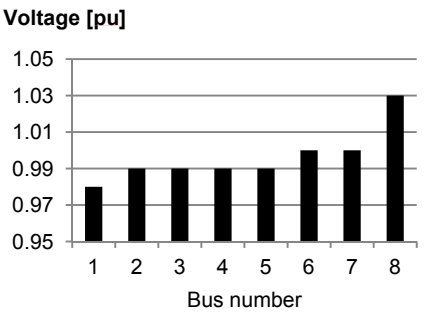

Fig. 3.4. Bus voltage profiles in the generic 12-bus system

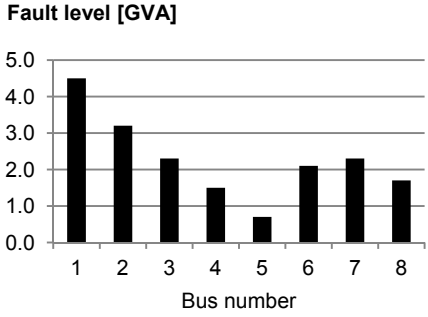

Fig. 3.5. Short-circuit power levels of the generic 12-bus system [3.1]

It can be observed that all voltage levels are within the limits of HV transmission systems (±5%). Considering the short-circuit levels, the installed capacity of CPPs without wind power is about 2 GW, thus the generic 12-bus system can be characterized as a weak islanded system.

3.2.3 Generic 12-bus System CPP Model

The CPP model is composed of two parts; the electrical part comprises the SG and excitation system (i.e. AVR, exciter, and PSS) models, the mechanical part comprises the prime mover and governor models. This structure is illustrated in Fig. 3.6.

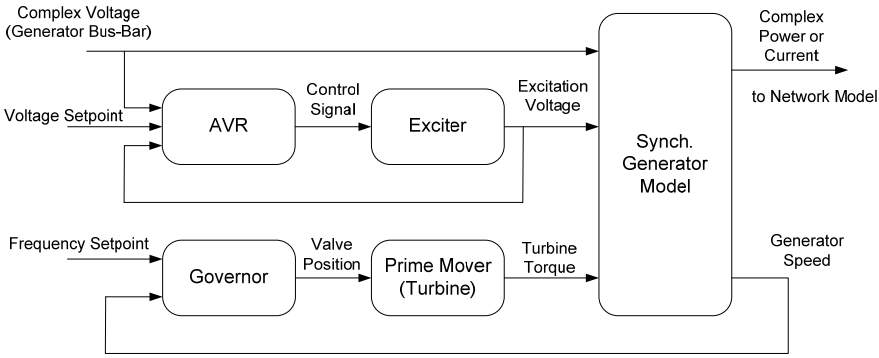

Fig. 3.6. Structure of a CPP model

The SG model represents symmetrical stead-state electro-mechanical dynamics with the differential and algebraic equations. The differential equations are in the two-axis (d-q axis) rotor reference frame. These differential equations describe the damper and field windings in terms of related currents and flux linkages. Further, the algebraic equations transfer the stator currents from the rotor reference frame to the common reference frame of the power system [3.10]. The differential and algebraic equations are given in [3.1] with the parameters implemented in the generic 12-bus system. Additionally, if a CPP consist of more than one SG, the aggregation approach is applied and SGs are modeled as single SG.

The excitation system of CPPs provide direct current to SG field winding in order to control voltage and reactive power flow, thus to enhance the power system stability. The exciter provides DC power to the SG field winding, constituting the power stage of the excitation system. Additionally, the AVR processes and amplifies voltage reference signal to a level and form appropriate for control of the exciter. Most of the CPPs have the PSS in their excitation system to damp power system oscillations by providing

additional input signal to the AVR [3.6]. Excitation system models [3.5], [3.11] implemented in the generic 12-bus system for CPPs are given in [3.1] with the related parameters.

Finally, the prime mover and governor provide a means of controlling active power and system frequency. The prime mover model represents the dynamics of the hydro and steam turbines. Accordingly, the governor model provides the necessary mechanical input signal to the prime mover in order to control the active power together with the system frequency. The dynamics of prime movers and governors is very important for the inertial response control studies of WPPs that are addressed in Chapter 4. The generic 12-bus system has the flexibility to utilize different prime mover and governor models which are grouped in three categories according to their performance. In Fig. 3.7, these different prime mover and governor models are illustrated in terms of system frequency response for the largest infeed loss. In Chapter 4, Case1 is employed to investigate the inertial response control methods of WPPs.

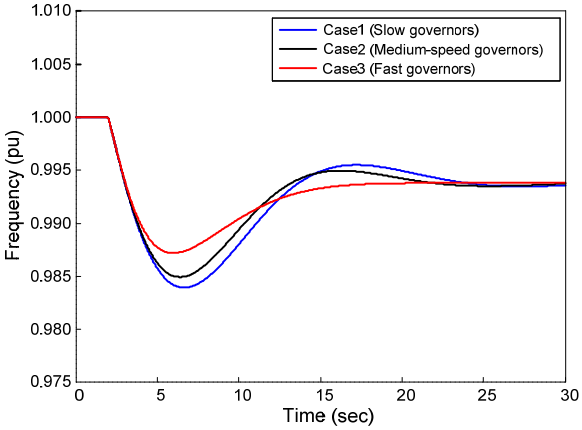

Fig. 3.7. Different frequency responses of generic 12-bus system with different prime mover and governor models

3.2.4 Generic 12-bus System Wind Power Penetration Scenarios

Various operational scenarios are considered for the generic 12-bus system model. These scenarios reflect different wind penetrations into the power system. Two trends in development of the power system have been considered. The first trend assumes that the increased loads are covered by the increase of wind power while the installed capacity of the CPPs is kept constant. This is a typical situation in countries with incentives for wind power in the early stages of wind power development. For these cases some levels of wind power penetration may require reinforcement of lines; however no major changes in the network layout are expected. The second trend assumes that the load will not change significantly, but new wind farm installations would replace some for the existing CPPs. This is typically in countries where wind power is reaching a relatively high penetration level e.g. more than 20%. A typical example for this trend is Denmark where 50% of electricity demand is planned to be covered from wind energy by 2025 [3.12]. Thus, the generic power system model can accommodate wind penetrations from 0% (base case) up to 50% as shown in Table 3.1. In these scenarios, the percentage of the wind power penetration is defined as the ratio of the installed wind power capacity to installed conventional power capacity. Additionally, the wind power penetration scenarios on the single-line diagram with UK wind power installations are illustrated in Fig. 3.8.

Table 3.1. Wind power penetration scenarios in generic 12-bus system [3.1]

	0%	**5%**	**10%**	**20%**	**30%**	**40%**	**50%**
CPPs (MW)	1480	1470	1470	1470	1260	1120	1020
Loads (MW)	1450	1550	1650	1850	1850	1850	1850
WPP-1 (MW)	0	100	200	400	400	400	400
WPP-2 (MW)	0	0	0	0	200	200	200
WPP-3 (MW)	0	0	0	0	0	150	250

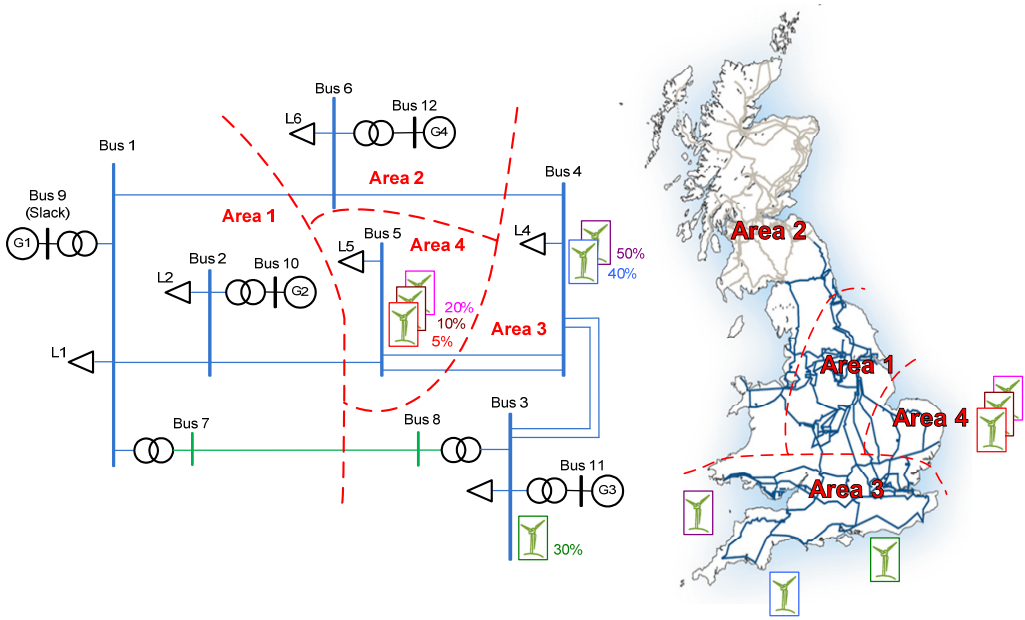

Fig. 3.8. Mapping of wind power penetration scenarios on the generic 12-bus system with UK wind power installations [3.1]

3.2.5 Generic 12-bus System Load Model

Since the stable operation of systems depends on the ability to continuously match the active and reactive output of CPPs with the loads in the power system [3.6], load representation is important for the power system stability studies, even more critical for the wind power integration studies. Load models are different from the SG models and more complicated due to the composition of large number of equipments in HV level. Mainly, there are three types of load representation; static, dynamic, and induction motor loads. The combinations of the different load types are also possible according to load behavior [3.13]. In this thesis, for the inertial response control studies the load model is expressed in terms of algebraic equations as the exponential static load types. Only the voltage dependency is enabled in the load models, and they are not dependent on the frequency. The active power demand of loads is assumed as constant power behavior, and the reactive power demand of the loads is assumed as constant

impendence behavior during the simulations in the generic 12-bus system. The load models are given in the following formulations with the parameters [3.14]:

$$P = P_0\left(aP\left(\frac{V}{V_0}\right)^{e\_aP} + bP\left(\frac{V}{V_0}\right)^{e\_bP} + (1-aP-bP)\left(\frac{V}{V_0}\right)^{e\_cP} \right) \tag{3.1}$$

$$Q = Q_0\left(aQ\left(\frac{V}{V_0}\right)^{e\_aQ} + bQ\left(\frac{V}{V_0}\right)^{e\_bQ} + (1-aQ-bQ)\left(\frac{V}{V_0}\right)^{e\_cQ} \right) \tag{3.2}$$

where $1-aP-bP=cP$, $1-aQ-bQ=cQ$, and the coefficients are aP=0, bP=0, e_aP=0, e_bP=0, aQ=1, bQ=0, e_aQ=2, e_bQ=0.

3.3 Wind Power Plant Model

Models of wind turbines and WPPs have been developed in the literature for the wind power integration studies with different modeling approaches [3.15]-[3.23]. The developed models have been employed in harmonic, sub-synchronous resonance, short-circuit, transient stability, frequency stability, voltage stability, and small-signal stability analyses of power systems. One type of wind turbine or WPP model cannot comprise all the dynamics in these studies, accordingly the most detailed model should not be utilized for simpler analyses. Main focus in the modeling studies is to develop a wind turbine model (e.g. fixed speed, variable speed with partial or full converter), and further the aggregated and full WPP models have been proposed to perform wind integration studies. Although, both wind turbine and WPP models have not been standardized yet, the IEEE and IEC working groups are working on this issue [3.17], [3.24].

In this section, a simplified WPP model and an aggregated WPP model based on a full-converter VSWT (FC-VSWT) with a permanent magnet synchronous generator (PMSG) are developed and employed to investigate the inertial response control and synchronizing power support in the generic 12-bus system. First, the simplified WPP model is proposed to simulate the overall WPP behavior for high wind speed

conditions (i.e. above rated wind speed). Second, the aggregated WPP model is proposed to capture the aerodynamical and mechanical features for the inertial response control studies.

3.3.1 Simplified Wind Power Plant Model

In a WPP, mainly there are two control layers; one of them is the WPP control level as a centralized and high level control, and the other level is the wind turbine control as distributed and individual control. The performance of the overall WPP is both dependent on these control levels. If the aim of the wind integration studies is to investigate the impact of WPPs on the frequency and transient (i.e. synchronizing power studies) stability or to specify the power system requirements, the overall WPP can be represented as a first order time delay. With this representation the WPP is treated as one single fast generation unit. It is assumed that all the wind turbines operate at high wind speed conditions and the inner current control loops of the full-converter are very fast compared to the power control loops. The simplified model (or PQ source model) is shown in Fig. 3.9 and is employed in the simulations of Chapter 4 and Chapter 5. Further improvements can be made by implementing current limits of the wind turbine converters and utilizing the aerodynamical and mechanical dynamics of the wind turbine into the simplified model [3.23].

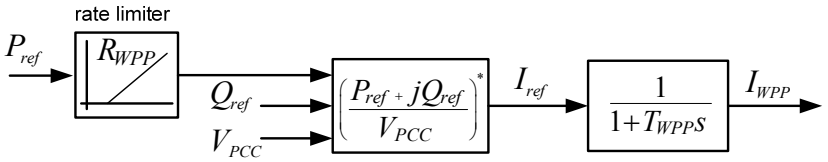

Fig. 3.9. Block diagram of simplified WPP model

3.3.2 Aggregated Wind Power Plant Model based on FC-VSWT

In order to propose an aggregated WPP model, first a generic FC-VSWT model is implemented which expresses the aerodynamical and mechanical dynamics of a generic wind turbine with the electrical and control dynamics of PMSG and FC. Including these dynamics the performance of the inertial response control can be investigated in

the generic power system (Chapter 4). Similar to the CPP model described above, there are three parts in the generic FC-VSWT model developed in this section. The first part is the wind turbine model which is the generic utility-scale multi-megawatt turbine (NREL 5MW) model adapted from [3.18], [3.19]. The second part is the electrical model of the PMSG and FC (MSC and GSC) which are developed with the author of [3.25]. Finally, the third part is the control structure of the FC model. The overall block diagram of the FC-VSWT is given in Fig. 3.10.

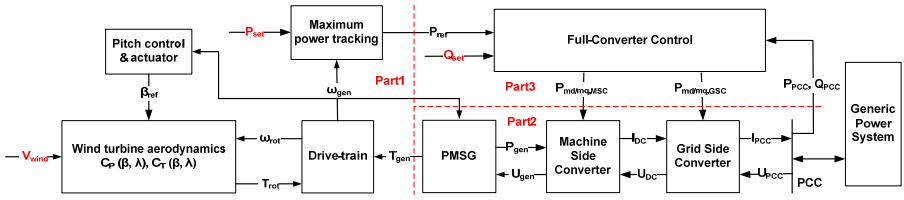

Fig. 3.10. Overall block diagram of FC-VSWT model

In the wind turbine model, the kinetic energy extracted from the wind is modeled using the algebraic equations of the rotor torque (T_{rot}) and the thrust force (F_t). The T_{rot} and F_t equations [3.19] are defined as

$$T_{rot} = \frac{\pi}{2\omega_{rot}} \rho R^2 V_{rot}{}^3 C_P(\lambda,\beta) \tag{3.3}$$

$$F_t = \frac{\pi}{2} \rho R^2 V_{rot}{}^2 C_T(\lambda,\beta) \tag{3.4}$$

where ρ is the air density, R is the rotor radius, V_{rot} is the effective wind speed on the rotor, C_P is the power efficiency coefficient, and C_T is the torque efficiency coefficient. As in the formulations above, the C_P and C_T from the lookup tables [3.18] are both dependent on tip speed ratio (λ) and blade pitch angle (β). In Fig. 3.10, the 'wind turbine aerodynamics' block comprises the above formulations.

The pitch control limits the active power at the rated value for high wind speeds. The pitch control is not enabled all the operation range, however a control logic activates only during the certain operating conditions such as, de-rated active power operation ($P_{set}{}^{*}<P_{available}$) and cases with above the rated generator speed ($\omega_{gen}<\omega_{rated}$) [3.19].

Furthermore, the drive-train is represented as a two-mass shaft model with spring and damping constants. The formulations of the drive train are expressed as follows:

$$\dot{\omega}_t = \frac{1}{2H_t}\left(T_m - \theta_{sh}K_{sh} - \dot{\theta}_{sh}D_{sh}\right) \tag{3.5}$$

$$\dot{\omega}_g = \frac{1}{2H_g}\left(T_e - \theta_{sh}K_{sh} - \dot{\theta}_{sh}D_{sh}\right) \tag{3.6}$$

$$\dot{\theta}_{sh} = \omega_t - \omega_g \tag{3.7}$$

The aerodynamic and mechanical dynamics of the wind turbine are represented adequately to observe the 'recovery period' with the aforementioned blocks (i.e. formulations). The recovery period can be described as the duration to recover its previous operating condition after releasing an additional power when it is operating at available power due to deceleration of the wind turbine rotor. Moreover, the active power reference (P_{ref}) is generated in the 'maximum power tracking' block by calculating the available active power ($P_{available}$) from the pre-defined torque-speed lookup table [3.18]. Fig. 3.11 presents both the torque-speed lookup table, and the relationship between the wind speed and $P_{available}$, respectively. Therefore, P_{ref} is selected as the minimum of the external active power set value (P_{set}) and $P_{available}$. All these modeling considerations are implemented in the 'maximum power tracking' block given in Fig. 3.12.

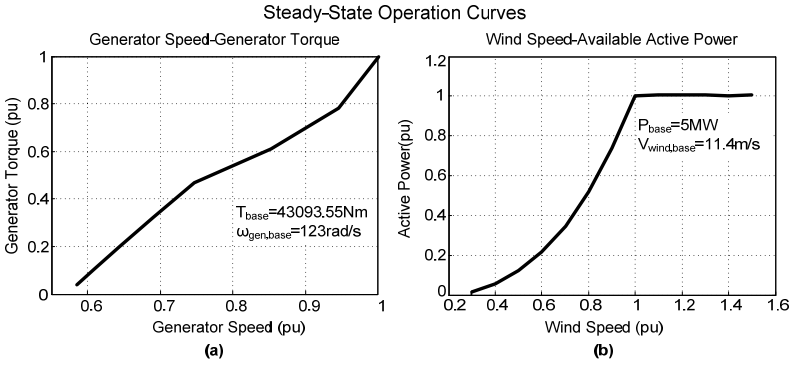

Fig. 3.11. Pre-defined operation curves of FC-VSWT; (a) generator speed to torque curve [3.18], (b) wind speed to available active power curve

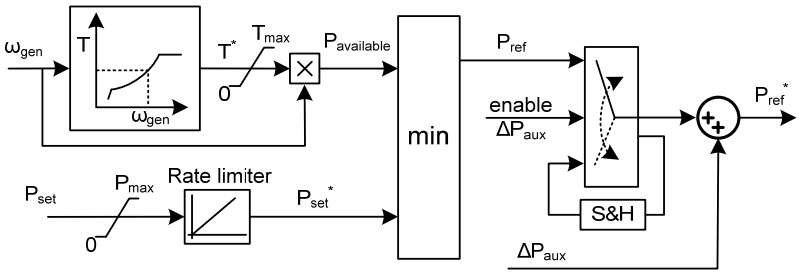

Fig. 3.12. Maximum power tracking block diagram

In the control structure of the FC-VSWT, the active power and the PMSG AC voltage are controlled with the machine-side converter (MSC) and the reactive power and the DC-link voltage are controlled with the machine-side converter (MSC). The inner current control loops of MSC and GSC are neglected, since the inner current control of the full-converter is very fast for the inertial response control studies (i.e. in the order of milliseconds [3.24]). The control dynamics of DC-link voltage and active power control are important for the inertial response control, thus the PI control loops retain in the FC control. Finally for the electrical model of the FC-VSWT (i.e. PMSG, MSC, and GSC), simplifications are made in order to reduce the computation time and complexity. The steady-state algebraic equations are implemented for the PMSG, MSC and GSC, additionally the DC-link is implemented as a differential equation to represent the charging of the capacitor [3.25].

The developed FC-VSWT model is utilized for the behavior of aggregated WPP model to investigate the inertial response control. The aggregation approach is simply modifying the base value of a single turbine to get overall WPP response [3.26]. The park layout of the WPP is not included in the aggregation approach, since the voltage variations at the wind turbine connection point are of no interest for the inertial response of the overall WPP performance in Chapter 4.

3.4 Validation of Aggregated WPP Model with RISØ Model

Active and reactive power control performance of the developed aggregated WPP model based on FC-VSWT is compared with another aggregated model developed in RISØ [3.16], [3.27]. The simulation results are shown in Fig. 3.13. The compared WPP models are not in the same structure such as the active power control of FC is implemented for the MSC in the developed model and the GSC in RISO model. Accordingly, the DC-link voltage control is also different between the models. However, the dynamics of the active power is not significantly different between the models (Fig. 3.13 (a)). For the reactive power control performance, there is a significant disturbance between the models due to the measurement point of the reactive power (Fig. 3.13 (b)). According to the simulation results presented below, the electrical model and control structure of the developed model can be used for the inertial response control studies.

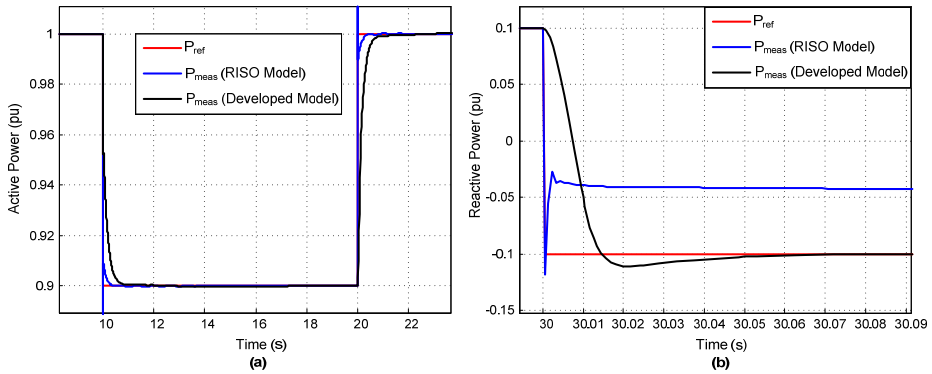

Fig. 3.13. Comparison of the performance of the developed and RISO WPP models; (a) step change in active power, (b) step change in reactive power

3.5 RMS Toolbox

For the simulations performed in Chapter 4 and Chapter 5, the generic power system and WPP models described in the previous sections are implemented in the RMS toolbox, which is developed in MATLAB/Simulink. The aim is to develop an RMS simulation platform for the wind integration studies. The RMS toolbox is open source and flexible in terms of implementing control methods for the WPPs. The other power

system simulation software toolboxes have their advantages and limitations according to the related power system analysis.

The power system simulations are generally solutions of the differential and algebraic equations. The models of the CPPs and WPPs with their controls and the dynamic loads are represented by a set of differential equations (3.8), and the rest of the power system describing the grid, the static loads, and the algebraic equations of the generator is described in (3.9).

$$\dot{x} = f(x, y) \tag{3.8}$$

$$0 = g(x, y) \tag{3.9}$$

To solve these two sets of equations in order to define the electromechanical states of the power system at any time instant with the bus voltage magnitudes and angles in the RMS simulations. There are two approaches solving the differential algebraic equations [3.28]:

- Partitioned-explicit (PE) method,
- Simultaneous-implicit (SI) method.

In the PE method, the differential equations are solved using numerical integration with the algebraic equations being solved separately. On the contrary, the SI method uses the numerical integration to convert the differential equations into algebraic equations which are formed overall power system model together with the network algebraic equations. In order to solve the algebraic equations, Newton-Raphson method is used at each time step. In the RMS toolbox the PE method is chosen and employed. The differential equations are solved by the differential equation solver (i.e. variable-step solver) of MATLAB/Simulink, and the implemented network solver handles the algebraic equations.

The PE method can be summarized as follows:

Step1: Solve the initial load flow to initialize the states (x_0) in the differential equations

Step2: After initialization, at $t=t_0$ make a disturbance in the system

Step3: Keeping the initial states constant solve the network algebraic equations to get the bus voltage magnitudes and angles

Step4: Using the bus voltages at $t=t_0+\Delta t$ integrate and solve the differential equations for $x_{t0+\Delta t}$

Step5: Go to Step3 and solve the network algebraic equations to get the bus voltage magnitudes and angles for $t=t+\Delta t$

Step6: This loop is repeated until the desired time has been reached (t<max. time).

The above mentioned steps are illustrated as a flow chart in Fig. 3.14. As an example, after a disturbance applied to the generic power system, the states are assumed constant during the following time step since the differential variables cannot change instantaneously. Using the previous state variables, the algebraic equations comprised of the network and stator equations are solved algebraically (at Step 4) in the current-balance form [3.27].

3.6 Summary

In this chapter, a generic power system model has been developed with various wind power penetration scenarios. Therefore, the developed power system model is realized as a realistic power system and is utilized for the wind power integration studies, particularly inertial response control studies conducted in Chapter 4. Accordingly, WPP models have been proposed in order to assess the impact on the generic power system and to develop new control methods considering the assessment results. The simplified WPP model is employed in the generic power system to demonstrate generic power system requirements for the inertial response control and synchronizing power support. It is the starting point of the investigations and high level control can be utilized with this model to analyze the impact on the power system dynamics. However, for the inertial response control studies the WPP model should comprise aerodynamic and mechanical dynamics of the wind turbine that have important impact on the power system frequency. Therefore, an aggregated WPP model based on FC-VSWT has been developed and the validation of the model is done with limited simulation results. Since the standardization of the models for both wind turbines and WPPs is still under

development, the developed models in this section are sufficient for the frequency stability studies (Chapter 4). On the other hand, the validity of the models should be improved further for the short-circuit fault (i.e. FRT). In Chapter 5, the synchronizing power support study is kept limited without considering the short-circuit fault cases. Consequently, all the developed models are implemented in the RMS toolbox which is developed in MATLAB/Simulink with the authors of [3.1]. The aim is to create an open source and flexible simulation platform for wind power integration studies. The developed RMS toolbox is also validated with DigSilent Power Factory software.

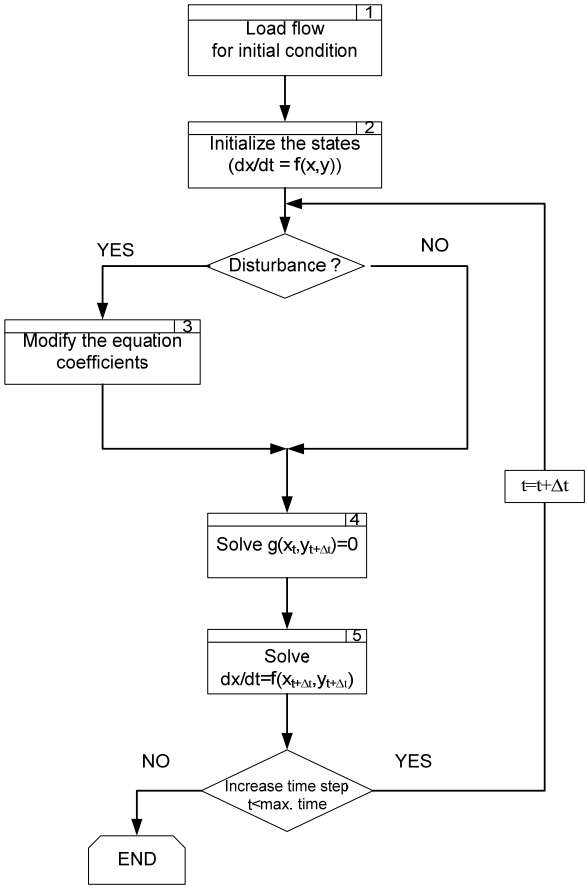

Fig. 3.14. Simplified algorithm for the PE method

3.7 References

[3.1] A. Adamczyk, M. Altin, Ö. Göksu, R. Teodorescu, F. Iov, "Generic 12-Bus Test System for Wind Power Integration Studies," *EPE Joint Wind Energy and T&D Chapters Seminar*, Aalborg, Denmark, Jun. 2012.

[3.2] Grid connection of wind turbines to networks with voltages above 100 kV, Regulation TF 3.2.5, Eltra and Elkraft System.

[3.3] G. Lalor, A. Mullane, and M. O'Malley, "Frequency Control and Wind Turbine Technologies," *IEEE Transactions on Power Systems,* vol. 20, no. 4, pp. 1905-1913, Nov. 2005.

[3.4] J. F. Conroy and R. Watson, "Frequency response capability of full converter Wind turbine generators in comparison to conventional generation," *IEEE Transactions on Power Systems,* vol. 23, no. 2, pp. 649-656, May 2008.

[3.5] P.M. Anderson, A.A Fouad, *Power System Control and Stability*, IEEE Press, 2003.

[3.6] P. Kundur, *Power System Stability and Control*, McGraw Hill, 1994.

[3.7] Shan Jiang, U. D. Annakkage, and A. M. Gole, "A platform for validation of FACTS models," *IEEE Trans. on Power Delivery*, vol. 21, no. 1, pp. 484-491, Jan 2006.

[3.8] CIGRE Working Group B4.39, "Integration of Large Scale Wind Generation using HVDC and Power Electronics," Feb. 2009.

[3.9] B. Pal, B. Chaudhuri, *Robust Control in Power Systems*, Springer, 2010.

[3.10] P. Sauer, *Power System Dynamic and Stability*, Prentice Hall, 1997.

[3.11] *IEEE recommended practice for excitation system models for power system stability studies*, IEEE Standard 421.5-1992, 1992.

[3.12] J. Østergaard, T. Ackermann, P. Bach, M. Lind, A. H. Nielsen, K. Nørregaard, P. Sørensen, B. Tennbakk, R. Teodorescu, M. Togeby, "EcoGrid.dk Phase I WP5 Report- Future step toward a Danish power system with 50% wind power," Energinet.dk, 2008.

[3.13] C. Concordia and S. Ihara, "Load Representation in Power System Stability Studies," *IEEE Trans. on Power Apparatus and Systems*, Vol. PAS-101, No. 4, Apr. 1982.

[3.14] DigSilent Technical Documentation, General Load Model, 2008.

[3.15] J. B. Ekanayake, L. Holdsworth, Wu XueGuang , N. Jenkins, "Dynamic Modeling of Doubly Fed Induction Generator Wind Turbines," *IEEE Transactions on Power Systems*, vol.18, no.2, pp. 803- 809, May 2003.

[3.16] A.D. Hansen, G. Michalke, "Multi-pole permanent magnet synchronous generator wind turbines' grid support capability in uninterrupted operation during grid faults," *Renewable Power Generation, IET*, vol.3, no.3, pp.333-348, Sept. 2009.

[3.17] M. Asmine, J. Brochu, J. Fortmann, R. Gagnon, Y. Kazachkov, C.-E. Langlois, C. Larose, E. Muljadi, J. MacDowell, P. Pourbeik, S. A. Seman, and K. Wiens, "Model Validation for Wind Turbine Generator Models," *IEEE Transactions on Power Systems*, vol. 26, no. 3, pp. 1769–1782, Aug. 2011.

[3.18] J. Jonkman, S. Butterfield, W. Musial, and G. Scott, "Definition of a 5-MW reference wind turbine for offshore system development," National Renewable Energy Laboratory (NREL), 2007.

[3.19] M. Soltani, T. Knudsen, J.D. Grunnet, and T. Bak, "AEOLUS Toolbox for Dynamic Wind Farm Model, Simulation, and Control," European Wind Energy Conference 2010, Warsaw, Poland, 20-23 April 2010.

[3.20] J. G. Slootweg, *Wind power: Modeling and impact on power system dynamics*, 2003.

[3.21] P. Sørensen, A. Hansen, F. Iov, F. Blaabjerg, M. Donovan, "Wind farm models and control strategies," Risø-R-1464(EN), Aug. 2005.

[3.22] V. Akhmatov, Analysis of Dynamic Behavior of Electric Power Systems with Large Amount of Wind Power, DTU 2003.

[3.23] N. W. Miller, J. J. Sanchez-Gasca, and W. W. Price, "Dynamic modeling of GE 1.5 and 3.6 MW wind turbine generators for stability simulations", Proc. IEEE Power Engineering Society General Meeting, vol. 3, pp.1977-1983, July 2003.

[3.24] *Electrical simulation models for wind power generation*, IEC 61400-27, 2012.

[3.25] A. Adamczyk, M. Altin, R. Teodorescu, F. Iov, P. C. Kjaer, U. D. Annakkage "Control of Full-Scale Converter Based Wind Power Plants for Damping of Low

Frequency System Osciullations," submitted to *IEEE Transaction on Power Systems.*

[3.26] F. Conroy and R. Watson, "Frequency response capability of full converter Wind turbine generators in comparison to conventional generation," *IEEE Trans. Power Systems,* vol. 23, no. 2, pp. 649-656, May 2008.

[3.27] P. Sørensen, A. Hansen, F. Iov, N. Cutululis, C. Jauch, F. Blaabjerg, "Dynamic wind turbine models in power system simulation tool DigSilent," Risø-R-1400(ed.2), Aug. 2007.

[3.28] P. W. Sauer and M. A. Pai, *Power System Dynamics and Stability*, Englewood Cliffs, NJ: Prentice–Hall, 1998

Chapter 4
Inertial Response Control of Wind Power Plants

4.1 Introduction

The frequency stability is reviewed in Chapter 2 with the inertial response control methods of WPPs which are proposed in the previous studies [2.16]-[2.32]. This chapter begins with analyzing these control methods to comprehend the requirements of the generic power system described in Chapter 3. The assessment of the analysis results is based on the operational metrics defined for the generic power system. Moreover, these results are employed to propose a new control method with a tuning methodology which has not been mentioned in previous studies. Eventually, the aim of the proposed control is to quantify the inertial response requirements from WPPs considering the VSWT capability for a given power system. The proposed control method determines the inertial response profile, and the tuning methodology specifies the parameters of the profile according to the power system characteristics. Finally, the proposed control method performance is compared with the existing control methods proposed in the previous studies.

4.2 Analysis of Inertial Response Control Methods

4.2.1 Operational Metrics for Inertial Response Control of WPPs

Operational metrics are critical to assess the impact of wind power penetration on power systems and the performance of the inertial response control methods. In the generic power system the operational metrics are defined for the largest infeed loss (i.e.

a critical N-1 contingency). These metrics are chosen from the GC requirements of TSOs and the studies regarding the frequency stability. TSOs have defined GC requirements for the frequency stability to keep the power system frequency in the limits to protect the power system equipments (e.g. SGs, motors, transformers, and distributed generation).

One of the well-known metric is the maximum frequency deviation or in other terms minimum frequency point (i.e. frequency nadir). This metric is very important with respect to the frequency stability of the power system and management of the CPPs' frequency control (i.e. performance of the primary and secondary control and coordination of the reserves). The value of the metric is 800 mHz in 50 Hz systems [4.1] and 900 mHz in 60 Hz systems [4.2] due to the under-frequency load shedding limits. For the analysis in this chapter, the operational metric is defined as 0.016 pu in 50 Hz base.

The second metric is the maximum ROCOF value employed for islanding detection relays in the MV distributed generation. These relays can measure ROCOF following a disturbance and once the threshold value is exceeded after a detection time, a trip signal is initiated. The initiated signal trips the distributed generation to protect the equipments during islanding. This protection scheme is defined as a passive method to detect islanding conditions [4.3], [4.4]. The threshold value for maximum ROCOF is dependent on the power system and varies from 0.3 Hz/s to 2 Hz/s (e.g. Hawaii:0.37 Hz/s, Ireland:0.5 Hz/s, New Zealand:0.75Hz/s, ENTSO-E: 2Hz/s) . Additionally, the detection time of the relays varies from 50 ms to 500 ms in 50 Hz systems [4.3]. Considering these values, the second metric is defined 0.008 pu/s (i.e. 0.4 Hz/s in 50 Hz) with 200ms.

Finally, the third metric is selected as the time to reach the minimum frequency point. The minimum frequency point and the time to reach this point are determined by the energy released during the inertial response stage. The time to reach the minimum frequency point has an influence on the frequency response stages. Thus, it affects the

management of the frequency control such as primary and secondary frequency performance and their reserve. In this chapter, the value is chosen as 4.68s due to the simulation result for the base case (20% wind penetration case) following the largest infeed loss in the generic power system.

Abovementioned operational metrics are summarized in Table 4.1, and used for assessing the impact of the wind power penetration and the performance of the inertial response control methods.

Table 4.1. Operational metrics for the generic power system

	Operational Metric	**Ranges/Values**	**Remarks**
1	max. dynamic frequency deviation (or min. frequency point)	0.016pu (=800mHz in 50 Hz)	Load shedding frequency limit (1 Hz) with a margin (200mHz)
2	max. df/dt with a given detection time	0.008 pu/s with 200ms (=0.4Hz/s in 50 Hz)	ROCOF relay settings for distributed generation
3	time to reach the min. frequency point	4.68s (20% wind scenario)	Not to exceed the time simulated for the base case

4.2.2 Existing Inertial Response Control Methods

As described in Chapter 2, there are several control methods which enable inertial response from WPPs. The first control concept is the derivative control which calculates the ROCOF and with a gain modifies the active power reference ($\Delta P_{inertia}$). Since the derivative control is sensitive to the noise, a low pass filter is added to the control method. Moreover, it may be further supported by a dead band. However, the derivative control should be quite fast and not be affected by the non-generation loss events (e.g. switching of transmission lines) that makes the appropriate filtering becomes challenging [2.15]. The block diagram is illustrated in Fig. 4.1 and the parameters of the control are summarized in Table 4.2. To conduct sensitivity analysis, H_{WPP} values are selected from the literature for the given range.

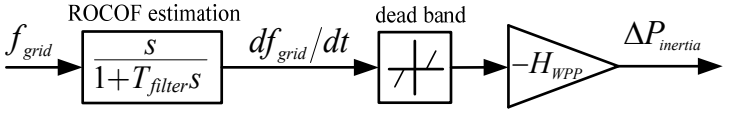

Fig. 4.1. Block diagram of derivative control

Table 4.2. Parameters of derivative control

Parameter Name	Unit	Parameter Value	Remarks
H_{WPP}	[s]	3.5, 5.3, 13.4, 28.3	Similar to SG inertia constant
T_{filter}	[ms]	20	Low pass time constant
Dead-band	[Hz/s]	±0.05	To reduce the activity of the control

The second inertial response control method is the temporary frequency control which enables an active power pulse (ΔP_{temp}) for a certain time (t_{temp}) after detection of the disturbance. In this chapter, ΔP_{temp} is varied for the sensitivity analysis of the temporary frequency control to investigate the impact on the power system frequency. The detection of the frequency disturbance is similar to the control blocks of the derivative control (i.e. ROCOF estimation and dead-band blocks). The block diagram is illustrated in Fig. 4.2 and the parameters of the control are summarized in Table 4.3.

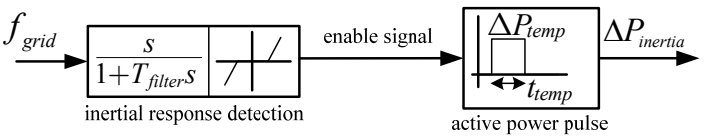

Fig. 4.2. Block diagram of temporary frequency control with ROCOF triggering

Table 4.3. Parameters of temporary frequency control

Parameter Name	Unit	Parameter Value	Remarks
ΔP_{temp}	[pu]	0.05, 0.1, 0.2, 0.3	Magnitude of the active power pulse
t_{temp}	[s]	2, 3, 5	Duration of the active power pulse
T_{filter}	[ms]	20	Low pass time constant
Dead-band	[Hz/s]	±0.05	To reduce the activity of the control

In order to utilize the control methods in the generic power system, the simplified WPP model (i.e. PQ source model), which is described in Chapter 3, is implemented in the simulations (Fig. 4.3), and the parameters for the sensitivity analysis is summarized in Table 4.4. The aim of the sensitivity analysis is to determine which parameters of the inertial response control method and the WPP model has an impact on the operational metrics. As mentioned in Chapter2, this model is valid only for high (i.e. above rated) wind speed conditions. Therefore, the inertial response requirements of the generic power system can be specified to improve the inertial response control.

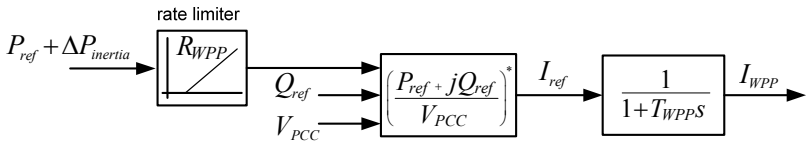

Fig. 4.3. Block diagram of simplified WPP model for sensitivity analysis (Chapter 3)

Table 4.4. Parameters of simplified WPP model

Parameter Name	**Unit**	**Parameter Value**	**Remarks**
R_{WPP}	[pu/s]	0.1, 0.5, 1	Rate limiter of the active power reference
T_{WPP}	[s]	0.025, 0.125, 0.25	Performance of the overall WPP active power control

4.2.3 Need for Inertial Response Control

The generic power system has been developed with the wind power scenarios which vary from 0% to 50% penetration levels. The details of the wind power penetration scenarios have been given in Chapter 3. In this section, the impact of these wind power penetration on the frequency stability of the generic power system is investigated in terms of the defined operational metrics. The disturbance is assumed as the largest infeed loss (i.e. 200 MW).

Fig. 4.4 indicates that the wind power penetration levels higher than 20% do not achieve the operational metric 1. For 40% and 50% wind penetration levels, the

minimum frequency point even reaches lower values exceeding the trip limit of load shedding relays. Accordingly, when the effect of the time constant of the WPP (T_{WPP}) is considered, there is no significant change in the minimum frequency point as shown in Fig. 4.5. For the 50% wind penetration, the slowest response (T_{WPP}=0.25s) gives 10 mHz improvement. Thus, the response time of the WPP active power control does not have substantial impact on the minimum frequency point.

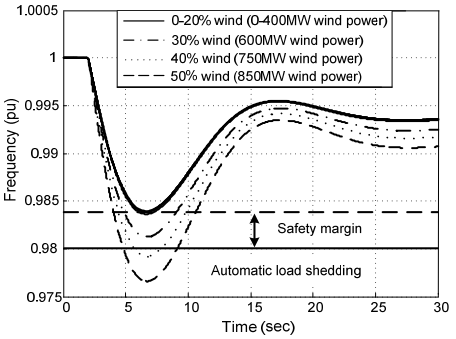

Fig. 4.4. System frequency of the generic power system following the largest infeed loss for different wind power penetration scenarios (T_{WPP}=0.025s)

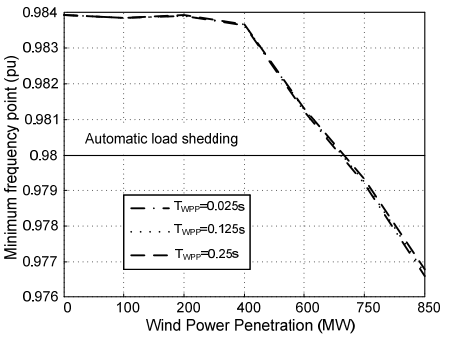

Fig. 4.5. Impact of T_{WPP} on the minimum frequency point for different wind power penetration scenarios

The impact of wind power penetration on the maximum ROCOF of the power system at 200ms after the disturbance (operational metric 2) is illustrated in Fig. 4.6. The wind power penetration is restricted due to the ROCOF relay settings and thus T_{WPP} affects the wind power penetration level. If a WPP has faster response (i.e. lower T_{WPP}), it will quickly recover to its pre-disturbance operating condition and the ROCOF will be smaller. In order to increase the wind power penetration level, there are two possible solutions: the first solution is to change the settings of the ROCOF relays, and the second solution is to enable inertial response control from WPPs. Therefore, in the generic power system for high wind power penetration scenarios which comprise replacement of CPPs, there is a need for the inertial response control from WPPs with respect to the simulation results regarding operational metric 1 and 2.

Further investigation is performed for the impact of T_{WPP} on the time to reach minimum frequency point (operational metric 3). The simulation results are given in Fig. 4.6. The difference between the fast and slow response is 30ms for the 50% wind penetration scenario. Following the largest infeed loss, WPPs regulate their active power output with T_{WPP} value and due to this response time, the frequency control of CPPs is affected just after the disturbance. However, the effect is minor and can be neglected as given in Fig. 4.6.

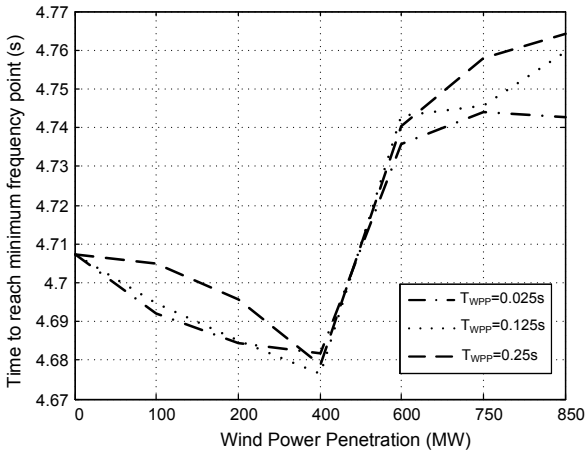

Fig. 4.6. Impact of TWPP on the time to reach minimum frequency point for different wind power penetration scenarios

When the CPPs' active power outputs are considered in terms of primary frequency control response, the used primary frequency reserve until the minimum frequency point is illustrated in Fig. 4.7. Up to 20% wind penetration level, the primary frequency response of each CPP is not changing significantly. However, for 30%-50% wind power penetration scenarios, activated primary frequency reserve from G1 and G2 is decreasing due to the replacement of the generating units (i.e. 2 units in G1 and 1 unit in G2). For G3 and G4, the activated primary frequency response is increasing due to increased maximum frequency deviation (Fig. 4.4).

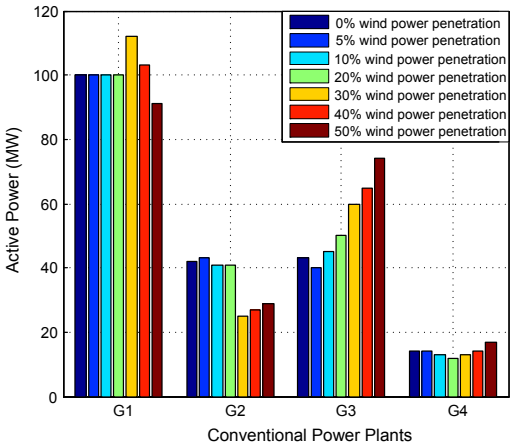

Fig. 4.7. Activated primary frequency reserve of CPPs at the minimum frequency point

4.2.4 Sensitivity Analysis of Derivative Control

In the previous section, need for the inertial response from WPPs is described in detail with the simulation results. According to results, above 20% wind power penetration, frequency response of the system is exceeding the operational metric 1. Moreover, in 40% and 50% wind penetration scenarios, the operational metric 2 is also exceeded. The first inertial response control method, the derivative control, is investigated by performing the sensitivity analysis with the parameters H_{WPP}, T_{WPP}, and R_{WPP} for all the wind power penetration scenarios. For the simulations, each time only one parameter is varied and the other parameters are kept constant. The simulation results regarding only 40% and 50% wind power penetration scenarios are summarized to assess the impact of the derivative control.

4.2.4.1 Impact of Derivative Control Gain (H_{WPP})

In this section, the effect of H_{WPP} is investigated in terms of the operational metrics for the 40% wind power penetration. H_{WPP} represents the inertia constant of a SG. Accordingly, in the derivative control, the H_{WPP} value determines how much additional active power is released from the WPPs following the largest infeed loss. Hence, this released power changes the ROCOF and the minimum frequency point. The effect on the power system frequency is illustrated in Fig. 4.8. When the H_{WPP} value is increased,

the minimum frequency point is increasing as expected and achieving the operational metric 1 where H_{WPP} value is close to 28.3pu. The important remark is that the ROCOF does not change immediately due to active power drop at the PCC point of the WPPs at the instant of the largest infeed loss (Fig. 4.9). After the loss of the largest infeed, the reactive power flow has been changed in the generic power system, and the voltage at the PCC point of the WPPs has been reduced, thus the active power poutput of WPP.

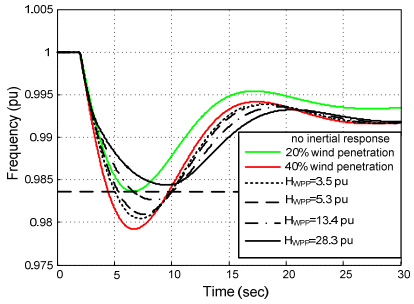

Fig. 4.8. System frequency for different H_{WPP} values where T_{WPP}=0.025s and R_{WPP}=0.1pu/s

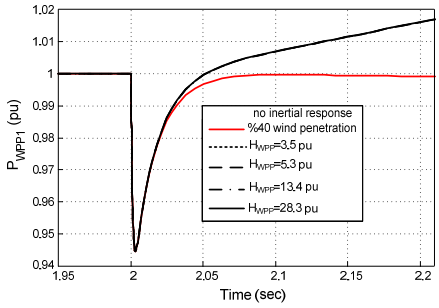

Fig. 4.9. Active power change of WPP-1 at Bus 5 during 200 ms after the loss of the largest infeed for different H_{WPP} values where T_{WPP}=0.025s and R_{WPP}=0.1pu/s

The ROCOF results are given in Fig. 4.10. It can be noticed that during the 200ms after the loss of largest infeed, the ROCOF has not been changed due to active power and voltage drop at the PCC point of the WPPs. Therefore, H_{WPP} does not affect the operational metric 2 when R_{WPP} is 0.1pu/s. Thus, R_{WPP} also specify the performance of the active power control. This is very important consideration while determining the derivative control parameters according to the power system requirements (i.e. ROCOF relay settings) and the WPP parameters (i.e. R_{WPP}). The active power output of the WPP also shows the reason of the impact of H_{WPP} on the ROCOF (Fig. 4.11); difference between the active power outputs of WPP-1 for different H_{WPP} values starts after 500 msec. following the disturbance. Moreover, the additional active power provided by the WPPs during the inertial response control varies between 5% and 15 % of the rated power which is in the pre-defined interval (i.e. 0.1pu to 0.3pu control output).

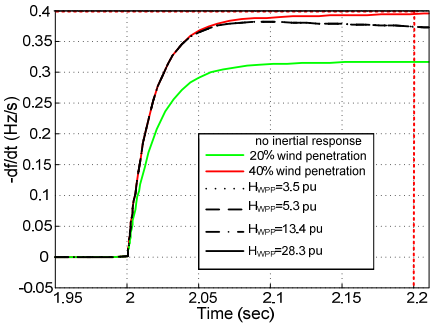

Fig. 4.10. ROCOF during 200ms after the largest infeed loss for different H_{WPP} values where T_{WPP}=0.025s and R_{WPP}=0.1pu/s

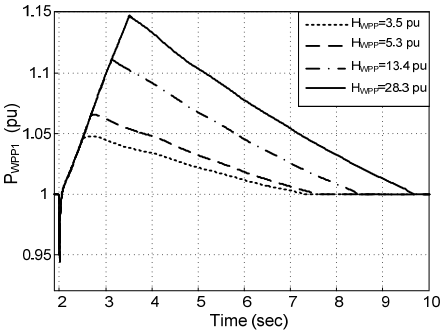

Fig. 4.11. Active power ouput of WPP-1 at Bus 5 for different H_{WPP} values where T_{WPP}=0.025s and R_{WPP}=0.1pu/s

For the last operational metric, the simulation results of the time to reach the minimum frequency point are summarized in Fig. 4.12 with different H_{WPP} values. The time increases while the additional active power provided by the WPPs is increased. The reason is shown in Fig. 4.13 as the active power change of the G3. When the additional active power is increased by H_{WPP}, the governors of CPPs detect the frequency drop slowly and increasing their mechanical power slowly as well. Thus, the minimum frequency point is delayed in time.

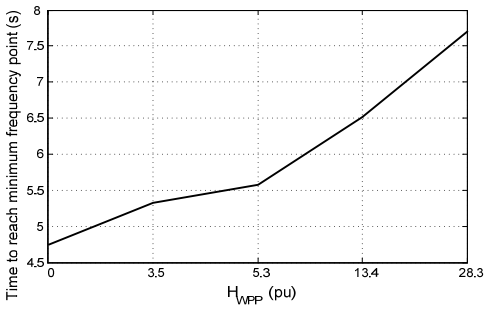

Fig. 4.12. Time to reach the minimum frequency point for different H_{WPP} values where T_{WPP}=0.025s and R_{WPP}=0.1pu/s

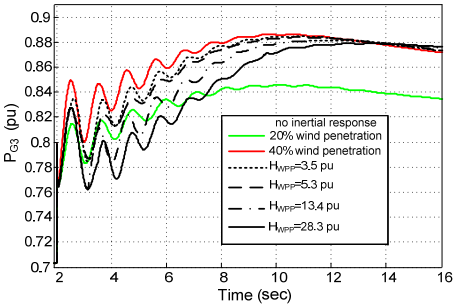

Fig. 4.13. Active power change of the G3 for different H_{WPP} values where T_{WPP}=0.025s and R_{WPP}=0.1pu/s

When the CPPs are replaced by the WPPs, the inertial response of these CPPs is considered to be transferred to the WPPs by the derivative control. However, if the replaced generating units are providing primary frequency control, this solution is not enough. Fig. 4.14 shows the total energy released from the WPPs for different H_{WPP} values and compared it to the calculated replaced inertial energy. The red straight line indicates the replaced inertial energy of the generating units (i.e. one unit from G1 and one unit from G2). From Fig. 4.12, even in the case of H_{WPP}=3.5pu the released energy is sufficient compared to the replaced inertial energy. However, in Fig. 4.8 the minimum frequency point of the derivative control with H_{WPP}=3.5pu does not achieve the operational metric 1. Consequently, implementing the derivative control is not a solution itself, the active power drop at the PCC of the WPPs and the replaced energy of the primary frequency control should be taken into account.

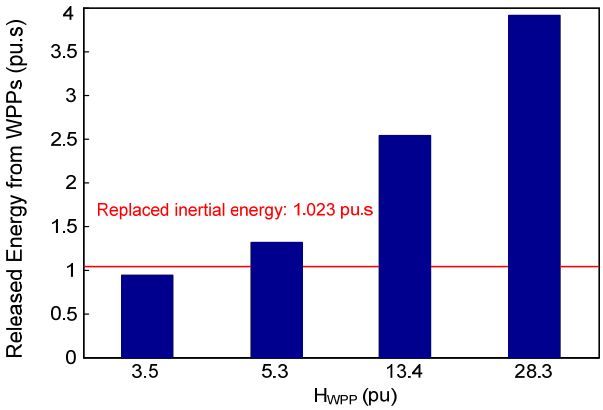

Fig. 4.14. Comparison of the total released energy from WPPs where T_{WPP}=0.025s and R_{WPP}=0.1pu/s

4.2.4.2 Impact of WPP Rate Limiter (R_{WPP})

R_{WPP} can represent a grid code requirement (e.g. ramp rates defined for the active and reactive power control of WPPs) or the active power control limitation for WTGs [4.5]. In this section, the effect of the R_{WPP} is investigated in terms of the operational metrics for the 40% wind power penetration scenario.

Fig. 4.15 shows the frequency response of the generic power system where the H_{WPP} value is kept constant at 28.3pu, and T_{WPP} is 0.025s. In the figure, the minimum frequency point is not affected significantly by R_{WPP} variation however; the time to reach this point has been changed. Fig. 4.16 illustrates this impact of R_{WPP}. The reason is that the energy released from WPPs is increased when the R_{WPP} value has increased, therefore the time to reach minimum frequency point is delayed.

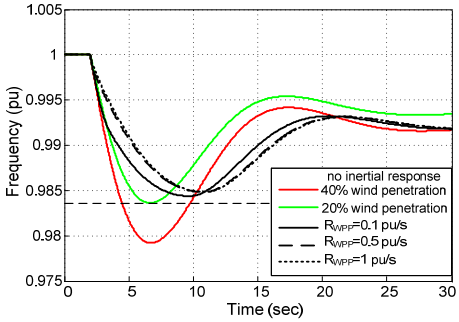

Fig. 4.15. System frequency for different R_{WPP} values where T_{WPP}=0.025s and H_{WPP}=28.3pu

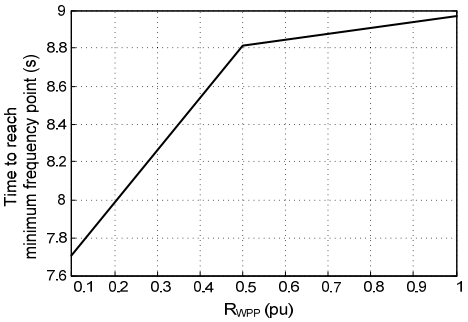

Fig. 4.16. Time to reach the minimum frequency point for different R_{WPP} values where T_{WPP}=0.025s and H_{WPP}=28.3pu

For the operational metric 2, the ROCOF during the first 200ms after the largest infeed loss is given in Fig. 4.17. With the chosen H_{WPP} (28.3pu) and T_{WPP} (0.025s) values, the operational metric 2 is achieved for every values of the R_{WPP} due to faster WPP response (T_{WPP}=0.025s). In Fig. 4.18, the additional active power output of WPPs is presented as 17%, 8%, and 2% to keep the ROCOF values at 0.37Hz/s, 0.29Hz/s, and 0.19Hz/s respectively. These results provide critical information how much and how fast the inertial response of WPPs should act in terms of not to trip ROCOF relays in the MV distributed generation. Additionally, the WPPs with R_{WPP}>0.5pu/s and T_{WPP}=0.025s performs better inertial response performance than the CPPs' inherent inertial response in the base case (20% wind penetration scenario).

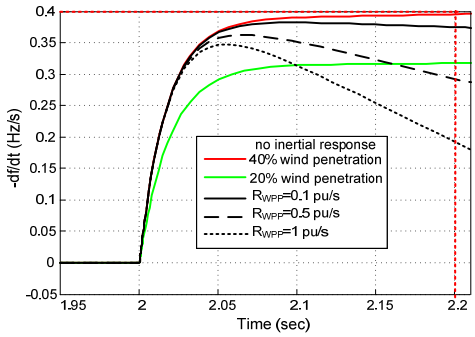

Fig. 4.17. ROCOF during 200ms after the largest infeed loss for different R_{WPP} values where T_{WPP}=0.025s and H_{WPP}=28.3pu

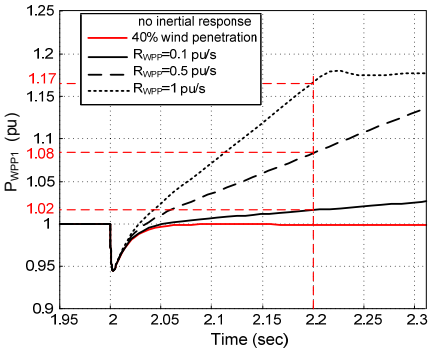

Fig. 4.18. Active power change of WPP-1 at Bus 5 during 200ms after the largest infeed loss for different R_{WPP} values where T_{WPP}=0.025s and H_{WPP}=28.3pu

The impact of R_{WPP} on the active power output of CPPs is shown in Fig. 4.19. For the value of R_{WPP} equals to 0.1pu/s, the magnitude of the power oscillations is less than the cases where R_{WPP} equals to 0.5pu/s or 1pu/s. Therefore, selecting a high gain and a high rate limiter for the derivative control can destabilize the power system due to the small signal stability. Consequently, when the total released energy from WPPs is considered in Fig. 4.20, the lowest energy is obtained with the lowest R_{WPP}. However, the frequency minimum point is almost same with different times to reach this point while R_{WPP} value is varied. This result indicates that the amount of energy should be determined considering the time to reach the minimum frequency point together with the minimum frequency point.

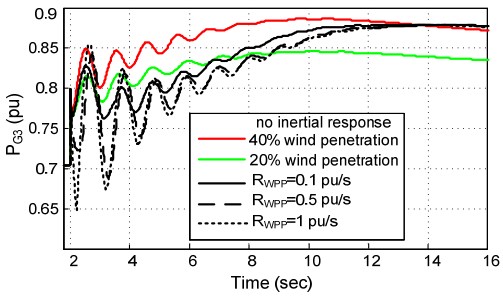

Fig. 4.19. Active power change of the G3 for different R_{WPP} values

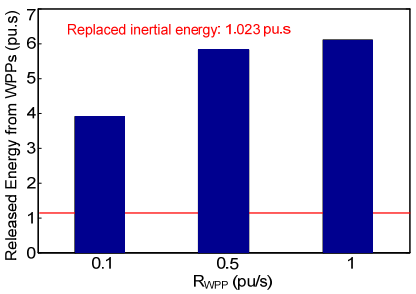

Fig. 4.20. Comparison of the total released energy from WPPs for different R_{WPP} values

4.2.4.3 Impact of WPP Time Constant (T_{WPP})

According to the modeling assumptions made in Chapter 3 for the simplified WPP model (i.e. PQ source model), T_{WPP} represents the overall WPP active and reactive control performance as a first order time delay. This assumption is sufficient to analyze the impact of the inertial response control of the WPP which operates at high wind speed on the power system. In this section, the impact of the T_{WPP} is investigated in terms of the operational metrics for the 40% wind power penetration.

Fig. 4.21 presents that the minimum frequency point is not significantly affected for different T_{WPP} values. Additionally, the impact on the time to reach this minimum frequency point is shown in Fig. 4.22, thus there is no major difference (approximately 250ms) obtained by varying the T_{WPP} values.

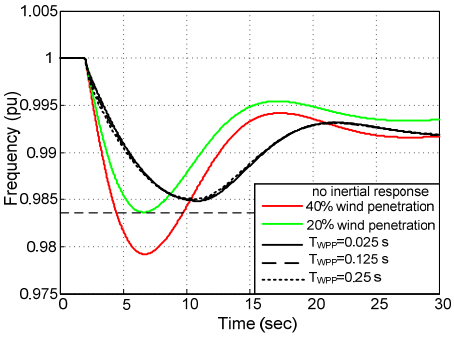

Fig. 4.21. System frequency for different T_{WPP} values where R_{WPP}=1pu/s and H_{WPP}=28.3pu

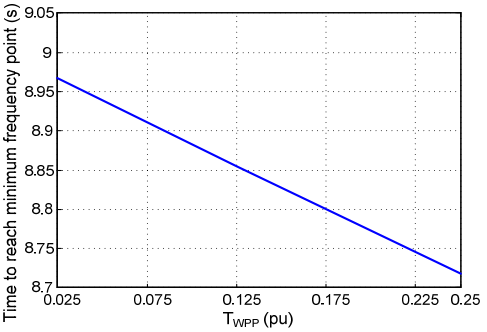

Fig. 4.22. Time to reach the minimum frequency point for different T_{WPP} values where R_{WPP}=1pu/s and H_{WPP}=28.3pu

T_{WPP} with high R_{WPP} value such as 1 pu/s has an impact on the ROCOF as seen in the Fig. 4.23 due to the active power output of the WPPs shown in Fig. 4.24. For all the cases given in the following figures, operational metric 2 has been achieved.

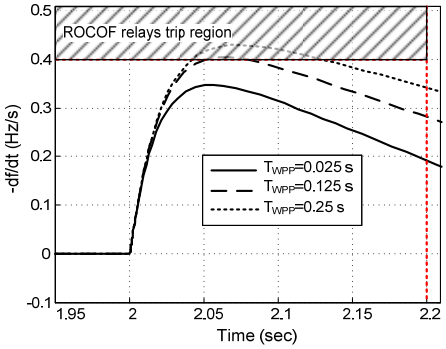

Fig. 4.23. ROCOF during 200ms after the largest infeed loss for different T_{WPP} values where R_{WPP}=1pu/s and H_{WPP}=28.3pu

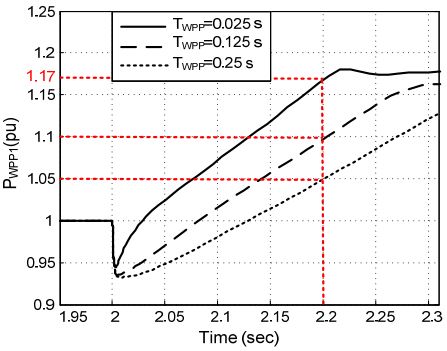

Fig. 4.24. Active power change of WPP-1 at Bus 5 during 200ms after the largest infeed loss for different T_{WPP} values where R_{WPP}=1pu/s and H_{WPP}=28.3pu

By changing the performance of the WPP active power control (i.e. varying T_{WPP}), CPPs' active power outputs have been affected such as the magnitude of the power oscillations increase when the T_{WPP} is decreased. The simulation result for the active power output of G3 is given in Fig. 4.25, and as stated before the small signal analysis is required for inertial response control studies in order to not to disturb the modes in the power system. Additionally, the energy released during the inertial response from WPPs (Fig. 4.26) is not changed significant amount as expected from the simulation results of the minimum frequency point (Fig. 4.21).

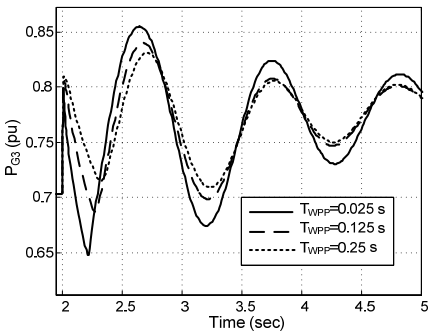

Fig. 4.25. Active power change of the G3 for different T_{WPP} values

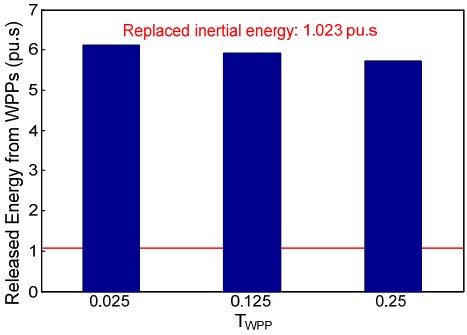

Fig. 4.26. Comparison of the total released energy from WPPs for different T_{WPP} values

4.2.5 Sensitivity Analysis of Temporary Frequency Control

The temporary frequency control (Fig. 4.2) of WPPs is simulated in the generic power system with the parameters specified above (Table 4.3) for all the wind power penetration scenarios. Since the sensitivity analyses of R_{WPP} and T_{WPP} are performed in the previous section, parameters of t_{temp} (duration of the active power pulse) and ΔP_{temp} (magnitude of the active power pulse) are analyzed in this section. Accordingly, the simulation results regarding 40% and 50% wind power penetration scenarios are summarized for assessing the impact of the temporary frequency control.

4.2.5.1 Impact of Active Power Pulse Duration (t_{temp})

The impact of t_{temp} on the power system frequency is illustrated in Fig. 4.27. When the t_{temp} value has been increased, the minimum frequency point increases as expected and satisfying the operational metric 1 where t_{temp} value is close to 5s. On the other hand, changing t_{temp} does not affect the ROCOF, while the ROCOF value is kept below the operational metric 2 limit as shown in Fig. 4.28.

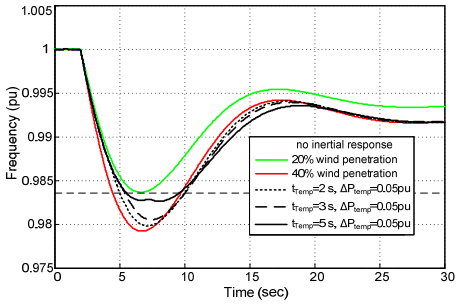

Fig. 4.27. System frequency for different t_{temp} values where ΔP_{temp}=0.05pu, T_{WPP}=0.025s, and R_{WPP}=0.1pu/s

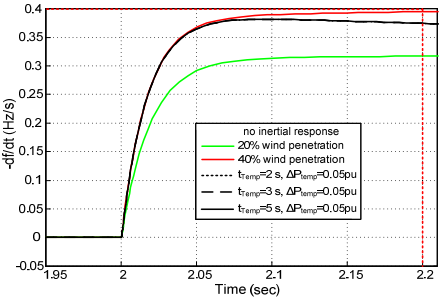

Fig. 4.28. ROCOF during 200ms after the largest infeed loss for different t_{temp} values where ΔP_{temp}=0.05pu, T_{WPP}=0.025s, and R_{WPP}=0.1pu/s

In Fig. 4.27, if the t_{temp} value equals to 5 s, the minimum frequency point is close to the operational metric 1 defined in Table 4.1. However, after this point a second small dip in the frequency occurs. The reason of the frequency dip is that when the inertial response control ends its action at t=7s, the system frequency starts to increase by the

governor action of CPPs. The active power outputs of WPP1 and G3 are given in Fig. 4.29 and Fig. 4.30, respectively.

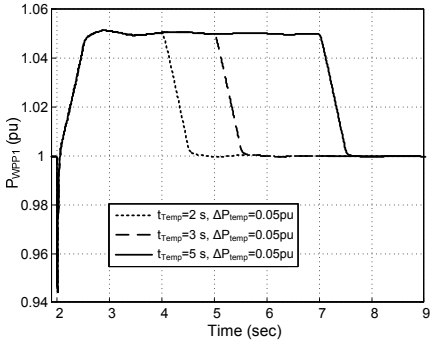

Fig. 4.29. Active power ouput of WPP-1 at Bus 5 for different t_{temp} values where ΔP_{temp}=0.05pu, T_{WPP}=0.025s, and R_{WPP}=0.1pu/s

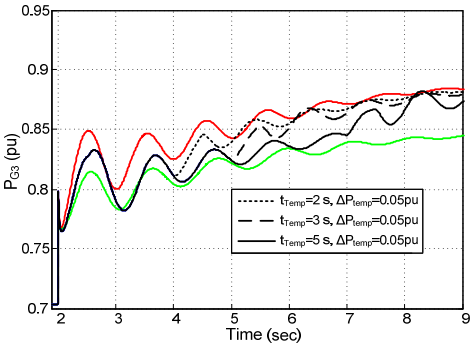

Fig. 4.30. Active power change of the G3 for different t_{temp} values where ΔP_{temp}=0.05pu, T_{WPP}=0.025s, and R_{WPP}=0.1pu/s

Fig. 4.31 presents the correlation between t_{temp} and the time to reach the minimum frequency point for simulated values of t_{temp}. Although the correlation seems linear, the time to reach the minimum frequency point proportionally increases with the duration of the inertial response control. Also, this correlation shows the amount of released energy increases with t_{temp}. The total released energy from WPPs is given in Fig. 4.32 for simulated values of t_{temp}.

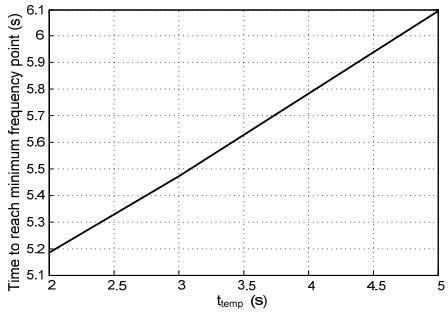

Fig. 4.31. Time to reach the minimum frequency point for different t_{temp} values where ΔP_{temp}=0.05pu, T_{WPP}=0.025s, and R_{WPP}=0.1pu/s

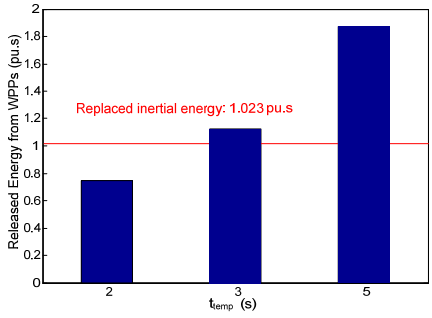

Fig. 4.32. Comparison of the total released energy from WPPs for different t_{temp} values where ΔP_{temp}=0.05pu, T_{WPP}=0.025s, and R_{WPP}=0.1pu/s

4.2.5.2 Impact of Active Power Pulse Magnitude (ΔP_{temp})

The effect of the active power pulse magnitude (ΔP_{temp}) is illustrated for the power frequency in Fig. 4.33. When the ΔP_{temp} value is increased (while keeping t_{temp}=2s), the minimum frequency point increases as expected. However, with this t_{temp} value, the temporary frequency control does not achieve the operational metric 1. It can be easily noticed that after t=4s, the ROCOF is reduced due to the decrase in ΔP_{temp}. Fig. 4.34 describes how the WPP1's active power output changes according to the temporary frequency control with different ΔP_{temp} values. In Fig. 4.33 and 34, the ΔP_{temp} value for 0.3pu is not presented due to the rate limiter value. Thus, the active power output cannot reach the additional 0.3pu during 2s. Additionally, the results for ROCOF are the same with the results of previous section (sensitivity analysis of t_{temp}), because R_{WPP} and T_{WPP} have not been changed in the simulations in this section (T_{WPP}=0.025s and R_{WPP}=0.1pu/s).

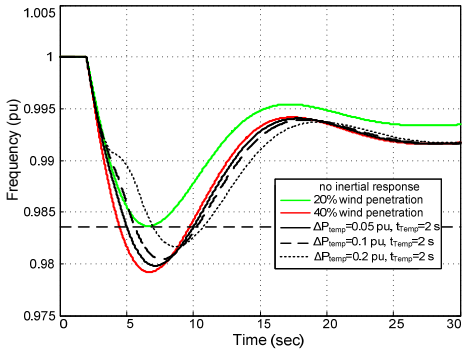

Fig. 4.33. System frequency for different ΔP_{temp} values where t_{temp}=2s, T_{WPP}=0.025s, and R_{WPP}=0.1pu/s

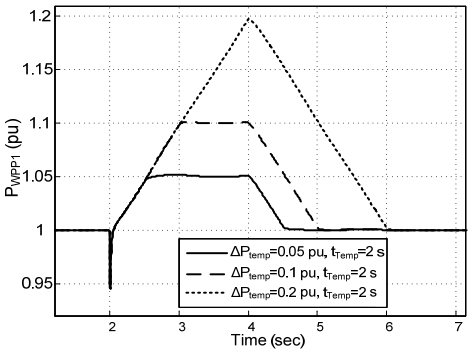

Fig. 4.34. Active power ouput of WPP-1 at Bus 5 for different different ΔP_{temp} values where t_{temp}=2s, T_{WPP}=0.025s, and R_{WPP}=0.1pu/s

Fig. 4.35 shows the correlation between t_{temp} and time to reach the minimum frequency point. The results are again similar to the results obtained in the previous section. Accordingly, when the released energy from WPPs during the inertial response has been analysed, the amount of the total energy cannot be considered as a requirement in order to achieve the operational metric 1. The total energy, when ΔP_{temp} equals to 0.2pu and t_{temp} equals to 2s, is higher than the energy which is given in the previous section as

ΔP_{temp} is 0.05pu and t_{temp} is 5s. However, in the first case the minimum frequency point is lower than the second case. The results are presented in Fig 36 and 37, respectively.

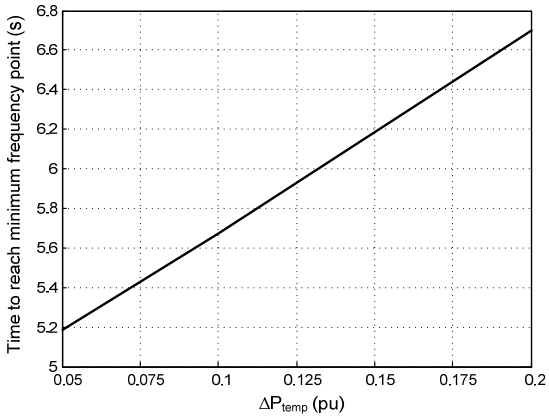

Fig. 4.35. Time to reach the minimum frequency point for different ΔP_{temp} values where t_{temp}=2s, T_{WPP}=0.025s, and R_{WPP}=0.1pu/s

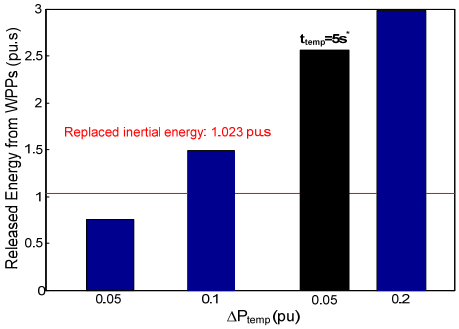

Fig. 4.36. Comparison of the total released energy from WPPs for different ΔP_{temp} values where t_{temp}=2s, T_{WPP}=0.025s, and R_{WPP}=0.1pu/s(*t_{temp}=5s and P_{temp}=0.05pu)

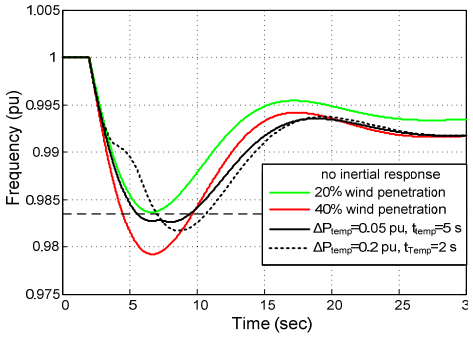

Fig. 4.37. Comparison of system frequency for different ΔP_{temp} and t_{temp} values

In the simulation results presented above, the t_{temp} value is kept constant at 2s, and the sensitivity analysis of ΔP_{temp} is performed. Moreover, the t_{temp} value is considered as 5s, and the simulations are repeated. The simulation results in Fig. 4.38 can be found undesirable for the frequency response of the generic power system. The power system has experienced double dip in the frequency, as the frequency goes up to the quasi-

steady state and the inertial response control completes its action. This is due to the lack of feedback loop of the temporary frequency control from the power system. The pre-defined power pulse without considering the power system frequency and ROCOF causes undesirable frequency dips similar to disturbances in the power system.

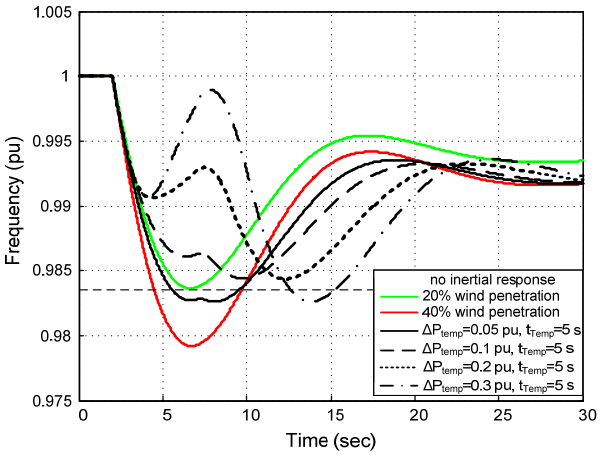

Fig. 4.38. System frequency for different ΔP_{temp} values where t_{temp}=5s, T_{WPP}=0.025s, and R_{WPP}=0.1pu/s

4.2.6 Summary of Sensitivity Analysis of Existing Inertial Response Control Methods

Performance of the first control method, the derivative control, for the inertial response of WPPs is dependent on the parameters such as H_{WPP} (derivative control parameter), R_{WPP} and T_{WPP} (WPP active power control parameters). Thus, the impact of the derivative control performance on the generic power system should be assessed in terms of these parameters to achieve the pre-defined operational metrics (Table 4.1). The following conclusions are obtained from the simulation results of both 40% and 50% wind penetration levels:

- H_{WPP} has an impact on the minimum frequency point (operational metric 1) and time to reach this point (operational metric 3).

- R_{WPP} has an impact on the ROCOF following the disturbance within 200ms (operational metric 2) and the time to reach the minimum frequency point (operational metric 3).
- T_{WPP} has an impact on the ROCOF following the disturbance within 200ms (operational metric 2) only.
- Replacement of CPPs should be realized not only providing the inertial response but also compensating the replaced primary frequency control by WPPs. Therefore, released energy for the inertial response control of WPPs should cover the energy of the replaced primary frequency control until the time to reach the minimum frequency point.
- Selecting proper R_{WPP} and H_{WPP} values WPPs can perform better than CPPs. The inertial response control of WPPs has the advantage of the programmable inertia by changing these values.
- High R_{WPP} and H_{WPP} values increase the magnitude of power oscillations in the generic power system. The derivative control should be tuned properly considering the small signal stability of the power system. Hence, the response of the active power control with inertial response control should not disturb the poorly damped modes in the power system.
- By using the simplified WPP model (i.e. PQ source model, Chapter 3), the ROCOF during 200ms after the largest infeed loss has been affected due to the voltage drop at the PCC point of the WPP. The accurate WPP model comprising the voltage and frequency dynamics of the power system should be utilized for the inertial response control studies.

In addition to the conclusions stated above, the simulation results are summarized in Table 4.5 and Table 4.6 for the 40% and 50% wind power penetration scenarios, respectively. The operational metrics are represented as *ROCOF* (ROCOF at 200ms after the largest infeed loss), f_{min} (minimum frequency point), t_{min} (time to reach the minimum frequency point), and $E_{WPP\text{-}total}$ (total released energy from WPPs during the inertial response, 100MW base). Additionally, $P_{max\text{-}WPP1}$ (peak active power output of WPP-1 connected to Bus 5), and $P_{@200ms\text{-}WPP1}$ (active power output of WPP-1 connected

to Bus 5 at 200ms after the largest infeed loss) are added for further information. The highlighted values in gray are the cases which do not achieve the operational metrics.

Table 4.5. Summary of the assessment of the derivative control for 40% wind penetration scenario

40% Wind Power Penetration Scenario								
H_{WPP} (pu)	R_{WPP} (pu/s)	T_{WPP} (s)	ROCOF	f_{min}	t_{min}	$E_{WPP\text{-}total}$	$P_{max\text{-}WPP1}$	$P_{@200ms\text{-}WPP1}$
-	-	0.25	0.42	48.96	4.76	-	-	-
		0.25	0.42	48.96	4.76	-	-	-
3.5	0.1	0.025	0.38	49.02	5.32	0.93	1.047	1.016
		0.25	0.42	49.03	5.27	0.88	1.046	0.985
	1	0.025	0.33	49.02	5.36	1.02	1.048	1.045
		0.25	0.38	49.03	5.34	1.00	1.048	1.008
5.3	0.1	0.025	0.38	49.05	5.58	1.31	1.066	1.016
		0.25	0.42	49.06	5.54	1.23	1.060	0.985
	1	0.025	0.31	49.05	5.68	1.50	1.067	1.063
		0.25	0.37	49.06	5.67	1.45	1.064	1.021
13.4	0.1	0.025	0.38	49.13	6.50	2.54	1.111	1.016
		0.25	0.42	49.14	6.33	2.32	1.100	0.985
	1	0.025	0.23	49.14	6.95	3.36	1.127	1.120
		0.25	0.34	49.15	6.87	3.21	1.117	1.048
28.3	0.1	0.025	0.38	49.22	7.71	3.91	1.150	1.016
		0.25	0.42	49.22	7.37	3.48	1.132	0.985
	1	0.025	0.20	49.24	8.97	6.11	1.185	1.164
		0.25	0.34	49.25	8.72	5.73	1.169	1.048

Table 4.6. Summary of the assessment of the derivative control for 50% wind penetration scenario

50% Wind Power Penetration Scenario								
H_{WPP} (pu)	R_{WPP} (pu/s)	T_{WPP} (s)	df/dt	f_{min}	t_{min}	$E_{WPP\text{-}total}$	$P_{max\text{-}WPP1}$	$P_{@200ms\text{-}WPP1}$
-	-	0.025	0.44	48.84	4.74	-	-	-
		0.25	0.48	48.83	4.76	-	-	-
3.5	0.1	0.025	0.42	48.91	5.42	1.16	1.054	1.015
		0.25	0.47	48.93	5.38	1.08	1.055	0.979
	1	0.025	0.36	48.92	5.49	1.28	1.055	1.047
		0.25	0.43	48.93	5.50	1.23	1.058	1.006
5.3	0.1	0.025	0.42	48.95	5.76	1.61	1.072	1.015
		0.25	0.47	48.96	5.76	1.48	1.069	0.979
	1	0.025	0.33	48.95	5.89	1.87	1.075	1.065
		0.25	0.41	48.97	5.92	1.79	1.075	1.019
13.4	0.1	0.025	0.42	49.05	6.84	3.05	1.114	1.015
		0.25	0.47	49.06	6.62	2.75	1.103	0.979
	1	0.025	0.24	49.06	7.39	4.14	1.137	1.120
		0.25	0.38	49.08	7.29	3.91	1.125	1.042
28.3	0.1	0.025	0.42	49.15	8.23	4.66	1.145	1.015
		0.25	0.47	49.15	7.74	4.07	1.128	0.979
	1	0.025	0.20	49.18	9.69	7.45	1.200	1.162
		0.25	0.38	49.20	9.37	6.90	1.170	1.042

The assessment of the derivative control method for inertial response has revealed the requirements of the generic power system with high wind power penetration scenarios. The need for the inertial response from WPPs is required for the wind penetration levels above 30%. The simulation results have showed that for 40% and 50% wind penetration levels the generic power system exceeds the limits of the operational metrics. The reason is the replacement of the CPPs by WPPs which do not have inertial response and primary frequency control action.

According to the simulation results given in Table 4.5 and Table 4.6, the following figure specifies the requirements of the generic power system (i.e. active power profile of the WPPs' inertial response control) in order to achieve the operational metrics for high wind power penetration scenarios.

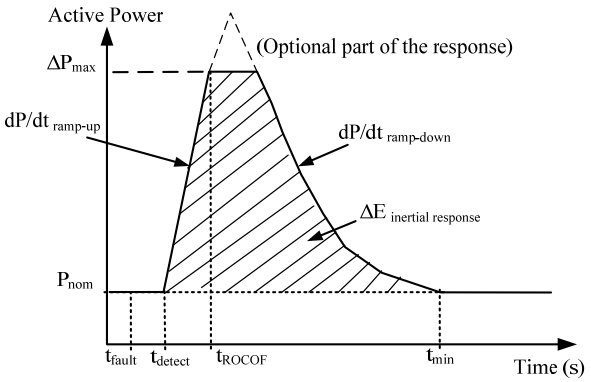

Fig. 4.39. Graphical representation of the generic power system requirements for the derivative control

The description of the parameters given in Fig. 4.39 is specified as follows:

- t_{fault}: time instance of the fault (e.g. largest infeed loss)
- P_{nom}: nominal power of WPPs
- t_{detect}: detection time for df/dt control (covering active power recovery time of WPPs)
- $dP/dt_{ramp\text{-}up}$: increase rate of active power (related to ROCOF relay settings)
- t_{ROCOF}: detection time setting for ROCOF relays
- ΔP_{max}: maximum additional active power from WPPs to limit ROCOF
- $dP/dt_{ramp\text{-}down}$: decrease rate of active power (e.g. ROCOF of the power system)
- $\Delta E_{inertial\ response}$: energy released from WPPs during the inertial response
- t_{min}: time to reach the minimum frequency point

The parameters obtained from the simulation results above are given in the following table:

Table 4.7. Summary of the assessment of the derivative control for 50% wind penetration scenario

Parameters	**Values**	**Explanation**
t_{detect}	≤50ms	Detection time + recovery time of WPP
$dP/dt_{ramp\text{-}up}$	0.35pu/s	Ramp-up rate to reach ΔP_{max} in order to limit the ROCOF
t_{ROCOF}	200ms	Detection time setting of ROCOF relays
ΔP_{max}	5%	Additional active power increase at t_{ROCOF} to limit the ROCOF
$dP/dt_{ramp\text{-}down}$	≤ROCOF	Ramp-down of the inertial response control action
$\Delta E_{inertial\ response}$	5 pu.s	Released energy during the inertial response (at 100 MW base)

t_{detect}, $dP/dt_{ramp\text{-}up}$, t_{ROCOF}, and ΔP_{max} are determined from the simulation results in order to achieve operational metric 2. t_{detect} is dependent on the frequency measurement and the ROCOF calculaiton. $dP/dt_{ramp\text{-}up}$ is determined by the generic power system, replaced CPPs, t_{detect}, t_{ROCOF}, and ΔP_{max}. Additionally, ΔP_{max} is dependent on the ROCOF relay settings. $dP/dt_{ramp\text{-}down}$ can be selected as the ROCOF of the generic power system by detection or smaller than the ROCOF as pre-defined value. $\Delta E_{inertial\ response}$ is defined as a result of the simulations. However, it can be calculated from the inertial response and the primary frequency control of the replaced generating units of CPPs. Consequently, these requirements and related parameters are going to be employed to propose the new inertial response control method for WPPs.

Similar to the assessment of the derivative control method, the second inertial response control method, which is the temporary frequency control, is also evaluated according to the operational metrics. Performance of the temporary frequency control is dependent on t_{temp} and ΔP_{temp} parameters together with R_{WPP} and T_{WPP}. The temporary frequency control is implemented as an open loop control which releases a pre-defined active power pulse triggered by ROCOF. The triggering event can be also defined in

terms of frequency deviation or combined consideration of voltage deviation, frequency deviation, and ROCOF for the future implementations. Accordingly, the detection time (t_{detect}) for these implementations has an effect on the minimum frequency point as given in the Fig. 4.40. In Fig. 4.40 (a), the t_{detect} value is varied from 0s to 2s when ΔP_{temp} is 0.05pu and t_{temp} is 2s. As a result the minimum frequency point is increased when the detection time is increased. On the contrary, if the t_{temp} value is chosen as 5s (ΔP_{temp}=0.05pu) and the same detection times are employed, the minimum frequency point will decrease (Fig. 4.40 (b)).

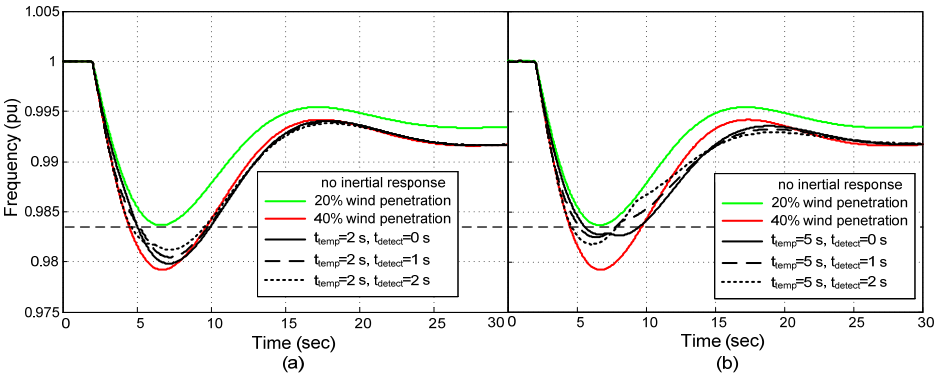

Fig. 4.40. System frequency for different t_{detect} values where t_{temp}=2s, ΔP_{temp}=0.05pu, T_{WPP}=0.025s, R_{WPP}=0.1pu/s (a) and t_{temp}=5s, ΔP_{temp}=0.05pu, T_{WPP}=0.025s, R_{WPP}=0.1pu/s (b)

The following conclusions are based on the simulation results given above for the temporary frequency control:

- The released energy during the inertial response control does not determine the operational metrics especially the minimum frequency point 1 directly How this energy is delivered during the inertial response control should be taken into account for the power system.
- The releasing of the energy for inertial response should be considered and separated into two parts; in the first part, the additional active power value is determined by the ROCOF relays to limit the ROCOF. The duration of this additional active power can be determined with respect to the power system

disturbance (or ROCOF). For the second part, the additional active power will be ramped down with the ROCOF of the power system (or less than ROCOF), in order not to disturb the power system such as a secondary frequency dip.

- For the delays of the detection time further investigation is required.

4.3 Improved Inertial Response Control

Based on the conclusions obtained from the sensitivity analysis of the existing inertial control methods, an improved inertial response control concept is proposed in this section. The design of the inertial response control is explained in the following sections in two steps; in the first step the background of the proposed control, the pre-designed implementation of the inertial response control, and the sensitivity analysis of the pre-designed inertial response control. In the second step, considering the simulation results of the pre-designed control the inertial response control is improved. Thereafter, the following section describes the tuning methodology of the proposed control. This section is very critical for a power system to implement the proposed inertial response control and has not been mentioned in the previous studies. The proposed control and its tuning methodology can be utilized for the generic inertial response control of any power system with high wind power penetration.

4.3.1 Pre-designed Inertial Response Control

The way of providing energy for inertial response control should be considered in two parts. The first part should be related to the boost of the additional active power. It should be fast and the magnitude of this active power is determined by the operational metric 2 in order not to trigger ROCOF relays, where the ramp-up rate of the active power can be determined with respect to the power system disturbance (i.e. ROCOF for the given generation loss). Moreover, the second part should consider both the duration and the ramp-down rate of the additional active power to achieve the operational metric 1 (the minimum frequency point). The duration and the ramp-down rate should be tuned in order not to disturb the frequency response of the power system for instance with a double dip in the system frequency.

In addition to above considerations, following a generation loss or a load increase (i.e. low frequency events) the ROCOF is maximum and the frequency deviation (Δf) is minimum. At this time instant, the WPP should provide an immediate active power boost not to trip the ROCOF relays considering the detection time and the performance of the active power control loop. Furthermore, at the time instant when the minimum frequency occurs, the mechanical power supplied from the CPPs is equal to electrical power of the total load in the power system. On the contrary to previous statement, at this time Δf is maximum and ROCOF is minimum (=0). These considerations are determined particularly by the operation of a CPP which is illustrated in Fig. 4.41.

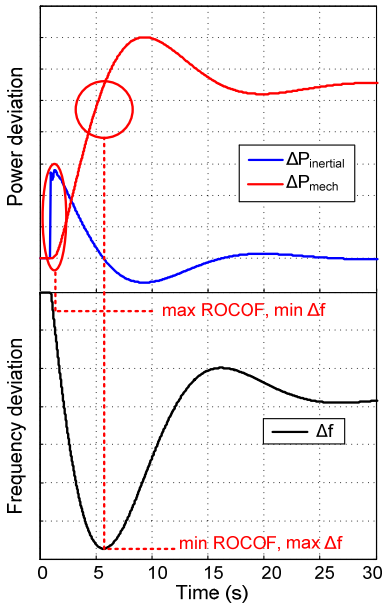

Fig. 4.41. Illustration of mechanical and inertial power deviations of a CPP with the system frequency deviation following a generation loss

Improved control method for inertial response of WPPs should provide additional energy to the power system taking into account aforementioned considerations and the behaviour of a CPP presented in Fig. 4.41. The following design criteria are going to be employed to propose the new improved inertial response control concept:

- The control should temporarily release an additional energy dependent on the dynamics of the power system frequency (e.g. ROCOF, Δf).
- The control should comprise two components; the first component increases the active power output of the WPP using the ROCOF signal (similar to the df/dt control). However, the gain of this component is not required to be as high as in the derivative control. The second component is a droop control similar to the primary frequency control of a CPP, however in this component the value of the droop is varying. The reason of the variable droop is to minimize the released energy compared to the existing inertial response control methods.
- The control should coordinate the energy provided by two components; derivative control and droop control.
- The control should provide less energy compare to the derivative and temporary frequency control methods in order not to force unnecessarily the WPP and decrease the recovery time when the aerodynamical capability is considered.
- The control should not cause any instability such as a double dip in the power system frequency.

These design criteria are transformed into the control block diagrams as illustrated in Fig. 4.42. In this figure, the first component is similar to the derivative control, but in this case, the gain of this component is less and determined in order not to trip the ROCOF relays or in other words to achieve the operational metric 2. The second component is similar to the primary frequency control of CPPs, however in this case it represents a droop control with a variable gain to provide an additional active power temporarily during the inertial response. In this study, this control action is defined as '*variable-droop*'. The variable-droop control is enabled by an external signal, which can be triggered by df_{grid}/dt or Δf_{grid} using a dead-band. After enabling the variable-droop control, the droop value starts to increase, and is multiplied by Δf_{grid}, then added as $\Delta P_{VarDroop}$ to ΔP_{ROCOF} in Fig. 4.42. During the ramp-up period of the variable-droop control, ΔP_{ROCOF} signal starts to decrease due to the declined df_{grid}/dt signal. Thus, the released energy during the inertial response is minimized compared to the existing control methods by coordinating the two components of the proposed control. Besides

releasing less energy, the variable-droop control is based on Δf_{grid} signal, which is easier and more reliable to detect compared to df_{grid}/dt signal. Taking the derivative of the power system frequency is challenging due to filtering of the noise. Another advantage is that, the variable-droop control represents a fast frequency control action with a smooth ramp-down rate which does not affect the power system frequency adversely.

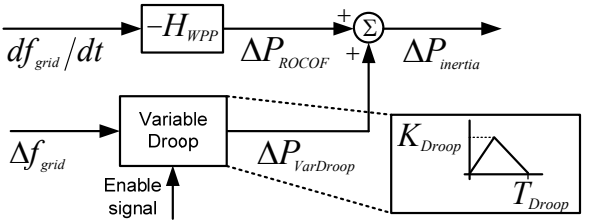

Fig. 4.42. Pre-designed inertial response control

4.3.2 Sensitivity Analysis of Pre-designed Inertial Response Control

The simplified WPP model and the pre-designed inertial response control in are implemented together in Fig. 4.43. The parameters (R_{WPP}, T_{WPP}, H_{WPP}, K_{Droop}, and T_{Droop}) are swept with predefined values which are given in Table 4.8 for each wind power penetration scenarios in the generic power system to perform the sensitivity analysis. The simulation results are assessed according to the operational metrics. In this section, the sensitivity analyses of H_{WPP}, K_{Droop}, and T_{Droop} are presented for the 40% and 50% wind power penetration scenarios.

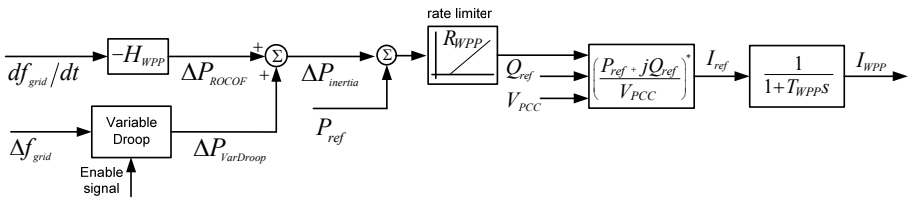

Fig. 4.43. Simplified WPP model with pre-designed inertial response control

Table 4.8. Parameters of simplified WPP model and pre-designed control

Parameter Name	**Unit**	**Parameter Value**	**Remarks**
R_{WPP}	[pu/s]	0.1, 0.5, 1	Rate limiter of the active power
T_{WPP}	[s]	0.025, 0.125, 0.25	Performance of the overall WPP
H_{WPP}	[pu]	5, 7.5, 10	Similar to SG inertia constant
K_{Droop}	[pu]	5, 7.5, 10	Gain of the variable-droop control
T_{Droop}	[s]	7, 9, 11	Duration of the variable-droop

4.3.2.1 Sensitivity Analysis of Inertial Response Gain (H_{WPP})

The effect of the H_{WPP}, which is the inertial gain of the first component of the pre-designed inertial response control, is investigated in terms of the operational metrics for the 40% and 50% wind power penetration scenarios. H_{WPP} represents the inertia constant of a SG similar to the derivative control. However, in this control structure, the H_{WPP} value has an impact on how much additional power is released from a WPP in order not trip the ROCOF relays in the distributed generation. Hence, this released power affects ROCOF directly and has less impact on the minimum frequency point (due to small H_{WPP} value). Furthermore, the impact on the frequency of the generic power system is illustrated in Fig. 4.44. Also, similar considerations are valid that was obtained for the derivative control.

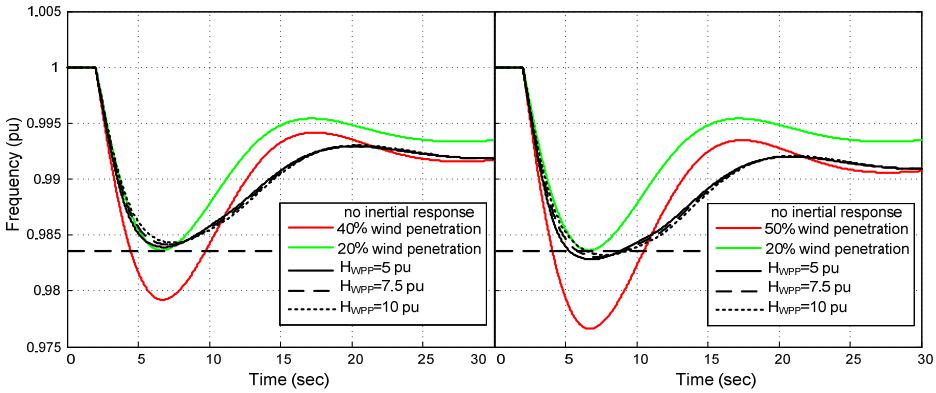

Fig. 4.44. System frequency for different H_{WPP} values where R_{WPP}=1pu/s, T_{WPP}=0.025s, K_{Droop}=5pu, and T_{Droop}=9s for 40% and 50% wind power penetration scenarios

ROCOF is given in Fig. 4.45 for 200ms following the disturbance. It can be noticed that during this time, ROCOF has been changed and come close to the CPP inertial

response for different H_{WPP}. Therefore, H_{WPP} affects the operational metric 2 when the R_{WPP} value is 1pu/s on the contrary to results found in derivative control section. This is a very important point to tune the inertial response gain of pre-designed inertial response control according to the power system requirements (i.e. ROCOF relay settings).

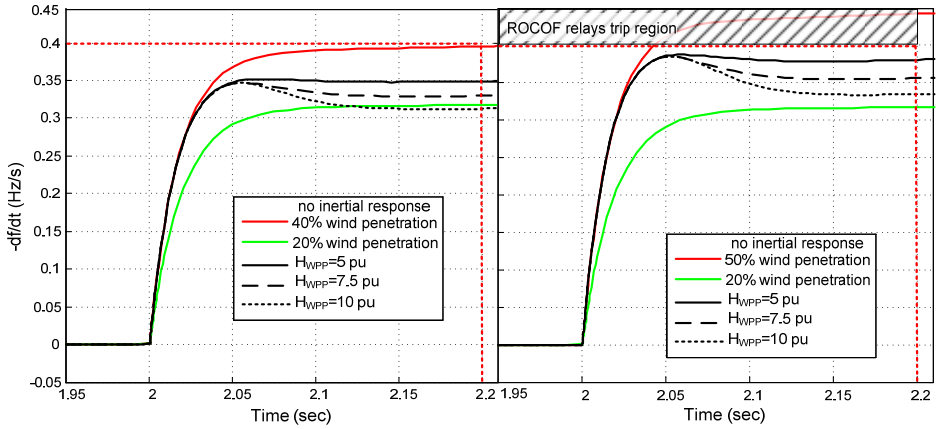

Fig. 4.45. ROCOF during 200ms after the largest infeed loss for different H_{WPP} values where R_{WPP}=1pu/s, T_{WPP}=0.025s, K_{Droop}=5pu, and T_{Droop}=9s for 40% and 50% wind power penetration scenarios

The reason of differences in plots given Fig. 4.45 is presented in Fig. 4.46 as the active power output of the WPP-1. The released active power by the inertial response component (i.e. the first component) is elevated when the H_{WPP} value is increased. The P_{max} value is not changed significantly for different H_{WPP} values in both of the scenarios however, the overall response of the WPP looks like a rectangular shape as in the temporary frequency control. In order to tune the H_{WPP} value not only is the operational metric 2 taken into account but also overall response of the WPP should be considered.

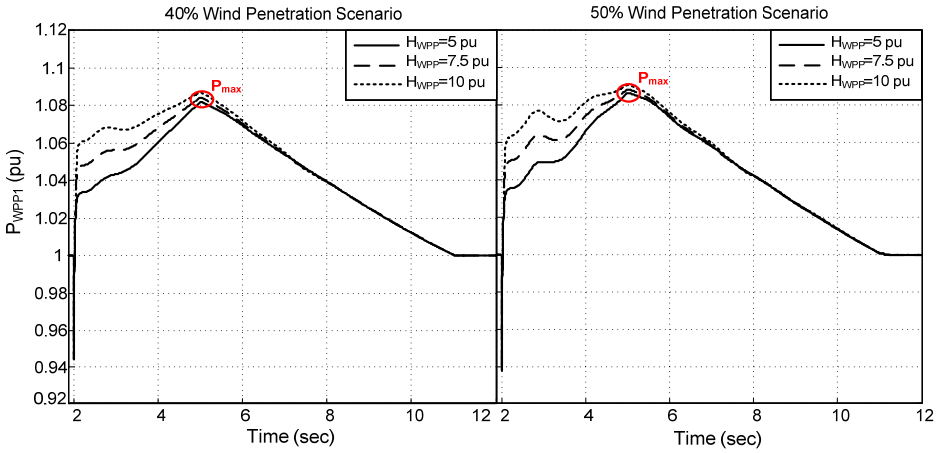

Fig. 4.46. Active power ouput of WPP-1 at Bus 5 for different H_{WPP} values where R_{WPP}=1pu/s, T_{WPP}=0.025s, K_{Droop}=5pu, and T_{Droop}=9s for 40% and 50% wind power penetration scenarios

The time to reach the minimum frequency point (operational metric 3) for the 40% and 50% wind power penetration scenarios is presented in Fig. 4.47 for different H_{WPP} values. The time is increasing slightly while the additional active power provided by the WPPs is increased. This is due to low values of the H_{WPP} in the first component of the pre-designed inertial response control.

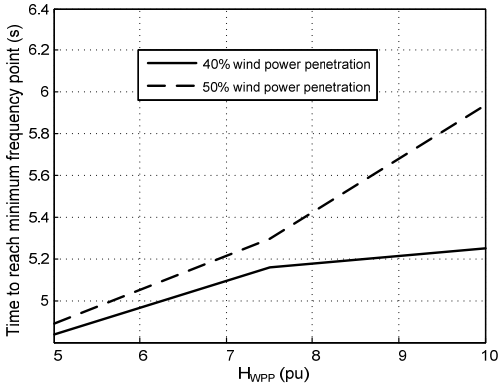

Fig. 4.47. Time to reach the minimum frequency point for different H_{WPP} values where R_{WPP}=1pu/s, T_{WPP}=0.025s, K_{Droop}=5pu, and T_{Droop}=9s for 40% and 50% wind power penetration scenarios

As explained above the variable-droop control is also replacing the primary frequency control temporarily until the time to reach the minimum frequency point. Fig. 4.48 shows the total energy released from the WPPs for different H_{WPP} and the calculated replaced inertial energy. The red straight line indicates the replaced inertial energy of the generating units (i.e. 1 unit from G1, 1 unit from G2 for 40% wind power and 2 units from G1, 1 unit from G2 for 50% wind power). Furthermore, the H_{WPP} value affects the released energy slightly during the inertial response control.

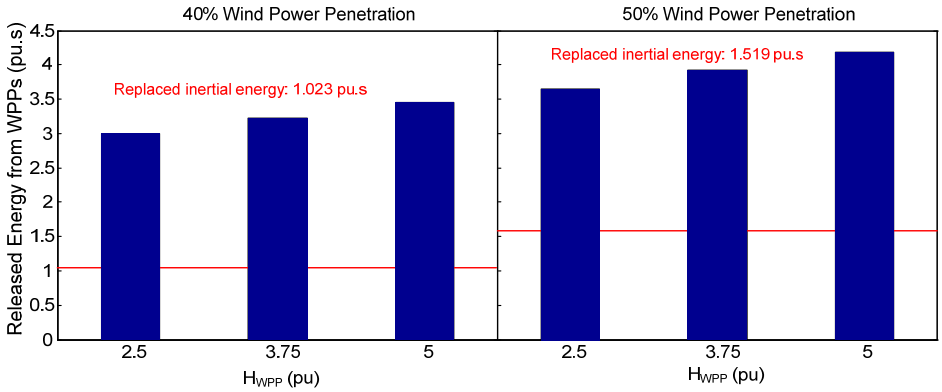

Fig. 4.48. Comparison of the total released energy from WPPs for different H_{WPP} values where R_{WPP}=1pu/s, T_{WPP}=0.025s, K_{Droop}=5pu, and T_{Droop}=9s for 40% and 50% wind power penetration scenarios

4.3.2.2 Sensitivity Analysis of Variable-Droop Gain (K_{Droop})

K_{Droop} is a variable gain of the second component of the pre-designed inertial response control which provides an additional active power with respect to the frequency deviation following the disturbance. The motivation of the variable-droop control is to utilize a similar control concept of governors in CPPs to provide a temporary energy in order to satisfy the operational metric 1. This can be also realized to delay the CPPs' primary frequency response while achieving the operational metrics by providing fast and temporary energy from WPPs. Additionally, considering the first component of the pre-designed inertial control which is the inertial response by the derivative control, the overall response of the WPP improves the frequency stability of the power system.

In this section, the effect of the K_{Droop} value is investigated by sensitivity analysis of the parameter. The important point in this sensitivity analysis is that only the K_{Droop} value is changed, not the time to reach this K_{Droop} value. The sensitivity analysis is illustrated in Fig. 4.49. The K_{Droop} value is varied where T_{Droop} and T_{KDroop} are kept constant. The aim is to investigate the impact of K_{Droop} on the power system frequency.

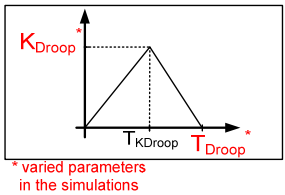

Fig. 4.49. Variable-droop control implementation of the pre-designed inertial response control

Fig. 4.50 presents the generic power system frequency when the K_{Droop} value is increased from 5pu to 10 pu. For 40% wind power penetration, all the K_{Droop} values improve the minimum frequency point. However, for the50% wind power penetration, when the value of the K_{Droop} value is 10 pu, a double dip occurs in the system frequency, and this situation is not preferred by the TSOs [4.7]. In Fig. 4.50, it is obviously seen that the time to reach the minimum frequency point is increasing to a higher value for K_{Droop}=10 pu.

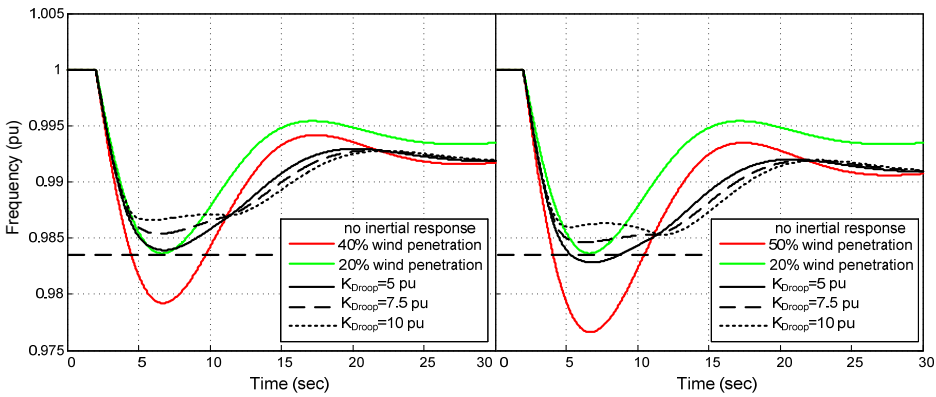

Fig. 4.50. System frequency for different K_{Droop} values where T_{Droop}=9s, H_{WPP}=5pu, T_{WPP}=0.025s, and R_{WPP}=1pu/s

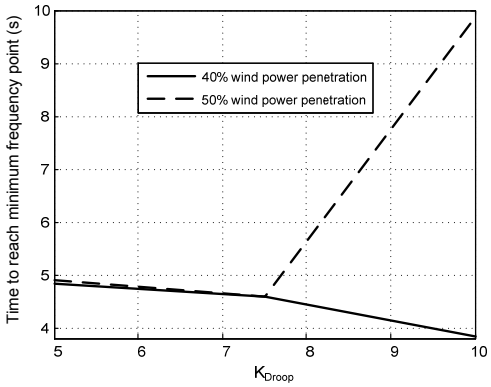

Fig. 4.51. Time to reach the minimum frequency point for different K_{Droop} values where T_{Droop}=9s, H_{WPP}=5pu, T_{WPP}=0.025s, and R_{WPP}=1pu/s

For the operational metric 2, there is no difference between the cases of different K_{Droop} values. Accordingly, the additional active power delivered from the WPP1 is shown in Fig. 4.52 for both of the wind power penetration scenarios. The reason of the increase in the minimum frequency point can be realized as the increase of the peak power from WPPs at the time where the minimum frequency occurs. However, when the peak value of the active power is increased, the active power ramp-down rate is also increased that cause a double dip in the power system frequency (e.g. K_{Droop}=10pu/s for 50% wind power penetration).

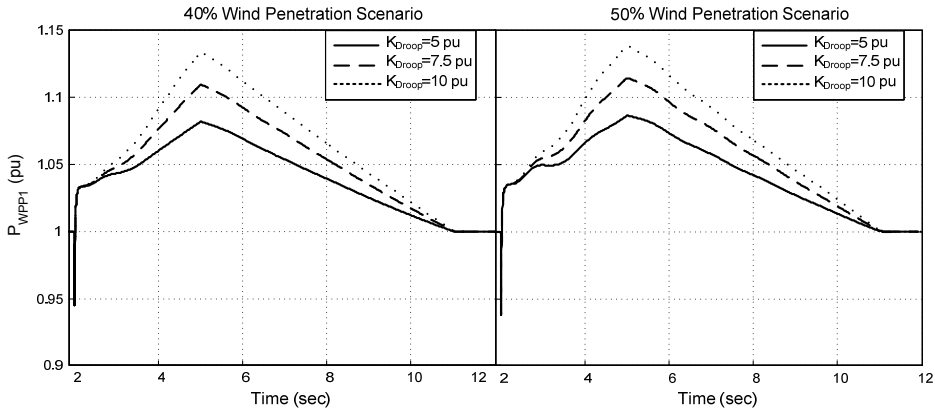

Fig. 4.52. Active power ouput of WPP-1 at Bus 5 for for different K_{Droop} values where T_{Droop}=9s, H_{WPP}=5pu, T_{WPP}=0.025s, and R_{WPP}=1pu/s

Consequently, in order to tune the variable-droop control, the ramp-down rate and the peak value of the inertial response should be considered carefully with the control performance of the CPPs' governors and the inertia of the power system.

Finally, the energy released during the inertial response control is given in Fig. 4.53 for both of the scenarios. The released energy is increased as an expected result, when the K_{Droop} value is increased. Another important remark is that the amount of energy does not specify the minimum frequency point directly due to the ramp-down rate of the variable-droop control.

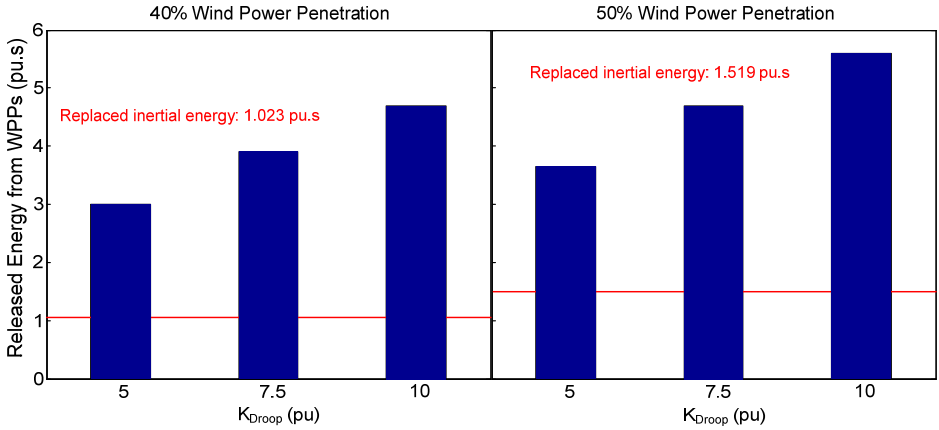

Fig. 4.53. Comparison of the total released energy from WPPs for different K_{Droop} values where T_{Droop}=9s, H_{WPP}=5pu, T_{WPP}=0.025s, and R_{WPP}=1pu/s

4.3.2.3 Sensitivity Analysis of Variable-Droop Duration (T_{Droop})

By sweeping the T_{Droop} parameter, the impact of the variable-droop control on the generic power system is investigated in this section. The important remark in this sensitivity analysis is that only the T_{Droop} value is changed not the time to reach this K_{Droop} value which is illustrated in Fig. 4.49. The frequency response given in Fig. 4.54 illustrates the effect of T_{Droop} after the minimum frequency point. Thus, the minimum frequency has not been affected significantly with the change of T_{Droop}. If the T_{Droop} value is selected a small value as 7s, the minimum frequency point is going down

further. Additionally, the effect on the time to reach the minimum frequency point is presented in Fig. 4.55. The reason is the same that is obtained in the previous section due to the increase in the ramp-down rate of the variable-droop control. However, in this case the peak value of the power is the same for all the T_{Droop} values (i.e. no change in K_{Droop}) with different duration of the additional active power.

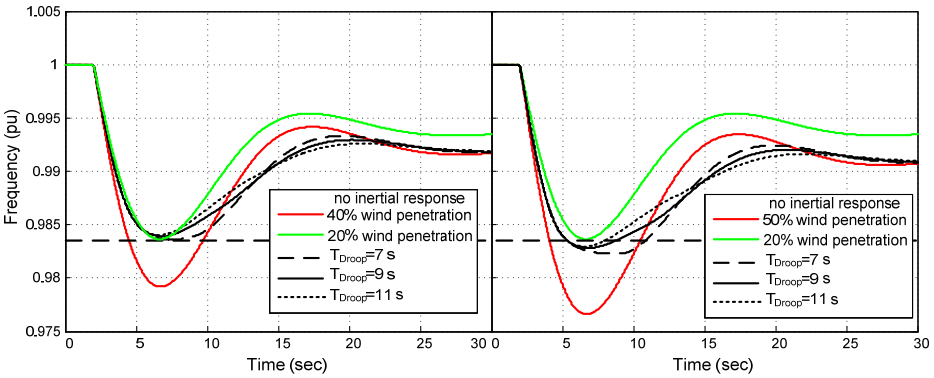

Fig. 4.54. System frequency for different T_{Droop} values where K_{Droop}=5pu, H_{WPP}=5pu, T_{WPP}=0.025s, and R_{WPP}=1pu/s

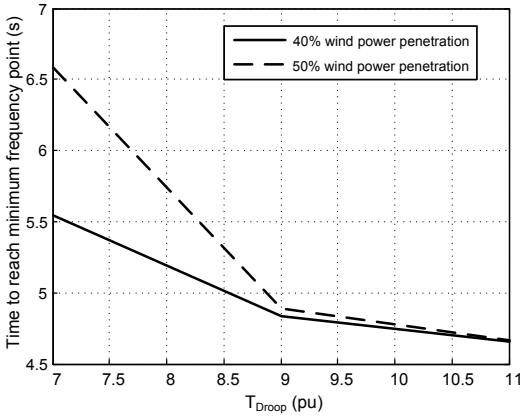

Fig. 4.55. Time to reach the minimum frequency point for different T_{Droop} values where K_{Droop}=5pu, H_{WPP}=5pu, T_{WPP}=0.025s, and R_{WPP}=1pu/s

The additional active power delivered from the WPPs is shown in Fig. 4.56 for both of the wind power penetration scenarios. As mentioned above, the minimum frequency point is not affected by changing the T_{Droop} value, thus the ramp-down rate is smooth (even for T_{Droop}=7s) enough not to cause a double dip in the frequency. When the rate of change of the active power from the minimum frequency point to pre-disturbance operating point is considered, the smoother rate is obtained for the higher values of T_{Droop}. High values of T_{Droop} help the governor control by slowing down the active power deviation of the CPPs. As a result, the frequency of the power system is deviating smoothly to the quasi steady-state frequency point after the minimum frequency point.

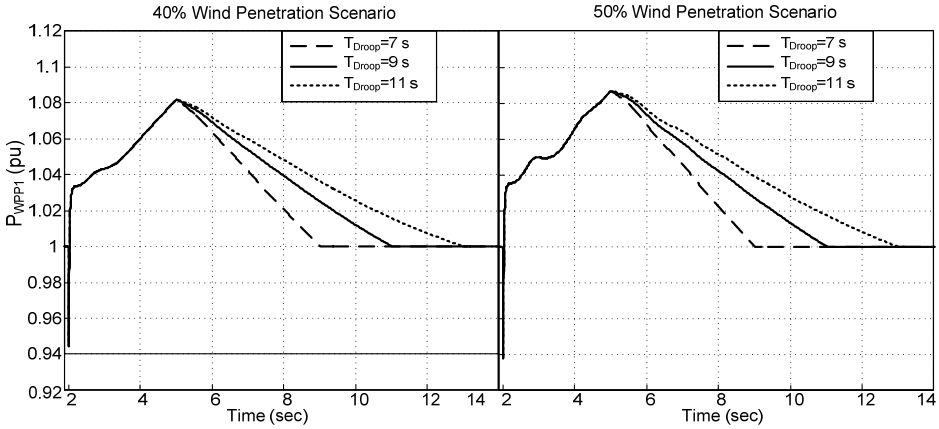

Fig. 4.56. Active power ouput of WPP-1 at Bus 5 for for different T_{Droop} values where K_{Droop}=5pu, H_{WPP}=5pu, T_{WPP}=0.025s, and R_{WPP}=1pu/s

As the final simulation result, the energy released during the inertial response control is given in Fig. 4.57. The released energy is increasing when the T_{Droop} value is increased. The same conclusion as with the sensitivity analysis of K_{Droop} is obtained that the amount of energy is not specifying the minimum frequency point directly due to the ramp-down rate of the variable-droop control.

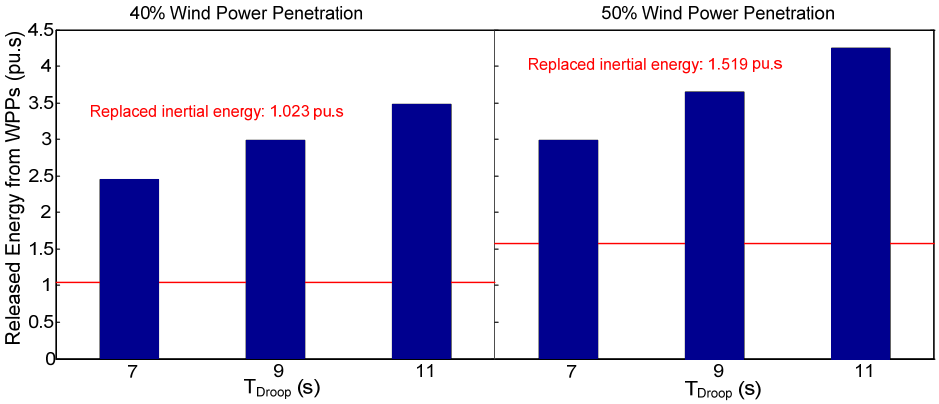

Fig. 4.57. Comparison of the total released energy from WPPs for different T_{Droop} values where K_{Droop}=5pu, H_{WPP}=5pu, T_{WPP}=0.025s, and R_{WPP}=1pu/s

4.3.3 Proposed Inertial Response Control

From the simulation results above, the following considerations are employed to improve the pre-designed inertial response control:

- R_{WPP} and T_{WPP} parameters of the simplified WPP model affect the ROCOF after the largest infeed loss (i.e. operational metric 2) together with the H_{WPP} parameter. These three parameters specify the active power boost value of the WPP during 500ms after the generation loss. The active power boost value is dependent on the ROCOF relay settings including the detection time and the threshold value. The inertia of the power system and the amount of the generation loss are the other factors.
- H_{WPP} is determined by the operational metric 2 in order not to trip ROCOF relays in the MV distributed generation. However, for the overall response of the proposed inertial response control, it can be adjusted after tuning the K_{Droop} parameter.
- The parameters of K_{Droop} and T_{Droop} affect the operation of the primary frequency control of CPPs (i.e. governor control), and if they haven't been tuned properly, a double dip can occur in the power system frequency.

According to these considerations and in order to implement more practical variable-droop control, the pre-designed inertial response control is improved as given in Fig.

4.58. Only the variable-droop control component has been updated and the derivative control component is kept same (Fig. 4.2). The variable-control gain profiles of the pre-designed and proposed inertial response controls are compared in Fig. 4.59. The tuning methodology of the proposed control is described in the next section.

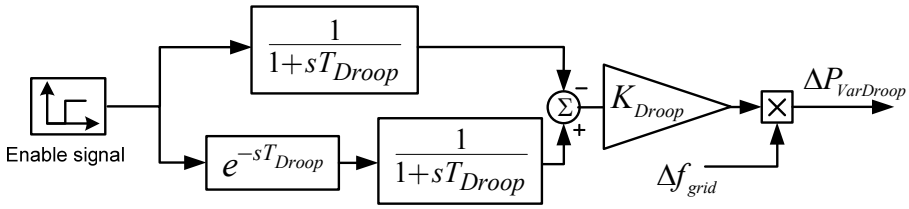

Fig. 4.58. Proposed variable-droop control

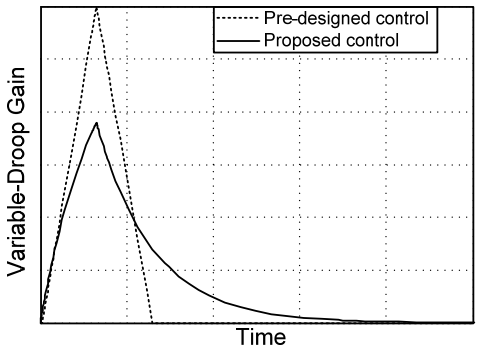

Fig. 4.59. Comparison of pre-designed and proposed inertial response variable-droop controls' gain

4.3.4 Tuning Methodology of Proposed Inertial Response Control

The tuning methodology for inertial response control concepts has not been described particularly in the previous studies (Chapter 2). Every specific power system model used in the inertial response control studies has different characteristics in terms of the inertia and the primary frequency control. These two features determine the frequency response of the power system, and should be taken into account in order to provide a temporary active power contribution from inertial response control of WPPs. Therefore, the tuning methodology of the variable-droop control aims selecting proper parameters (K_{Droop} and T_{Droop}) not to cause potential frequency instability while achieving the operational metric 1. Since, the H_{WPP} parameter of the derivative control

in the proposed inertial response control is tuned according to the operational metric 2, the tuning methodology of the variable-droop control is explained in this section.

The tuning methodology is based on a simplified model which is employed to estimate the minimum frequency point and the time to reach this point for low frequency events without simulations. The generic power system model is simplified in two steps; the first simplification is an average system frequency model (i.e. single mass model) [4.8], and the second simplification is a delay model adapted from [4.9], [4.10]. The delay model for power systems with different generation mixes is developed to estimate the maximum frequency deviation (Δf_{min}) and the time to reach the minimum frequency point (t_{min}). Consequently, these estimated values are used to tune the T_{Droop} and K_{Droop} values of the variable-droop control.

4.3.4.1 Average System Frequency Model

In the average system frequency model, all CPPs are represented as one equivalent mass, which has the average inertia constant (H_{eq}) with damping constant (D_{eq}) and is driven by the difference between the mechanical power change (ΔP_m) and the electrical power change (ΔP_L). The largest infeed loss can be represented by ΔP_L. The model is presented in Fig. 4.60 where two types of CPPs are modeled as an illustration, but can be extended to N number of CPPs [4.6].

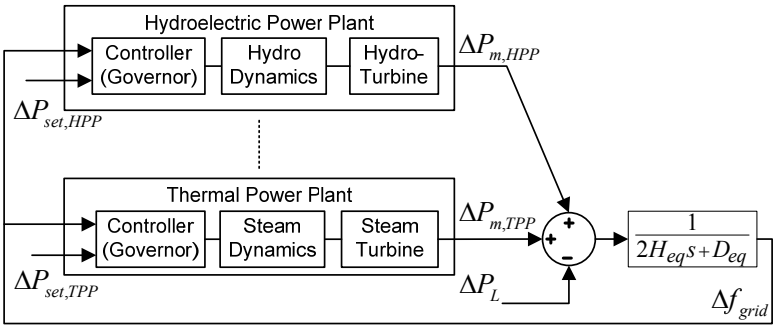

Fig. 4.60. Average system frequency model representation

4.3.4.2 Delay Model

The delay model, which is based on the average system frequency model, uses pure time delays to model the time constants of the governor, steam and hydro dynamics (e.g. valve motion, steam bowl dynamics), and converts the closed loop model (i.e. Fig. 4.10) into an open loop delay model [4.9]. The hydro and thermal turbine models can be kept as they are, or they can be assumed also as time delays with respect to their response characteristics. The equivalent representation of the average system frequency model (i.e. Fig. 4.60) as a delay model is illustrated in Fig. 4.61.

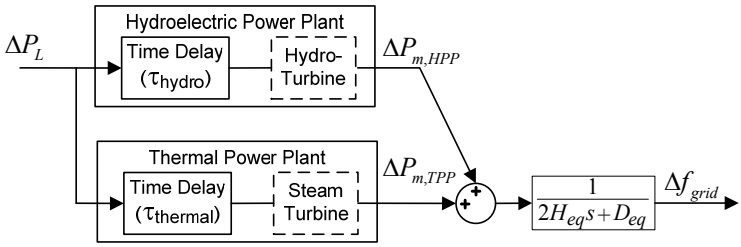

Fig. 4.61. Delay model representation

The simplification approach of the delay model for the hydroelectric power plant (HPP) is described in [4.10], which is adopted from [4.9]. In this approach, the first assumption is to represent governor dynamics, which is a transfer function of the form $1/(1+sT_G)$, with a pure time delay of T_G. The second assumption is considered for the transfer function of the transient droop compensation $((1+sT_R)/(1+s(R_{T,hydro}/R_P)T_R))$, and the exact response of this transfer function is transformed into linear function by using the slope of the overall response. Additionally, this linear function is simplified to a delay representation as illustrated in Fig. 4.62. This simplification is based on the equality of the Area1 and Area2 in Fig. 4.62.

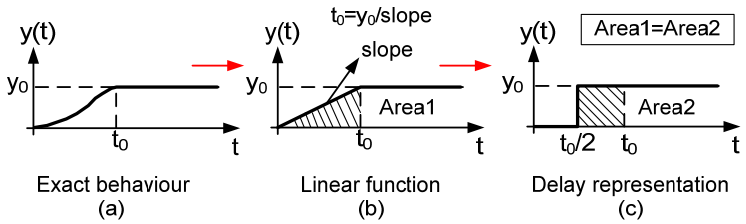

Fig. 4.62. Illustration of the second assumption [4.9]

In the third assumption, the hydro-turbine response is also modeled as a time delay. Due to the non-minimum phase characteristic of the hydro-turbine, the transfer function of the turbine is assumed as a time delay considering the energy balance of the response (i.e. Area1=Area2 in Fig. 4.63). Finally, the governor-turbine model of a HPP in the average system frequency model is simplified to a pure time delay (t_{HPP}) and calculated as follows:

$$t_{HPP} = t_G + t_0/2 \tag{4.1}$$

$$t_G = T_G + t_{hydro} \tag{4.2}$$

where T_G is governor time constant (1st assumption).

2nd assumption:

$$t_0/2 = H_{eq} R_{T,hydro} \left(1 - \frac{D_{eq}}{\frac{1}{R_p} + D_{eq}} \right) \tag{4.3}$$

where $R_{T,hydro}$ is temporary droop, and R_p is permanent droop.

3rd assumption:

$$t_{hydro} + 1.5T_W e^{-2t_{hydro}/T_W} = 1.5T_W \tag{4.4}$$

where T_W is the water starting time of the hydro-turbine.

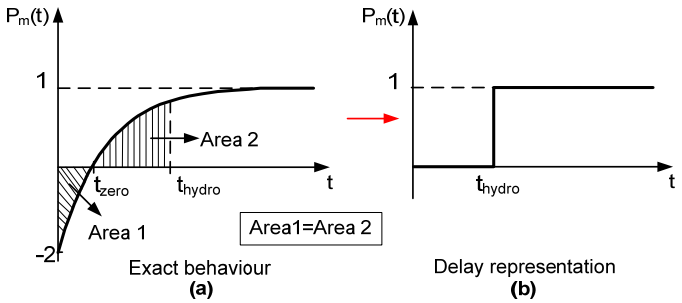

Fig. 4.63**.** Illustration of the third assumption for hydro-turbines [4.10]

For thermal power plants (TPP), the first assumption of the HPP delay model is valid, therefore governor dynamics (e.g. control time constant, servo, and steam valve bowl time constant) is assumed as a pure time delay of T_G. The transfer function of the steam turbine $((1+sFT_R)/(1+sT_R))$ is similar to the transient droop compensation, and accordingly $R_{T,thermal}$ is defined in order to calculate the time delay of the steam turbine. The derivation of $R_{T,thermal}$ is shown in Fig. 4.64.

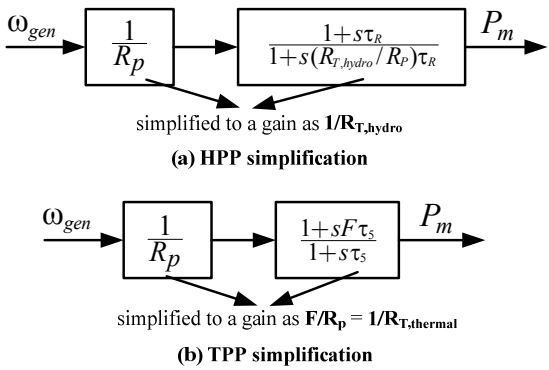

Fig. 4.64. $R_{t,thermal}$ parameter calculation of TPP

Consequently, after the simulations to validate the t_{min} and Δf_{min} values for a TPP with the average system frequency model, an additional correction time delay ($t_0/2$) is added to t_{TPP} and $t_{TPP,corr}$ is calculated. The difference between these two parameters is that

t_{TPP} is associated to calculated Δf_{min} and $t_{TPP,corr}$ is used to calculate t_{min}. So the t_{TPP} and $t_{TPP,corr}$ are as follows:

$$t_{TPP} = t_G + t_0/2 \tag{4.5}$$

$$t_{TPP,corr} = t_G + t_0 \tag{4.6}$$

$$t_G = T_G + T_S + T_V \tag{4.7}$$

where T_G is governor time constant T_S is servo time constant, and T_V is steam valve bowl time constant (1st assumption).

2nd assumption:

$$t_0/2 = H_{eq} R_{T,thermal} \left(1 - \frac{D_{eq}}{\frac{1}{R_p} + D_{eq}} \right) \tag{4.8}$$

where R_p is permanent droop.

Aforementioned assumptions are considered for TPPs and HPPs when there is one type of CPP is employed in the average system model frequency model (e.g. only a TPP or a HPP) [19]. Accordingly, with the calculated time delays (i.e. t_{HPP} and t_{TPP}), Δf_{min} and t_{min} values of the power system can be estimated according to the following formulations:

$$\Delta f_{\min} = \Delta P_L \frac{1}{D_{eq}} \left(e^{-t_{CPP} D_{eq}/2H_{eq}} - 1 \right) \tag{4.9}$$

where t_{CPP} equals to t_{HPP} for only one type of HPP or t_{TPP} for only one type of TPP.

$$t_{\min} = t_{HPP} \tag{4.10}$$

if there is only one type of HPP.

$$t_{\min} = t_{TPP,corr} \tag{4.11}$$

if there is only one type of TPP.

Five test cases are defined and simulated in MATLAB/Simulink in order to verify formulations above for both power system with one type HPP and one type of TPP. The average system frequency model of the test cases and the parameters are given in Table 4.9and Fig. 4.65, respectively. The models and related parameters are used from Chapter 3, [4.8], [4.10].

Table 4.9. Parameters of average system frequency models for only one type of HPP and TPP

Power System with HPP	$\mathbf{T_G(s)}$	$\boldsymbol{\tau_R}$**(s)**	$\mathbf{R_T}$	$\mathbf{R_p}$	$\mathbf{T_W(s)}$	$\mathbf{H_{eq}}$	**D**
(a)	0.2	5	0.38	0.05	1	3	1
(b)	0.25	8.59	0.7245	0.05	1.48	6.5457	1
Power System with TPP	$\mathbf{T_G(s)}$	$\boldsymbol{\tau_R}$**(s)**	**F**	$\mathbf{R_p}$	$\mathbf{T_S(s)}$	$\mathbf{H_{eq}}$	**D**
(a)	0.2	7	0.3	0.05	0.3	5	1
(b)	0.2	10	0.237	0.05	0.3	5	1
(c)	0.2	5	0.28	0.05	0.05	5	1

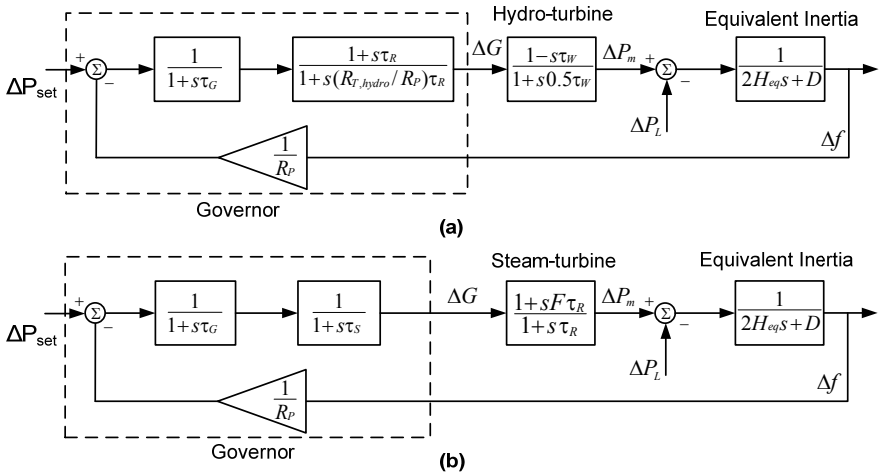

Fig. 4.65. Average system frequency models for only one type of HPP (a) and TPP (b)

For the given parameters above, the simulation results and estimated values (according to the given formulations above) for Δf_{min}, t_{min} and $t_{min,corr}$ are given in Table 4.10. The simulation results are consistent with the estimated values for the power system with HPP (a) and the power system with TPP (a), (b), (c). For the power system with HPP

(b), due to the large time constant of governor and inertia of the power system, the error between the simulation result and the estimated value is higher than the other cases. It can be realized that the assumptions become invalid. However, regardless of the mismatch value, the variable-droop control can be tuned using the Δf_{min}, t_{min} and $t_{min,corr}$ values.

Table 4.10. Comparison of the simulation results and the estimated values of the power system models (Table 4.9)

	t_{min} (s) (Simulated)	**t_{min} (s)** (Estimated)	**Δf_{min} (Hz)** (Simulated)	**Δf_{min} (Hz)** (Estimated)
PS with HPP (a)	2.8230	2.6957	-1.810	-1.692
PS with HPP (b)	8.8810	6.8545	-1.746	-2.038
PS with TPP (a)	2.2470	2.0873	-0.587	-0.607
PS with TPP (b)	2.6660	2.5092	-0.674	-0.698
PS with TPP (c)	2.1690	1.9507	-0.519	-0.521

The formulations (4.1)-(4.11) can be employed for power systems which comprise different types of generation with different types of governor and turbine parameters (e.g. 3 TPPs and 1 HPP in the generic 12-bus system). Therefore, the delay model of a generic power system with different generation mixes is developed considering the response of each CPP independently. The calculation is based on the weighted average of time delay values of each CPPs (i.e. t_{CPP}) according to their power ratings (i.e. n_{CPP}). The derivation of the time delay of the generic power system ($t_{min,eq}$) and maximum frequency deviation ($\Delta f_{min,eq}$) are defined as follows:

$$t_{\min,eq} = \sum n_{CPP} t_{CPP} \Big/ \sum n_{CPP} \tag{4.12}$$

where n_{CPP} is power rating of the CPP in system MVA base.

$$t_{CPP} = t_{G,CPP} + t_{0,CPP} \Big/ 2 \tag{4.13}$$

where $t_{G,CPP}$ is (2) for a HPP, and (7) for a TPP.

$$t_{0,CPP}/2 = H_{eq}\frac{R_{T,CPP}}{r_{CPP}}\left(1-\frac{D_{eq}}{\frac{1}{R_{p,CPP}}+D_{eq}}\right) \tag{4.14}$$

where $R_{T,CPP}$ is $R_{T,hydro}$ for a HPP or $R_{T,thermal}$ for a TPP.

$$r_{CPP} = \sum R_{p,CPP}/R_{p,CPP} \tag{4.15}$$

$$\Delta f_{\min,eq} = \Delta P_L \frac{1}{D_{eq}}\left(e^{-t_{\min,eq}D_{eq}/2H_{eq}}-1\right) \tag{4.16}$$

Similar to the above calculations for the power system with one type of CPP (4.1)-(4.8), $t_{min,eq}$ is amended by adding $t_{0,CPP}/2$ for TPPs in (4.13) in order to estimate the time to reach the minimum frequency point ($t_{min,eq,corr}$) consistently with the simulation results. With the developed formulations, $t_{min,eq}$, $t_{min,eq,corr}$, and $\Delta f_{min,eq}$ are estimated for the generic power system. The comparison of the simulation results and delay model estimation are presented in Table 4.11.

Table 4.11. Comparison of the simulation results and delay model estimation

$t_{min,eq,corr}$ (s) (Estimated)	**$t_{min,eq,corr}$ (s)** (Simulated)	**$\Delta f_{min,eq}$ (Hz)** (Estimated)	**$\Delta f_{min,eq}$ (Hz)** (Simulated)
4.81	4.79	-1.44	-1.1

After estimating both $t_{min,eq,corr}$ and $\Delta f_{min,eq}$, which are the former values before the implementation of the variable-droop control, the parameters (i.e. T_{Droop} and K_{Droop}) are tuned considering the delay model response of the power system. The tuning methodology of T_{Droop} and K_{Droop} is designed in order not to disturb the primary frequency response of CPPs which is represented as $t_{min,eq,corr}$ and $\Delta f_{min,eq}$ in the delay model. $t_{min,eq,corr}$ defines the duration of the variable-droop control, and $\Delta f_{min,eq}$ determines how much additional power is released in order to increase frequency as

demanded ($\Delta f_{increase}$). The response of the variable-droop control is illustrated in Fig. 4.66, and the parameters are calculated as follows:

$$T_{Droop} = t_{\min,eq,err} \Big/ 2 \tag{4.17}$$

$$K_{Droop} = \frac{-H_{eq}\left(R_T^{*} D_{eq} + \Delta f^{*}\right) - T_d D_{eq}}{\Delta f^{*} + R_T^{*} D_{eq}} \tag{4.18}$$

where

$$R_T^{*} = \sum n_{CPP} \frac{R_{T,CPP}}{r_{CPP}} \left(1 - \frac{D_{eq}}{\frac{1}{R_{p,CPP}} + D_{eq}} \right) \Bigg/ \sum n_{CPP} \tag{4.19}$$

$$\Delta f^{*} = 2 \ln\left(\left(\Delta f_{\min,eq} + \Delta f_{increase} \right) \frac{D_{eq}}{\Delta P_L} + 1 \right) \tag{4.20}$$

$$T_d = \sum n_{CPP} t_{G,CPP} \Big/ \sum n_{CPP} \tag{4.21}$$

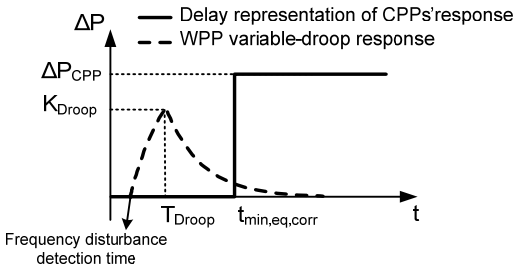

Fig. 4.66. Illustration of the tuning methodology of the variable-droop control

According to the formulations (4.17)-(4.18) for the generic power system with the 50% wind penetration scenario, T_{Droop} value is calculated as 2.5 s (i.e. $t_{min,eq,corr}/2 \approx 2.5$s), and K_{Droop} value is 15 pu in the WPP installed capacity base (i.e. 850 MW, Chapter 3) to increase the minimum frequency point by 250 mHz (i.e. $\Delta f_{increase}$=250 mHz).

4.4 Comparison of Inertial Response Control Methods

In the simulations, the largest infeed from G2 (Chapter 3) is tripped to demonstrate the performance of the proposed inertial response control and to compare it with the existing control concepts for the 50% wind power penetration scenario. The advantages of the proposed control are presented in terms of the peak value of the additional active power and the released energy during the inertial response. The simulation results are shown in the following subsections; in the first subsection, all the aggregated WPPs are assumed to operate high wind speed (i.e. average wind speed (V_{wind}) =14m/s). In the second subsection, the WPP-2, which is connected at Bus 3 (Fig. 4.1), operates at low wind speed (i.e. V_{wind}=10m/s) to assess the impact of the recovery period of the FC-VSWT on the power system frequency.

4.4.1 Simulation Results for High Wind Speed Operations

In Fig. 4.67, the minimum frequency point of the generic power system is compared for the proposed inertial response control and the existing control concepts. All three control concepts achieve the first operational metric 1 (Table 1), however the temporary frequency control creates a double dip in the power system frequency due to the steep ramp-down rate of the released active power (Fig. 4.68). Additionally, the derivative control method has the highest value for the time to reach the minimum frequency point. The reason is that in the derivative control more energy is released when the ramp-down rate equal to ROCOF compared to the proposed control. This can be seen in Fig. 4.68 which illustrates the active power output of the WPP-1 connected to Bus 5. For the operational metric 2, all the control concepts provide sufficient active power within 200 ms after the detection of the disturbance. Only difference between the control concepts is the ramp-up rate of the released active power (Fig. 4.68), where the impact on the ROCOF is insignificant.

For the operational metric 2, all the control concepts provide sufficient active power within 200 ms after the detection of the disturbance. Only difference between the

control concepts is the ramp-up rate of the released active power (Fig. 4.68), and the impact on the ROCOF of the generic power system is given in Fig. 4.69.

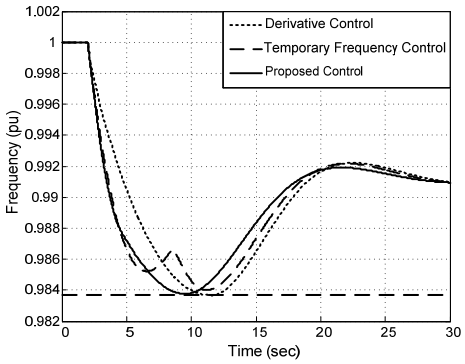

Fig. 4.67. Comparison of the system frequency with the proposed and the existing control concepts for high wind speed operation

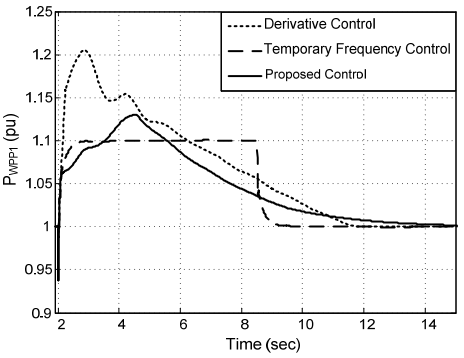

Fig. 4.68. Comparison of the active power output of WPP-1 with the proposed and the existing control concepts for high wind speed operation

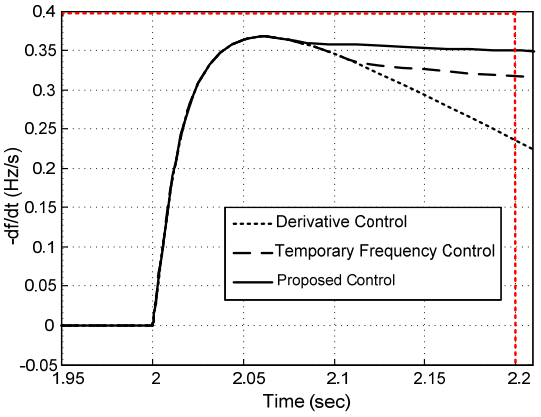

Fig. 4.69. Comparison of the ROCOF within 200 ms with the proposed and the existing control concepts for high wind speed operation

One of the advantages of the proposed control is to achieve operational metric 1 and 2 with releasing less than 15% additional active power. Accordingly, the total energy released during the inertial response for the proposed control is also less than the other control strategies. The released energy from the WPP-1 during the inertial response is

compared for the control concepts in Fig. 4.70. Another advantage of the proposed control is that the dependency on the derivative component is limited selecting a small H_{WPP} value, which is implemented to achieve the operational metric 2. On the contrary, the derivative control does not have this flexibility due to the large H_{WPP} value and is only dependent on the df/dt signal. Furthermore, the temporary frequency control does not have the adaptive ramp-up and ramp-down rate for the released active power causing the frequency instability (double dip in Fig. 4.67).

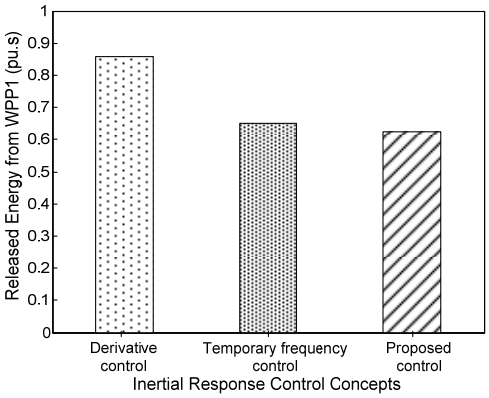

Fig. 4.70. Comparison of the released energy from WPP-1 with the proposed and the existing control concepts for high wind speed operation

4.4.2 Simulation Results for Low Wind Speed Operations

For low wind speed conditions, the recovery period occurs after boosting the active power by the inertial response control. The active power reduction due to the recovery period is highly dependent on the wind speed, released energy during the active power boost, and the duration of the active power boost [4.11], [4.12]. Considering the recovery period, the simulations are performed by taking the wind speed of the aggregated WPP-2 (200 MW) as 10m/s (WPP-1 and WPP-3 are operated at high wind speed conditions). Since the wind speed has been modified in the simulations, the gain for the aggregated WPP-2 (explained in Chapter 3) has increased not to change the load flow of the 50% wind power penetration scenario. In Fig. 4.71, the impact of the recovery period on the system frequency (a) is presented with the active power output of WPP-2 (b). The double dip in the system frequency has become deeper for the

temporary control due to the drop in the active power output of the WPP-2 (Fig. 4.71 (b)). Both the temporary frequency control and the derivative control do not satisfy the operational metric 1 for the below rated wind speed operation of the WPP-2. Moreover, the proposed control has better performance than the other two control concepts in terms of the minimum frequency point, and the recovery period has a small impact when the system frequency tries to reach the quasi-steady state value. This is due to the less energy provided during the inertial response of the proposed control than the other control concepts. In addition to simulation results, the proposed control has less sensitive to the ROCOF measurement noise compared to the derivative control, also more stable and flexible than the temporary frequency control.

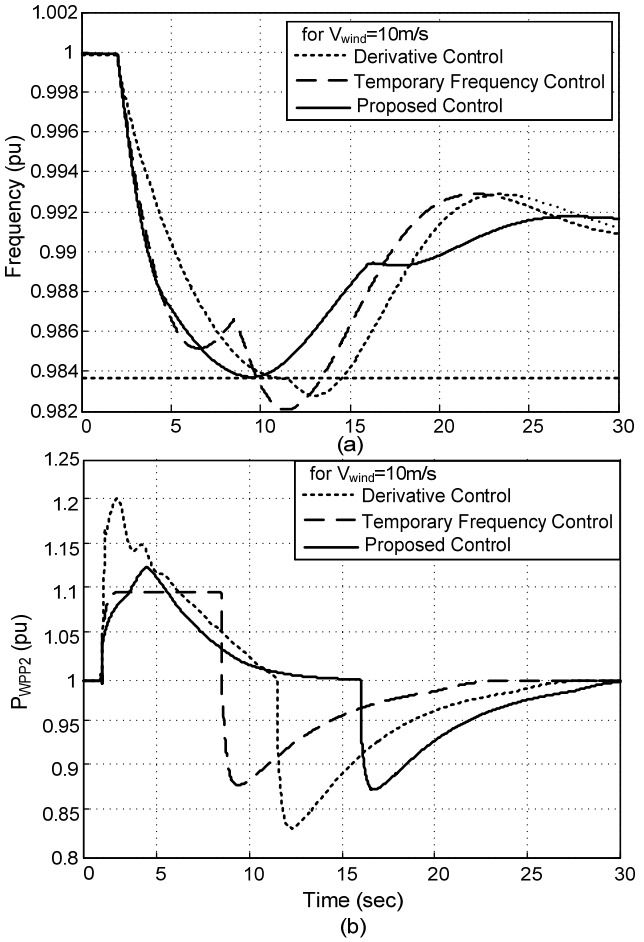

Fig. 4.71. Comparison of the system frequency (a) and the active power output of

WPP-2 (b) with the proposed and the existing control concepts for low wind speed operation

In Fig. 4.71, V_{wind} is assumed 10m/s for the aggregated WPP-2. However, for different wind speeds the recovery period of FC-VSWT would be different [4.11]. The impact of different wind speeds on the generic power system frequency is illustrated in Fig. 4.72. In order not to change the load flow of the 50% wind power penetration scenario, the gain for the aggregated WPP-2 has increased also for the cases with different wind speeds. From Fig. 4.72, it is observed that there is no significant difference between the wind speed conditions, which are lower than the rated wind speed. However, when the WPP is operated at the rated wind speed, the double dip occurs in the power system frequency occurs. The result is consistent with the simulation results presented in [4.11]. Therefore, the wind speed conditions should be considered while enabling the inertial response control.

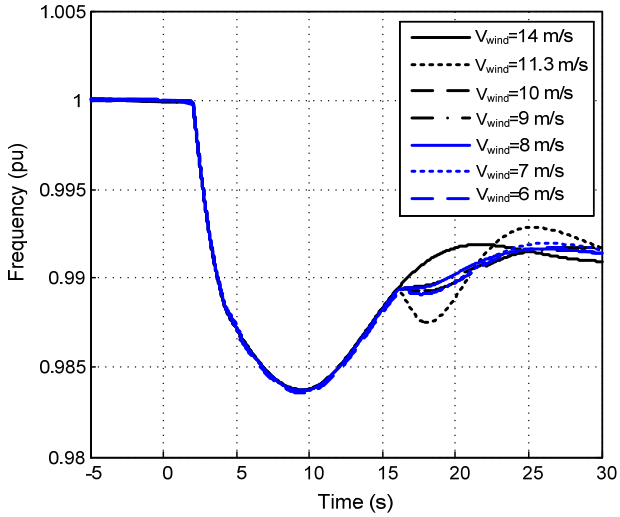

Fig. 4.72. Comparison of the system frequency for different wind speed conditions of WPP-2

4.5 Summary

In this chapter, a new inertial response control for WPPs is proposed and demonstrated considering the inertial response requirements of a generic power system. Before

developing the new inertial response control, the existing control methods are investigated by the sensitivity analysis. The advantages and disadvantages of the existing control methods are summarized to guide the new control method. Additionally, the tuning methodology for the proposed control is described in detail taking into account the power system characteristics (i.e. inertia, governor response of the CPPs). Using the tuning methodology, the proposed control can be applied to any power system with high wind power penetration.

In order to assess the inertial control and the existing control concepts (i.e. the derivative control and temporary frequency control), the generic power system with wind power penetration scenarios, and the aggregated WPP model are utilized with the operational metrics. According to these metrics, the simulation results are evaluated in terms of the power system requirements and the operational constraints of the FC-VSWT (i.e. aggregated WPP). The proposed control provides less energy and peak active power compared to the existing control methods while achieving the operational metrics. Another improvement has been made for the below rated wind speed operation where the impact of the recovery period has been reduced with the proposed inertial response control.

4.6 References

[4.1] ENTSO-E, "Load-Frequency Control and Performance," Jun. 2004.

[4.2] EPRI, "Power System Dynamics Tutorial,"2005.

[4.3] C.F, Ten, P.A Crossley, "Evaluation of ROCOF Relay Performances on Networks with Distributed Generation," IET 9th International Conference on Developments in Power System Protection, pp.523-528, 17-20 Mar. 2008.

[4.4] S. Conti , "Analysis of distribution network protection issues in presence of dispersed generation," *Electric Power Systems Research Journal*, 2009, Vol. 79, Issue 1, pp. 49-56.

[4.5] EirGrid and SONI, "DS3: Frequency Control Workstream".

[4.6] "General Specification V112–3.0 MW 50/60 Hz", Vestas Wind Systems A/S.

[4.7] National Grid Code Frequency Response Working Group UK, "Requirements for System Inertia," July 2010.

[4.8] P. Kundur, *Power System Stability and Control*, 1993, McGraw-Hill.

[4.9] M. Chan, R. Dunlop, and F. Schweppe, "Dynamic Equivalents for Average System Frequency Behavior Following Major Disturbances," *IEEE Trans. Power Apparatus and Systems*, vol. PAS-91, no. 4, pp. 1637–1642, Jul. 1972.

[4.10] N. R. Ullah and T. Thiringer, "Temporary primary frequency control support by variable speed wind turbines-potential and applications," *IEEE Trans. Power Systems*, vol.23, no.2, pp.601-612, May 2008.

[4.11] G. C. Tarnowski, P C. Kjaer, P. E. Sorensen, and J. Ostergaard, "Variable speed wind turbines capability for temporary over¬-production," in *IEEE Power & Energy Society General Meeting*, pp. 1-7, Calgary, USA, July 2009.

[4.12] G. C. Tarnowski, "Coordinated Frequency Control of Wind Turbines in Power Systems with High Wind Power Penetration," Ph.D. dissertation, Dept. Elect. Eng., Technical University of Denmark, Copenhagen, Denmark, 2012

Chapter 5
Synchronizing Power Support from Wind Power Plants

5.1 Introduction

Rotor angle stability of power systems determines how CPPs can remain in synchronism following a disturbance such as short-circuit fault, loss of generation, increase in mechanical power or step increase in load. These disturbances cause an imbalance between generation and consumption. According to source of the imbalance, the electromagnetic torque/power (T_e/P_e) or mechanical torque (T_e/P_e) decelerates or accelerates rotors of SGs connected to a power system. Equations (2.1) and (2.2) given in Chapter 2 describe these dynamics for the rotor speed and angle of SGs. In order to illustrate these dynamics, a generation loss or a step load increase as a disturbance can be considered for a power system operating at steady-state. Following the generation loss, SGs start to accelerate or decelerate with respect to each other according to their characteristics. If one generator temporarily runs faster than another, the angular position of its rotor relative to that of the slower SG will advance. The resulting angular difference transfers part of the load (i.e. T_e or P_e) from the slow SG to the fast SG, depending on the *power-angle relationship*. Beyond a stability limit, an increase in angular separation between SGs results in a decrease of the power transfer such that the angular separation is increased further. Thus, the instability occurs if the power system cannot absorb the kinetic energy corresponding to these rotor speed differences. Loss synchronism may occur between one SG and the rest of the system, or groups of SGs

[5.1]. The power-angle characteristic of a SG represents both the steady-state and transient rotor angle stability of the SG with the infinite bus. Considering the power-angle characteristic, the synchronizing power of the SG can be realized as the ability of the SG remaining in synchronism with the rest of the power system. In this chapter, the steady-state and transient power-angle characteristics of a SG are described in order to understand the synchronizing power of the SG in the single machine-infinite bus (SMIB) model. However, the integration of WPPs requires the synchronizing power analysis of the multi-machine systems. Therefore, the dynamic ward equivalencing approach is introduced and modified to include the WPP impact on the multi-machine systems. Accordingly, the following sections investigate the possible impacts on a simplified generic power system regarding the lack of synchronizing power with the integration of WPPs. After analyzing the impacts, the control concepts are proposed and simulated to compensate both the steady-state and transient power-angle characteristics. Finally, the simulation results are discussed in the summary section.

5.2 Steady-State Power-Angle Characteristic

In SMIB system model given in Fig. 5.1, the steady-state stability of a SG can be analyzed. The active power supplied by the SG to the power system is calculated as follows for the salient-pole and round-rotor types respectively:

$$P_e = \frac{E_q V_s}{x_d} \sin\delta + \frac{V_s^2}{2} \frac{x_d - x_q}{x_d x_q} \sin 2\delta \tag{5.1}$$

where E_q is the internal emf, Vs is the infinite bus voltage, $x_d=X_d+X_{ext}$, and $x_q=X_q+X_{ext}$ which are the combined reactance of the generator and external grid.

$$P_e = \frac{E_q V_s}{x_d} \sin\delta \tag{5.2}$$

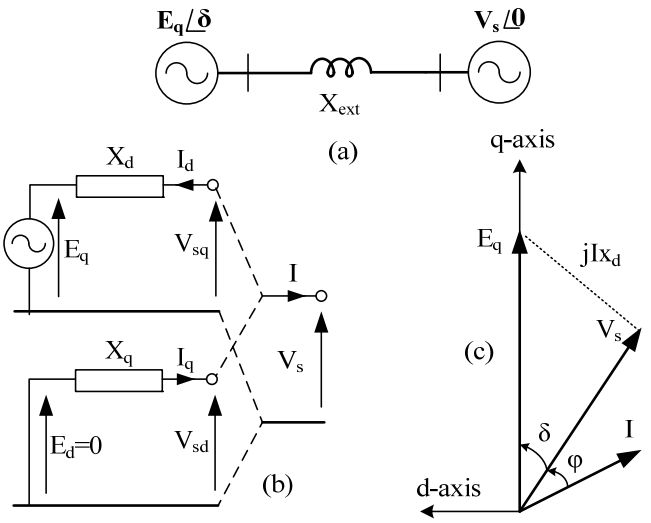

Fig. 5.1. SMIB model in steady-state; (a) single line, (b) circuit, and (c) phasor diagrams

Equation (5.1) is simplified to (5.2) by assuming X_d=X_q, can be used for the steady-state analysis of the SG. The resistances and shunt admittances are neglected, and constant excitation emf (E_q) is assumed for (5.1) and (5.2). According to (5.2), the power-angle characteristic is illustrated in Fig. 5.2. For the operating conditions on the left hand side of the power-angle characteristic curve, the SG is steady-state stable where it can reach an equilibrium point after subjected to a disturbance (e.g. increase in P_m). On the other hand, if the SG is operating at the operating conditions, which is higher than 90°, it will lose the synchronism due to lack of equilibrium point. From these considerations, it can be concluded that if $dP_e/d\delta$ is higher than 0, the SG is steady-state stable for the SMIB model with constant excitation. The $dP_e/d\delta$ is referred as the steady-state synchronizing power coefficient, K_{Eq}, and given in (5.3).

$$K_{Eq}\Big|_{\delta=\delta_0} = \frac{E_q V_s}{x_d}\cos\delta_0 \tag{5.3}$$

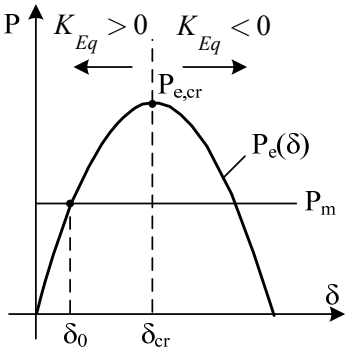

Fig. 5.2. Illustration of the power-angle characteristic of a SG

5.3 Transient Power-Angle Characteristic

Any disturbance acting on a SG produces a sudden change in the armature currents and flux. This flux change induces additional currents in the rotor which will affect the E_q which is proportional to the field current. Thus, the steady-state power-angle characteristic is not valid for the post-disturbance rotor dynamics [5.2]. In order to modify the power-angle characteristic the transient emfs E_d' and E_q' are assumed constant. Additionally, the transient saliency can be ignored by assuming $x_d' \approx x_q'$ (i.e. classical model), and as a result the active power equation becomes

$$P_e(\delta') = \frac{E'V}{x_d'} \sin\delta' \tag{5.4}$$

where $x_d' = X_d' + X_{ext}$ and the circuit and phasor diagrams are given in Fig. 5.3.

According to (5.4) and Fig. 5.3, the transient power-angle characteristic is illustrated with the steady-state characteristic for the SMIB model in Fig. 4. As $x_d' > x_d$, the values of the transient characteristic is higher than the steady-state characteristic. The angle shift of the curve comes from the angle difference between q-axis and E' (Fig. 5.3). Furthermore, these characteristics are illustrated for the unregulated SG which does not have an automatic voltage regulator (AVR). In Fig. 5.4, the AVR effect is also included and the details of the calculations are given in [5.2]. As it can be seen clearly from Fig.

4, when the effect of the rotor circuits, damper windings, field flux variation, and AVR is included, the synchronizing power of the SG is increasing in SMIB model. The

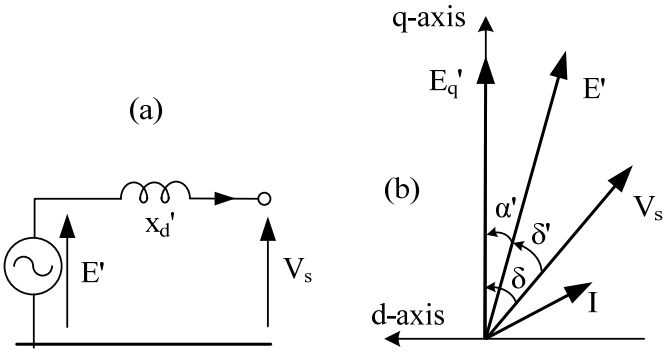

Fig. 5.3. SMIB model in transient state; (a) circuit and (b) phasor diagrams

transient synchronizing power coefficient ($K_{E'}$) is greater than steady-state (K_{Eq}), and lower than regulated synchronizing power coefficient (K_{Vg}), $K_{Vg} > K_{E'} > K_{Eq}$ at the operating point A in Fig. 5.4.

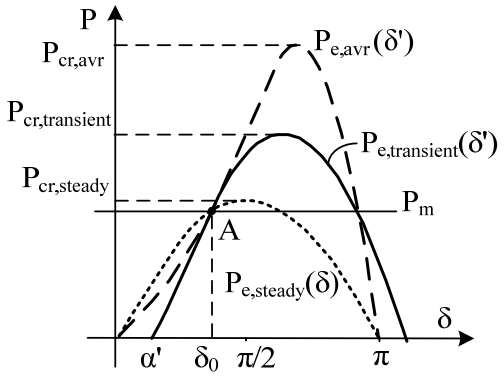

Fig. 5.4. Illustration of the power-angle characteristic of a SG for steady-state, unregulated transient, and regulated transient cases [2.3]

Regardless of power-angle characteristics, the synchronizing power coefficient should be positive for stable operation of the SG connected to the infinite bus (i.e. SMIB model). It is also the indication of the stiffness of the SG's electrical connection to the power system. Up to this point, single SG connected to an infinite bus system has been

analyzed to capture the theory of the synchronizing power. However, in order to analyze the impact of WPPs on the rotor angle stability of power systems, the analysis should be expanded to multi-machine systems by using (5.4) between each SG. The details are given in the following section.

5.4 Synchronizing Power Analysis of Multi-Machine Systems

Transient power-angle characteristic derived in the previous section can be used for the synchronizing power analysis of multi-machine systems. The advantage of the classical model (5.4) used in the transient characteristic is that the SG transient reactance is added directly to the reactance of the transmission lines and transformers in the power system. To employ the classical model of SGs for multi-machine systems, the power system model should be reduced to a simplified representation which consists of only SGs' internal buses (i.e. *E'*). When the loads are assumed as constant impedances, they can be included in the admittance matrix of the power system. For a given multi-machine power system, the current and voltage equations are obtained as follows:

$$I_{gk} = \frac{E_k' - V_k}{x_{dk}'} \quad for\, k = 1,..,n \tag{5.5}$$

$$0 = \sum_{l=1}^{N} Y_{kl} V_l - I_{gk} \quad for\, k = 1,..,n \tag{5.6}$$

$$0 = \sum_{l=1}^{N} Y_{kl} V_l \quad for\, k = n+1,..,N \tag{5.7}$$

where E_k' is the kth generator transient emf, V_k is the kth bus voltage, I_{gk}' is the kth generator current, and Y_{kl} is klth element of the modified admittance matrix by the addition of load impedances.

Above equations can be written in compact form:

$$\begin{bmatrix} I_G \\ 0_N \end{bmatrix} = \begin{bmatrix} Y_A & Y_B \\ Y_C & Y_D \end{bmatrix} \begin{bmatrix} E_G' \\ V_N \end{bmatrix} \tag{5.8}$$

where Y_A, Y_B, Y_C, and Y_D is the related sub-matrices of the modified admittance matrix and diagonal matrix $1/x_d'$. Using second row of the matrix equation above V_N is substituted in the first row and the following relation is obtained between generator currents (I_G) and internal emfs (E_G')

$$I_G = \left(Y_A - Y_B Y_D^{-1} Y_C\right) E_G' \tag{5.9}$$

where Y_A-$Y_B Y_D^{-1} Y_C$ matrix is referred as the reduced network matrix (Y_{RNM}).

The synchronizing power analysis for multi-machine systems is based on the reduced network model [5.2], [5.3]. According to active power flow equations (5.10), the *self* and *mutual synchronizing power* is calculated in (5.11) and (5.12). The mutual synchronizing power indicates how the output of the active power output of the SG changes in relation to its rotor angle difference with the other SGs. It determines the stiffness of the connection between SGs regarding the loading of SGs.

$$P_{ei} = E_i'^2 G_{ii} + \sum_{j \neq i}^{N} E_i' E_j' G_{ij} \cos\left(\delta_i' - \delta_j'\right) + \sum_{j \neq i}^{N} E_i' E_j' B_{ij} \sin\left(\delta_i' - \delta_j'\right) \tag{5.10}$$

where $Y_{ij}=G_{ij}+jB_{ij}$ are the elements of the reduced admittance matrix. In order to simplify the analysis the transmission losses are neglected [5.2] and synchronizing powers are

$$K_{E,self} = \frac{\partial P_{ei}}{\partial \delta_i} = \sum_{j \neq i}^{N} E_i' E_j' B_{ij} \cos\left(\delta_i' - \delta_j'\right) \tag{5.11}$$

$$K_{E,mutual} = \frac{\partial P_{ei}}{\partial \delta_j} = -E_i' E_j' B_{ij} \cos\left(\delta_i' - \delta_j'\right) \tag{5.12}$$

In the classical synchronizing power analysis of power systems, the above formulations are sufficient and can be also used for the transient stability analysis (e.g. in transient energy calculation [5.2] and in time domain analysis [5.4]). However, in order to employ the load characteristic, which may be dependent on the bus voltage of the load,

another approach should be considered. Therefore, in [5.5] the dynamic ward equivalencing method was developed to include the voltage dependent loads when the operating point moves away from the steady-state conditions for the transient stability studies. The current injections from load buses are included in (5.8) and the sensitivity matrix is defined for equivalent current increments (ΔI_G^{eq}) as a function of the rotor angle of SGs (5.14).

$$\begin{bmatrix} I_G \\ I_L \end{bmatrix} = \begin{bmatrix} Y_A & Y_B \\ Y_C & Y_D \end{bmatrix} \begin{bmatrix} E_G' \\ V_L \end{bmatrix} \tag{5.13}$$

where I_L is load currents, and V_L is load bus voltages. From (5.8), equivalent current

$$I_G^{eq} = Y_{eq} E_G' \tag{5.14}$$

where the equivalent current injection and equivalent admittance matrix as follows

$$I_G^{eq} = I_G - Y_B Y_D^{-1} I_L \tag{5.15}$$

$$Y_{eq} = Y_A - Y_B Y_D^{-1} Y_C \tag{5.16}$$

I_G^{eq} is re-derived with ΔI_G^{eq} considering the sensitivity matrix (W) which is defined by taking the partial derivatives of the load flow equations, load and generator current injection equations [5.4]. W includes load dynamics and indicates how much rotor angle deviation ($\Delta\delta_G'$) changes the equivalent current injection from generator buses. Further, active power deviations (ΔP_{Gi}) are calculated according to ΔI_G^{eq} which is dependent on $\Delta\delta_G$.

$$I_G^{eq} = I_{G0}^{eq} + \Delta I_G^{eq} \tag{5.17}$$

$$\Delta I_G^{eq} = Y_A \Delta E_G' + Y_B \Delta V_L - Y_B Y_D^{-1} \Delta I_L \tag{5.18}$$

In (5.18), $\Delta E_G'$, ΔV_L, and ΔI_L can be written in terms of $\Delta\delta_G'$ with W [5.5].

$$\Delta I_G^{eq} = W \Delta\delta_G' \tag{5.19}$$

$$\Delta P_{Gi} = \sum_{j} E_i' W_{ij} \cos(\delta_i' - \varphi_{ij}) \Delta\delta_j' \tag{5.20}$$

Although the dynamic equivalencing method is utilized for the transient stability studies to increase the accuracy of equivalent current injections, it can be used to assess the contribution of WPPs for the synchronizing power support as given in (5.21). In the next sections, the analysis of synchronizing power with presence of WPPs and the assessment of the synchronizing power support of WPPs using the dynamic ward equivalencing method are addressed with a simplified test system.

$$\Delta I_G^{eq} = Y_A \Delta E_G' + Y_B \Delta V_L - Y_B Y_D^{-1} \left(\Delta I_L - \Delta I_G \right) \tag{5.21}$$

5.5 Synchronizing Power Analysis of Power Systems with WPPs

In [5.6], a generic power system model was developed to assess dynamic and transient performance characteristics of WPPs. The model comprises one WPP, one CPP (e.g. thermal or hydro power plant), and one main system which may be a CPP or an infinite bus. Moreover, an aggregated load is modeled. Modified version of this generic power system model, which is presented in Fig. 5.5, is employed for synchronizing power analysis. The aim of using the modified generic model is to illustrate the theory of the synchronizing power between two CPPs (or SGs) without increasing the complexity of the power system. The base case is designed with three CPPs (i.e. G1, G2, and G3) for the synchronizing power study, and then one of the CPP (i.e. G3) is replaced with a WPP to investigate its impact on the synchronizing power between the remaining CPPs. In the analysis, AVR and governor of CPPs are not modeled, and the simulations are performed for one second (i.e. duration for the first swing stability). The parameters of the G1, G2, and G3 are given in [3.1]. The WPP is modeled as the first order time delay which is mentioned in the modeling chapter (Chapter 3). Since the time frame for the synchronizing power is in the order of a few seconds, the detailed model of the wind turbine is not preferred for the simulations. Additionally, in the simulations the limitations of the active and reactive power control are not exceeded where the overall WPP response is assumed to provide the required power for the control method. For

the replacement of CPP case, the load flow conditions are kept same as the base case. The CPP under investigation is G2 in Fig. 5, thus the rotor angle and active power deviations are going to be compared between two cases. First, the lack of the synchronizing power due to the replacement of CPP is addressed, and then how the WPP can support the synchronizing power of CPPs is presented by using the dynamic ward equivalencing method.

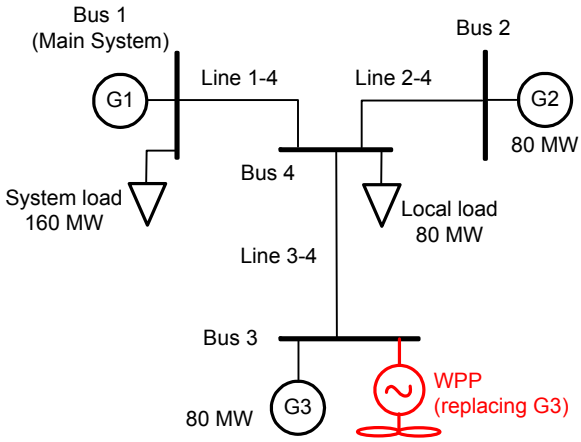

Fig. 5.5. Simplified generic power system model for synchronizing power studies

Using (5.9), (5.11), (5.12), and (5.14) self and mutual synchronizing powers of two cases are compared in Table 1 for G2. From Table 5.1, it can be concluded that the replacement of the CPP with the WPP reduce the synchronizing power between remaining CPPs. This impact of the WPP is illustrated with time domain simulations in Fig. 5.6. The load connected to Bus1 is increased with the step of 25% and 50% as a disturbance for both cases.

Table 5.1. Comparison of Synchronizing Powers of Two Cases

Cases	$K_{E,self,G2}$	$K_{E,mutual,G1\text{-}G2}$	$K_{E,mutual,G3\text{-}G2}$
Base Case	2.09	-1.02	-1.07
WPP Case	1.49	-1.49	-

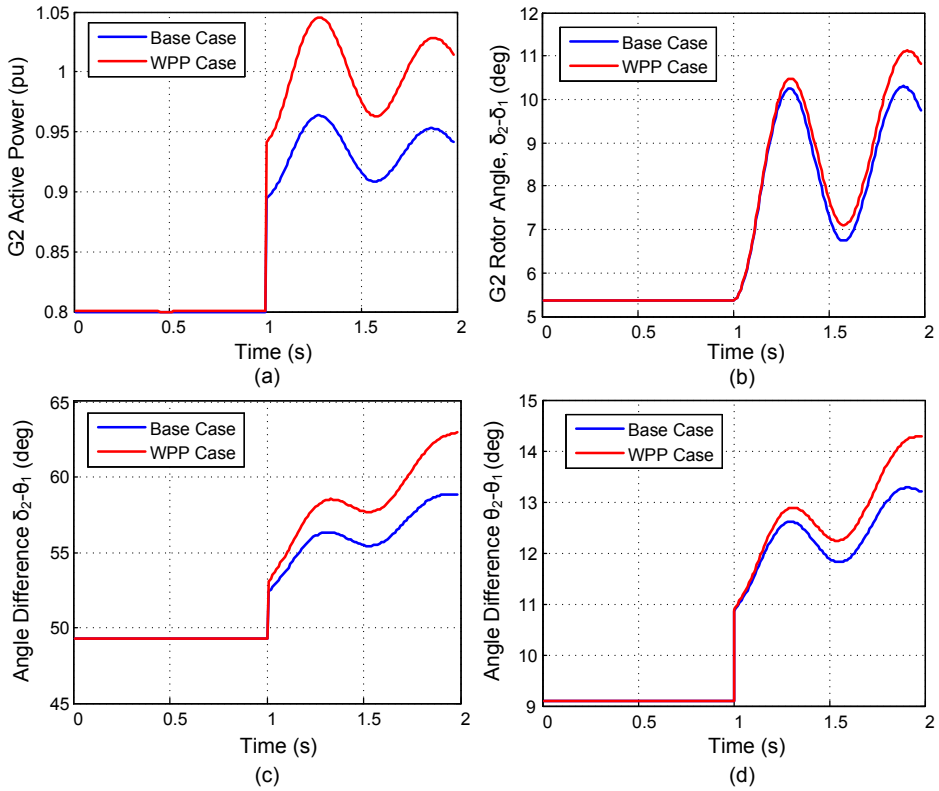

Fig. 5.6. Comparison of two cases for 25% load increase in terms of active power output of G2 (a), rotor angle of G2 with reference to G1 ($\delta_{2\text{-}1}$) (b), angle difference between rotor angle of G2 and Bus-1 angle (c), angle difference between Bus-2 and Bus-1 (d)

According to the Fig. 5.6, G2 is stable for both of the cases. However, in WPP case the active power output of G2 at the instant of the disturbance is increased compared to base case. The reason is that the WPP does not increase its active power output like the G3. Thus, the synchronizing power is reduced compared to base case. This can also be observed from the mutual synchronizing power of G2 in Table 5.1. Furthermore, the power system is forced towards the stability limits by increasing the system load connected to Bus5 50% step as another disturbance. The results are given in Fig. 5.7. According to these results, G2 is unstable regarding the high load increase related to the voltage stability. During the simulations excitation voltage is constant and bus voltages decrease to low values that the loads cannot be fed through. However, in both of the cases for different disturbances, only change is the replacement of G2 with the

WPP. Therefore, the lack of synchronizing power or in other words the lack of WPP's active power contribution following the disturbance leads the power system towards instability quickly compared to the base case. It is obvious that if the WPP has voltage control or reactive power support after the disturbance, it will stabilize the power system similar to the FACTs [5.7]. Reactive power support is important however, the loading of G2 will not be changed after the reactive power support following the disturbance. In the next section, different input signals, such as rotor angle deviation, bus voltage angle and magnitude deviations, are considered to increase active and reactive power output of the WPP in order to support synchronizing power and the power system stability.

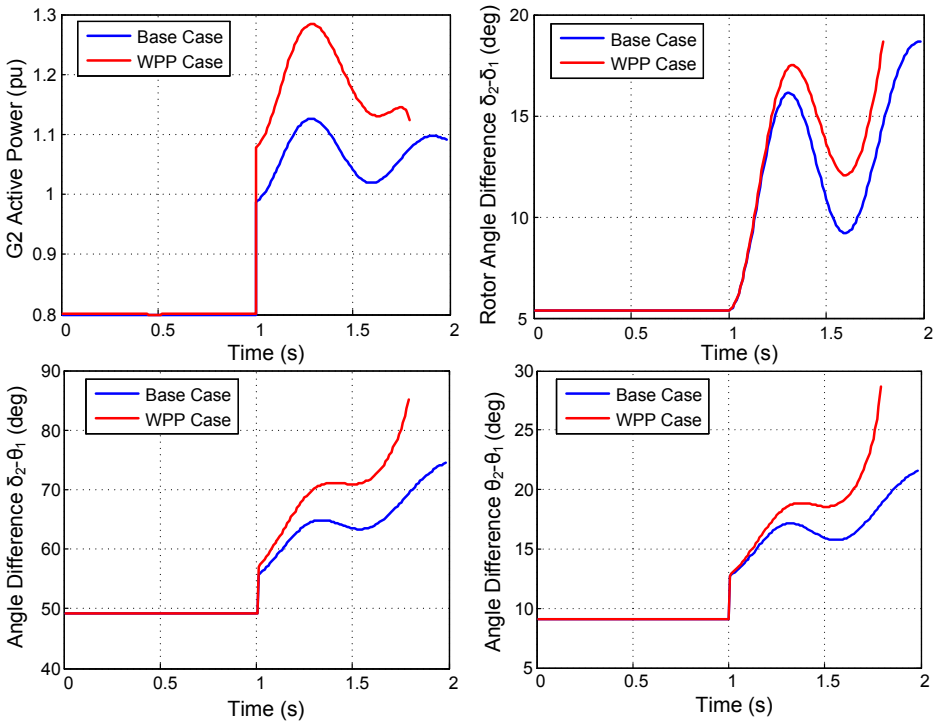

Fig. 5.7. Comparison of two cases for 50% load increase in terms of active power output of G2 (a), rotor angle of G2 with reference to G1 ($\delta_{2\text{-}1}$) (b), angle difference between rotor angle of G2 and Bus-1 angle (c), angle difference between Bus-2 and Bus-1 (d)

The dynamic ward equivalencing method is employed to assess the control method based on different input and output correlation (e.g. input: angle deviation output: active power or reactive power). The performance criterion of the synchronizing power support is to come close the base case performance.

5.6 Control Methods for Synchronizing Power Support from WPPs

To support the synchronizing power between G1 and G2, various input signals have been selected for the WPP. These signals can be angle difference and voltage deviation such as rotor angle deviation between G2 and G1 ($\Delta\delta_{21}$), angle difference between Bus2 and Bus1 voltage ($\Delta\theta_{21}$), angle difference between Bus2 and Bus3 voltage ($\Delta\theta_{23}$), angle difference between Bus3 and Bus1 voltage ($\Delta\theta_{21}$), and Bus3 voltage magnitude deviation (ΔV_3). The correlation between these input signals and WPP active and reactive power output is illustrated in Fig. 5.8. The control methodology of the synchronizing power support is to enable temporary active or reactive power according to the related input signal. The duration of the response is assumed two seconds. After the disturbance, this support will compensate the lack of the synchronizing power released by the replaced CPP (G3). For this reason, several configurations are proposed in Fig. 5.8. The dead-band block is optional and can be implemented within the enable signal. The dynamic ward equivalent method is modified and used to assess these control methods considering their impact on the active power increase of G2 (ΔP_2) with respect to rotor angle deviation of G1 ($\Delta\delta_1$).

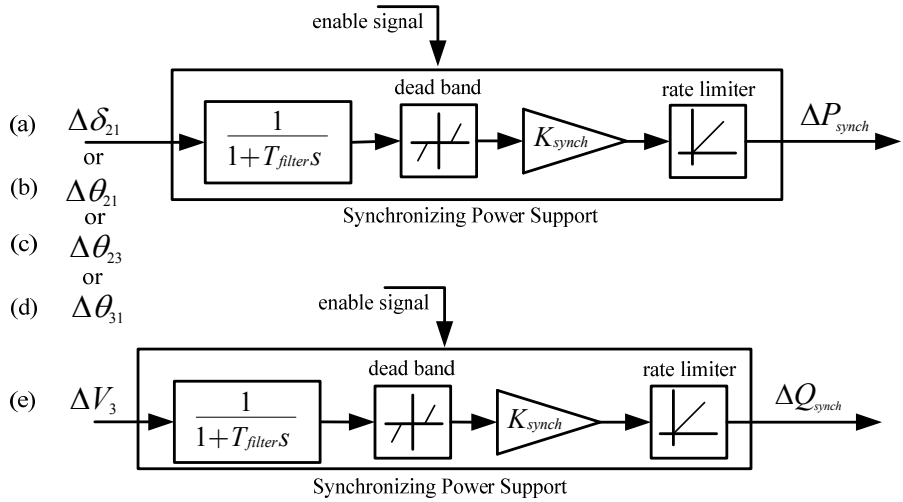

Fig. 5.8. Control candidates for the synchronizing power support; temporary active power increase based on rotor angle deviation (a), various angle deviations (b), (c), (d), and temporary reactive power increase based on voltage deviation (e)

According to the modified dynamic ward equivalencing analysis, $\Delta P_2/\Delta\delta_1$ is calculated for the proposed control methods above. This ratio can be treated as the mutual synchronizing power which is defined in (5.12). The difference is that when the modified dynamic ward equivalent analysis is employed, the reduced admittance matrix is not used but the load flow equations and the impact of the WPP is included (i.e. current injection of WPP). This analysis is applied to assess the proposed control methods above, and the results are given in Table 5.2. In the assessment of the proposed control methods, K_{synch} is assumed 1 pu, and the current and voltage dependency of the WPP's active and reactive power are modified with respect to the control methods.

Table 5.2. Assessment of Proposed Control Methods according to $\Delta P_2/\Delta\delta_1$

Control Methods	$\Delta P_2/\Delta\delta_1$
Without control	1.4
ΔP_{synch} dependent on $\Delta\delta_{21}$ (Fig 7. a)	1.8
ΔP_{synch} dependent on $\Delta\theta_{21}$ (Fig 7. b)	1.7
ΔP_{synch} dependent on $\Delta\theta_{23}$ (Fig 7. c)	1.5
ΔP_{synch} dependent on $\Delta\theta_{31}$ (Fig 7. d)	1.5
ΔQ_{synch} dependent on ΔV_3 (Fig 7. e)	1.4

Table 5.2 shows that the control method, which is using the rotor angle difference between G2 and G1 as an input signal and changing the active power output according to this signal, has more impact on $\Delta P_2/\Delta\delta_1$ (i.e. mutual synchronizing power) than the other methods. This is an expected result due to the control method which is directly dependent on the rotor angle deviations. This assessment is verified with the time domain simulations as shown in Fig. 5.9 and Fig. 5.10 for the 25% and 50% load increase, respectively. From the simulation results below, the modified dynamic ward equivalencing method has accurate results however, the performance criterion has not been achieved completely with the control methods due to slow variation of the input signals. The active power increase of G2 at the instant of the disturbance has not been changed immediately with the control methods. When the control methods increase the active/reactive power output of the WPP, the synchronizing power is increased between G2 and G1 which can be obtained from Fig. 5.9 and 5.10 (a). Only for the control method based on ΔV_3 input signal does not have sufficient impact on the mutual synchronizing power of G2. The damping of the power system oscillations has not been affected adversely by the proposed control methods. The prony analysis is conducted for the controls and the results are summarized in Table 5.3.

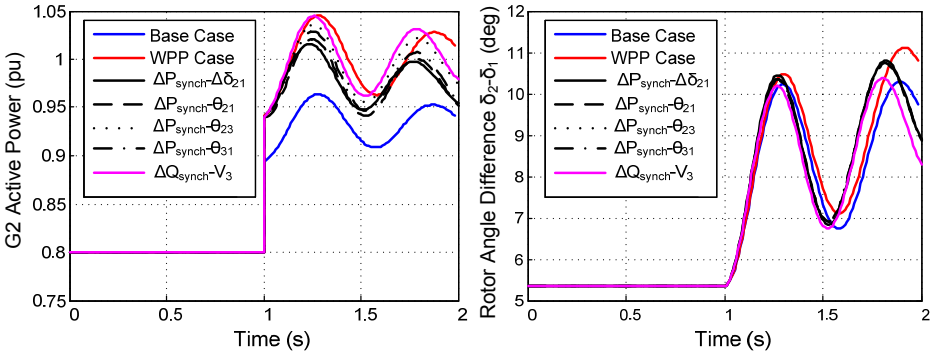

Fig. 5.9. Comparison of the control candidates for the 25% load increase in terms of active power output of G2 (a), and rotor angle of G2 with reference to G1 (δ_{21}) (b)

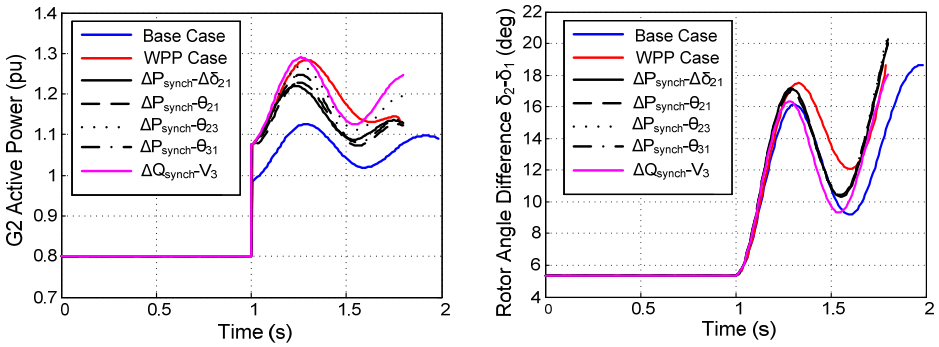

Fig. 5.10. Comparison of the control candidates for the 50% load increase in terms of active power output of G2 (a), and rotor angle of G2 with reference to G1 (δ_{21}) (b)

Table 5.3. Comparison of the Dominant Mode Frequency and Damping Ratio

Control Methods	**Frequency (Hz)**	**Damping (%)**
Without control	1.86	6.4
ΔP_{synch} dependent on $\Delta\delta_{21}$ (Fig 7. a)	1.87	6.9
ΔP_{synch} dependent on $\Delta\theta_{21}$ (Fig 7. b)	1.87	6.6
ΔP_{synch} dependent on $\Delta\theta_{23}$ (Fig 7. c)	1.86	6.4
ΔP_{synch} dependent on $\Delta\theta_{31}$ (Fig 7. d)	1.86	6.0
ΔQ_{synch} dependent on ΔV_3 (Fig 7. e)	1.88	6.1

Hitherto, the synchronizing power support for the transient conditions has been analyzed. In other words, the transient-power angle characteristic of G2 has been analyzed with the proposed control methods. The control methods can be also employed for the support of the steady-state characteristic. In order to analyze the impact of the proposed control on the steady-state synchronizing power, the system load is increased by a ramp-up rate which has the duration of five seconds. It represents slowly increasing load events in power systems. For this disturbance, due to time frame of the disturbance, excitation systems and governors of the CPPs have to be included into the CPPs' model. The structures and parameters of these controls have been chosen from the models in Chapter 3. The ramp increase of system load is applied as a disturbance in the modified generic power system to assess the proposed controls, and the simulation results are shown in Fig. 5.11. As it can be seen obviously, when there is an active power increase of the WPP by any control method regardless of the contribution amount, the steady-state characteristic of the G2 has been improved

compared to the without control case. The assessment of the control methods, which is given in Table 2, is also valid for this disturbance (Fig. 5.11 b). The control methods can be also realized as the de-loading of the CPPs by increasing WPP's active power output. The last control method has not been demonstrated in Fig. 5.11 due to the negligible voltage deviations.

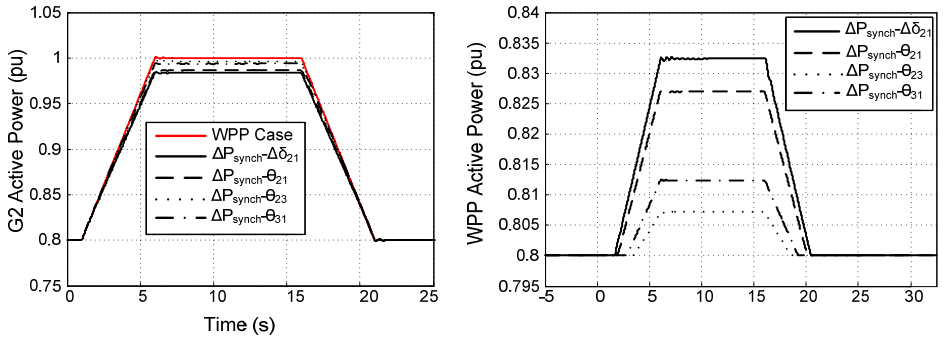

Fig. 5.11. Comparison of the control candidates for the ramp-load increase in terms of active power output of G2 (a) and WPP (b)

5.7 Summary

In this chapter, the impact of WPPs on the synchronizing power of CPPs for high wind power penetration scenarios which include replacement of some of the CPPs with the WPPs has been analyzed by means of extensive simulation studies. The synchronizing power of a SG has investigated from the literature in terms of the steady-state and transient characteristics. These characteristics have been reviewed for SMIB system which describes the rotor angle stability of one SG connected to infinite bus. Furthermore, the synchronizing power analysis of the multi-machine systems has been investigated, thus the self and mutual synchronizing powers of a SG have been defined. These synchronizing power definitions have been employed to assess the WPP impact on the rotor angle stability. When the WPPs are integrated to a power system, there are two ways to assess the impact; in the classical approach reduced network model has been utilized and the load and WPP impacts cannot be included. In the dynamic ward equivalencing approach, the load impact is included by the sensitivity matrix which is

calculated by the partial derivatives of the power flow equations and current injections of loads. The dynamic ward equivalencing approach has been modified in order to assess the WPP impact, and the active power deviations dependent on the rotor angle variations has been calculated considering the WPP current injections.

The generic power system model has been utilized for the synchronizing power analysis. In this model, for the base case there are three CPPs, and for the WPP case one of the CPP has been replaced by a WPP. The reason is to investigate the impact of the WPP on the synchronizing power of the remaining CPPs. Accordingly the investigation is conducted for both cases using the modified dynamic ward equivalent approach and time domain simulations. The consistency of the modified approach is verified with the time domain simulations. Furthermore, the control methods to support the synchronizing power have been proposed. The assessment of these control methods has been carried out, and as a result the control method, which increases the active power output of the WPP based on rotor angle deviation, has more impact on the synchronizing power. Other control methods based on bus voltage angle deviation can be also considered and their gain parameters can be increased to obtain the same impact of the control based on rotor angle deviation according to the modified dynamic ward equivalent approach. On the other hand, the control method which modifies the reactive power output of the WPP based on the voltage deviation at its PCC point has smaller impact compared to other control methods, however in the generic power system model the PCC point short circuit ratio and the effect of the excitation systems are important for this control method. For the future work, real power system models which comprise congested lines and bottlenecks for the active power transfer can be investigated. Additionally, the practical consideration of the bus voltage angle measurements should be implemented into the simulations, such as sampling time, communication delays, etc.

5.8 References

[5.1] IEEE/CIGRE Joint Task Force, "Definition and Classification of Power System Stability," Jun. 2003.

[5.2] J. Machowski, J. W. Bialek, and J. R. Bumby, *Power system dynamics: stability and control*, 2008, John Wiley & Sons.

[5.3] H. Rudnick, F. M. Hughes, A. Brameller, "Steady State Instability: Simplified Studies in Multimachine Power Systems," *IEEE Trans. Power Apparatus and System,* PAS-102, no.12, 3859-3867, Dec. 1983.

[5.4] G. W. Stagg, A. H. El-Abiad, *Computer methods in power system analysis*, 1968, Mc-Graw-Hill.

[5.5] T. Baldwin, L. Mili, and A. G. Phadke, "Dynamic ward equivalents for transient stability analysis," *IEEE Trans. Power Syst.*, vol. 9, pp.59-67, 1994.

[5.6] O. Anaya-Lara, F. M. Hughes, and N. Jenkins, "Generic network model for wind farm control scheme design and performance assessment," *Proc. EWEC*, London, UK, 2005.

[5.7] E. Acha, C. R. Fuerte-Esquivel, H. Ambriz-Pérez, C. Angeles-Camacho, *FACTS: Modeling and Simulation in Power Networks*, 2004, Wiley.

Chapter 6
Conclusions and Future Work

With the integration of large WPPs, the power system stability will be affected for the high wind power penetration scenarios in the future particularly for the island power systems such as UK, Ireland, etc. According to the initial wind integration studies conducted by TSOs have claimed that WPPs should behave like CPPs. According to these studies, the draft versions of grid codes for integration of wind power have been published and discussed with the WPP owners and WT manufacturers. However, the details of these requirements are not clearly specified in terms of the generic parameters considering the power system characteristics, and this situation leads to the manufacturers' objections. More studies and discussions are still required for investigating the power system requirements and enhancing the capability of WPPs according to these investigation results.

The main focus of this thesis is the analysis of power system requirements for the synchronizing power support and inertial response control of WPPs in high wind power penetration scenarios. Considering the performance of a generic power system obtained analysis results are evaluated thus, a new control method has been proposed for inertial response of WPPs. Additionally, an assessment methodology of the synchronizing power support from WPPs has been developed. In order to implement and simulate the generic power system, WPPs and proposed control method, appropriated models are presented with an RMS simulation platform.

In this chapter, the conclusions of this thesis and the possible future works associated with this thesis are elaborated as follows.

6.1 Conclusions

In this thesis, WPPs consist of FC-VSWT are main concern in power systems with high wind power penetration levels. Therefore, symmetrical stead-state representation of a generic power system with various wind power penetration scenarios and a WPP (simplified and aggregated models) have been presented for the wind integration studies. Moreover, for the simulations of the inertial response control and synchronizing power support studies an RMS toolbox has been developed. According to the simulation results, which include the operation of WPPs in the island and weak power systems, the controller parameters should be carefully tuned to represent the realistic behavior of the WPP and not to cause any instability. In order to validate the aggregated WPP model, step response of active and reactive power controls are compared with the model developed in RISO, Wind Energy Systems Department. As a result of the comparison of two models, there is no significant difference for the electrical and control part of the WPP model. However, for the wind turbine part standard models are required, and further concern is needed for the aggregation approach of WPPs and the tuning methodology of the control loops considering the connected power system characteristics.

For the inertial response control, classification of the existing control methods has been made regarding the profile of the active power support. Accordingly, the sensitivity analysis of these control methods has been performed to investigate the requirements of the power systems. Based on the results of the sensitivity analysis a new control method is proposed which improves the performance of WPPs' inertial response in terms of less energy release and peak active power compared to the existing control methods. The tuning methodology of the proposed control can help TSOs about the requirement specification of the inertial response control for any power systems with high wind power penetration. Additionally, for the operation of low wind speed the

recovery period has less impact on the system frequency again compared to the previous methods.

As a result of the synchronizing power support investigations, the replacement of CPPs in high wind power penetration scenarios reduces the synchronizing power between the remaining CPPs. Based on the simulations, the instability situations have not been experienced with the sudden load increase as a disturbance; however the weak synchronizing power links may cause instability of power systems in N-2 contingency or in quasi-steady state points. The developed assessment methodology describes the impact of WPPs and also the contribution of WPPs to support synchronizing power in different ways.

To summarize, the contributions below are presented in this thesis:

- The proposed control method provides improved inertial response for WPPs in high wind power penetration scenarios. With the tuning methodology of the proposed control, parameters of the proposed control are specified for any power system.
- The assessment of the proposed control and existing control methods have been performed in the generic power system with various wind power penetration scenarios.
- The assessment methodology for the synchronizing power between CPPs is developed in the case of the replacement of CPPs.

6.2 Future work

The objectives stated for the thesis are achieved within the scope and limitations. However, further improvements can be done as follows:

- WPP model can be improved including each wind turbine operating conditions and collector system.
- Analysis of dispatch algorithm for the proposed inertial response control method can be performed aiming the minimum recovery period of the overall WPP.

- Real power system models can be employed for both the inertial response control and synchronizing power support studies in cooperation with TSOs.
- The realistic estimation of frequency deviation and ROCOF can be implemented and with the real frequency measurements in the simulations.
- Coordination of WPPs for the inertial response control can be analyzed to reduce the impact of the recovery period of WPPs.
- Realistic N-1 and N-2 contingencies can be used for the synchronizing power studies to highlight the importance of the synchronizing power support from WPPs with collaboration of TSOs.
- The measurement and calculation of angles can be considered with the representation of phasor measurement units to improve the synchronizing power support.

6.3 List of publications

P1. M. Altin, R. Teodorescu, B. Bak-Jensen, P. Rodriguez and P. C. Kjær, "Aspects of Wind Power Plant Collector Network Layout and Control Architecture," The Danish PhD Seminar on Detailed Modeling and Validation of Electrical Components and Systems 2010.

P2. M. Altın, Ö. Göksu, R. Teodorescu, P. Rodriguez, B. Bak-Jensen, L. Helle, "Overview of Recent Grid Codes for Wind Power Integration," 12th International Conference on Optimization of Electrical and Electronic Equipment (OPTIM), 2010.

P3. M. Altin, R. Teodorescu, B. Bak-Jensen, P. Rodriguez, F. Iov, P. C. Kjær, "Wind Power Plant Control - An Overview," 9th International Workshop on Large-Scale Integration of Wind Power into Power Systems, pp. 581-588, 2010 Proceedings ISBN 978-3-9813870-2-5.

P4. M. Altin, R. Teodorescu, B. Bak-Jensen, U. D. Annakage, F. Iov, P. C. Kjaer, "Methodology for Assessment of Inertial Response from Wind Power Plants," IEEE Power and Energy Society General Meeting 2012.

P5. A. Adamczyk, M. Altin, O. Goksu, R. Teodorescu, F. Iov, "Generic 12-Bus Test System for Wind Power Integration Studies," EPE Joint Wind Energy and T&D Chapters Seminar, Aalborg, Denmark, Jun. 2012.

P6. M. Altin, A. Adamczyk, R. Teodorescu, B. Bak-Jensen, U. D. Annakage, F. Iov, P. C. Kjaer, "Improved Inertial Response Control for Wind Power Plants," submitted to *IEEE Transactions on Power Systems*.

Publications

[P1] published in The Danish PhD Seminar on Detailed Modeling and Validation of Electrical Components and Systems 2010

Aspects of Wind Power Plant Collector Network Layout and Control Architecture

M. Altin, R. Teodorescu, B. Bak-Jensen, P. Rodriguez and P. C. Kjær

ABSTRACT

Recent developments in wind turbine technology go towards the installation of larger Wind Power Plants (WPPs) both onshore and offshore. As wind power penetration level increases, power system operators are challenged by the penetration impacts to maintain reliability and stability of power system. Therefore, connection topology and control concepts of large WPPs should be carefully investigated to improve the overall performance of both the WPP and the power systems. This paper aims to present a general overview of the design considerations for the electrical layout of WPPs and the WPP control strategy for optimum power generation while fulfilling the power system operators' requirements.

I. INTRODUCTION

As fossil fuel energy sources have dwindled and global warming increases, renewable energy sources attract more attention. Wind energy is one of the leading alternatives among these sources. The rapid growth of wind industry over the last decades brings along a lot of study and research for integration of wind energy to conventional power systems. In addition to technological and economical developments in wind turbine technology, governments have granted funds for research and support in renewable energy sources.

The important benefits of wind energy are reduced CO_2 emission, reduced operational cost (as no fuel is required) and adding capacity value to a power system (ability to contribute to peak demands). However, these advantages are available only when WPPs operate according to the regulations that are prescribed by power system operators for the stability and reliability of the system [1], [2]. Considering these regulations, WPP designers should design internal electrical system, as well as control structure of the WPP.

The main function of the internal electrical system is to collect power from each Wind Turbine Generator (WTG) spread over the entire WPP and to transmit it to the power system. Electrical collector systems can be designed using different topologies depending on the size, location (onshore or offshore), and terrain of the WPP [3], [4]. Because of the practical limitations, collector system design must be evaluated from economic and reliability point of view [5], [6].

Furthermore, the WPP control structure, which consists of centralized controller and individual WTG controllers, regulates the WPP power production [7]. WPP operators are able to control entire power plant by a centralized controller which is an interface between the power system operator and the WPP. The centralized controller should be implemented to satisfy the requirements of the power system operator in coordination with the WTG controllers [8], [9].

In this paper considerations for the collector system design regarding power loss optimization, reliability and economics are presented. Additionally, a hierarchical WPP control structure for optimum active and reactive power generation is introduced. Thereby, the overall WPP should be able to satisfy the power system operators' requirements.

In Section II, an overview of the grid codes of Germany and Denmark is briefly introduced as a general instance of common requirements. The collector system design considerations including optimization of power losses, economic and reliability evaluations are presented in Section III. Section IV introduces WPP control strategies in a coordinated and hierarchical structure. In the closing section, future work and milestones of the work is provided.

II. GRID CODE REQUIREMENTS

The transmission system operators (TSOs) are responsible for network operations in steady-state and transient conditions. According to TSOs' perspective, it must be proven for the power plants connected to transmission network that the reliability and stability of the grid should not be adversely affected. Thus the technical requirements, which are commonly referred to as grid codes, must clearly define the connection criteria of the WPPs into the transmission network. Recently there has been a lot of research and study on revising grid codes. However, it has to be considered, that every country has different connection criteria for the wind power and national regulatory frameworks require continuous changes due to the developments in the wind turbine technology.

This work was supported by Vestas Wind Systems A/S.

M.A. is a PhD student at Department of Energy Technology, Aalborg University, 9220 Aalborg, Denmark (e-mail: mua@iet.aau.dk, phone no. +45 9940 9283).

R.T. is with Department of Energy Technology, Aalborg University, 9220 Aalborg, Denmark (e-mail: ret@iet.aau.dk)

B.B-J. is with Department of Energy Technology, Aalborg University, 9220 Aalborg, Denmark (e-mail: bbj@iet.aau.dk,).

P. Rodriguez is with the Technical University of Catalonia, Spain. (e-mail: pro@iet.aau.dk).

P.C.K. is with the Vestas Wind Systems A/S, 8200 Århus, Denmark (pck@vestas.com)

Paper submitted to the PhD Seminar on Detailed Modelling and Validation of Electrical Components and Systems 2010 in Fredericia, Denmark, February 8th, 2010

The new grid codes treat the WPPs in such a way that they should contribute power system control similar to conventional power plants [1]. In the literature, technical analysis and overview of technical requirements regarding the connection of large WPPs to the transmission system are provided [10], [11]. In [11], the grid codes of several countries and comparison of their most recent available editions are presented. This paper narrows down the overview to Germany and Denmark grid codes, just to give an idea of the common requirements.

According to the grid codes, the technical requirements are defined for the connection and operation of WPPs connected to transmission system [1], [2]. These requirements cover:

- FRT requirements,
- Active power and frequency control,
- Reactive power control,
- Frequency and voltage operating range.

The FRT or low voltage ride through (LVRT) requirements are described in such a way that WPPs must withstand voltage dips to a certain percentage of the voltage level for a specified duration in the grid codes. These voltage characteristics depend on protection system of the network and fault location. The FRT requirements also include fast active and reactive output power restoration after a fault clearance.

The active power and frequency control requirements define the regulation of WPP active power output and the frequency response to control their active power outputs with respect to frequency deviations. Moreover, WPPs can actively participate in active power regulation using various control strategies [2]. This control should require ancillary services such as participation in primary and secondary frequency control.

Reactive power control capabilities are also required by the grid codes. It is performed either by setting a reactive power value or power factor value. Further, reactive power control should be extended for controlling voltage at the WPP grid connection point or at the distant node (secondary voltage control).

In addition to control and response capabilities, grid codes stated that WPPs must operate over an extended range of system voltages and frequency deviations from the nominal operating values. For these operating ranges, limited period of continuous operation and active power reduction is allowed.

A. Germany [1]

1) FRT Requirements

According to the *Transmission Code 2007* [1], the FRT requirements are given in Fig. 1 for single, dual, and triple pole short circuits (with and without earth contact) or fault induced symmetrical and asymmetrical voltage dips. The curve characteristic represents the voltage magnitude associated with the time duration during which the WPP must remain connected.

The grid code defines the following FRT requirements:

- Above the borderline 1, voltage drops should not lead to WPP disconnection.
- The voltage dips within the shaded area between the borderline 1 and borderline 2 should not lead to instability or disconnection of the WPP. However, in case of WPP instability, short-time disconnection is allowed. The resynchronization must be completed at most 2 s and after fault clearance active power feed-in must be increased with a gradient of 10% of the nominal capacity per second.

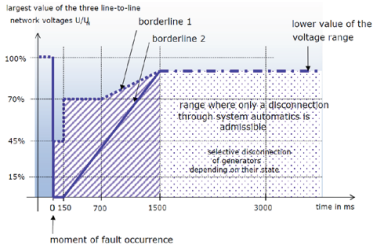

Fig. 1. Limit curve for the FRT requirements of the *Transmission Code 2007* [1]

- Below the borderline 2, disconnection of the WPP is allowed and also a short-time disconnection of the WPP from the network is always permitted (Resynchronization period may be more than 2 s and the active power gradient may be less than 10%).
- For all WPPs which are not disconnected during the fault, active power must be maintained immediately after the fault clearance and increased to the original value with a gradient of at least 20% of the nominal capacity per second.
- For reactive current feed-in for voltage backup, in the case of network voltage above the borderline 1, the requirements are shown in Fig. 2. *K* value should be in the range of 0 and 10 and it must be adjustable. Additionally, WPP disconnection time delays associated with voltage level are specified in *Transmission Code 2007*.

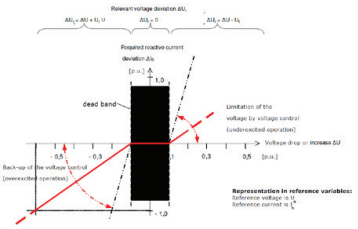

Fig. 2. Reactive output current during disturbances [1]

2) Active power and frequency control

The active power reduction must be satisfied with at least 10% of the network connection capacity per minute. And frequency response of the WPP is shown in Fig. 3 similar to the droop characteristic of a conventional power plant for over-frequencies. However, there is no limitation for the frequency band between 47.5 and 50.2 Hz. WPP is allowed to disconnect below 47.5 Hz and above 51.5 Hz.

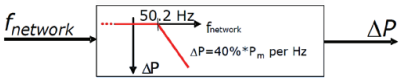

Fig. 3. Active power reduction of WPPs in the case of over-frequency [1]

3) Reactive power control

The reactive power control requirements are defined for various ranges of reactive power or power factor at rated active power. Each WPP must meet the requirements at the grid connection point to one of the variants of Fig. 4. The TSO shall select one variant with respect to the relevant network conditions. The reactive power output of the WPP must be able to reach the set value within 4 minutes.

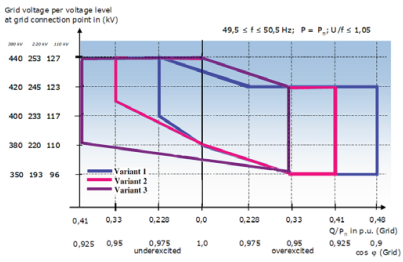

Fig. 4. WPP reactive power (or power factor) requirements at the grid connection point (Variants 1-3) [1]

4) Frequency and voltage operating range

WPP must operate continuously within certain voltage and frequency variation limits during the normal operation of the system. Further, they must remain in operation even in case of voltage and frequency disturbances outside the normal operating limits. Fig. 5 shows the operating voltage (at the grid connection point) and frequency limits for WPPs.

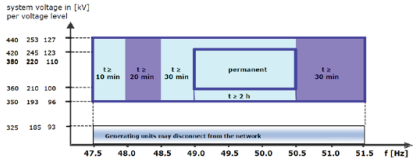

Fig. 5. Operating frequency and voltage limits for WPPs [1]

B. Denmark [2]

The Danish requirements which are presented in this paper should apply to WPPs connected to grids with voltages above 100 kV (the transmission system) [2].

1) FRT Requirements

The FRT requirements define that the WPP must remain connected after the faults or sequence of faults that are shown in Table I.

TABLE I
FRT REQUIREMENTS OF DANISH GRID CODE FOR WPPS CONNECTED TO THE GRIDS ABOVE 100 KV [2]

Type of the fault	**Duration of the fault**
Three-phase short circuit	Short circuit in 100 ms
At least two three-phase short circuits	Shorts circuits within 2 mins
Two-phase short circuit (with/without earth contact)	Short circuit in 100 ms followed by new short circuit 300-500 ms later, also with a duration of 100 ms
At least two two-phase short circuits	Shorts circuits within 2 mins
Single-phase short circuit to earth (earth fault)	Single-phase earth fault 300-500ms later, also with a duration of 100 ms
At least two single-phase earth faults	Shorts circuits within 2 mins

According to Danish grid code, behavior of the grid during a three-phase fault is illustrated in Fig. 6 for simulation purposes. Technical details are defined in the grid code [2].

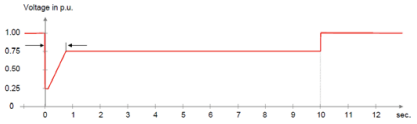

Fig. 6. Voltage profile for simulation of three-phase faults in Danish grid code [2]

Additionally, WPPs must have sufficient energy reserves in terms of emergency power, hydraulics and pneumatics for the following three independent sequences:

- At least six three-phase short circuits with 5-min intervals
- At least six two-phase short circuits with 5-min intervals
- At least six single-phase earth faults with 5-min intervals

2) Active power and frequency control

The grid code [2] demands WPPs to have ability of active power regulation speed (both upward and downward) with a ramp rate 10-100 % of rated power per minute.

By frequency regulation WPPs must change the active power production with respect to the grid frequency deviations. Fig. 7 shows two cases of frequency control. In case 1, the frequency control can only regulate the active power production in downward direction, whereas in case 2, it can also make upward regulation due to the previous

downward regulation. The frequencies applied to this figure are depicted in the grid code [2].

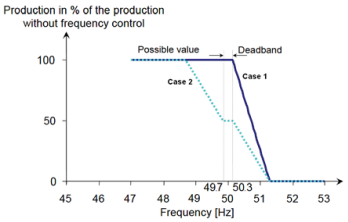

Fig. 7. Active power-frequency response [2]

3) Reactive power control

WPP must control its reactive power output that as a mean value over 10 seconds must be kept within the control band, as shown in Fig. 8.

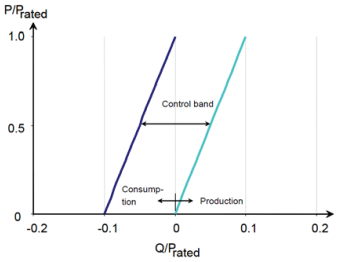

Fig. 8. Requirements concerning the WPP's exchange of reactive power at the grid connection point [2]

4) Frequency and voltage operating range

WPP must continue power production at voltages and frequencies that deviate from normal operating conditions. Fig. 9 indicates normal and time-limited operating conditions of the WPP. Abnormal voltages and frequencies will occur in less than ten hours per year.

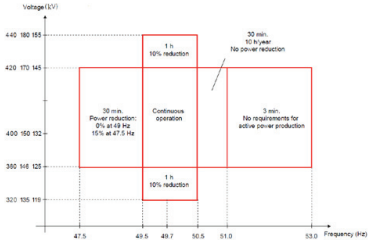

Fig. 9. Operating frequency and voltage limits for WPPs [2]

C. Comparison of German and Danish Grid Code Requirements

From the grid codes presented above, it can be clearly noticed that the interconnection requirements for WPPs have common concepts. However, they vary from country to country due to the inherent network structure.

In the German grid code, there are more options regarding FRT and reactive power control requirements for the WPP operator. In the Danish grid code, however, for the FRT requirement point of view, fault types and duration of the faults, which may occur in the transmission system, are clearly described. On the other hand, WPP operational voltage and frequency ranges are much flexible in Danish grid code. Active power control and frequency control requirements are very similar in both transmission codes, but they leave WPP primary and secondary frequency control issues to the bilateral agreements between the TSO and WPP operator.

III. WPP COLLECTOR SYSTEM DESIGN

The WPP collector system generally consists of WTGs, step-up transformers, network of cables which collect the power from each WTG, switching equipments, protection relays and collector substation where the collected power is transmitted to the transmission system. If WPP capacity increases, collector system performance becomes particularly important.

WPP location (onshore or offshore) and terrain are significant factors for designing collector system. Terrain characteristics determine whether the collector system consists of overhead lines, underground or subsea cables. Furthermore, WTG locations in the wind farm are optimized with respect to wind regime and site [12], [13]. Collector substation location and grid connection point can also be constrained by the terrain.

Once the WTG locations and grid connection point are decided, collector system layout, which is also referred to as feeder topology, must be configured by selecting and routing the cables. The number of WTGs located on a collection feeder is limited by the cable ampacity and the voltage level of the collector system. System reliability is another design consideration to maintain sustainable power. The reliability aspect covers redundancy, protection system, fault location, and service restoration systems. Typical configurations that have different levels of redundancy are illustrated in Fig. 10 [3]:

- Radial designed and radial operated feeder structure Fig. 10a ,
- Ring designed and radial operated feeder structure Fig. 10b and Fig. 10c,
- Star designed and radial operated feeder structure Fig. 10d.

The solutions that provide adequate reliability will increase capital investments and can increase power losses. A technique that translates power losses (fixed, variable losses and losses

due to unavailability of the system) into initial capital investment should be used for economic evaluation of the collector system. By using expected financial return investment in the economic evaluation for WPP economic factors (fixed losses factor, variable losses factor, and system unavailability losses factor), design alternatives are shown to be favorable [5].

On the other hand, collector layout affects protection system design such that in some cases, it may be difficult to distinguish faults and make selective coordination of the layout. Therefore, in the early stage of the collector system design, protection scheme should be considered and protection evaluation factor may be introduced such as reliability assessment factor [14]. Short circuit current capacity, types and numbers of protection relays, additional switching equipment and relay cost, and selective coordination level (numbers of relays, which can be coordinated) can be the protection evaluation factors.

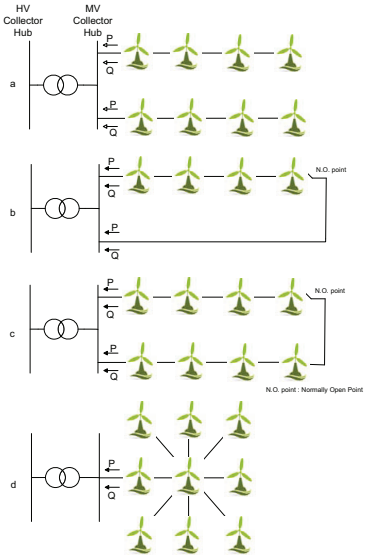

Fig. 10. Typical feeder configurations of WPPs.

IV. WPP CONTROL

The grid code specifications mentioned in Section II force the WPPs to participate in power system control similar to conventional power plants. WPP control structure should be designed including control of output power fluctuations (because of the intermittent nature of wind), primary frequency control, secondary frequency control, reactive power regulation, and secondary voltage control. To perform these control functions, the WPP must have a hierarchical structure such as a centralized (main) controller and WTG controllers. The main controller determines active and reactive power set points, which are ordered by the TSO, for each WTG. At the local control level, WTG controller ensures that the received set points are reached. In this scheme the main controller is responsible for the overall optimum power production of the plant considering the collector system power losses and availability of wind power [15]. In Fig. 11, an overall diagram of the centralized controller is shown [8].

The control functions mentioned above should be distributed among the main and WTG controllers in the following manner:

- Main controller functions:
  - Active power control of WPP,
  - Secondary frequency control,
  - Reactive power control of WPP,
  - Voltage control of WPP (at the grid connection point and a distance point).
  - Wind Prediction
- WTG control functions:
  - Active power control of WTG,
  - Reactive power control of WTG,
  - Primary frequency control,
  - FRT control.

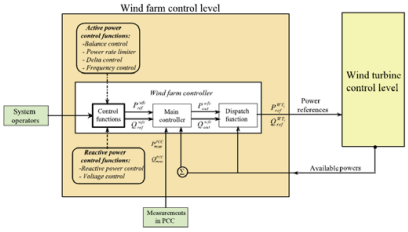

Fig. 11. WPP main controller [8].

Furthermore, the centralized controller should operate in coordination with each WTG controller to satisfy stability and robustness of the WPP, thus it is operated as a conventional plant. A *cluster controller* shown in Fig. 12 can be a novel option to satisfy this coordination. It can be basically described as a control level between the main controller and a group (cluster) of WTG controllers. The centralized controller shares its responsibilities with the distributed cluster controllers. These controllers are responsible for a group of WTGs (with respect to the collector layout) in a decentralized way. The cluster controller should include fault location and service restoration functions, which are automated processes, for the collector system, short-term wind forecasting function for optimum generation, and redundant control in case of emergency. Hereafter the centralized and WTG controller

hierarchy is defined as 2-level control, and the centralized, cluster and WTG controller hierarchy is named as 3-level control structure.

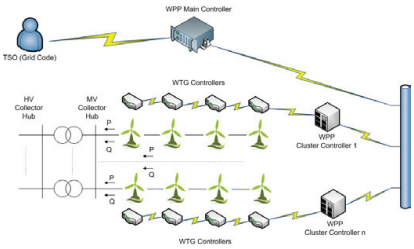

Fig. 12. WPP cluster controller concept.

In 2-level control structure, the centralized controller sends out set points, WPP operator commands to WTGs and gets related measurement data from the WTGs. All data should be processed in the centralized controller, thus there is a lot of network traffic in the WPP. However, the cluster controllers in 3-level control structure manage the network traffic and optimize the bandwidth of the network for faster communication. 3-level control structure is more reliable due to redundant control that during a communication failure between the cluster and centralized controller, the cluster control can perform the centralized controller's functions. In 3-level control structure, protection scheme will also have additional features such as group tripping of WTGs, faster fault detection and service restoration concerning a sub-area of the WPP not the whole WPP.

V. CONCLUSION

In this paper, an overview of German and Danish grid code requirements, the WPP collector system design considerations and the WPP control structure were presented. The objective of the grid codes is to specify WPPs' regulation and control capabilities for safe, reliable and economic operation of the power system. Grid codes may also be used for the modelling of the transmission system.

WPP collection system design decisions have been playing a critical role to efficient operation of the WPP. There are many challenges regarding power losses, economics, protection system and reliability. The tradeoffs between these challenges point out the importance of the design considerations and evaluation techniques to decide optimum configuration. Further study can integrate economic evaluation, steady state analysis (load-flow, loss calculation, short-circuit calculation), reliability assessment, protection and generation automation system analysis to develop an optimization platform.

To fulfill grid code requirements, the WPP control structure should have the functions presented in Section IV. The control strategy is similar to the Automatic Generation Control (AGC) concept of centralized dispatch centre in transmission system. For future study AGC experiences can be used to improve WPP control algorithm including optimization active and reactive power control due to the collector system layout and availability of the generation. Fast communication and redundant control are the primary drivers for the 3-level control structure. This structure should be required for redundancy, reliability, fault detection and service restoration functions in the WPP. To compare 2-level and 3-level control structure, communication time sensitivity and economic evaluation analyses should be required.

VI. REFERENCES

[1] 'Transmission Code 2007, Network and System Rules of the German Transmission System Operators' (VDN, Verband der Netzbetreiber August 2007).

[2] 'Grid connection of wind turbines to networks with voltages above 100 kV, Regulation TF 3.2.5' (Energinet, Denmark, December 2004).

[3] G. Quinonez-Varela, G. W. Ault, O. Anaya-Lara, and J.R. McDonald, "Electrical collector system options for large offshore wind farms," *IET Renewable Power Generation*, vol. 1, pp. 107-114, June 2007.

[4] IEEE PES Wind Plant Collector System Design Working Group, "Wind power plant collector system design considerations," in *2009 Power & Energy Society General Meeting*, pp. 1–7.

[5] R. A. Walling, T. Ruddy, "Economic optimization of offshore windfarm substations and collection systems," in *Proc. 2009 V-th International Workshop on Large-Scale Integration of Wind Power and Transmission Networks for Offshore Wind Farms*, pp. 396–402.

[6] M. Scutariu, "Techno-economical optioneering of offshore wind farms electrical systems," in *2007 PowerTech Conf.*, pp. 2195–2200.

[7] J. R. Kristoffersen, P. Christiansen, "Horns Rev offshore windfarm: its main controller and remote control system," *Wind Engineering*, vol. 27, pp. 351-359, Sept. 2003.

[8] A. D. Hansen, P. Sorensen, F. Iov, F. Blaabjerg, "Centralised power control of wind farm with doubly fed induction generators,"*Renewable Energy*, vol. 31, pp. 935-951, May 2006.

[9] J. L. Rodriguez-Amenedo, S. Arnalte, J. C. Burgos, "Automatic generation control of a wind farm with variable speed wind turbines," *IEEE Transactions on Energy Conversion*, vol. 17, pp. 279-284, June 2002.

[10] I. Erlich, U. Bachmann, "Grid code requirements concerning connection and operation of wind turbines in Germany," in *Proc. IEEE Power Engineering Society General Meeting, 2005*, pp. 1253 - 1257.

[11] M. Tsili, S. Papathanassiou, "A review of grid code technical requirements for wind farms," *IET Renewable Power Generation*, vol. 3, pp. 308-332, Sept. 2009.

[12] S.H. Jangamshetti, V.G. Ran, "Optimum siting of wind turbine generators," *Power & Energy Society IEEE Transaction on Energy Conversion*, vol. 16, pp. 8 - 13, March 2001.

[13] G. Marmidis, S. Lazarou, E. Pyrgioti, "Optimal placement of wind turbines in a wind park using monte carlo simulation," *Elsevier Renewable Energy*, vol. 33, pp. 1455–1460, July 2008.

[14] E. Clarke, *Reliability Evaluation of Power Systems*, 2nd edition, New York: Plenum Publishing Corporation, 1996.

[15] R. G. D. Almeida, E. D. Castronuovo, J. A. P. Lopes, "Optimum Generation Control in Wind Parks When Carrying Out System Operator Requests," *IEEE Transactions On Power Systems*, vol. 21, pp. 718-725, May 2006.

[P2] published in Proceedings of Conference on Optimization of Electrical and Electronic Equipment (OPTIM), 2010

Overview of Recent Grid Codes for Wind Power Integration

Müfit Altın*, Ömer Göksu*, Remus Teodorescu*, Pedro Rodriguez**, Birgitte-Bak Jensen*, Lars Helle***
* Aalborg University, Dept. of Energy Technology, Denmark
**Universitat Politecnica de Catalunya, Spain
***Vestas Wind Systems A/S, Denmark
mua@iet.aau.dk

***Abstract*- As wind power penetration level increases, power system operators are challenged by the penetration impacts to maintain reliability and stability of power system. Therefore, grid codes are being published and continuously updated by transmission system operators of the countries. In this paper, recent grid codes, which are prepared specially for the large wind power plants, are analyzed and compared. Also, harmonization of different grid codes in a common manner and future trends are assessed.**

I. INTRODUCTION

Wind power penetration to power systems increases in large amounts worldwide. The transmission system operators (TSO) have revised their grid codes which are technical interconnection requirements for the wind power plants (WPP). There are also different requirements for the distribution system operators (DSO) however, the grid codes, which are surveyed in this paper, are related only for transmission systems.

The grid codes are significant due to the following statements:

- TSOs must maintain stability and reliability of power dispatch regardless the generation technology.
- The technical negotiations between TSOs and power plant operators must be clear, transparent and reduced as much as possible.
- On the power plant manufacturer side, they must design equipments and controllers considering these grid codes, and they should not make changes without the TSO's permission.

Conventional power plants, which are composed of synchronous generators, are able to support the stability of the transmission system by providing inertia response, synchronizing power, oscillation damping, short-circuit capability and voltage backup during faults. These features allow the conventional power plants comply with the grid codes, thus today TSO have a quite stable and reliable grid operation worldwide.

Wind turbine generator technical characteristics, which are mainly fixed and variable speed induction generators, doubly fed induction generators and synchronous generators with back to back converters, are very different to those of the conventional generators. As the installation of WPPs, which consist of these wind turbine generators, has reached important levels that they have a major impact on the characteristics of the transmission system [1]. Therefore, the grid codes demand WPPs to behave as much as similar to the conventional power plants for maintaining power system stability and reliability. Simultaneously the wind turbine manufacturers have been challenged by the new grid codes as they must adapt their technology to satisfy these grid codes. After adaptations and developments in the wind turbine technology, TSOs and WPP developers will work together and revise the grid codes in order to assist the future WPP connections without destabilizing the transmission system [2]. This is an iterative process regarding TSOs, WPP developers and operators.

As grid codes have evolved especially in the countries with already or planned high wind power penetration, technical analyses of the main issues related to the WPP connection are provided in the literature [3], [4]. This paper provides first, main requirements of the WPP connection in different countries and then, compares the resent available grid code versions. The current grid codes of these countries are listed in Table I.

In Section II, the common technical issues for connection of WPPs are described briefly. Section III compares the latest available versions of the grid codes listed in Table I. Grid codes harmonization and future trends are discussed in Section IV.

TABLE I
GRID CODES IN COUNTRIES WITH HIGH WIND POWER PENETRATION

Country	TSO	Release Date	Ref
Denmark	Energinet.dk	December 2004	[5]
Germany	E.ON, EnBW, Vattenfall, RWE	August 2007	[6]
		2009	[7]
		2008	[8]
Spain	Red Electrica	March 2006	[9]
		October 2008	[10]
		2007	[11]
		2000	[12]
UK	NGET	June 2009	[13]
Ireland	EIRGRID	April 2008	[14]
US	FERC, WECC	June 2005	[15]
		July 2009	[16]
China	CEPRI	July 2009	[17]

II. COMMON TECHNICAL REQUIREMENTS IN GRID CODES

According to the grid codes, the technical requirements are defined for the connection and operation of WPPs in the transmission system. The following requirements, which are common in most of the grid codes, have been considered in this paper:

- Normal operation:
  - Frequency and voltage ranges
  - Active power (P) control
  - Reactive power (Q) control
- Behavior under grid disturbances
  - Voltage ride through (VRT)
  - Reactive current injection (RCI)

WPPs must be required to operate within a range around the rated voltage and frequency at point of common coupling (PCC) to avoid instabilities due to the grid disturbances. Typically this requirement can be described as the following frequency/voltage operation zones:

- Continuous operation in a limited range below and above the nominal point.
- Time limited operation with possible reduced output in extended ranges.
- Immediate disconnection.

For normal grid operations, active power control requirement is defined as an ability to adjust the active power output with respect to the frequency deviations and the orders coming from the TSO. According to this requirement, WPPs can participate both in primary and secondary frequency control.

Reactive power control in normal operation is generally reactive power regulation in response to the PCC voltage variations. The reactive power requirement is related to the characteristics of each grid as a voltage changing capability, which depends on the grid short-circuit power. There are three different ways for this requirement; reactive power set point control, power factor (PF) control, and voltage control.

Grid disturbances in the form of voltage sags or swells can typically lead to WPP disconnections that may cause instability and yield in blackouts. To avoid this, the grid code requires continuous operation even if the voltage dip reaches very low levels (in some cases 0 pu), support the voltage recovery by injecting reactive current and active power restoration after the fault clearance with a limited ramp values. These typical features are generally defined in grid codes as follows

- VRT in terms of minimum (low VRT) and maximum (high VRT) voltage ride through and recovery slope for symmetrical and asymmetrical faults that WPPs must be able to withstand without disconnection from the grid.
- Active power and reactive power limitation during faults and recovery.
- RCI for voltage support during fault and recovery.
- Restoration active power with limited ramp after fault clearance.

III. COMPARISON OF THE GRID CODE REQUIREMENTS

A. Frequency and voltage deviations under normal control

The voltage-frequency operational window for grid codes is graphically represented in Fig. 1. The strictest continuous operation limits for frequency appear in the British code [13] (47.5-52 Hz) and for voltage in the Chinese grid code [17] (90-110% nominal voltage). It is obvious that the most extreme frequency limits 46.5 Hz and 53.5 Hz are for EON offshore [8].

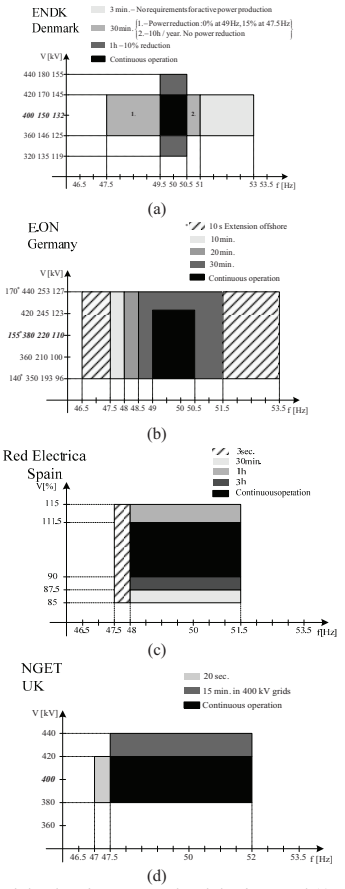

Fig. 1. Limit Voltage-frequency operation window for Denmark (a), Germany (b), Spain (c), UK (d) grid codes.

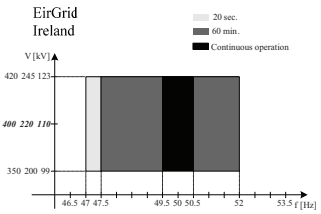

(e)

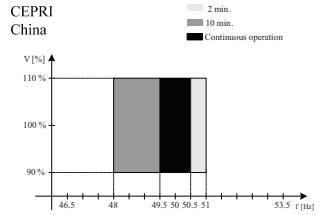

(f)

Fig. 1. Limit Voltage-frequency operation window for Ireland (e), China (f) grid codes.

B. Active Power Control in Normal Operation

Active power curtailment requirements are different across the countries as given in Table II.

As a particularity in Denmark, various types of power curtailment are requested [5].

The frequency control participation is varying with respect to transmission system characteristics.

According to the German code [7] when frequency exceeds the value 50.2 Hz, wind farms must reduce their active power with a 0.4 pu/Hz gradient (WPP 40% of the available power).

The British code [13] requires that wind farms larger than 50 MW to have a frequency control device capable of supplying primary and secondary frequency control, as well as over-frequency control. It is remarkable that it also prescribes tests, which validate that wind farms indeed have the capability of the demanded frequency response.

In Spanish grid code, WPPs must be able to give active power increase or decrease active power output proportional to the frequency deviation at the connection point. The frequency control must work as a droop controller of which values vary between 0.02 and 0.06 pu based on wind power plant ratings. Speed of the response will be adjustable 10% of the rated capacity in 250 ms.

The Irish code [14] demands a frequency response as described in the curve in Fig. 2.

TABLE II
ACTIVE POWER CURTAILMENT RATES

Country	Active Power Ramp Rate Range		
Denmark	20 – 100% with accuracy of 5% (5 min average)		
Germany	At least 10% of grid connection capacity per 1 min. (to a set level higher than 10%)		
Spain	-		
UK	-		
Ireland	over 1 min 1–30 MW per min. (activation time less than 10 s)	over 10 min 1–30 MW per min. (activation time less than 10 s)	
China	Inst. capacity <30 MW	Inst. capacity 30-150 MW	Inst. capacity >150 MW
	over 1 min. max ramp: 6 MW	over 1 min. max ramp: inst. cap. / 5	over 1 min. max ramp: 30 MW
	over 10 min. max ramp: 20 MW	over 10 min. max ramp: inst. cap. / 1.5	over 10 min. max ramp: 100 MW

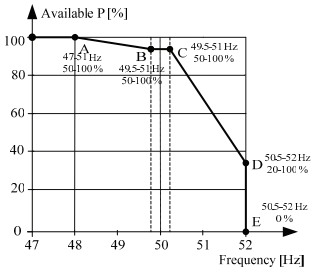

Fig. 2. Irish P-f curve.

The values for the power and frequency of ABCDE points should be online modified by the TSO within the ranges shown in the Fig. 2. This is due to the fact that in order to obtain a smooth participation of WPP in the TSO frequency control, the active power ramp should be imposed by TSO in harmony with the frequency response of the other participants to the balancing act.

C. Reactive Power Control in Normal Operation

1. Germany

The minimum requirements for reactive power generation [7] are given in the form of areas as function of voltage at nominal active power and as function of active power for the cases when the WPP is working at derated power for different ranges of voltages inside the normal operation range. The requirement can be given as a reactive power requirement or a power factor requirement. As the characteristics of the grid may differ depending on location and strength, three variants are defined by the Germans TSO's as depicted in Fig. 3 and Fig. 4.

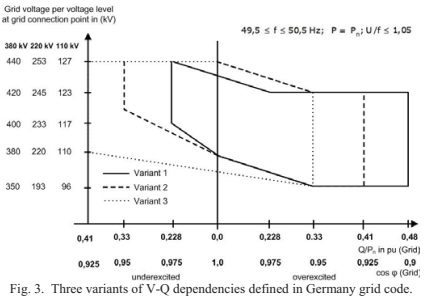

Fig. 3. Three variants of V-Q dependencies defined in Germany grid code.

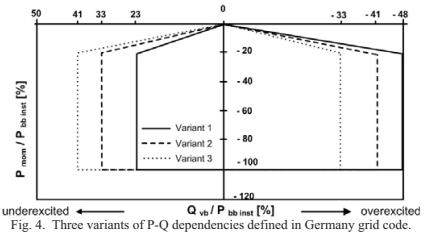

Fig. 4. Three variants of P-Q dependencies defined in Germany grid code.

2. Spain

The reactive power requirements during normal operations are defined by the directive [12], which applies to all generation on high voltage (HV) level both conventional and renewable. The following requirements are defined as a function of active power and transmission voltages as follows:

- Min. range 0.15 inductive - 0.15 capacitive for all technical active power range and nominal voltage
- Min. range 0.30 inductive - 0.30 capacitive as a function of the voltage shown in Fig. 5

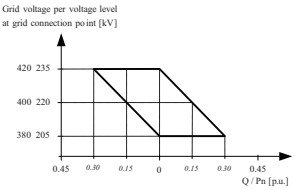

Fig. 5. V-Q dependence in Spain grid code.

3. Denmark

In the Danish grid code [5], the 10 s average PQ diagram is given as shown in Fig. 6 which applies for the whole range of voltage during normal operation. Basically it defines a control

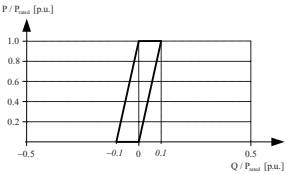

Fig. 6. P-Q dependence in Denmark grid code.

band of 0.1 pu. In comparison with the Germany and Spanish grid codes, the minimum required reactive power is lower.

4. UK

The British [13] code is specifically formulated for non-synchronous embedded generation and requires a power factor in the range 0.95 inductive to 0.95 capacitive at 1 pu active power for connection to the HV system (132/275/400 kV). This requirement equivalent to 0.33 pu reactive power should be maintained for active power down to 0.2 pu for lagging power factor and down to 0.5 pu for leading power factor. The grey area in Fig. 7 is an extension of the reactive power requirements in the dashed are for active power lower than 0.2 pu a lower band of pu of reactive power is required at low power leading power factor that can be required after agreement with the TSO (NGET).

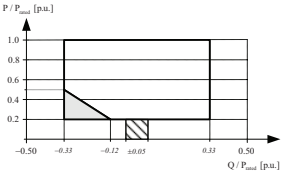

Fig. 7. P-Q dependence in UK grid code

5. Ireland

The Irish code [14] is quite similar but with 0.33 pu reactive power for both lagging and leading power factor as shown in Fig. 8 and with the reactive power requirements decreasing linearly to zero proportional to active power for lower than 0.5 pu.

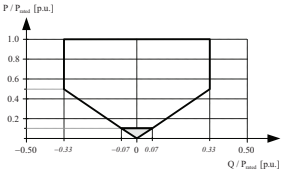

Fig. 8. P-Q dependence in Ireland grid code.

6. US

The US FERC 661 code [15] is specifying that reactive power in the power factor range 0.95 inductive to 0.95 capacitive can be required by TSO on a situation, which is not permanent operation but dynamically employed.

D. Behavior Under Grid Disturbance

1. Germany

The VRT and RCI are described in Fig. 9 and Fig. 10, respectively.

VRT

- Within the black area no interruptions is allowed. The WPP must stay connected even when the PCC voltage is zero. The 150 ms accounts for typical operating time of protection relays.
- Within the dark grey area, if the facility is facing stability issues, short time interruptions (STI) with resynchronization in maximum 2 s are allowed.
- The voltage value in Fig. 9 refers to the highest value of all three phase grid voltages measured at the low voltage side of the transformer in each wind turbine.

P and Q limitation during faults and recovery

- During faults, the active current can be reduced in order to fulfill the reactive current requirements

Minimum reactive current injection

- In case of significant deviation of the voltage, proportional reactive current has to be injected/absorbed as shown in Fig. 10, which indicates that rated reactive current can be requested for a voltage deviation of 10%.
- The response time of reactive current controller should be max 30 ms and the control band should be between –10% and +20% of the rated current.

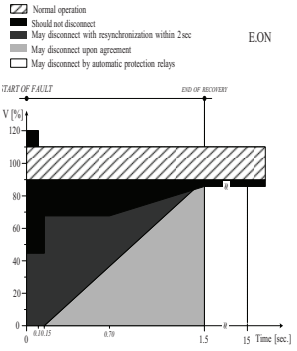

Fig. 9. VRT requirements in German grid code.

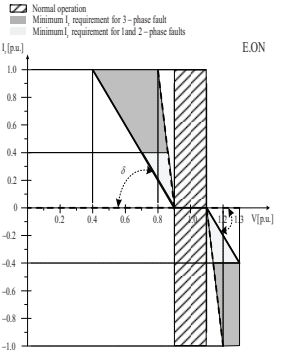

Fig. 10. Reactive Current Injection Requirements in German grid code.

- The reactive current requirements in Fig. 10 apply for the highest value of the three phase voltages in case of faults within the black area.
- For 1 and 2-phase faults, the maximum reactive current can be limited to 40% of the rated current.
- After fault clearance, the reactive current reference should not change stepwise in order to avoid stability issues.
- For voltages below 0.85 pu, if the facility is unable to supply the reactive power required for voltage support, the so called “Safeguard I” implemented in PCC will trip the wind farm after 0.5 s. “Safeguard II” at the wind turbine level is implemented as system protection acting after 1.5 s and includes the stepwise tripping of wind turbines.

Resuming Active power

- After fault clearance without disconnection, the active power feed-in must be continued immediately after fault clearance and increased to the original value with a gradient of at least 20%/s.
- In case of short disconnection, the active power feed-in must be resumed immediate after fault clearance with a gradient of at least 10%/s.

2. Spain

The VRT and RCI requirements of Spain are described in Fig. 11 and Fig. 12, respectively.

VRT

- During the whole transient regime, the facility must be able to inject to the grid at least the nominal apparent current.

P and Q limitation during faults and recovery

- The facility might not consume active and reactive power at the grid connection point during both, fault

duration and the duration of voltage recovery following fault clearance.

- Momentary active or reactive power consumption (<0.6 pu) is allowed during just the first 40 ms after the start of the fault and the first 80 ms after the clearance of balanced (three-phase) faults.
- Momentary active or reactive power consumption (<0.4 pu) is allowed during just the first 80 ms after the start of the fault and the first 80 ms after the clearance of unbalanced faults (single-phase and two-phase).

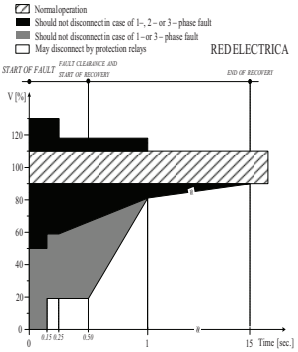

Fig.11. VRT requirements in Spain grid code.

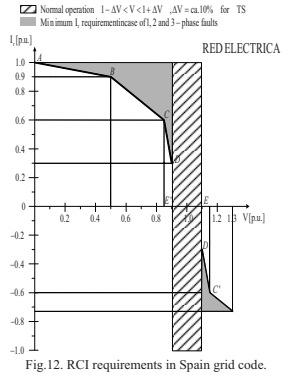

Fig.12. RCI requirements in Spain grid code.

Reactive current injection

The requirements of reactive power generation under voltage faults (V<0.85 pu) are implemented similarly as for the case of automatic voltage regulation (AVR) in conventional synchronous generation, i.e. in the form of a PI voltage controller with reactive current reference I_r as output, as shown in Fig. 13. V_c is the voltage set point (rms), V is the PCC voltage (rms) and I_r is the instantaneous reactive current reference. The saturation levels are voltage dependent as explained in Fig. 13.

The following particularities apply:

- The controller will be enabled for any voltage outside the normal operation range.
- If the WPP was working in voltage control mode in normal operation, the voltage set point during fault will remain unchanged.

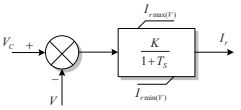

Fig.13. Reactive current injection requirements in Spain during FRT.

- If the WPP was working in reactive power or power factor control mode, during the disturbance the voltage set point will be the voltage prior to the fault if the normal operation set to reactive power or power factor allocation.
- During the fault, the facility should inject/absorb positive sequence reactive currents based on the action of the voltage controller with minimum saturation levels defined by the polygonal curve ABCDE as shown in Fig. 12. In case of overvoltage, the saturation levels are mirrored but for voltages higher than 1.3 pu, disconnection is required by protection relays.
- These levels should be implemented as saturation levels for the voltage controller that runs in both normal and faulty operation.
- For the range 0.85≤V≤1.15 pu, the injected reactive current will react according to the voltage control, possibly saturating the regulator limits.
- Once the fault is cleared, the voltage controller will keep be enabled for at least 30 s after voltage level reenter the normal operation range. Afterwards, the voltage controller will be disabled and the reactive power requirements for normal operation will apply

Active current injection

- During faults, the facility should limit the active current within the grey area as shown in Fig. 14 (excluding the active current increments/reductions due to frequency control or, if applicable inertia emulation).

As it can be seen, the active current limitation is a function of P_{ao}, the active power that the facility was generating prior to the disturbance and voltage level.

- For voltage levels lower than 0.5 pu, the active current can be reduced to zero.
- Any possible violation of these active current limits must be corrected before 40 ms.

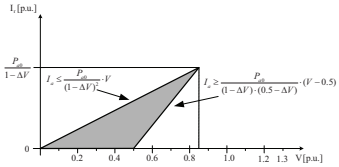

Fig.14. Active power limitation in Spain during FRT.

- In case of current saturation, reactive current limitation given by voltage controller saturation has priority over active current limitation.
- For voltages higher than the normal operation, the facility will seek if possible, to maintain the active power level prior to the disturbance.
- The gain of the active current controller should ensure dynamic response (90% rise) in less than 40 ms for V<0.85 pu and 250 ms for V>0.85 pu

Resuming Active power

- The voltage dependent active current control previous mentioned ensures that after the fault clearance without disconnection, the active power level prior to disturbance will be restored smoothly within 250 ms.

3. Denmark

The VRT requirement for Danish grid code is as shown in Fig. 15, which is valid only for three-phase faults. For single or double-phase faults, wind power plant should be able to withstand unsuccessful reclosures in the transmission network [5].

During the voltage dip the wind farm must as a maximum take a reactive current measured in at the grid connection point corresponding to 1.0 times the nominal current of the wind farm.

1. US

The recent WECC LVRT standard [16] is an effort to create compliance with the federal regulation FERC Order

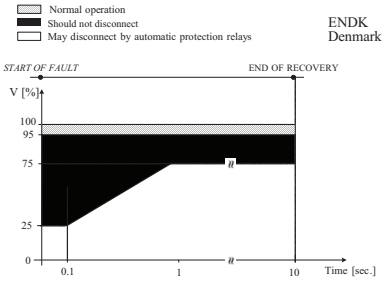

Fig.15. VRT in Denmark Grid Code.

661-A [14] in terms of fault voltage level and duration (0V for 9 cycles) and boundaries for time of voltage recovery for both LVRT (until voltage became higher than 90%) and HVRT (until voltage became lower than 110%) shown in Fig. 16.

VRT

- All generators are required to remain in-service during three-phase faults with normal clearing (for a maximum of 9 cycles) unless clearing the fault disconnects the generator from the transmission system
- The voltage is measured at high voltage side of the WPP step-up transformer
- For single-phase faults, delayed clearing times apply unless clearing the fault disconnects the generator from the transmission system
- TSO should provide to the WPP owner the normal breaker clearing time for three-phase faults and delayed clearing time for single-line-to-ground faults at the high voltage side of the generating plant step-up transformer
- There is no requirement for power limitation during fault or reactive power injection during fault or recovery.

IV. Discussion of Harmonization of Grid Codes

From the survey presented above, it can be observed that the interconnection regulations vary considerably from country to country. It is often difficult to find a general technical justification for the existing technical regulations that are currently in use worldwide due to the different wind power penetration levels in different countries and operational methodology of power systems.

For instance, countries with a weak power system, such as Ireland, have considered the impact of wind power on network stability issues, which means that they require fault ride-through capabilities for wind turbines already at a lower wind power penetration level compared with countries that have very robust systems. The inclusion of FRT regulations for DFIG noticeably increase overall cost by 5%. The European Wind Energy Association (EWEA) recommends that regulations for the European grid connection (or other nations) are to be developed in a more consistent and harmonized manner [18].

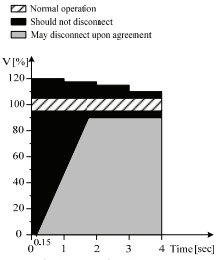

Fig.16. VRT in US-WECC.

Harmonized technical requirements will bring maximum efficiency for all parties and should be employed wherever possible and appropriate. While this applies to all generation technologies, there is a particular urgency in the case of wind power. As wind penetration is forecasted to increase significantly in the short to medium term, it is essential that grid code harmonization should be tackled immediately. It will help manufacturers to internationalize their products/services, developers to reduce cost, and TSOs to share experience, mutually, in operating power systems. It is also important that the national grid code should aim at an overall economically efficient solution, i.e., the costly technical requirements such as ''fault ride through'' capability for wind turbines should be included only if they are technically required for reliable and stable power system operation. Hence, it can be summarized that grid codes should be harmonized at least in the areas that have little impact on the overall costs of wind turbines. In other areas, grid codes should take into account the specific power system robustness, the penetration level, and/or the generation technology.

V. Future Trends

The following requirements are expected to be included in the future grid codes:

Local Voltage control

Both the Spanish and the German grid codes have increased the complexity of the reactive current injection during fault and recovery and a continuous local voltage control may prove to be necessary, particularly for offshore wind farms [19].

Inertia Emulation

The Spanish grid code [10] mention that even if for the moment the ability to emulate inertia is not yet compulsory it is strongly recommended and it may be introduced as a requirement later.

The implementation of emulated inertia should be in the form of proportional-derivative controller acting on frequency variation as input and outputting the necessary power variation as shown in Fig. 17.

The following particularities apply:

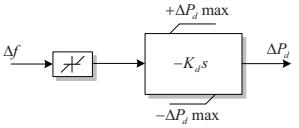

Fig.17. VRT in US-WECC.

- The gain K_d should be adjustable between 0 and 15 s, and the response time should be such that in 50 ms the active power should increase at least by ΔP=5%.
- In order to be able to generate the required saturation levels: $\pm\Delta P_d$max, energy storage of any technology is required able to inject or absorb at least 10% active power for at least 2 s.
- The deadband of frequency variation will be limited to $\pm$ 10 mHz.
- The Inertia Emulation should be disabled for voltages lower than 0.85 pu.

Power Oscillation Damping (POD)

This is another feature strongly recommended by the Spanish grid code [10], where just like in the case of the synchronous generators, the system should be able to increase or decrease the output power in such a way to reduce the power oscillations in the low frequency range (0.15 – 2.0 Hz). The following specific requirements apply:

- The POD can be implemented by "sharing" the existing power-frequency regulator.
- The POD can "share" the energy storage used for Inertia Emulation.
- The deadband of frequency variation will be limited to $\pm$ 10 mHz.
- The POD should be disabled for voltages lower than 0.85 pu.

VI. Conclusion

In this paper, the grid code technical requirements were presented for the connection of wind farms to the power systems, basically at the HV level. A comparative overview and analysis of the main requirements were conducted, comprising several national codes from many countries where high wind penetration levels have been achieved or are expected in the future. The objective of these requirements is to provide wind farms with the control and regulation capabilities encountered in conventional power plants and are necessary for the safe, reliable and economic operation of the power system. Current wind turbine technology, particularly developed over the last years, has been heavily influenced by these requirements. Modern wind turbines are indeed capable of meeting all requirements set, with the exception of the constant speed machines, which are practically not marketed anymore for large scale applications.

Acknowledgment

This work was supported by Aalborg University-Vestas Wind Systems A/S partnership under Vestas Power Program. Any opinions, findings, and conclusions or recommendations expressed in this material are those of the authors and do not necessarily reflect those of Vestas Wind Systems A/S.

References

[1] C. Hilger Wind power and impacts on power system operation—Eltra, In: Denmark. Wind power and impacts on power systems conference, Oslo, 17–18 June 2002.

[2] A. Causebrook and B. Fox, "Modernising grid codes to accommodate diverse generation technologies, especially modern wind farms," *Wind Engineering*, 28, pp. 75-86, 2004.

[3] I. Dealegria, J. Andreu, J. Martin, P. Ibanez, J. Villate, and H. Camblong, "Connection requirements for wind farms: A survey on technical requirements and regulation," *Renewable and Sustainable Energy Reviews*, vol. 11, pp. 1858-1872, 2007.
[4] M. Tsili and S. Papathanassiou, "A review of grid code technical requirements for wind farms," *IET Renewable Power Generation*, vol. 3, p. 308, 2009.
[5] Grid connection of wind turbines to networks with voltages above 100 kV, Regulation TF 3.2.5, Eltra and Elkraft System.
[6] Transmission Code 2007. Networks and System Rules of the German Transmission System operators, VDN-e.v. beim VDEW, August 2997, www.vdn-berlin.de.
[7] Ordinance on System Services by Wind Energy Plants (System Service Ordinance – SDLWindV) - Draft, 2009, www.erneuerbare-energien.de.
[8] Requirements for Offshore Grid Connections in the E.ON Netz Network" by E.ON, 2008, www.eon-netz.com.
[9] Resolution-P.O.12.3-Response requirements against voltage dips in wind installations, by Red Electrica in March 2006, www.ree.es (translated in English by Spanish Wind Association AEE www.aeolica.es).
[10] Annex of O.P. 12.2 Restricted to the technical requirements of wind power and photovoltaic facilities (Draft), by Red Electrica in October 2008 www.ree.es (translated in English by Spanish Wind Association AEE www.aeolica.es).
[11] Spanish Verification, Validation, and Certification Procedure for the Assessment of the Response of Wind Installations against Voltage Dips according to the requirements of P.O.12.3 (VV&CP), 2007, by Spanish Wind Association AEE www.aeolica.es.
[12] Resolution-P.O.7.4 - Servicio complementario de control de tension de la red de transporte, by Red Electrica in March 2000, www.ree.es.
[13] The Grid Code, Issue 4, by National Grid Electricity Transmission plc, - NGET, June 2009.
[14] Grid Code, Ver.3.1 3, elaborated by The EirGrid April, 2008.
[15] Order 661 - Interconnection with Wind Energy, issued by Federal Energy Regulatory Commission (FERC) of United States, June 2, 2005.
[16] WECC-0060 - PRC-024-WECC-1-CR – Generator Low Voltage Ride-Through Criterion –Regional Criterion (draft) – 2009 www.wecc.biz.
[17] Revised national grid code (draft), report no. WED-QR-C01-E-06 – elaborated by CEPRI as part of the Sino-Danish Wind Energy Development Program (WED), July 2009 www.dwed.org.
[18] Wind Power Interconnection into the Power System: A Review of Grid Code Requirements – Singh, Elsevier, 2009.
[19] Erlich, I.; Feltes, C.; Shewarega, F.; Wilch, M., "Interaction of large offshore wind parks with the electrical grid," *Electric Utility Deregulation and Restructuring and Power Technologies*, pp.2658-2663, 6-9 April 2008.

[P3] published in Proceedings of 9th International Workshop on Large-Scale Integration of Wind Power into Power Systems

Wind Power Plant Control - An Overview

Mufit Altin, Remus Teodorescu, Birgitte Bak-Jensen, Pedro Rodriguez, Florin Iov, Philip C. Kjær

***Abstract*-- Recent developments in wind turbine technology go towards installation of larger Wind Power Plants (WPPs). Therefore, power system operators have been challenged by the WPP penetration impacts in order to maintain reliability and stability of the power system. The revised grid codes have concentrated on the WPP connection point and as a result a WPP is considered as a single power plant. Nevertheless, compared to conventional power plants, WPPs have different inherent features such as converter-based grid interface technology, internal electrical layout, and asynchronous operation of turbines. Taking these into account, a WPP controller is the key factor in order to satisfy the grid code requirements. This paper presents a comprehensive overview of various WPP controller strategies comprising active power, reactive power, voltage, frequency, and emulated inertia control. The WPP control architecture composed of WPP control level and wind turbine control level is also discussed considering the hierarchy and coordination of these levels.**

***Index Terms*— active and reactive power control, emulated inertia control, frequency control, wind power, wind power plant control,**

I. Introduction

BEFORE the rapid increasing of the wind power generation, wind turbines had been considered as distributed energy sources in medium and low voltage distribution systems. The wind turbine technology was not adequate to participate in power system control in response to voltage or frequency disturbances [1]. Common practice during a system disturbance was to disconnect the wind turbines and reconnect them after the fault clearance. However, recent developments in wind turbine technology have changed this picture and TSOs have revised their grid codes for connection and operational requirements to reduce the impacts of the large WPP installations. Denmark and Germany have led these grid code revisions among the other countries due to their high wind power capacity [2], [3]. In Spain, the TSO has also revised the grid code including future requirements that are introduced for planned wind power installations in order to maintain stable and reliable integration [4]. Technical analyses and comparison of the most recent available grid code editions with the wind turbine technologies are surveyed in the literature [5], [6]. All these studies with the experiences from recent years have pointed out that WPPs should be treated like conventional power plants. Accordingly, grid codes have concentrated on the WPP connection point rather than the wind turbines connection points.

Furthermore, in a conventional power plant, generating units usually have identical controllers, i.e. governors and excitation system, with similar controller settings. They are connected to the same bus through common or individual step-up transformers. Thus, the general approach for modeling and evaluating the performance of the power plant is that one synchronous generator with its controllers can represent the overall power plant response. In some applications, conventional power plants are equipped with joint control functionality which provides the power plant operator to control the generating units as a group, working together on the basis of single active and reactive power generation set points [7]. As a result, the power plant control features are implemented with a single generating unit and should satisfy the grid code requirements.

WPPs have completely different aspects from the above discussion which bring additional considerations to the control system. The control structure is not straightforward as in the conventional power plant case mentioned above. The characteristic aspects of the WPPs can be summarized as follows [8]:

- WPPs have wind turbines with converter-based grid interface technology (permanent magnet synchronous generators and squirrel cage induction generators with full-scale converters or doubly-fed induction generators with partial-scale converters).
- The rotor speed of the wind turbines is varying and fluctuates due to the wind (variable wind speed turbines). In other words, wind turbines rotor speed is eventually decoupled from the frequency of the transmission system due to the usage of the induction generators and full-scale converters.
- In WPPs, the typical size of the wind turbines is much smaller with respect to conventional units (from kW to MW range).
- WPPs are not simply collections of individual wind turbines, they have collector systems and other devices (energy storage, FACT, etc.) with controllers. This means each individual wind turbine terminals face different operating

This work was supported by Vestas Wind Systems A/S.

M. Altin is a PhD student at Department of Energy Technology, Aalborg University, 9220 Aalborg, Denmark (e-mail: mua@et.aau.dk).

R. Teodorescu is with Department of Energy Technology, Aalborg University, 9220 Aalborg, Denmark (e-mail: ret@et.aau.dk)

B. Bak-Jensen is with Department of Energy Technology, Aalborg University, 9220 Aalborg, Denmark (e-mail: bbj@et.aau.dk).

P. Rodriguez is with the Technical University of Catalonia, Spain. (e-mail: pro@et.aau.dk).

F. Iov is with Vestas Wind Systems A/S, 8200 Århus, Denmark (e-mail: fliov@vestas.com)

P. C. Kjær is with Vestas Wind Systems A/S, 8200 Århus, Denmark (e-mail: pck@vestas.com)

conditions from the point of connection during the steady-state and the transient situations.

- Each individual wind turbine has its own electrical and mechanical control systems (wind turbine control level).
- Active and reactive power controls are decoupled in the converter-based wind turbines.

Therefore, in large WPPs wind turbines have to be managed from a higher and centralized control level, here called as WPP control level. The WPP control level is an interface between the WPP (wind turbines and if available, reactive compensation or energy storage devices) and the transmission system, and therefore, also the WPP operator and TSO. The WPP control usually regulates the production of the WPP based on the TSO demands and the connection point measurements. Additionally, the WPP control level is a key factor to control the wind turbines centrally in an efficient and hierarchical way while satisfying the grid codes.

To be able to implement the WPP control level, aggregated models are used in the literature [9]-[11] for the overall WPP, which is represented as a single wind turbine without losing the wind and collector system characteristics. Another approach is to model the WPP as individual wind turbine and the WPP control functions are implemented at this wind turbine control level. This approach aims to gain wind turbines the required WPP functionalities. After implementing the control structure, evaluation is performed for the proposed controller in order to fulfill the grid code requirements [12], [13].

So far, the mentioned approaches are based on a single control level without a hierarchical architecture or distribution of the control functions among several control levels (i.e. WPP and wind turbine control levels, if available FACTs and energy storage controllers). But, in this paper, a comprehensive overview of WPP control strategies [14]-[19], which are implemented at the WPP control level in the WPP two-level control architecture, is presented regarding active power, reactive power, voltage, frequency, and emulated inertia controls. Moreover, WPP and wind turbine control level functions are discussed considering the hierarchy and coordination of these levels.

II. Grid Code Requirements for WPPs

Grid codes define the connection and operational requirements for all parties such as power plant owners, large consumers, and ancillary service providers, connected to the transmission system. Recent grid codes for the power plants were specified in terms of synchronous machines. However, wind turbines are based on different technologies which have significant impacts on the conventional transmission system [20]. TSOs have revised their grid codes to sustain reliable and stable power generation to the loads while enabling the large scale integration of wind power generation [2]-[4]. Although the requirements depend on the inherent characteristics of each transmission system, structural harmonization study of the grid codes has been intended to establish a generic common grid code format where the general layout and specifications, not the values, are fixed and agreed upon by all the TSOs, WPP developers, and wind turbine manufacturers [21]. The most common requirements comprise:

- Active power and frequency control,
- Reactive power and voltage control,
- Fault ride through (FRT) capability,
- Frequency and voltage operating ranges.

The given requirements and more detailed discussions have already been made in the literature [5], [6], [20], [21]. Here a brief review of the mentioned common requirements is included for the WPP control functions.

A. Active Power and Frequency Control

WPPs have to dynamically participate in the grid operation control by regulating their active power output. Active power regulation in the grid codes include active power control functions, which limit the maximum active power, balance the active power output, and define the ramp rates upward or downward direction.

The control functions provide TSOs to control WPPs in a predictable way reducing the uncertainties caused by the wind. They might also be the supervisory tools to integrate WPPs into existing transmission planning and market operations. Additionally, reserve power can be maintained through using these functions for the frequency control. Active power reference update rate, start-up ramp rate, shut down ramp rate, and system protection functions are the additional requirements specified under the active power control title in the grid codes [2]-[4], [21], [23], [24].

Frequency control is performed by the power plants under the supervision of TSO in different stages which depend on each other [22]. Primary frequency control is one of the stages and allows a balance to be re-established between generation and consumption at a frequency other than the system frequency reference (50 or 60 Hz) in response to a frequency deviation.

In the WPPs, the wind turbines don't have a synchronously rotating rotor like in conventional power plants, and they are therefore following the system frequency. If there is a frequency excursion, they can change their active power output by the additional converter or the wind turbine controllers according to the grid code requirements [8]. The grid codes generally demand active power curtailment for frequencies above the normal operating limits (i.e. higher than 50.2 Hz in [3]) and immediate disconnection for lower frequencies (i.e. lower than 47 Hz in [3]). However, these limits can vary according to the bilateral agreements between the TSO and WPP owner. If the TSO demands same primary frequency control performance as for the conventional power plants, active power reserve should be deployed in the turbine kinetic energy, energy storage equipments or by de-rated operation of the wind turbine.

Moreover, emulated inertia control is another form of active power control for WPPs. This control idea comes from the conventional power plant natural response to the load changes in the grid operation. However, in WPPs wind turbine rotor speed is decoupled from the system frequency. The controller for inertia emulation should increase or decrease the active power output proportional to the derivative of the frequency, and as a result reduces the drop/rise of the frequency deviations. But, specifications for the emulated inertia control rely on the power system characteristics, such as the overall inertia of the system and the wind power penetration level in the transmission system. This controller structure is not a common requirement now in the grid codes, but is defined for a future implementation in the Spanish grid code [4].

B. Reactive Power and Voltage Control

WPPs have to regulate their reactive power output in response to the voltage deviations at the grid connection point and the reactive power references sent by the TSO. The reactive power requirements depend on the grid connection point characteristics, which include short-circuit power of the connection point, X/R ratio, and wind power penetration level. For the grid operation, there are three different possibilities for reactive power references set by the TSO; reactive power, power factor and voltage references. Grid codes have stated these reactive power operating conditions, such as P/Q and V/Q curves or voltage slope characteristics. Additionally, the reactive power ramp rate, reactive power control and measurement accuracy, settling and rise times for reactive power change are specified in the grid codes [2]-[4], [21], [23], [24].

C. Fault Ride Through (FRT) Capability

During grid disturbances, voltage dips can typically lead to WPP disconnections that will cause instability and yield into blackouts. To avoid these problems, the grid codes require continuous operation even if the voltage dip reaches very low levels, support to the voltage recovery by injecting reactive current and active power restoration after the fault clearance with a limited ramp values. All these features are defined as FRT capability of the wind turbines and described by the FRT voltage profile given in the grid codes. During the fault, the reactive current injection is defined by another figure, and in addition to these capabilities, reactive current injection, dead, rise, and settling time with the post fault support time are specified correspondingly in the grid codes [2]-[4], [23], [24].

III. WPP CONTROL

In order to satisfy the mentioned grid codes, the WPP control level is responsible for the active and reactive power dispatch for the wind turbines. In addition to the steady state performance, the WPP control level can dynamically provide stability, or if it is not possible to react due to the response time of the WPP controller and WPP communication system, it should not affect the transmission system operation adversely during the transient conditions (i.e. faults, switching operations, and load/wind variations). The challenge increases further when there are other components, such as energy storages, capacitor banks, and FACTs in the WPP. Therefore, the WPP control architecture should be structured in a hierarchical and coordinated way for efficient, reliable and stable grid operation as a single generating unit.

Generally, two-level control, which comprises the WPP control level and the wind turbine level, has been implemented as a benchmark of WPP control architecture in the literature and industry [14]-[19]. In this architecture, the WPP control level determines the active and reactive power set points for each wind turbine based on the grid connection point measurements and TSO demands.

The wind turbine control level on the other hand, ensures that the sent out references from the WPP control level are reached. Moreover, if any operational changes occur, such as available wind power or fault situations, the WPP control level should be acknowledged through a SCADA (Supervisory Control and Data Acquisition) system. In the following subsections, the WPP control level is described in more details.

A. WPP Active Power Control

In the WPP control level, the active power control main purpose is to control the injected active power at the point of connection into the transmission system. Therefore, the WPP active power controller calculates the active power set points of each wind turbine in the WPP with respect to the active power reference received from the TSO. As illustrated in Fig. 1, the inputs of the active power control are the received power reference, measured active power at the connection point, available active power values from each wind turbines, and the outputs are the reference signals to each wind turbine. The WPP active power control typically contains an active power control functions block, main controller block and dispatch function block as shown in Fig. 1.

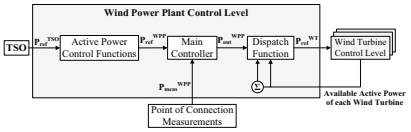

Fig. 1. WPP level active power control [16]

1) Active Power Control Functions

In Danish grid code [2], active power control functions are clearly defined, thus in Horns Rev I all the functions are implemented and in operation [17]. The active power control functions block in Fig. 1 can decide which control function will be active for the WPP. For instance, balance control or delta control can work at the same time with the power rate limiter function. These control functions are simulated in [16] and the results are given in Fig. 2.

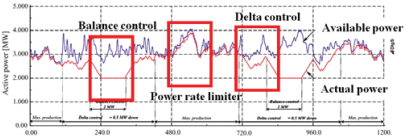

Fig. 2. WPP active power control functions [16]

2) Active Power Main Controller

The main controller block, illustrated in Fig. 3, is a simple PI controller with anti wind-up limiter that calculates the active power error and decides the overall WPP active power reference (P_{out}^{WPP}).

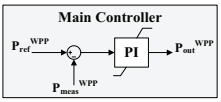

Fig. 3. WPP active power main controller based on [16]

3) Active Power Dispatch Function

There are various ways in order to distribute the active power reference signals to individual wind turbines (P_{ref}^{WT}) as a dispatch function. The simplest algorithm directly sends the input signal (P_{out}^{WPP}), which is expressed in per unit (pu), to all wind turbines. It should be noticed that if the power reference signal sent to a wind turbine exceeds the maximum available power of the wind turbine, in the next error computation step the rest of the wind turbines will automatically increase their outputs in order to reset the active power error. However, this algorithm does not check the available power of the overall WPP, thereby a steady state error may remain [19], [25].

Another strategy, which is mentioned in [16]-[18], calculates the wind turbine active power set points based on a proportional distribution of each wind turbine available active power. Equation (1) is simply formulated as a proportional distribution of the available active power by dividing each wind turbine available active power to the total available active power, where P_{av}^{WTi} is the available active power of i^{th} wind turbine and P_{av}^{WPP} is the total available active power of the WPP.

$$P_{ref}^{WT_i} = \frac{P_{av}^{WT_i}}{P_{av}^{WPP}} \times P_{out}^{WPP}, \quad P_{av}^{WPP} = \sum_{i=1}^{n} P_{av}^{WT_i} \qquad (1)$$

Further, an optimized dispatch control strategy is implemented that defines the active power set points of each wind turbines and closely follows the TSO active power reference taking the WPP internal active power losses and availability of the wind power into consideration [14]. This optimization problem defined in (2) is composed of three sub-objective functions: the first and second part aim to decrease the deviation between the WPP active and reactive power outputs and the TSO reference value respectively, and the last part seeks to reduce the active power losses in the collector system.

$$\min \left\{ \begin{array}{l} p_1\left(P_d - P_{total}\right)^2 + p_2\left(Q_d - Q_{total}\right)^2 + \\ p_3\left[\left(P_{out1} - P_d\right)^2 + \sum_{i=2}^{n}\left(P_{outi} - P_{s_{i-1}}\right)^2\right] \end{array} \right\} \qquad (2)$$

,where P_d and Q_d is active and reactive power demand received from the TSO, P_{total} and Q_{total} is the total active and reactive power of the WPP, P_{outi} is the sending side active power flow of branches and P_{Si} is the receiving side active power flow of branches from the wind turbine side to the connection point. For this objective function a primal-dual predictor corrector interior point optimization method is used in [14].

As a result, using the above active power control the WPPs can operate at the maximum power or at a de-rated power that would be used for the primary and secondary frequency control purposes or to support voltage stability in contingency situations (curtailment of the active power).

B. WPP Reactive Power Control

The grid codes demand reactive power support in several ways; reactive power, power factor or voltage control specified as set points sent by the TSOs. Among these control strategies, the appropriate strategy is selected by the TSO and WPP developer with respect to the short-circuit ratio, X/R ratio at the connection point and the currently installed reactive compensation in the vicinity of WPP connection point.

The WPP reactive power control structure is similar to the active power control mentioned above. It is briefly shown in Fig. 4 that possible set points from the TSO are reactive power, power factor or voltage. The inputs of reactive power control are the set points (Q_{ref}^{TSO}, V_{ref}^{TSO}, pf_{ref}^{TSO}), the measurement of the related signal (Q_{meas}^{TSO}, V_{meas}^{TSO}, pf_{meas}^{TSO}) according to the set point, and in some cases the available active power of the wind turbines, are needed in order to calculate the individual reactive power or voltage reference of the wind turbines (Q_{ref}^{WT}, V_{ref}^{WT}) [16].

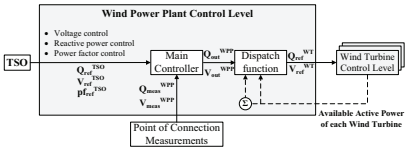

Fig. 4. WPP level reactive power control [16]

1) Reactive Power Control Strategies

Power factor control is a passive reactive power control related to the active power output of the WPP. In other words, when the active power output is increased, the power factor control will also increase the reactive output. The significant disadvantage is that when the active power changes due to wind or TSO reference, these changes will lead to reactive power changes at the connection point [15].

Another strategy is the reactive power control which receives the reactive power reference signal from the TSO. Same disadvantage can take place, if the wind power

change is very rapid. Thus a very fast reactive control will be required from both the TSO operator and the WPP reactive power controller in order to sustain the voltage constraints.

On the other hand, the voltage control strategy is more robust and active power changes do not affect the set points coming from the TSO as in the previous strategies. But practical drawbacks, such as communication delays, should be carefully handled. However, undesired voltage changes cannot be avoided at the point of connection [15].

2) Reactive Power Main Controller

The main controller, which is illustrated as a block in Fig. 4, is a simple PI controller with anti wind-up limiter that calculates the reactive power or voltage error and decides the overall WPP reactive power reference (Q_{out}^{WPP}) or connection point voltage reference (V_{out}^{WPP}). In addition to this structure in reactive power control strategy, the reactive power reference can be modified by adding output of the voltage control as a reactive power correction. It is shown in Fig. 5 and the additional voltage loop is realized to assure the voltage constraints at the connection point [16]. Similar control structure with the reactive power additional loop can also be implemented in the voltage control strategy. Another similar main controller structure, which is based on reactive power control and a subordinated voltage control loop, is illustrated in Fig. 6 [25]. The implementation of the subordinated loop is to enable the voltage constraints while following the reactive power reference. In other words it s a protection to sustain the WPP availability such that the WPP connection point voltage remains between the voltage limits.

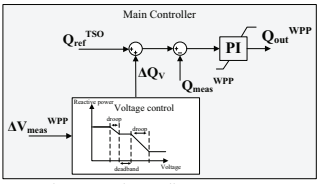

Fig. 5. WPP reactive power main controller [16]

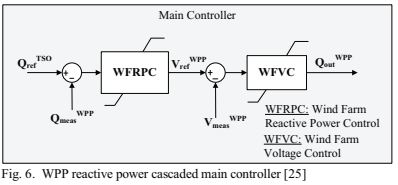

Fig. 6. WPP reactive power cascaded main controller [25]

3) Reactive Power Dispatch Function

Similar to the active power dispatch function, there are various ways in order to distribute the reactive power/voltage reference signals to individual wind turbines (Q_{ref}^{WT} or V_{ref}^{WT}) similar to active power control as a dispatch function. The simplest algorithm directly sends the input signal that is reactive power reference (Q_{out}^{WPP}) to all wind turbines. It should be noticed that in the voltage control strategy, the voltage reference (V_{out}^{WPP}) must be converted to reactive power set point, and then it can be distributed as the reactive power references (Q_{ref}^{WT}) [25]. However, the disadvantage of the reactive control strategy with this distribution function is that the identical reactive power set values sent to each wind turbine would cause excessive voltage variations within the collector feeders. In case of high voltage profile, there could be trip of the wind turbines because of the voltage instability and equipment voltage ratings [19].

Another strategy, which is mentioned in [16]-[17], calculates wind turbine reactive power set points based on a proportional distribution of each wind turbine available reactive power. Equation (3) is simply formulated as a proportional distribution of the available reactive power by dividing each wind turbine available reactive power to the total available reactive power, where P_{av}^{WTi} and Q_{av}^{WTi} is the available active and reactive power of ith wind turbine respectively, Q_{av}^{WPP} is the total available reactive power of the WPP, and $S_{gen\_rate}^{WTi}$ is MVA rating of the i^{th} wind turbine.

$$Q_{ref}^{WT_i} = \frac{Q_{av}^{WT_i}}{Q_{av}^{WPP}} \times Q_{out}^{WPP}, Q_{av}^{WPP} = \sum_{i=1}^{n} Q_{av}^{WT_i}, Q_{av}^{WT_i} = \sqrt{\left(S_{gen\_rate}^{WT_i}\right)^2 - \left(P_{av}^{WT_i}\right)^2} \quad (3)$$

Further, an optimized dispatch control strategy is implemented that defines the reactive power or voltage set points of each wind turbines and closely follows the TSO active power reference taking the WPP internal active power losses and availability of the wind power into consideration [14]. This optimization problem is defined in (2) and the details are mentioned in the active power dispatch function part.

Another optimization algorithm focuses on the WPP collector system losses which are the sum of no-load and load losses in the collector system [26]. In (4), the total loss (P_{LOSS}) is formulated in two parts; the first part is the load loss at any operating point in terms of total power (S) and voltage (V) which is related to the load loss ($P_{LL\text{-}rated}$) at the rated power (S_{rated}) and nominal voltage (V_{rated}). The second part is the no-load loss of the collector system transformers at any V which is also related to the no-load loss ($P_{NL\text{-}rated}$) at the nominal voltage (V_{rated}).

$$P_{LOSS} = \left(\frac{V_{rated}}{V}\right)^2 \left(\frac{S}{S_{rated}}\right)^2 P_{LL-rated} + \left(\frac{V}{V_{rated}}\right)^2 P_{NL-rated} \quad (4)$$

4) WPP Coordinated Reactive Power Control

The WPP reactive power control level is surveyed as a single central unit in order to satisfy grid codes reactive power and voltage requirements. Likewise, the wind turbine control level has reactive power and voltage control strategies, which affect the overall performance of the WPP. The coordination of these two control levels is very important. For instance, reactive power control can be implemented as a slow control loop on the WPP control level and a fast voltage control loop, which is able to

operate in the wind turbines (Fig. 7). Another possible structure is that both WPP control and wind turbine control level have the voltage control capability. The voltage control on the WPP level can stabilize the connection point voltage within the limits regardless the active power variations. On the other hand, voltage controllers at the wind turbines are able to reduce the fast voltage variations in the collector system and the grid (Fig. 8) [15], [27]. On the contrary to this control structure, there has been an implementation where the voltage control loop is the inner control and the relatively slower reactive power control loop is the outer control loop [28]. The claim for this structure, which is depicted in Fig. 9, is that it is more stable than the reactive power control loop inside of the voltage control loop. However, if the wind turbines react with their very fast voltage control with respect to the disturbances, there might be some intra-plant stability problems due to the WPP collector system and interaction of these controllers.

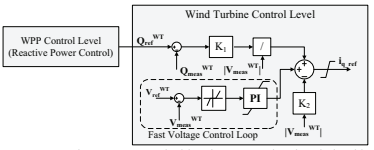

Fig. 7. WPP reactive power control with voltage control at the wind turbine [15]

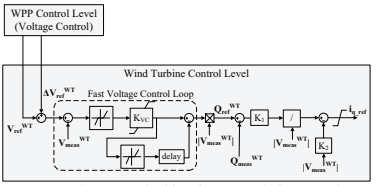

Fig. 8. WPP voltage control with voltage control (inner reactive power control loop) at the wind turbine [15]

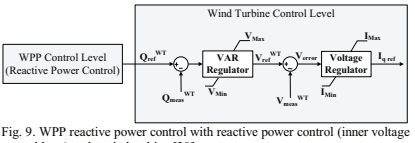

Fig. 9. WPP reactive power control with reactive power control (inner voltage control loop) at the wind turbine [28]

C. WPP Frequency Control

In the power system, the active power generated and consumed must be in balance during steady state conditions. When a disturbance has occurred, the system frequency will deviate with respect to the angular momentum of the synchronous machines and spinning loads connected to the system. For these frequency excursions, power plants are required to provide frequency response which is specified in the grid codes by the TSOs.

The primary frequency control is the response of the power plant during the frequency deviation by changing its active power output in order to stabilize the frequency at a level different than the nominal frequency (50 Hz or 60 Hz) within 10 sec. – 30 sec. (BC period in Fig. 10).

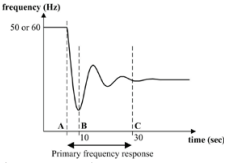

Fig. 10. Primary frequency control

In the last 5 years, there have been a lot of studies about primary frequency control both implemented on the WPP control and wind turbine control level. Most of the studies have implemented the primary frequency control in the pitch control system or active power control loop of the converters by either using the inertial response of the rotor, reserve power of the wind turbine (de-rated operation mode) or energy storage devices. In [16] and [17], the primary frequency control is implemented on the WPP control level and the reason is stated to avoid that WPP can counteract the frequency controllers in the wind turbines. This control structure is illustrated in Fig. 11. On the other hand, in [14] and [17], all the all the wind turbines are able to response to frequency deviations and they can change their active power autonomously regardless of the WPP controller.

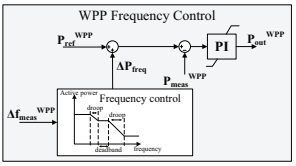

Fig. 11. WPP frequency control [16]

D. WPP Emulated Inertia Control

As mentioned in the frequency control, any imbalance such as the difference between generation and consumption leads to deviations in the system frequency. The frequency drop during the AB period (in Fig. 10) depends on the total inertia of the system, which can be described as the available stored energy in the rotor of the conventional power plants. This stored energy is instantaneously released to cease the frequency drop.

If the wind power penetration level is expected to increase with the converter based wind turbines, the system inertia response will be reduced. As a result, the system frequency drop during an imbalance will drop very rapidly to lower values than the previous case. Therefore, TSOs let WPPs contribute to system inertia by emulating synchronous machine inertial response [4]. In [29], the active power output of a WPP is controlled by an algorithm in order to contribute to the system frequency. This control

is emulating the inertia response behavior of the synchronous power plant. It detects the frequency of the power system and then calculates a variation rate in the detected system frequency. Afterwards, an active power output change of the WPP is calculated based on a value of the WPP overall inertia and the previously calculated frequency variation rate. The calculated active power change for the overall WPP is distributed with respect to two embodiments, the first one is just by dividing the number of the wind turbines, and the second approach is by taking account of the WPP equivalent rotational speed and every individual rotational speed of the wind turbines. Furthermore, the method comprises the detection of the incoming wind speed at the WPP, and the calculation of the energy residing in the rotational masses of the WPP from the detected wind speed. Fig. 12 illustrates the whole detection and calculation steps of the control methodology.

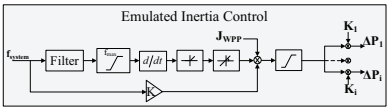

Fig. 12. WPP emulated inertia control based on [29]

IV. Discussion and Conclusion

The installation of larger WPPs at both onshore and offshore are rapidly increasing by virtue of the recent developments in wind turbine technology and the incentives provided by the governments. According to the wind integration studies performed by the TSOs and organizations from academy and industry, the grid code requirements have been revised, wind turbine manufacturers have been implementing new developments to the market, and the WPP developers have been conducting the connection studies considering grid codes and wind turbine technology. In this paper, a comprehensive overview of WPP control strategies is presented regarding active power, reactive power, voltage, frequency, and emulated inertia controls.

The WPP control level is the key factor for steady state and dynamic operational performance of the WPP. The WPP control architecture as a usual concept consists of mainly two levels, the WPP control level and the wind turbine control level. The general functions of the WPP control level are discussed in the related part of the report that comprises the following functions required from the system operator; active power, frequency, emulated inertia, and reactive power (voltage control, pf control).

FRT control function is much more related to the wind turbine level with respect to the response time and elimination of the disturbances. In the literature the functions of each WPP control level and the coordination of these levels haven't been covered in detail. Furthermore, more detailed WPP models including the communication latency and sampling time should be developed. According to the grid code requirements and wind turbine technology a brief provision of the functions for the each level can be classified as follows:

WPP Control Level Functions:

- Active power control of WPP
- Secondary frequency control
- Primary frequency control
- Reactive power control (or Voltage control) of WPP

Wind Turbine Control Level Functions:

- Active power control of wind turbine
- Reactive power control of wind turbine
- Emulated inertia control
- FRT control

On the other hand, AGC (Automatic Generation Control) for the secondary frequency control and secondary voltage control functions utilized in conventional transmission systems can be implemented to improve the WPP control algorithm which includes optimization of the active and reactive power control considering the collector system layout, wind prediction, and availability of the generation.

Finally, communication time delays between the control levels should be taken into account for the WPP control architecture. For instance, the arrival time of the available wind power information from the wind turbine to the WPP controller will affect the primary frequency control performance.

V. Acknowledgment

This work was supported by Aalborg University-Vestas Wind Systems A/S partnership under Vestas Power Program. Any opinions, findings, and conclusions or recommendations expressed in this material are those of the authors and do not necessarily reflect those of Vestas Wind Systems A/S.

VI. References

[1] T. Ackermann, *Wind Power in Power Systems*, Chichester: Wiley, 2005.
[2] Eltra and Elkraft System, "Wind turbines connected to grids with voltages above 100 kV, Regulation TF 3.2.5", Dec. 2004.
[3] VDN, "TransmissionCode 2007, Network and system rules of the German transmission system operators", Aug. 2007.
[4] Red Electrica, "Offprint of the outline of O.P. 12.2 Restricted to the technical requirements of wind power and photovoltaic facilities", 2008.
[5] I. Dealegria, J. Andreu, J. Martin, P. Ibanez, J. Villate, and H. Camblong, "Connection requirements for wind farms: a survey on technical requirements and regulation," *Renewable and Sustainable Energy Reviews*, vol. 11, pp. 1858-1872, 2007.
[6] M. Tsili and S. Papathanassiou, "A review of grid code technical requirements for wind farms," *IET Renewable Power Generation*, vol. 3, p. 308, 2009.
[7] L. O. Long, "Joint control of electric governors for hydraulic turbines," *IEEE Transactions Power Apparatus and Systems,* vol.PAS-87, no.9, pp.1754-1762, 1968.
[8] O. A.-Lara, N. Jenkins, J. Ekanayake, P. Cartwright, and M. Hughes, *Wind Energy Generation, Modelling and Control*, Chichester: Wiley, 2009
[9] M. P. and S. Achilles, "Aggregated wind park models for analyzing power system dynamics," in *4th International Workshop on Large Scale Integration of Wind Power and Transmission Networks 2003*.
[10] L. Fernandez, C. Garcia, J. Saenz, and F. Jurado, "Equivalent models of wind farms by using aggregated wind turbines and equivalent winds," *Energy Conversion and Management,* vol. 50, pp. 691-704, 2009.

[11] E. Muljadi, C. P. Butterfield, A. Ellis, J. Mechenbier, J. Hochheimer, R. Young, N. Miller, R. Delmerico, R. Zavadil, and J. C. Smith, "Equivalencing the collector system of a large wind power plant, " in *Proc. 2006 IEEE Power Engineering Society General Meeting*.
[12] J. Morren, J. Pierik, S. W.H. de Haan, "Inertial response of variable speed wind turbines," *Electric Power Systems Research,* vol.76. Issue 11, pp.980-987, 2006.
[13] J.G. Slootweg, S.W.H. de Haan, H. Polinder and W.L. Kling, "Voltage control methods with grid connected wind turbines: a tutorial review," *Wind Engineering,* vol.25. no. 6, pp.353-365, 2001.
[14] R. deAlmeida, E. Castronuovo, and J. PecasLopes, "Optimum generation control in wind parks when carrying out system operator requests," *IEEE Transactions on Power Systems,* vol. 21, 2006.
[15] J. Fortmann, M. Wilch, F. Koch, and I. Erlich, "A novel centralised wind farm controller utilising voltage control capability of wind turbines," in *Proc. 2008 Power System Computation Conf.*, pp. 1-7, 2008.
[16] A. Hansen, P. Sorensen, F. Iov, and F. Blaabjerg, "Centralised power control of wind farm with doubly fed induction generators," *Renewable Energy*, vol. 31, pp. 935-951, 2006.
[17] J.R. Kristoffersen and P. Christiansen, "Horns Rev offshore windfarm: its main controller and remote control system," *Wind Engineering*, vol. 27, pp. 351-359, 2003.
[18] B. Liu, X. Peng, and T. Undeland, "Centralized power control strategy of offshore wind farm with permanent magnetic generators," in *Proc. 2009 IEEE 6th International Power Electronics and Motion Control Conference,* vol. 3, pp. 1075-1079.
[19] J. Rodriguez-Amenedo, S. Arnaltes, and M. Rodriguez, "Operation and coordinated control of fixed and variable speed wind farms," *Renewable Energy*, vol. 33, 2008, pp. 406-414.
[20] J.C. Smith, M.R. Milligan, E.A. DeMeo, B. Parsons, "Utility Wind Integration and Operating Impact State of the Art," *IEEE Transactions on Power Systems,* vol.22, no.3, pp.900-908, Aug. 2007.
[21] European Wind Energy Association (EWEA) Working Group, "Generic Grid Code Format for Wind Power Plants,"Nov. 2009.
[22] UCTE Operation Handbook, 2009: http://www.entsoe.eu/index.phpid57
[23] EirGrid, "Grid Code," ver.3.1 3, Apr. 2008.
[24] NGET, "The Grid Code," Issue 4, June 2009.
[25] J. Rodriguez-Amenedo, S. Arnalte, and J. Burgos, "Automatic generation control of a wind farm with variable speed wind turbines," *IEEE Transactions on Energy Conversion*, vol. 17, pp. 279-284, 2002.
[26] General Electric Company Patent, "Windfarm collector system loss optimization", EP2108828 A2.
[27] Repower Systems AG, "Wind park with robust reactive power adjustment system and method for the operation thereof", US2008/0073912 A1
[28] Einar V. Larsen, "Voltage Control for Wind Generations", US 2006/0012181 A1.
[29] Vestas Wind Systems A/S, "Method and system for controlling a wind power plant comprising a number of wind turbine generators", PCT/EP2009/057943828.

VII. BIOGRAPHIES

Mufit Altin (S'09) was born in Denizli, Turkey, 1982. He received B.S. and M.S. degrees in electrical and electronics engineering from Middle East Technical University (METU), Ankara, in 2004 and 2009, respectively. He was a research engineer with Power System Group in the Scientific and Technological Research Council of Turkey (TUBITAK), from 2004 to 2009. He is currently working toward the PhD. degree in the Department of Energy Technology, Aalborg University, Denmark. His research interest includes distribution automation, wind power plant control, wind energy, and power systems.

Remus Teodorescu received the Dipl.Ing. degree in electrical engineering from Polytechnical University of Bucharest, Romania in 1989, and PhD. degree in power electronics from University of Galati, Romania, in 1994. In 1998, he joined Aalborg University, Department of Energy Technology, power electronics section where he currently works as full professor. He is the co-recipient of the Technical Committee Prize Paper Awards at IEEE IAS Annual Meeting 1998, and Third-ABB Prize Paper Award at IEEE Optim 2002. His areas of interests are: design and control of power converters used in renewable energy systems, distributed generation mainly wind power and photo-voltaics, computer simulations, digital control implementation. Remus Teodorescu is the coordinator of the Vestas Power Program.

Birgitte Bak-Jensen (M'88) received the M.Sc. degree in electrical engineering in 1986 and the Ph.D. degree in "Modeling of High Voltage Components" in 1992, both from the Institute of Energy Technology, Aalborg University, Aalborg, Denmark. From 1986 to 1988, she was with Electrolux Elmotor A/S, Aalborg, Denmark as an Electrical Design Engineer. She is currently an Associate Professor in the Institute of Energy Technology, Aalborg University, which she joined in August 1988. Her fields of interest are modeling and diagnosis of electrical components and power quality and stability in power systems. During recent years, integration of dispersed generation to the network grid has become one of her main fields, where she has participated in many projects concerning wind turbines and their connection to the grid.

Pedro Rodriguez (S'99-M'04) received the M.S. and Ph.D. degrees in electrical engineering from the Technical University of Catalonia (UPC), Barcelona, Spain, in 1994 and 2004, respectively. In 1990, he joined the faculty of UPC as an Assistant Professor, where he is currently an Associate Professor. In 2005, he was a visiting researcher in the Center for Power Electronics Systems, Virginia Tech, USA. He is now the Head of the Research Group on Renewable Electrical Energy Systems at the UPC and co-Supervisor of the Vestas Power Program in partnership collaboration with the AAU. His research interest is focused on applying power electronics to distributed energy systems and power quality. Dr. Rodriguez is a Member of the IEEE Power Electronics, IEEE Industry Application, and IEEE Industrial Electronics Societies. Currently, he is a member of the IEEE IES Technical Committee on Renewable Energy Systems and the chair of the IEEE Industrial Electronics Student Forum.

Florin Iov was born in Galati, Romania, in 1968. He received the Dipl. Eng. degree in electrical engineering from Brasov University, Brasov, Romania, in 1993. He served as a faculty member in the Department of Electrical Machines and Drives, Galati University, Galati, Romania, from 1993 to 2000. In November 2000, he joined the Department of Electrical Energy Conversion, Aalborg University, Denmark, where he worked on the Low Inductance IGBT Fuse Project in cooperation with Cooper Bussmann, Inc. Currently, he is with Vestas Wind Systems. His fields of interest are electrical machines, power electronics and drives, wind turbines, modeling, and simulation.

Philip Carne Kjaer received the M.Sc. degree in electrical engineering from Aalborg University, Aalborg, Denmark, in 1993, and the Ph.D. degree from the University of Glasgow, Glasgow, U.K., in 1997. From 1993 to 1998, he was a Research Assistant at the University of Glasgow, working with advanced control of switched reluctance machines and drives. From 1998 to 2003, he was with ABB Corporate Research, Vasteras, Sweden, where, as a Development Engineer, he worked on servo-motor-based high-voltage circuit breaker drives, factory testing of synchronous machines, power converters for HVDC power transmission, and multi-megawatt variable-speed drives. Beginning in 2000, he also functioned as Deputy Department Manager and, most recently, as Group Manager for a team of 18 scientists. In October 2003, he joined Vestas Wind Systems, Arhus, Denmark, where he currently holds the position as Chief Specialist for power plants. His research covers control and application of electrical machines and power electronic converters. Dr. Kjaer is a Chartered Engineer in the U.K., a Member of the Institution of Electrical Engineers, U.K., and the recipient of the 2004 Richard M. Bass Outstanding Young Power Electronics Engineer Award.

[P4] published in Proceedings of IEEE Power and Energy Society General Meeting 2012

Methodology for Assessment of Inertial Response from Wind Power Plants

M. Altin, *Student Member, IEEE*, R. Teodorescu, *Fellow, IEEE*, B. B. Jensen, *Member, IEEE*, U. D. Annakkage, *Senior Member*, *IEEE,* F. Iov, *Senior Member, IEEE*, and P. C. Kjaer, *Senior Member, IEEE*

***Abstract*—High wind power penetration levels result in additional requirements from wind power in order to improve frequency stability. Replacement of conventional power plants with wind power plants reduces the power system inertia due to the wind turbine technology. Consequently, the rate of change of frequency and the maximum frequency deviation increase after a disturbance such as generation loss, load increase, etc. Having no inherent inertial response, wind power plants need additional control concepts in order to provide an additional active power following a disturbance. Several control concepts have been implemented in the literature, but the assessment of these control concepts with respect to power system requirements has not been specified. In this paper, a methodology to assess the inertial response from wind power plants is proposed. Accordingly, the proposed methodology is applied to one of the inertial response control concepts from the literature.**

***Index Terms*—wind energy, frequency stability, wind power plant, frequency control, inertial response**

I. Introduction

Electricity generation from wind energy has rapidly increased for the last five years by 27.4% worldwide [1]. In many countries, wind energy targets have been set in the range of 20% to 50% of all electricity generation due to the concerns of CO_2 emissions, fossil fuel costs, and energy efficiency [2]-[4]. In order to maintain sustainable and reliable operation of the power system for these targets, transmission system operators (TSOs) have revised the grid code requirements [5]. Also, the TSOs are planning the future development of the power system to integrate more wind power according to their grid codes. Various future wind penetration scenarios have been specified covering low levels to high levels of wind penetration with low and high levels of power consumption [6]. In the scenarios with high wind power penetrations, conventional power plants (CPPs) such as old thermal power plants are planned to be replaced with wind power plants (WPPs) [7]. Consequently, the power system inertia is reduced due to the replacement of CPPs and the wind turbine (WT) technology which does not respond like a physical inertia of synchronous generators [8].

The power system inertia determines the sensitivity of system frequency which indicates how fast and deep the system frequency deviates after a imbalance between generation and consumption. The total inertial response of each synchronous generator determines the power system inertia. The power system inertia helps to stabilize the system frequency by providing time for primary frequency controllers to respond [9], [10]. However, the inertial response cannot be provided inherently by WPPs. In the high wind power penetration scenarios which have the replacement plans of CPPs, the power system frequency stability may be affected more adversely for the islanded systems such as UK, Ireland, and Bornholm. Therefore, frequency stability studies should take into account the capability of WPPs providing short-term additional active power [11]. This capability has been defined as 'synthetic inertial response' in the grid code recommendations and studies [12], [13].

The wind power industry has focused on the inertial response capability of WTs in the last years. A comprehensive summary regarding this topic is given in [14]. Different control concepts enabling inertial response have been proposed for WPPs and WTs in the literature [15]-[28]. These control concepts can be divided into two main categories with respect to the input signal and the inertial response shape. The first category is the derivative control for the rate of change of frequency (ROCOF) and referred as derivative control [15]-[22]. The idea is to emulate the inertial response of a synchronous generator using the electromechanical equation. Due to the sensitivity of the derivative control, a low-pass filter is added to eliminate noise from measurement. In the second category, the control provides an additional active power temporarily proportional to frequency deviation or predefined constant value [23]-[28]. In this paper, it is defined as temporary frequency control. These control concepts should be analyzed by the TSOs in order to define the requirements for WPPs' inertial response in their grid codes.

In the literature, aforementioned control concepts have been applied to various power system models such as single-mass model [19], [26] and single-bus model [20], [21], [27], [28]. However, these power system models are insufficient to analyze the impacts of WPPs' inertial response on power systems.

Besides the power system model, realistic wind power penetration scenarios should be specified in order to analyze the impact of the WPP inertial response on the power system.

This work was supported in part by Vestas Wind Systems A/S under the Vestas Power Programme.

M. Altin, R. Teodorescu and B. B. Jensen are with the Department of Energy Technology, Aalborg University, Aalborg, 9220, Denmark. (e-mail: mua@et.aau.dk, ret@et.aau.dk and bbj@et.aau.dk).

U. D. Annakkage, with the Department of Electrical and Computer Engineering, University of Manitoba, Winnipeg, MB R3T 5V6,Canada (e-mail: annakkag@ee.UManitoba.ca)

F. Iov and P. C. Kjaer are with Vestas Wind Systems A/S, Århus, 8200, Denmark (e-mail: fliov@vestas.com and pck@vestas.com).

However, in the literature these scenarios have been implemented simply by changing the inertia constant of the synchronous generators [27] or increasing the amount of generation loss (or load) [28], which are not representing the realistic situations. Accordingly, a methodology to assess the WPP inertial response should include a realistic power system model with wind power penetration scenarios.

In this paper, a methodology is proposed for assessment of inertial response from WPPs. The methodology covers a power system model with wind power penetration scenarios, operational metrics, and a WPP model. The power system model used in this methodology captures frequency and voltage response dynamics of a power system. In the power system model, realistic wind power penetration scenarios are performed and operational metrics regarding frequency stability are specified to determine the inertial response requirements from WPPs. Moreover, a simplified WPP model with an inertial response controller is included in the power system model. Finally, the inertial response controller is assessed using this methodology.

II. Background

Frequency stability is defined as the ability of a power system to maintain steady frequency after a disturbance resulting in a significant imbalance between generation and consumption. It depends on the control performance at the generation side and the protection settings at the consumption side. Generally, frequency stability problems are associated with inadequacies in power system component responses, poor coordination of control and protection equipment, or insufficient generation reserve [29].

In frequency stability studies, the power system frequency response stages should be investigated following a disturbance. The largest infeed loss is an example of significant imbalance, which is one of the (N-1) contingency criteria in transmission system planning. The power system progresses through the frequency response stages described in Table I after the largest infeed loss [9], [10].

Table I
Frequency Response Stages following a Generation Loss

	Stage	Impact	Origin
1	Electromagnetic energy release	Maintain synchronism	Magnetic field of synchronous generator
2	Inertial response	Slow down ROCOF	Kinetic energy from rotor
3	Primary frequency control	Bring frequency to a steady-state level	Frequency responsive reserve
4	Automatic generation control	Bring frequency back to its nominal value	Contingency reserve

The first two stages are inherent responses from synchronous generators in CPPs. In the electromagnetic energy stage, the synchronous generators release immediately an additional active power depending on their electrical distance from the point of the generation loss. However, the additional active power sustains approximately 1/3 of a second, and it comes from the magnetic field of the synchronous generator. In the following stage, which is defined as the inertial response stage, the system frequency starts to decrease due to the difference between the mechanical power input and the electrical power output of each synchronous generator. The relation is described as the electromechanical equation in (1), where ω is the rotational speed, H is the inertia constant, P_{mech} and P_{elec} are the mechanical and electrical power of the synchronous generator, respectively.

$$2H\frac{d\omega}{dt} = P_{mech} - P_{elec} \quad (1)$$

During the second stage, the additional power comes from the stored rotational energy of the synchronous generator. The change of the active power depends on the inertia constant (H) and the rotational speed change rate ($d\omega/dt$).

The inertial response of the synchronous generator is illustrated in Fig. 1. The dashed curve is the active power delivered from the rotational kinetic energy and the dotted curve shows the active power given by the primary frequency control after a loss of generation.

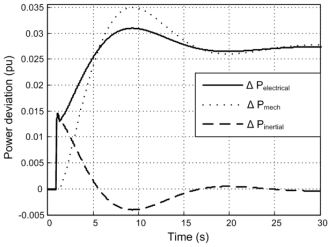

Fig. 1. Synchronous generator frequency response

The power system inertia is the overall inertial response of each synchronous generator in CPPs. However, WPPs do not provide inertial response inherently due to the converter based grid interface of WTs. Therefore, for high wind power penetration scenarios comprising CPPs' replacement, the power system inertia is reduced due to the replacement of CPPs and the frequency stability is technically challenging. The power system requires a control capability from WPPs for these scenarios. National Grid in UK, ENTSO-E in EU, Red Electrica in Spain, and Hydro-Quebec in Canada have been working on grid code requirements for the implementation of an inertial response from WPPs. Table II summarizes the recent requirements and studies from TSOs with the illustration in Fig. 2.

Table II
Summary of The Requirements and Studies for Inertial Response from WPPs

TSO	Requirements
Red Electrica	derivative control (future requirement) (Fig. 2)
Hydro Quebec	emulating a synchronous generator with H=3.5s (grid code requirement) [14]
National Grid	similar to inertial response of a synchronous generator (discussion and recommendation [13]) (Fig. 2)
ENTSO-E	similar to inertial response of a synchronous generator (pilot grid code draft [12]) (Fig. 2)

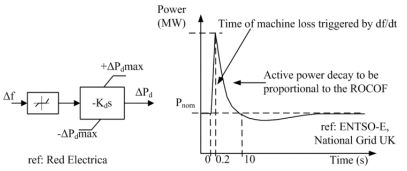

Fig. 2. Requirements and studies for WPP inertial response

In order to fulfill the future requirements and recommendations, several inertial response control concepts have been implemented in the literature [15]-[28]. These concepts can be grouped generally in two categories.

A. Derivative Control

The proportional control method based on ROCOF was proposed to emulate the inertial response of a synchronous generator [15]-[28]. The control modifies the active power or torque set point by an additional active or torque value using (1). The derivative control is sensitive to the noise in the frequency measurements. To solve this problem, a low-pass filter is added to the control as shown in Fig. 3.

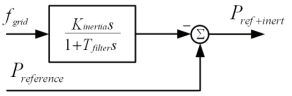

Fig. 3. Block diagram of the derivative control

B. Temporary Frequency Control

In this control method, an additional active power is released temporarily after the detection of a disturbance [23]-[28]. The magnitude of the additional active power can be either proportional to the frequency deviation [25] or a predefined value [26], [27]. The temporary frequency control is similar to a fast primary frequency control of a CPP, except the additional power is temporary in this control. The controller output is illustrated in Fig. 4.

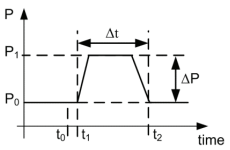

Fig. 4. Temporary frequency control response

The discussions and studies are still being carried out by the TSOs, academia, and industry. In these studies, the control concepts have been implemented in several power system models. Single-mass model is one of the models to analyze the impact of the WPP inertial response on the frequency stability (Fig. 5) [19], [26]. This model is valid for the frequency stability studies for governor control of CPPs. Using this model, the simulation results for the WPP inertial response studies present for how much the minimum frequency is changing. However, the model assumes that WPPs behave similar to CPPs after the disturbance, which is not the real case. WPPs are not able to have inherent electromagnetic release and inertial response stages. Additionally, the single-mass model is neglecting voltage deviations and power system oscillations after the disturbance.

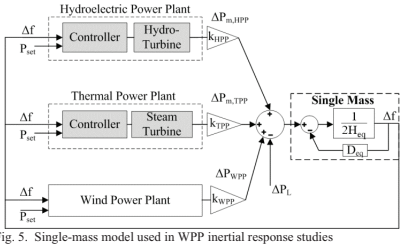

Fig. 5. Single-mass model used in WPP inertial response studies

Another power system model used for WPP inertial response analysis, the single-bus model, is used where all the power plants are connected to the same bus [20], [21], [27], [28]. This model is more realistic than the single-mass model however it is still missing the voltage response dynamics and power oscillations in the power system. Consequently, a power system model including voltage response dynamics and power oscillations is required in order to assess control concepts of WPP inertial response.

In these power system models, system inertia has been changed by reducing the power system inertia constant or increasing the loss of generation (or load) to indicate the need for the WPP inertial response control. These disturbances don't reflect realistic wind power penetrations, particularly for high wind power scenarios. Furthermore, the operational metrics regarding frequency stability have not been defined completely. For instance, the results have been compared only to the minimum frequency point not considering ROCOF.

In the following section, a methodology is proposed to assess the impact of the inertial response from WPPs on the power system. The methodology includes a power system model with wind power penetration scenarios, operational metrics, and a WPP model.

III. Methodology for Assessing Inertial Response from WPPs

The proposed methodology intends to assess the inertial response from WPPs including power system model, different wind power penetration scenarios, operational metrics for frequency stability, and a WPP model. These topics are presented in following subsections.

A. Power System Model: Generic 12-Bus Test System

The power system model should represent power system dynamics associated with the inertial response stage. Excitation system control and governor play an important role during this stage in power systems. Therefore, to investigate the impact of the WPP inertial response, multi-bus multi-machine model with excitation system control and governor is required.

Different multi-bus multi-machine models are available in the literature [30], [31]. However, these models have not been developed to conduct wind integration studies. Among these models, the original 12-bus test system [32], [33] has been selected and modified regarding the needs for WPP inertial response studies. As a result, the generic 12-bus test system for wind integration studies is modified and shown in Fig. 6. The modifications can be summarized as follows; realistic generators' loading, realistic voltage profile, updating load and excitation system models, adding governor and turbine models. The models and parameters in [31] are used for the modifications.

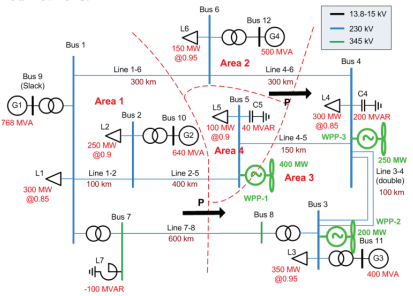

Fig. 6. Generic 12-bus test system

B. Wind Power Penetration Scenarios

In order to show the need for the inertial response from WPPs, detailed wind power penetration scenarios have been established for the generic 12-bus test system. The scenarios reflect different wind penetration levels from 0% to 50% in a power system. Two trends are assumed in establishing the wind penetration scenarios:

1. Increase load covered by an increase of wind power while CPPs' installed capacity is kept at the same level. This is a typical situation in countries with incentives for wind power in the early stages of development.
2. Increase wind power for the same load while closing some thermal power plants. This is typically in countries where wind power is reaching a relatively high penetration level e.g. 20% and there is no increase in the load.

The trends are summarized in Table III. Additionally, the distribution of WPPs to bus-3 and bus-4 is assumed more realistic for higher penetration levels (>20%). The total active power capacity of the generic 12-bus test system is 2248 MW including frequency responsive reserve. For the base case (0%), total active power of the load is established as 1450 MW and the total active power from CPPs is 1480 MW including the active power losses in the generic 12-bus test system.

TABLE III
WIND POWER PENETRATION SCENARIOS IN GENERIC 12-BUS TEST SYSTEM

	0%	5%	10%	20%	30%	40%	50%
CPP (MW)	1480	1470	1470	1470	1260	1120	1020
Load (MW)	1450	1550	1650	1850	1850	1850	1850
WPP (MW)	0	100	200	400	600	750	850

C. Operational Metrics

In order to assess the impact of wind power penetration on the power system, the operational metrics should be defined for the largest infeed loss. The operational metrics for the inertial response studies are chosen from the GC requirements of TSOs and literature regarding the frequency stability. The well-known metric is the maximum frequency deviation or in other terms minimum frequency point after the largest infeed loss. This metric is very important with respect to the frequency stability and the primary control response. The value is 800 mHz in 50 Hz systems and 900 mHz in 60 Hz systems due to the under-frequency load shedding limit [34].

The second metric is the maximum df/dt for islanding detection relays in the distributed generation. These relays measure df/dt and once the threshold value is exceeded after a detection time, a trip signal is initiated to disconnect distributed generation. The threshold value for maximum df/dt varies from 0.1 Hz/s to 1 Hz/s in 50 Hz systems, and the detection time varies from 50 ms to 500 ms [35].

Finally, the third metric is selected as the time to reach the minimum frequency point. The minimum frequency point and the time to reach this point are determined by the energy released during the inertial response stage. This time has an influence on the frequency response and should be considered carefully by the TSOs. It affects the management of the frequency control such as primary and secondary frequency reserve.

Abovementioned operational metrics are summarized in Table IV, and used for assessing the impact of the WPP inertial response in the generic 12-bus test system with the wind power penetration scenarios.

TABLE IV
OPERATIONAL METRICS FOR GENERIC 12-BUS TEST SYSTEM

Operational Metric	Ranges/Values	Remarks
max. dynamic frequency deviation (or min. frequency point)	0.016pu (=800mHz in 50 Hz)	Load shedding frequency limit (1 Hz) with a margin (200mHz)
max. df/dt (ROCOF) with a given detection time	0.008 pu/s with 200ms (=0.4Hz/s in 50 Hz)	ROCOF relay settings for distributed generation
time to reach the min. frequency point	4.68s (0% wind scenario)	Not to exceed the time simulated for the base case

D. Wind Power Plant Model

In the WPP inertial response studies, the proposed control concepts are implemented in a WT or WPP control level. In this paper, the WPP model is implemented as a first order transfer function. The block diagram is shown in Fig. 7. This simplification is sufficient enough to determine the power system requirements of the inertial response from WPPs. Also, the simplification is based on the following assumptions:

- Wind turbines are operating above the rated wind speed. (for no recovery period)
- Current controllers in the converter interface are very fast with respect to the active and reactive power controllers.

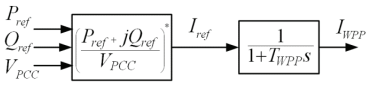

Fig. 7. Simplified WPP model

IV. Assessment Of The Derivative Control

The derivative control concept has been implemented in the generic 12-bus test system for all the WPPs. The block diagram of the derivative controller with the WPP is shown in Fig. 8. The parameters are the inertial response control gain (H_{WPP}), the rate limiter ramp-up rate (R_{WPP}), and the time constant of the WPP (T_{WPP}). In order to use the methodology described above, the parameters are swept with predefined values which are available in the literature for each wind power penetration scenarios. The results are assessed with respect to the operational metrics given in Table IV.

The values of the parameters are chosen from the literature as follows:

- R_{WPP} represents a grid code requirement or a limitation for wind turbines. R_{WPP} (pu/s) = 0.1 [25], 0.5 [11], 1
- T_{WPP} represents response time of the WPP. T_{WPP} (s) = 0.025, 0.125, 0.25 [12], [24], [25]
- H_{WPP} represents a gain of the inertial response controller. H_{WPP} (pu) = 3.5 [14], 5.3, 13.4, 28.3 (corresponding to 0.1,0.2, and 0.3 pu controller output respectively)

V. Results

The power dispatch is employed in the generic 12-bus test system performing the load flow calculations for all the wind power penetration scenarios. The power system is initialized and operating at steady-state with the generation and consumption balanced. At t = 2 s, the largest infeed, which is specified as 200 MW (2 units from G2, Fig. 6), is tripped resulting in a frequency deviation. Simulation time is 30 s covering the inertial response and primary frequency control stages of the power system. For each wind power penetration scenario, the impact of the disturbance on the operational metrics is examined.

The power system frequency after the loss of largest infeed is shown in Fig. 9 for different wind power penetration scenarios. The ROCOF of the system at 200ms after the largest infeed loss is given in Fig. 10 with T_{WPP} values swept from 0.025s to 0.25s.

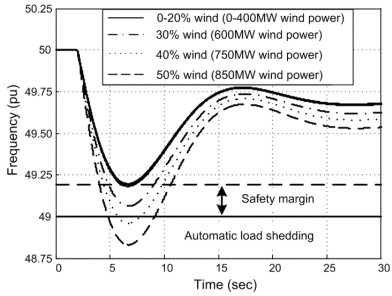

Fig. 9. System frequency deviation following the largest infeed loss for different wind power penetration scenarios (T_{WPP}=0.025s)

The impact of the increasing wind power penetration is the reduction of the power system inertia in terms of minimum frequency and ROCOF values. Due to the replacement of the CPPs for the penetration levels higher than 30%, there is a need for inertial response from WPPs.

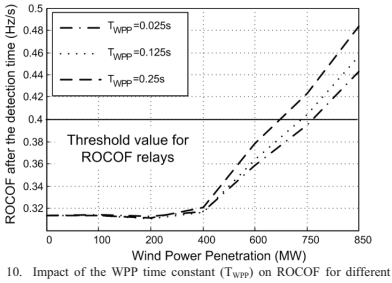

Fig. 10. Impact of the WPP time constant (T_{WPP}) on ROCOF for different wind power penetration scenarios

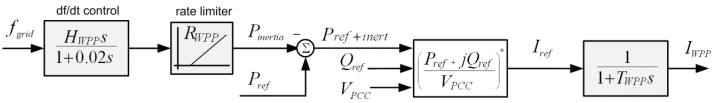

Fig. 8. WPP model with derivative control

Additionally, time constant of the WPPs (T_{WPP}) have a significant impact on the ROCOF due to the voltage deviations at the point of common coupling (PCC). Following the largest infeed loss, the reactive power from CPPs is changed and the bus voltages close to the loss will fluctuate. Consequently, it takes a certain time for the active and reactive power output of the WPPs to reach the pre-disturbance set values due to the T_{WPP}. In Fig. 10, when the response time is increased (higher T_{WPP}, slow response), the ROCOF threshold value is reached at the lower penetration levels.

ROCOF is the main limitation for the derivative controller parameters according to the results (sweeping H_{WPP}, T_{WPP}, R_{WPP} values) presented in Table V. The values in gray exceed the specified limits in Table IV.

TABLE V
RESULTS OF PARAMETER SWEEP FOR 40% AND 50% WIND PENETRATION SCENARIOS

			Wind Power Penetration Scenarios			
			40 %		50 %	
H_{WPP} (pu)	R_{WPP} (pu/s)	T_{WPP} (s)	f_{min}	df/dt	f_{min}	df/dt
-	-	0.025	48.97	0.40	48.84	0.44
		0.25	48.96	0.42	48.83	0.48
3.5	0.1	0.025	49.02	0.38	48.91	0.42
		0.25	49.03	0.42	48.93	0.47
	1	0.025	49.02	0.33	48.92	0.36
		0.25	49.03	0.38	48.93	0.43
5.3	0.1	0.025	49.05	0.38	48.95	0.42
		0.25	49.06	0.42	48.96	0.47
	1	0.025	49.05	0.31	48.95	0.33
		0.25	49.06	0.37	48.97	0.41
13.4	0.1	0.025	49.13	0.38	49.05	0.42
		0.25	49.14	0.42	49.06	0.47
	1	0.025	49.14	0.23	49.06	0.24
		0.25	49.15	0.34	49.08	0.38
28.3	0.1	0.025	49.22	0.38	49.15	0.42
		0.25	49.22	0.42	49.15	0.47
	1	0.025	49.24	0.20	49.18	0.20
		0.25	49.25	0.34	49.20	0.38

In 40% wind penetration scenario, the slowest response (T_{WPP}=0.25s and R_{WPP}=0.1pu/s) is not fulfilling the operational metric related to the ROCOF relay settings for all the inertial response gains (H_{WPP}). Furthermore, considering the smaller gain values lower than 13.4 pu, the minimum frequency point is very close to the load-shedding limit (49 Hz).

In 50% wind penetration scenario, the impact of the parameters on the power system is more substantial than the 40% scenario. According to the Table V, with the R_{WPP}=0.1 pu/s, the ROCOF is exceeding the limits in the operational metrics regardless of the T_{WPP} and the H_{WPP}. In other words, if the WPPs have lower ramp rates, the ROCOF relays will trip the distributed generation.

When the R_{WPP} is changed keeping the T_{WPP} constant, the minimum frequency point is affected slightly (50 mHz) in the case of a high gain (H_{WPP}=28.3pu). The R_{WPP} value for 1 pu/s keeps the ROCOF within the limits specified in the operational metrics. The active power output variation of the WPP-1 connected to bus-5 and the frequency deviation are given in Fig. 11 with different R_{WPP} values.

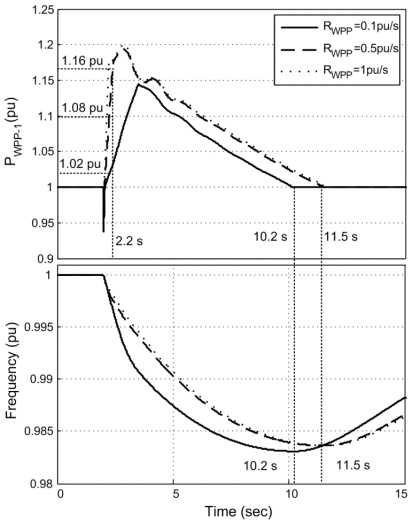

Fig. 11. Impact of the rate limiter gain (R_{WPP}) on WPP-1 active power output and system frequency (H_{WPP} = 28.3pu and T_{WPP} = 0.025s).

The effect of the T_{WPP} for the minimum frequency point is negligible (≈20 mHz). On the contrary, the T_{WPP} has an impact on the ROCOF similar to the R_{WPP} due to the regulation performance of the WPP active power control. This can be clearly seen in Fig. 12 for different T_{WPP}.

For the operational metric 2 (ROCOF), WPPs should act rapidly in 200 ms by releasing additional 0.047 pu active power in their MW base value (Fig. 12). Consequently, the first drop in active power due to voltage variation does not trigger the ROCOF relays, and therefore the duration of the active power recovery can be realized as a detection time needed for the WPP inertial response control. The requirement for both additional active power and detection time can be rearranged with respect to the ROCOF relay settings.

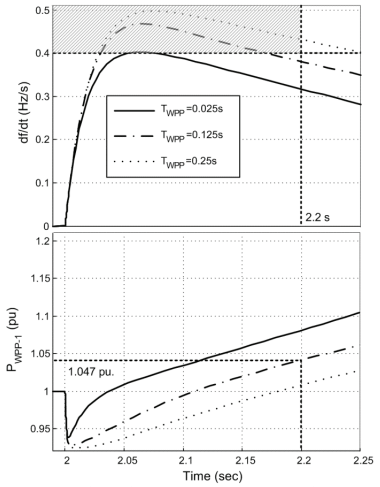

Fig. 12. Impact of the rate limiter gain (T_{WPP}) on ROCOF and WPP-1 active power output (H_{WPP} = 28.3pu and R_{WPP} = 0.5pu/s).

The first operational metric is related primarily to the governor response of the CPPs. Following the loss of largest infeed, the governors detect the frequency deviation and increase mechanical input of the turbine in order to compensate the power mismatch. The speed of the governor performs the frequency response in terms of the minimum frequency point and time to reach this point. For the WPP inertial response, the control releases an additional power for a certain time. Therefore, an additional energy is given to the system like the kinetic energy release of the CPPs. In Table VI, the minimum frequency point is compared with respect to the released energy from WPPs and time to reach the minimum frequency point for 50% wind penetration. The minimum frequency points are relatively close such as 49.15 Hz and 49.18 Hz with different released energy (4.66pu.s and 7.45pu.s) where H_{WPP} = 28.3, T_{WPP} = 0.025s, R_{WPP} = 0.1 pu/s and 1pu/s. This can be realized also from the WPP-1 active power output in Fig. 11. Accordingly, by keeping the R_{WPP} constant and increasing the T_{WPP}, the released energy is reduced, but the same minimum frequency point is obtained (Table VI). The third operational metric, time to reach minimum frequency point, is dependent on the released energy from WPPs. In Table VI, the more energy is provided by the WPPs to system, the longer time is obtained to reach the minimum frequency point.

The assessment results of the derivative control are illustrated in Fig. 13. The illustration can be realized as power system requirements from the derivative control. The ramp rate of the inertial response can be set to 0.5 pu/s from Fig. 12.

TABLE VI
COMPARISON OF MINIMUM FREQUENCY POINT FOR 50% WIND PENETRATION WITH RESPECT TO THE INERTIAL RESPONSE ENERGY FROM WPPS

H_{WPP} (pu)	T_{WPP} (s)	R_{WPP} (pu/s)	Wind Power 50 %		
			f_{min} (Hz)	ΔE_{WPP} (pu.s)	t_{min} (s)
13.4	0.025	0.1	49.05	3.05	6.84
		1	49.06	4.14	7.39
	0.25	0.1	49.06	2.75	6.62
		1	49.08	3.91	7.29
28.3	0.025	0.1	49.15	4.66	8.23
		1	49.18	7.45	9.69
	0.25	0.1	49.15	4.07	7.74
		1	49.20	6.90	9.37

Furthermore, the additional active power value at t = 2.2s is selected as 0.047 pu which is obtained from Fig.12. Additionally, the energy released during the inertial response control is taken from Table VI as 4.07 pu.s. With these values, the derivative control used in the methodology is achieving the operational metrics. However, Fig. 13 does not comprise the complete range of the parameters for the derivative control response since these values are the results obtained from certain H_{WPP}, R_{WPP}, T_{WPP} parameters.

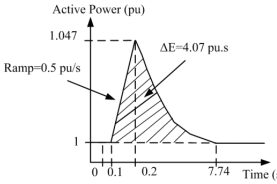

Fig. 13. Power system requirements for the inertial response from WPPs using derivative control.

VI. CONCLUSION

In this paper, a methodology is proposed to assess the inertial response from WPPs. The methodology is composed of a generic 12-bus test system with wind power penetration scenarios, operational metrics, and a WPP model. Using the proposed methodology, derivative control, which is a well-known control concept in the literature, is assessed and the results are summarized to determine the power system requirements for the WPP inertial response. In this study, the aerodynamic and mechanical dynamics are not included. The wind speed is assumed to be over the rated speed to neglect the recovery period of the WTs. The study is the first approach for determining the power system requirements for the WPP inertial response. As a future work, the temporary frequency response control concept, dynamics of a WT, and the detailed WPP model will be implemented, and analyses will be performed with the proposed methodology.

VII. ACKNOWLEDGMENT

This work was supported by Aalborg University-Vestas Wind Systems A/S partnership under Vestas Power Program. Any opinions, findings, and conclusions or recommendations expressed in this material are those of the authors and do not necessarily reflect those of Vestas Wind Systems A/S.

VIII. References

[1] BTM Consult ApS, "International Wind Energy Development, World Market Update 2010," Mar. 2010.

[2] Ecofys Final Report for Work Package-3 prepared for EirGrid, "All Island TSO Facilitation of Renewables Studies," June 2010.

[3] EcoGrid Phase 1 Work Package 3, "Step toward a Danish Power System with 50% Wind Energy", Jan. 2007.

[4] IEA Wind Task 25 Final Report Phase 1, "Design and Operation of Power Systems with Large Amounts of Wind Power," 2009.

[5] M. Altın, O. Göksu, R. Teodorescu, P. Rodriguez, B.-Bak Jensen, L. Helle, "Overview of recent grid codes for wind power integration," in *Optimization of Electrical and Electronic Equipment (OPTIM), 2010 12th International Conf.*, pp.1152-1160.

[6] National Grid UK, "Frequency Response Technical Sub Group Meeting Summary," Mar. 2011.

[7] National Grid UK, "*National Electricity Transmission System Seven Year Statement*," May 2011.

[8] M. Altın, R. Teodorescu, B.-Bak Jensen, P. Rodriguez, F. Iov, P. C. Kjær,"Wind Power Plant Control-An Overview", in Proc. *9th International Workshop on Large-Scale Integration of Wind Power into Power Systems as well as on Transmission Networks for Offshore Wind Power Plants 2010*, pp. 581-588

[9] J. Machowski, J. W. Bialek, and J. R. Bumby, *Power System Dynamics: Stability and Control*, Wiley, 2008, p. 353

[10] EPRI, "EPRI Power Systems Dynamics Tutorial, Final Report," July 2009.

[11] National Grid UK, "Grid Code Review Panel Paper, Future Frequency Response Services," Sept. 2010.

[12] ENTSO-E, "Requirements for Grid Connection Applicable to all Generators including dedicated requirements for specific generating unit facilities, working draft," Oct. 2010

[13] National Grid Code Frequency Response Working Group UK, "Requirements for System Inertia," July 2010.

[14] P. W. Christensen, G. C. Tarnowski, "Inertia for Wind Power Plants-State of the Art Review Year - 2011 ", in Proc. *10th International Workshop on Large-Scale Integration of Wind Power into Power Systems as well as on Transmission Networks for Offshore Wind Power Plants 2011,* pp. 457-463.

[15] J. Morren, J. Pierik, and S. Dehaan, "Inertial response of variable speed wind turbines," *Electric Power Systems Research,* vol. 76, no. 11, pp. 980-987, Jul. 2006.

[16] J. Morren, S. W.H. de Haan, W L. Kling, and J. A. Ferreira, "Wind turbine emulating inertia and supporting primary frequency control," *IEEE Transactions on Power Systems,* vol. 21, no. 1, pp. 433-434, 2006.

[17] L. Holdsworth, J. B. Ekanayake, and N. Jenkins, "Power system frequency response from fixed speed and doubly fed induction generator-based wind turbines," *Wind Energy*, vol. 7, no. 1, pp. 21-35, Jan. 2004.

[18] O. Anaya-Lara, F. Hughes, N. Jenkins, and G. Strbac, "Contribution of DFIG-based wind farms to power system short-term frequency regulation," in *Generation, Transmission and Distribution, lEE Proceedings*, 2006, vol. 153, no. 2, pp. 164-170.

[19] G. Lalor, A. Mullane, and M. O'Malley, "Frequency Control and Wind Turbine Technologies," *IEEE Transactions on Power Systems,* vol. 20, no. 4, pp. 1905-1913, Nov. 2005.

[20] J. F. Conroy and R. Watson, "Frequency response capability of full converter Wind turbine generators in comparison to conventional generation," *IEEE Transactions on Power Systems,* vol. 23, no. 2, pp. 649-656, May 2008.

[21] A. Mullane and M. O'Malley, "The Inertial Response of Induction-Machine-Based Wind Turbines," *IEEE Transactions on Power Systems,* vol. 20, no. 3, pp. 1496-1503, Aug. 2005.

[22] G C. Tarnowski, P C. Kjaer, P. E. Sorensen, J. Ostergaard, "Study on variable speed wind turbines capability for frequency response" in *Proceedings of the European Wind Energy Conference EWEC* 2009, p. 16-19

[23] G. C. Tarnowski, P C. Kjaer, P. E. Sorensen, and J. Ostergaard, "Variable speed wind turbines capability for temporary over-production," in *IEEE Power & Energy Society General Meeting,* 2009. pp. 1-7

[24] G. C. Tarnowski, P. C. Kjaer, S. Dalsgaard, and A. Nyborg, "Regulation and frequency response service capability of modem wind power plants," in *IEEE Power & Energy Society General Meeting,* 2010, pp. 1-8.

[25] S. Wachtel and A. Beekmann, "Contribution of wind energy converters with inertia emulation to frequency control and frequency stability in power systems," in *Proc. 2009 8th Workshop on Large-Scale Integration of Wind Power into Power Systems,* pp. 460-465.

[26] N. R. Ullah and T. Thiringer, "Temporary primary frequency control support by variable speed wind turbines-potential and applications," *IEEE Transactions on Power Systems,* vol.23, no.2, pp.601-612, May 2008.

[27] M. Kayikci and J. V. Milanovic, "Dynamic Contribution of DFIG-Based Wind Plants to System Frequency Disturbances, " *IEEE Transactions on Power Systems,* vol. 24, no. 2, pp. 859-867, May. 2009.

[28] K. Ping-Kwan, L. Pei, H, Banakar, B. T. Ooi, "Kinetic Energy of Wind-Turbine Generators for System Frequency Support," *IEEE Transactions on Power Systems,* vo1.24, no.1 , pp.279-287, Feb. 2009

[29] IEEE/CIGRE Joint Task Force, "Definition and Classification of Power System Stability," Jun. 2003.

[30] P. Kundur, *Power System Stability and Control*, 1994, McGraw-Hill

[31] P. M. Anderson, A A. Fouad, *Power System Control and Stability,* Wiley-IEEE Press, 2003.

[32] CIGRE Working Group B4.39, "Integration of Large Scale Wind Generation using HVDC and Power Electronics," Feb. 2009.

[33] J. Shan, U.D. Annakkage, AM. Gole, "A platform for validation of FACTS models," *IEEE Transactions on Power Delivery,* vo1.21, no. I, pp, 484- 491, Jan. 2006.

[34] ENTSO-E, "Load-Frequency Control and Performance," Jun. 2004.

[35] C.F, Ten, P.A Crossley, "Evaluation of ROCOF Relay Performances on Networks with Distributed Generation," *IET 9th International Conference on Developments in Power System Protection,* pp.523-528, 17-20 Mar. 2008.

IX. Biographies

Mufit Altin is currently working toward the PhD. degree in the Department of Energy Technology, Aalborg University, Denmark. His research interest includes distribution automation, wind power plant control, wind energy, and power systems.

Remus Teodorescu currently works as full professor Aalborg University, Department of Energy Technology. His areas of interests are: design and control of power converters used in renewable energy systems, distributed generation mainly wind power and photo-voltaics, computer simulations, digital control implementation.

Birgitte Bak-Jensen currently works as full professor Aalborg University, Department of Energy Technology. Her fields of interest are dispersed generation, smart grid systems, and power quality and stability in power systems.

Udaya Annakkage is a professor at the University of Manitoba, Winnipeg, MB, Canada. His research interests are power system stability and control, security assessment and control, operation of restructured power systems, and power system simulation.

Florin Iov currently holds the position as power system research specialist in Vestas Technology R&D/Global Research. His research covers control and application of electrical machines and power electronic converters for grid integration of renewable energy sources, operation and control of wind power plants in modern power systems.

Philip Carne Kjaer currently holds the position as chief specialist for power plants in Vestas Technology R&D/Global Research. His research covers control and application of electrical machines and power electronic converters.

[P5] published in EPE Joint Wind Energy and T&D Chapters Seminar, 2012

Generic 12-Bus Test System for Wind Power Integration Studies

Andrzej Adamczyk, *Student Member, IEEE,* Mufit Altin, *Student Member, IEEE*, Ömer Göksu, *Student Member, IEEE,* Remus Teodorescu, *Fellow, IEEE*, and Florin Iov, *Senior Member, IEEE*

***Abstract*--High wind power penetration levels into power systems requires an appropriate power system model when assessing impact on the overall system stability. The model should capture the wide range of dynamics related to the wind integration studies, such as voltage control, synchronizing power control, inertial response, frequency control, damping of electromechanical oscillations, balanced and unbalanced fault management, etc. Hence, the power system components: conventional power plants with controls, transmission lines, transformers and loads should be represented accurately to achieve realistic power system characteristics. Additionally, the power system model should be simple and computationally manageable in order to simulate multiple scenarios with different control parameters in a reasonable time. In this paper, a generic power system model is presented in order to comprehend the wind integration studies with different penetration scenarios.**

***Index Terms*-- wind power, integration studies, power system stability and dynamics, power system modeling**

I. Introduction

Wind energy generation has increased by 27.4% worldwide over five recent years [1]. Moreover, targets for total electricity generation, ranging from 20% to 50%, have been set for wind energy installations by many countries, considering CO_2 emissions, fossil fuel costs and energy efficiency [2]-[4]. Transmission system operators (TSOs) of these countries have revised their grid codes for wind power integration in order to provide the stable operation of the power systems while reaching these targets [5], and power systems are planned for more wind power integration. Wind power penetration scenarios have been defined for varying levels of penetration and consumption [6]. When wind power penetration is reaching high levels, it is planned that wind power plants (WPPs) replace old thermal conventional power plants (CPPs) [7].

Beyond a certain level wind power penetration into a power system poses challenges regarding wind power control and stable power system operation. Nowadays, the wind power can offer capabilities for ancillary services that can contribute to the power system stability. It is expected that these offerings for ancillary services will expand in the future with new functionalities such as inertial response, power system damping, secondary voltage control, etc. These services will play an important role especially in networks with high wind power penetration levels. In order to study the impact of these new ancillary services on the power system, simulation studies must be performed on a test system.

Numerous test systems variants were proposed in the literature. A simple test system represented by a voltage source behind an impedance is proposed in Danish grid code [8] to assess the stability of a wind turbine for symmetric three-phase faults. However, this test system does not include the dynamics regarding the frequency response, voltage control, and electromechanical oscillations. Furthermore, for inertial response and frequency control studies the single-mass model is implemented in the literature [9]. The rotating masses of all synchronous generators in CPPs are lumped as a single-mass; and governor controls are acting on this single-mass. The single-mass model represents the frequency control dynamics however neglecting the voltage variations and electromechanical oscillations. Another simplified model comprising these two models' behavior is implemented as a single-bus model in the literature [10], where all the generating units are connected to a single bus with their voltage and frequency controllers. In the single-bus model, the voltage dynamics are limited due to the small electrical distances between the synchronous generators. Nevertheless, this model is sufficient enough to analyze power system oscillations and balanced/unbalanced faults. However, in order to cover the wind integration studies thoroughly, a multi-machine multi-bus system is required with appropriate voltage and frequency controls.

Different multi-machine multi-bus power system models that can exhibit particular phenomena exist in the available literature, e.g. 9-bus system [11], 2-area 4-machine system [12], 12-bus system [13], [14], and 68-bus 16-generator system [15].

The 9-bus system is not adequate to create various generation mixes, voltage profiles and electromechanical oscillation modes. The 2-area 4-machine system has been developed for studying the theory of the small signal stability; however it is not representing a realistic power system layout. The voltage profile of the 2-area 4-machine system is relatively stiff due to small electrical distances between the system buses and the radial and symmetrical system structure does not allow flexibility in mode creation. The original 12-bus system was developed to test FACTS devices and it is

This work was supported in part by Vestas Wind Systems A/S under the Vestas Power Programme.

A. Adamczyk, M. Altin, Ö. Göksu and R. Teodorescu are with the Department of Energy Technology, Aalborg University, Aalborg, 9220, Denmark. (e-mail: mua@et.aau.dk, ana@et.aau.dk, omg@et.aau.dk and ret@et.aau.dk).

F. Iov is with Vestas Wind Systems A/S, Århus, 8200, Denmark (e-mail: fliov@vestas.com)

supporting small signal stability analysis. However, it does not include a wide range of parameters and settings for CPPs. The 68-bus 16-generator system gives great flexibility in formulating system dynamics and enables approaching a realistic system behavior. However, due to the system size it is too complex to handle it analytically in a small-signal stability analysis or other wind integration studies.

The existing power system models described above are not able to accommodate wind integration studies when they are used in their current form. For wind integration studies, the wind power locations in the power system and different wind penetration scenarios should be specified in detail. Thus, a test system that is able to support wind power studies should be relatively weak – system should be stressed close to a stability limit. Still, the test system should be stable under steady-state conditions. In the base case, voltage profile of the network should not be uniform - i.e. deviations around 1pu should exist, while staying in the limits of ±5% from the nominal values, as commonly required by the grid codes. Moreover, some of the system load buses should be relatively weak -i.e. be electrically distant from the conventional generating units.

The primary frequency control requires a network with different conventional generation mixes, including settings for governors as well as load variations. Inertial response studies have the similar requirements with different wind penetration scenarios. On the other hand, studies regarding electromechanical oscillation damping capabilities from wind power are requiring presence of different oscillation modes in the power system that are mainly coming from CPPs in combination with the network parameters and layout.

Taking into account the abovementioned requirements, a number of test cases should be defined (e.g. line and generator tripping, step load change) to impose abnormal conditions on the system and excite different kinds of instabilities. Since wind integration studies are targeted, different realistic wind penetration scenarios should be established based on existing trends seen around the world. Overall, it is possible to relate a generic test system used for wind integration studies with real power grids including their trends in accommodating wind power.

The present paper is proposing a generic test system model based on the 12-bus test system [13], [14] that is able to address all the above mentioned characteristics.

II. Generic 12-Bus Test System

A. Model structure

The layout of the generic 12-bus system for wind integration studies is given in Fig. 1. The system represents a small islanded power system with four areas dominated by thermal power plants like power systems in UK, USA and Germany. Area 1 is the biggest thermal power generation area with industrial and residential loads. Area 2 has dominant hydro power generation with small amount of rural loads. Area 3 is a heavily industrial load center with thermal power generation, while Area 4 is rich in wind resources. Hence, it is considered to have wind power connected mainly at bus-5.

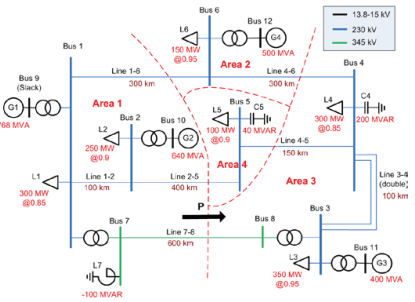

Fig. 1. Structure of generic 12-bus system for wind power integration studies.

There is a large power flow, over long lines, from Area 1 to Area 3. The infinite bus in the original 12-bus system (bus-9) is replaced with a CPP, G1. Traditionally, it is assumed that in power system studies the reference machine is the largest plant in the system. Therefore, size of G1 is set to 768 MVA to make its capacity largest among the generation mix. Most of the loads in Area 2 are shifted to Area 1 in order to balance the power flow.

Active power control for CPPs is included by implementing the prime mover and governor models. Active power dispatch between the areas is adjusted to improve voltage profile and achieve N-1 contingency criterion.

Instead of simplified 1st order exciters, more detailed models with realistic parameters are used for each CPP. The main buses exhibit a poor voltage profile and different electromechanical oscillations occur when triggered. Furthermore, both the residential and industrial loads in the test system are modeled as voltage and frequency dependent.

The system can be considered to be similar to UK power system in terms of direction of power flows as shown in Fig. 2, where Area 4 is representing offshore WPPs, Area 2 is hydro dominant Scotland, finally Area 1 and 3 are the congested central-south generation regions of the country.

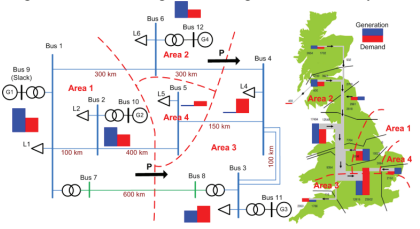

Fig. 2. Generic 12-bus system in context of UK grid [16].

B. Load Flow

The load flow for the base case without any wind power contribution is presented in Fig. 3.

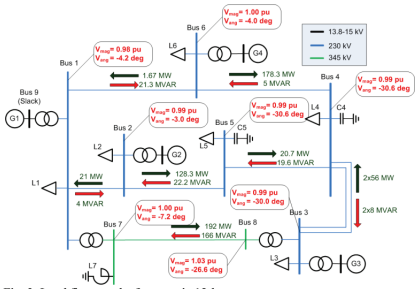

Fig. 3. Load flow results for generic 12-bus system.

In the base case, voltage profiles and load flows are balanced in order to represent steady-state operating conditions of the test system with proper reactive power compensation. Bus voltages are within the specified limits as ±5% of the nominal value, and accordingly the generator loadings (around 70%) and line loadings (around 50%) are within the acceptable limits. N-1 contingency criterion is achieved except the tripping of the longest line between bus-7 and bus-8. In addition to the steady-state analysis, the stiffness of the system buses is evaluated by a short circuit power calculation, and illustrated in Fig.4.

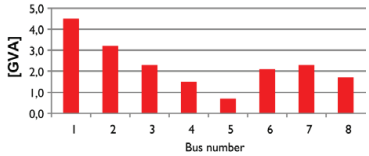

Fig. 4. Short-circuit power levels for each buses in generic 12-bus system.

C. Operational Scenarios

Various operational scenarios are considered for the generic power system model. These scenarios reflect different wind penetrations into the power system. Two trends in development of the power system have been considered. The first trend assumes that the increased loads are covered by the increase of wind power while the installed capacity of the CPPs is kept constant. This is a typical situation in countries with incentives for wind power in the early stages of wind power development e.g. Denmark, Germany, UK, etc. For these cases some levels of wind power penetration may require reinforcement of lines; however no major changes in the network layout are expected. The second trend assumes that the demand will not change significantly, but new wind farm installations would replace some for the existing CPPs. This is typically in the countries where wind power is reaching a relatively high penetration level e.g. more than 20%. A typical example for this trend is Denmark where 50% of electricity demand is planned to be covered from wind energy by 2025. Thus, the generic power system model can accommodate wind penetrations from 0% (base case) up to 50% as shown in Fig. 5

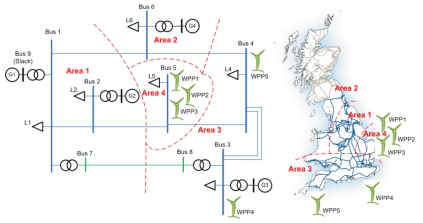

Fig. 5. Wind penetration scenarios for generic 12-bus system.

First, the wind power is inserted at bus-5 for penetration levels up to 30%. Then, the distribution of wind power to bus-3 and bus-4 is assumed to be more realistic for higher penetration levels (>30%). The total active power capacity of the generic 12-bus test system is 2248 MW, including frequency responsive reserve. For the base case (0%), total active power of the load is established as 1450 MW and the total active power from CPPs is 1480 MW including the active power losses.

TABLE I
WIND POWER PENETRATION SCENARIOS IN GENERIC 12-BUS TEST SYSTEM

	0%	5%	10%	20%	30%	40%	50%
CPP (MW)	1480	1470	1470	1470	1260	1120	1020
WPP (MW)	0	100	200	400	600	750	850
Load (MW)	1450	1550	1650	1850	1850	1850	1850

The sharing of production and consumption for the considered wind penetration levels is given in Table I. It should be noticed that the active power losses are included in the CPP generation.

III. CONVENTIONAL POWER PLANT MODEL

The structure of the CPP model implemented in the test system is shown in Fig. 6.

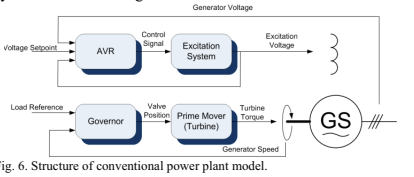

Fig. 6. Structure of conventional power plant model.

As given in the literature [17] this model comprises of a synchronous generator, prime mover, governor, excitation system, and automatic voltage control (AVR). In the following subsections, brief descriptions of those components are given.

A. Generator

The generator model is described by a set of six differential equations in a synchronous reference frame that describe rotor circuit dynamics as defined in [17]. Two additional steady-state equations are describing the stator circuit.

B. Prime mover and governor

The CPPs considered for the model are of fossil, steam and hydro types. Various types of governors in the power system for CPPs are available on literature. However, it is difficult to find parameters for a wide range of sizes. Thus, a governor and turbine model as defined in [11] is selected and shown in Fig. 7. The different parameters for the model are tested and selected with respect to the response rates. Three sets of parameters are benchmarked for different power system characteristics.

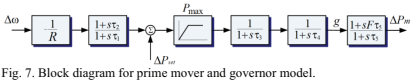

Fig. 7. Block diagram for prime mover and governor model.

C. Excitation system

Excitation systems can be categorized into three main groups [11], [18]:

- DC excitation systems,
- AC excitation systems,
- Static excitation systems.

Such categorization is also adopted in this paper. Nevertheless, for each category many models exist in the literature. Additionally, a wide scope of realistic parameters for excitation systems is hardly available in the literature. The parameters for abovementioned categories are selected from [11]. These models can be viewed as equivalent or simplified versions of models recommended by the current IEEE standard [18]. Hence adopting notation used in [11], for the generic 12-bus test system:

• DC exciters are modeled as Type A (equivalent to DC1A in [18]),

• AC brushless exciters are modeled as Type C (simplified version of AC1A in [18]),

• Static exciters are modeled as Type G (simplified version of ST1A in [18]).

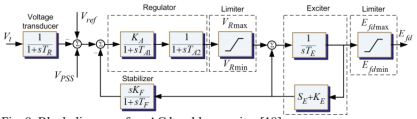

Fig. 8. Block diagram of an AC brushless exciter [18].

The different parameters for the model are tested according to the related IEEE standard [18]. Three sets of parameters are benchmarked for different power system characteristics.

IV. System Implementation

The proposed generic 12-bus test system model for wind integration studies is implemented in Matlab/Simulink and tested against an implementation in Power Factory DigSilent. Currently, the model is available in the RMS toolbox developed by the authors in Matlab/Simulink. The power system is represented algebraically in a complex current form while CPPs and WPPs are described by differential equations. The implemented approach in RMS toolbox to solve these equations is defined as partitioned-explicit method using a current-balance form [17]. The Matlab/Simulink RMS toolbox currently includes the analyses such as load flow, short-circuit calculation for symmetrical and asymmetrical faults, small-signal stability analysis, and time domain simulations for power system stability studies.

An alternative implementation has been accomplished in RSCAD, running in real time on RTDS. This model is suitable for Hardware-In-the-Loop (HIL) electro-magnetic transient (EMT) studies with detailed models of network components.

V. Small-Signal Stability Analysis

In order to select suitable types of excitation systems that meet the requirements for the base case of the test system a comprehensive small-signal stability analysis is performed.

Final selection of parameters regarding the excitation system and generator models is done to obtain a desired mode profile for electromechanical oscillations in the generic 12-bus test system. Based on the analysis, two sets of parameters are selected which correspond to two mode shape profiles.

Mode profile 1 is characterized by low damping of all electromechanical modes. All damping ratios are in the critical range of 0 to 10%. Moreover, for all modes of interest, a WPP at bus-5 has a relatively high potential (controllability index) to contribute to damping of this mode profile. For some modes active power controllability is higher, while for others reactive power controllability is higher. Mode profile 2 is characterized by highest average controllability index for reactive power modulation at bus-5, where most of the wind power is connected.

Frequency and damping ratio for mode shapes corresponding to the mode profile 1 are given in Table II. The generic 12-bus test system exhibits swing modes as well as control modes in the typical range for a power system. The participation factors for all swing modes in the mode profile 1 are shown in Fig. 11 for all CPPs.

TABLE II
OSCILLATORY MODES FOR MODE PROFILE 1

Mode No.	Damped requency	Damping ratio	
1	0.95 Hz	7.6 %	Swing modes
2	0.93 Hz	5.1 %	
3	0.77 Hz	0.5 %	
4	4.24 Hz	57.6 %	Control modes
5	1.16 Hz	47.4 %	
6	0.77 Hz	25.0 %	
7	0.58 Hz	33.2 %	

The response of the generators' speed in time domain for a small step in the voltage reference is shown in Fig. 13. Poorly damped mode in which G4 is highly participating is clearly noticed in Fig. 13. Two groups are swinging with respect to each other; the first group is G1 with G2, and the second group is G3 with G4.

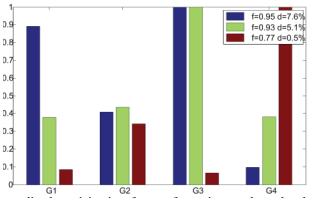

Fig. 9. Normalized participation factors for swing modes related to Mode Profile 1; Blue; Mode 1, Green: Mode 2, Red: Mode 3.

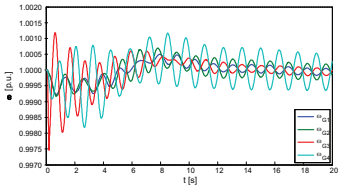

Fig. 10. Time domain responses of generators' speed to a step in voltage reference.

VI. System Frequency Response during Network Events

For the grid frequency performance profile, there are indices available in the grid codes such as the minimum frequency point (nadir or dynamic frequency deviation), quasi-steady-state frequency deviation, and rate of change of frequency (ROCOF) [19]. In the load-frequency control regulations of ENTSO-E, the maximum permissible frequency deviation is defined as ±800 mHz (0.016 pu) including a safety margin for the automatic load shedding frequency (1 Hz). Moreover, the quasi steady-state frequency deviation is specified between ±180 mHz (0.0036 pu) range.

In islanded power systems like UK and Ireland, TSOs defined ROCOF relay settings for the distributed generation connected to distribution system. The ROCOF relay trip value for EirGrid is 0.6Hz/s (0.012 pu/s). Taking into account the above regulations and practical implementations, a set of operational metrics is defined for the generic 12-bus test system. Based on a comprehensive analysis involving different sets of parameters for governors and prime movers, three sets of parameters are selected for each CPP. The system frequency response for the N-1 contingency which is the largest infeed loss is given in Fig. 14 considering the defined operational metrics. These parameter sets correspond to slow, medium and fast response of the CPPs respectively.

The voltage variations and electromechanical oscillations should be taken into account for the frequency control and inertial response studies of the WPPs. It is possible to observe these variations and oscillations in the generic 12-bus test system. An example of these variations at the connection bus of the WPP (bus-5) for the base case following the largest infeed loss is shown in Fig. 15.

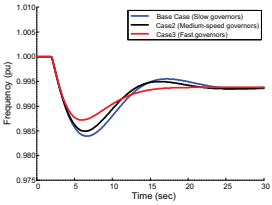

Fig. 11. Generic 12-bus test system frequency response for different governor and prime mover settings.

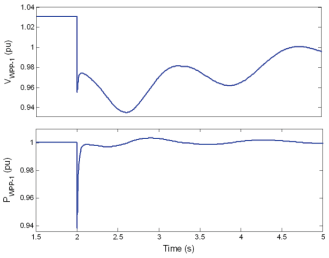

Fig. 12. Voltage and power variations at the connection point of WPP (bus-5).

VII. Future Work

As described in the previous sections, the developed generic 12-bus test system is appropriate for wind integration studies and can be used for analysis purposes such as small-signal stability, electromechanical oscillation damping, frequency response, etc. Additionally, the generic 12-bus test system is open for modifications and gives the opportunity to be improved by enhancements.

In order to analyze the impact of wind integration on the power systems for cases where HVDC connections and FACTS devices are installed, the generic 12-bus test system can be expanded with these units as shown in Fig. 16. For instance, the electromechanical oscillations in the power system can be analyzed where the HVDC and STATCOM units are also contributing in damping of oscillations.

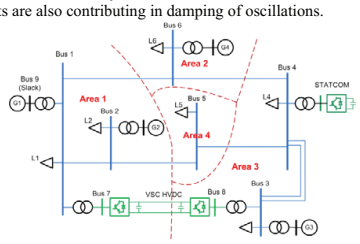

Fig. 13. Future expansion of generic 12-bus system with FACTS devices.

Moreover, WPPs can be installed in the generic 12-bus test system through HVDC connections, when analysis of wind integration with DC connection is under interest.

VIII. Summary

This paper presents a generic 12-bus test system with wind power penetration scenarios for wind integration studies. The developed test system is based on [13], but the original 12-bus test system has been modified in order to investigate and demonstrate the requirements of wind power on the power system. The scope of the analysis includes voltage control, synchronizing power control, inertial response, frequency control, damping of electromechanical oscillations, balanced and unbalanced fault management.

The realistic power system characteristics are demonstrated briefly using small-signal and frequency stability analysis. Accordingly, the generic 12-bus test system is simple and computationally manageable to simulate multiple scenarios with different control parameters. The test system is open for modifications regarding different power system components with control concepts such as HVDC, FACTs, and WAMs.

IX. Appendix – system data

Here is summarized data for the generic 12-bus system. Layout of the network is the same as show in Fig. 1. Line lengths and impedances are shown in Table III. Transformer data is given in Table IV. Bus configuration is shown in Table VI. Generator data, including controllers, is given in Table V. Due to space limitation only unit names, as used in the source references, are given. Hence, the detailed list of parameters for CPPs can be found in, according to [11] and [18]. Tables III-VI describe the base case cofiguration of the system.

Table III
Line data for 12-bus system base case scenario (100MVA base)

Line	Length [km]	R [pu]	X [pu]	B [pu]
1-2	100	0.01131	0.08998	0.18377
1-6	300	0.03394	0.26995	0.55130
2-5	400	0.0453	0.3599	0.7351
3-4	100 (x2)	0.0057	0.0450	0.3675
4-5	150	0.0170	0.1350	0.2757
4-6	300	0.03394	0.26995	0.55130
7-8	600	0.0159	0.1721	3.2853

Table IV
Transformer data for 12-bus system base case scenario

From-To Bus	Type	MVA Capacity	Uk (%)	Vector Group
1-7	Autotransformer	500	13	Y_NyN
1-9	Step-up	800	12	Y_Nd_{11}
2-10	Step-up	700	12	Y_Nd_{11}
3-8	Autotransformer	500	13	Y_NyN
3-11	Step-up	400	10	Y_Nd_{11}
6-12	Step-up	500	11	Y_Nd_{11}

Table V
CPP data for 12-bus system base case scenario

CPP	# of units	Total MVA Capacity	Generator type	Exciter type	Governor type
1	6	750	F6	H13	F10
2	4	640	F8	H13	F10
3	2	384	F9	F8	F10
4	3	474	H15	ST1A	H16

Table VI
Bus data for 12-bus system base case scenario (100MVA base)

Bus	V [kV]	Type	P_{gen} [pu]	P_{load} [pu]	Q_{load} [pu]	B_{shunt} [pu]	V_{mag} [pu]
1	230	PQ	-	3.00	1.86	-	-
2	230	PQ	-	2.50	1.21	-	-
3	230	PQ	-	3.50	1.15	-	-
4	230	PQ	-	3.00	1.86	2	-
5	230	PQ	-	1.00	0.48	0.4	-
6	230	PQ	-	1.50	0.49	-	-
7	345	PQ	-	-	-	-1	-
8	345	PQ	-	-	-	-	-
9	15.5	SL	-	-	-	-	1.00
10	15	PV	4.0	-	-	-	1.01
11	18	PV	2.7	-	-	-	1.01
12	13.8	PV	3.3	-	-	-	1.01

X. Acknowledgements

This work was supported by Aalborg University-Vestas Wind Systems A/S partnership under Vestas Power Program. Any opinions, findings, and conclusions or recommendations expressed in this material are those of the authors and do not necessarily reflect those of Vestas Wind Systems A/S.

XI. References

[1] BTM Consult ApS, "International Wind Energy Development, World Market Update 2010," Mar. 2010.

[2] Ecofys Final Report for Work Package 3 prepared for EirGrid, "All Island TSO Facilitation of Renewables Studies," June 2010.

[3] EcoGrid Phase 1 Work Package 3, "Step toward a Danish Power System with 50% Wind Energy", Jan. 2007.

[4] IEA Wind Task 25 Final Report Phase 1, "Design and Operation of Power Systems with Large Amounts of Wind Power," 2009.

[5] M. Altın, O. Goksu, R. Teodorescu, P. Rodriguez, B.-Bak Jensen, L. Helle, "Overview of recent grid codes for wind power integration," in *Optimization of Electrical and Electronic Equipment (OPTIM), 2010 12th International Conf.*, pp.1152-1160.

[6] National Grid UK, "Frequency Response Technical Sub Group Meeting Summary," Mar. 2011.

[7] National Grid UK, "*National Electricity Transmission System Seven Year Statement*," May 2011.

[8] Grid connection of wind turbines to networks with voltages above 100 kV, Regulation TF 3.2.5, Eltra and Elkraft System.

[9] G. Lalor, A. Mullane, and M. O'Malley, "Frequency Control and Wind Turbine Technologies," *IEEE Transactions on Power Systems,* vol. 20, no. 4, pp. 1905-1913, Nov. 2005.

[10] J. F. Conroy and R. Watson, "Frequency response capability of full converter Wind turbine generators in comparison to conventional generation," *IEEE Transactions on Power Systems,* vol. 23, no. 2, pp. 649-656, May 2008.

[11] P.M. Anderson and A.A Fouad, *Power System Control and Stability*, IEEE Press, 2003, ISBN 0-471-23862-7.

[12] P. Kundur, *Power System Stability and Control*, McGraw Hill, 1994, ISBN 0-07-035958-x.

[13] Shan Jiang, U. D. Annakkage, and A. M. Gole, "A platform for validation of facts models", Power Delivery, IEEE Transactions on, 21(1):484{491, 2006.

[14] CIGRE Working Group B4.39, "Integration of Large Scale Wind Generation using HVDC and Power Electronics," Feb. 2009.

[15] B. Pal, B. Chaudhuri, *Robust Control in Power Systems*, Springer, 2010, ISBN 978-1-4419-3853-4.

[16] www.nationalgrid.com/uk/

[17] Sauer, Pai, *Power System Dynamic and Stability*, Prentice Hall, 1997, ISBN-13: 978-0136788300.

[18] *IEEE recommended practice for excitation system models for power system stability studies*, IEEE Sandard 421.5-1992, 1992

[19] A. Adamczyk, R. Teodorescu and P. Rodriguez "Adaptation of 12-bus System for Wind Power Integration Studies".

[20] ENTSO-E, "Load-Frequency Control and Performance," Jun. 2004.

[P6] submitted to IEEE Transactions on Power Systems (under review)

Improved Inertial Response Control for Wind Power Plants

Mufit Altin, *Student Member, IEEE*, Andrzej Adamczyk, *Student Member, IEEE*, Remus Teodorescu, *Fellow, IEEE*, Birgitte Bak-Jensen, *Senior Member,* Udaya D. Annakkage, *Senior Member*, *IEEE*, Florin Iov, *Senior Member, IEEE*, and Philip Carne Kjær, *Senior Member, IEEE*

***Abstract*—. High wind power penetration scenarios demand additional control capability from wind power plants in order to enhance the frequency stability of power systems. Replacement of conventional power plants with wind power plants based on variable speed wind turbine technology reduces the power system inertia in these scenarios. Consequently, the rate of change of frequency and the maximum frequency deviation increase after a disturbance (e.g. loss of a conventional power plant). Having no inherent inertial response, wind power plants need supplementary control methods to provide additional active power following the disturbance. In this paper, a new inertial response control is proposed and simulated considering inertial response requirements of a generic power system with high wind power penetration. Furthermore, the tuning methodology of the proposed controller is described in detail. With the tuning methodology, the proposed control is generic and can be applied to any power system accommodating high wind power penetration. Accordingly, performance of the proposed control is compared with the existing control concepts in the literature by means of extensive simulation studies.**

***Index Terms*—Frequency stability, wind energy, wind power generation, inertial response, power system control.**

I. Introduction

THE variable speed wind turbines (VSWT), which dominate the current wind industry market [1], with converter-based grid interface provide decoupled, fast, and flexible control of active and reactive power [2], [3]. However, due to this control strategy, a VSWT does not have characteristics of a synchronous generator (SG) in terms of contributing to the power system inertia. With integration of wind power plants (WPP) employing VSWTs, the power system inertia is reduced for high wind power penetration scenarios which include replacement of conventional power plants (CPP) [4], [5]. Therefore, in the future, the frequency stability of power systems with high wind power penetration will be affected adversely and the control capability of WPPs should be reconsidered to enhance the frequency stability.

The wind power industry has focused on the inertial response capability of VSWTs in the last five years [6]. Transmission system operators (TSO) have been working on grid code requirements for implementation of a generic inertial response from WPPs [7]. Although some reports and recommendations for future grid codes have been published [8], there are no mandatory requirements at present.

This paper focuses on the inertial response control of WPPs in isolated power systems for high wind power penetration. In this study, the term 'inertial response' does not refer the emulation of a SG, but represents the temporary additional active power contribution from WPPs. Several control concepts have been proposed related to the inertial response of VSWTs in the previous studies [9]-[19]. The derivative control, which estimates the rate of change of frequency (ROCOF) with a low-pass filter, is implemented to emulate the inherent inertial response of a SG [9]-[15]. The impact of the derivative control on the power system is studied without considering the converter limitations of the VSWT in [9]. In [10], the influence of the derivative control on the converter and generator limitations of the VSWT is addressed and a novel control algorithm, which extracts the maximum energy from the turbine, is proposed. However, the proposed control algorithm provides a pre-defined temporary active power which is independent from the frequency deviation. In [11]-[13], the inertial response control of the VSWT is improved by implementing primary frequency control as an additional control loop. Further improvement for the DFIG based VSWT is achieved by employing the generator slip control [14], and coordinating WPPs with the CPPs' frequency response [15]. Besides the derivative control, the temporary frequency control, which is provision of an additional active power for a certain time period after detection of the frequency deviation, has been introduced [16]-[19]. The temporary frequency control response is determined with respect to the frequency deviation in [16] or a predefined active power pulse in [17]-[19]. Similar to the derivative control studies, the capability of VSWTs is evaluated for the temporary frequency control in [19], and evaluation results are utilized to tune the parameters of the temporary frequency control in [17]. Briefly, the previous studies are focused on either capability of VSWTs or simulation of the control concepts, however, without considering the power system requirements for the inertial response. Additionally, the description of the methodology for tuning the control parameters has not been mentioned in the previous studies. In fact, the inertial response control should consider power system requirements and the tuning methodology of the control concept should be developed

This work was supported in part by Vestas Wind Systems A/S under the Vestas Power Program.

M. Altin, A. Adamczyk, R. Teodorescu, and B. Bak-Jensen are with the Department of Energy Technology, Aalborg University, Aalborg, 9220, Denmark. (e-mail: mua@et.aau.dk, ana@et.aau.dk, ret@et.aau.dk and bbj@et.aau.dk).

U. D. Annakkage, with the Department of Electrical and Computer Engineering, University of Manitoba, Winnipeg, MB R3T 5V6,Canada (e-mail: annakkag@ee.UManitoba.ca)

F. Iov and P. C. Kjær are with Vestas Wind Systems A/S, Århus, 8200, Denmark (e-mail: fliov@vestas.com and pck@vestas.com).

according to power system characteristics. Furthermore, in future grid code revision studies, a generic inertial response control with the tuning methodology should be available for power systems with high wind power penetration.

This study begins with investigating the previous control concepts to comprehend requirements for a generic power system. The investigation results are employed to propose a new control concept with a tuning methodology for the generic power system. Eventually, the aim of the proposed control is to quantify the inertial response requirements from WPPs considering the VSWT capability for a given power system. The proposed control concept determines the inertial response profile, and the tuning methodology specifies the parameters of the profile according to the power system characteristics.

In this paper, first, the generic power system model is introduced with various wind power penetration scenarios and the performance criteria for the inertial response control are defined. Second, the aggregated WPP model is described comprising aerodynamical and mechanical dynamics of the VSWT. Following the modeling sections, the proposed control and tuning methodology are presented for the generic power system model. By means of extensive simulations, the proposed control and previous control concepts are evaluated and compared considering the impact on the power system and operational constraints of the VSWT.

II. Power System Model

The generic 12-bus test system given in Fig. 1 is utilized to assess the performance of the inertial response control in this study [20]. It represents a small isolated power system with four areas dominated by thermal power plants. Moreover, the generic test system has the flexibility for modeling different governor and prime mover settings in order to represent different frequency response of the power system. Thus, the impact of the inertial response control on different power systems can be analyzed using this test system. The data regarding governors and prime movers are given in Appendix.

Various wind penetration scenarios are implemented to have more realistic simulation cases for the generic 12-bus test system [20]. Two trends are assumed in establishing these scenarios. The first trend assumes that increased loads are covered by an increase of wind power while the installed capacity of the CPPs is kept constant. The second trend assumes that the demand will not change significantly, but new WPP installations will replace some of the existing old thermal CPPs. According to these trends, the generic 12-bus system accommodates wind power penetration from 0% up to 50% as shown in [20]. The percentage of the wind power penetration is defined as the ratio of the installed wind power capacity to installed conventional power capacity.

III. VSWT Model

In this study, aggregated WPP model based on a full-converter VSWT (FC-VSWT) with a permanent magnet synchronous generator (PMSG) is developed and employed to investigate the inertial response control in the generic power

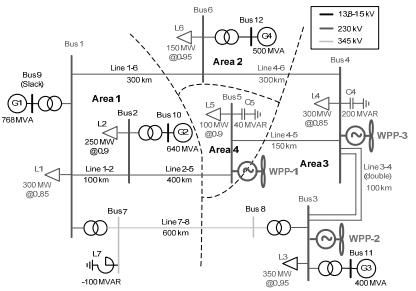

Fig. 1. Generic 12-bus test system [20]

system. Several generic FC-VSWT models are proposed in the literature by e.g. IEC [21] and IEEE working groups [22]. The proposed models are generally focused on the fault ride-through and voltage/reactive power control studies. However, for the inertial response study the generic FC-VSWT model should include aerodynamic and mechanical dynamics of the turbine as well as the generator and converter RMS representations. The generic utility-scale multi-megawatt turbine (NREL 5MW) model is utilized [23], [24] and adapted for RMS simulations in the generic power system.

The representation of aerodynamic and mechanical dynamics of the wind turbine is important for the inertial response control considering the overloading of the wind turbine. In the simulations, the wind turbine is operated at available power (i.e. maximum power for the given wind speed), and the inertial response control overloads the wind turbine by increasing the power reference of full-converter (FC) above the available power. Therefore, 'recovery period' is observed after the inertial response control action. The recovery period can be described as the duration to recover its previous operating condition after releasing an additional power when it is operating at available power due to deceleration of the wind turbine rotor.

For the electrical dynamics of the FC and PMSG, RMS models are implemented to represent the behavior of FC-VSWT in the inertial response control studies. Since the inner current control of the full-converter is very fast for the frequency stability studies (i.e. in the order of milliseconds [21]), the inner current control loops of machine side and grid side converters are neglected. The control dynamics of DC-link voltage and active power control are relevant for the inertial response control, thus the PI control loops of these controls retain in the FC control.

The developed FC-VSWT model is utilized for the aggregated WPP behavior to investigate the inertial response control. The aggregation approach is simply modifying the base value of a single turbine to get overall WPP response [12]. The park layout of the WPP is not included in the aggregation approach, since the voltage variations at the wind turbine connection point are of no interest for the inertial response of the overall WPP in this study.

IV. Proposed Inertial Response Control

In this section, the assumptions used in simulations of the inertial response control, the performance criteria to assess the impact of the inertial response control, the evaluation of the previous control concepts, and finally the proposed control concept are explained.

A. Assumptions for Inertial Response Control Simulations

Assumptions regarding the generic power system are employed in order to simulate the inertial response control and compare the various control concepts under the same operating conditions of the generic power system. First, to simulate a low frequency event, N-1 contingency is defined as the largest infeed loss (i.e. 200MW from G2). Second, for primary frequency control of CPPs, the allocation of active power reserve is sufficient in all the wind power penetration scenarios. Finally, all the wind power penetration scenarios are simulated for the inertial response control, however only the results of the 50% wind penetration scenario is presented in this paper due to lack of space.

In addition to the assumptions made for the generic power system, operating conditions of the aggregated WPP model are also specified to simulate and analyze the impact of the inertial response control on the frequency stability. WPPs are operated at high wind speed (i.e. above rated wind speed) to evaluate the inertial response control concepts and quantify generic power system needs. In high wind speed conditions, the tuning methodology is applied to the proposed control without taking into account the recovery period of the VSWT. After demonstration of the proposed control, low wind speed operating condition (i.e. below rated wind speed) is also simulated to present the impact of the recovery period on the frequency stability.

B. Performance Criteria

The performance criteria for the generic power system are defined in order to evaluate the inertial response control concepts. They are chosen from the grid code requirements and literature regarding the frequency stability. The details are given in [25] and summarized in Table I.

C. Assessment of Existing Inertial Response Control Concepts

In the literature, several control concepts are proposed to enable the inertial response of WPPs. The control concepts for inertial response control can be grouped into two categories according to the response profiles [25]. The derivative control is the proportional control method based on the ROCOF in order to emulate the inertial response of a SG [9]-[15]. The control modifies the active power or torque set point by an additional active or torque value which is equal to the product of ROCOF and a gain (H_{WPP}). The derivative control is sensitive to the noise in the frequency measurements. To solve this problem, a low-pass filter is added to the controller. Overall response of the derivative control is the ROCOF triggered inertial response similar to a SG. Moreover, the temporary frequency control is the additional active power release method of which the magnitude and the duration are predefined or proportional to the frequency deviation [16]-[19]. The block diagrams of these control concepts are given in Fig. 2.

TABLE I
Operational Metrics for the Generic Power System [25]

Operational Metric		Values
1	max. dynamic frequency deviation (min. frequency point)	0.016pu (=800mHz in 50 Hz)
2	max. ROCOF (df/dt) for a given detection time	0.008 pu/s with 200ms (=0.4Hz/s in 50 Hz)
3	time to reach the min. frequency point	4.68s (20% wind power penetration scenario)

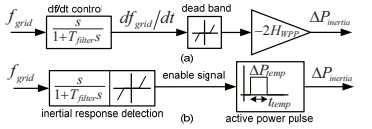

Fig. 2. Block diagrams of derivative control (a) and temporary frequency control (b)

Both of the control concepts are evaluated with various control parameters in order to investigate the inertial response control requirements for the generic power system [25]. Final parameters of the control concepts which meet the performance criteria are selected for the 50% wind power penetration scenario. The selected parameters are given in Appendix. According to these parameters, the simulation results are presented in Fig. 3 and Fig 4.

Replacement of the CPPs is realized not only by providing inertial response from WPPs but also by compensating the replaced primary frequency control temporarily by the WPPs (Fig. 3). Therefore, the parameters of the existing control concepts are chosen considering the minimum frequency point. Another important remark from Fig. 3 (b) is that the inertial response control should be tuned properly by taking into account the small signal stability of the power system. Thus, the inertial response control should not decrease damping of power system oscillations.

The temporary frequency control is an open loop control releasing the energy with respect to a predefined amount and duration of the active power that is triggered by the ROCOF (Fig. 2) or the frequency deviation. However, the inertial response control from WPPs should be dependent on the power system frequency deviations for different power system operating conditions (e.g. different wind power penetration scenarios). Finally, the amount of the released energy during the inertial response control does not determine directly the minimum frequency point and the time to reach this point according to Fig. 3 (a) and Fig. 4. Therefore, the way of providing the energy during the inertial response control, such as the duration and the ramp-down rate of the released active power, affects the frequency stability in terms of a double dip as shown in Fig. 4.

D. Proposed Inertial Response Control

Based on the conclusions above, a new inertial response control is developed considering the frequency deviation (Δf) and the df/dt as input signals. The developed controller has two components dependent on these input signals in order to

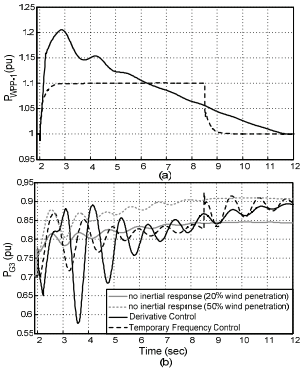

Fig. 3. Comparison of active power output of WPP-1 (connected to Bus 5 in Fig.1) (a) and G3 (connected to Bus 11 in Fig.1) (b) for the existing control concepts

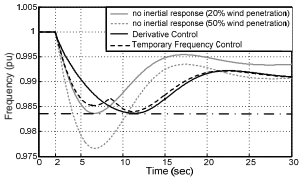

Fig. 4. Comparison of system frequency for the existing control concepts according to minimum frequency point

achieve the operational metrics (Table I). The first component is similar to the derivative control, but in this case, the gain of this component is determined in order not to trip the ROCOF relays or in other words to achieve the operational metric 2. The second component is similar to the primary frequency control of CPPs, however in this case it represents a droop control with a variable gain to provide an additional active power temporarily during the inertial response. In this study, this control action is defined as 'variable-droop'. Consequently, the proposed control, which is presented in Fig. 5 (a), coordinates the additional active power ($\Delta P_{inertia}$) provided by these two components to minimize the released energy during the inertial response compared to the existing control concepts.

The variable-droop control (i.e. the second component) is enabled by an external signal, which can be triggered by df_{grid}/dt or Δf_{grid} using a dead-band. After enabling the variable-droop control, the droop value starts to increase, and is multiplied by Δf_{grid}, then added as $\Delta P_{VarDroop}$ to ΔP_{ROCOF} in Fig. 5 (a). During the ramp-up period of the variable-droop control, ΔP_{ROCOF} signal starts to decrease due to the declined df_{grid}/dt signal. Thus, the released energy during the inertial response is minimized compared to the existing control

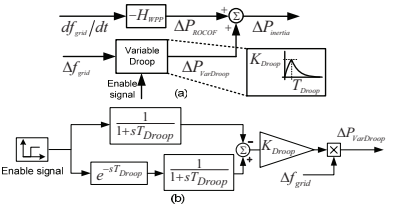

Fig. 5. Proposed inertial response control (a) and variable-droop control (b)

concepts by coordinating the two components of the proposed control. Besides releasing less energy, the variable-droop control is based on Δf_{grid} signal, which is easier and more reliable to detect compared to df_{grid}/dt signal. Taking the derivative of the power system frequency is challenging due to presence of the noise [6]. Another advantage is that, the variable-droop control represents a fast frequency control action with a smooth ramp-down rate which does not affect the power system frequency adversely (e.g. in Fig. 4).

The structure of the variable-droop control is presented in Fig. 5 (b). In this structure, there are two parameters which determine the duration and the magnitude of the inertial response, T_{Droop} and K_{Droop}, respectively. The tuning of these parameters is described in the next section according to the power system characteristics.

V. Tuning Methodology of Proposed Control

The tuning methodology for inertial response control concepts has not been described particularly in the previous studies [9]-[19]. Every specific power system model used in the inertial response control studies has different characteristics in terms of the inertia and the primary frequency control. These two features determine the frequency response of the power system, and should be taken into account in order to provide a temporary active power contribution from inertial response control of WPPs. Therefore, the tuning methodology of the variable-droop control aims selecting proper parameters not to cause potential frequency instability while achieving the operational metric 1. The tuning methodology is based on a simplified model which is employed to estimate the minimum frequency point and the time to reach this point for low frequency events without simulations.

The generic power system model is simplified in two steps; the first simplification is an average system frequency model (i.e. single mass model) [26], and the second simplification is a delay model adapted from [17], [27]. The delay model for power systems with different generation mixes is developed to estimate the maximum frequency deviation (Δf_{min}) and the time to reach the minimum frequency point (t_{min}). Moreover, these estimated values are used to tune the T_{Droop} and K_{Droop} values of the variable droop control.

A. Average System Frequency Model

In the average system frequency model, all CPPs are

represented as one equivalent mass, which has the average inertia constant (H_{eq}) with damping constant (D_{eq}) and is driven by the difference between the mechanical power change (ΔP_m) and the electrical power change (ΔP_L) [26]. In this study the largest infeed loss is represented by ΔP_L.

B. Delay Model

The delay model, which is based on the average system frequency model, uses pure time delays to model the time constants of the governor, steam and hydro dynamics (e.g. valve motion, steam bowl dynamics), and converts the closed loop model into an open loop delay model [27]. The hydro and thermal turbine models can be kept as they are, or they can be assumed also as time delays with respect to their response characteristics.

The simplification approach of the delay model for the hydroelectric power plant (HPP) is described in [17], which is adopted from [27]. In this approach, the delay representation of a HPP is developed based on three assumptions considering governor time constant, transient droop compensation dynamics, and hydro-turbine response. As a result, the total delay (t_{HPP}) is calculated for power systems only consisting of one type of HPPs. Therefore, the delay model for power systems with different generation mixes is required for the realistic estimation of Δf_{min} and t_{min}. First, the delay model of a power system consisting of only one type of thermal power plant (TPP) is developed with the approach adapted from [17]. Then, the delay model of power systems with different generation mixes is developed considering delay of HPPs and TPPs together.

For a TPP, the first assumption of the HPP delay model is the same [27], therefore governor dynamics (e.g. control time constant, servo, and steam valve bowl time constant) is treated as a pure time delay, t_G in (2). The second assumption is employed for the time delay of the steam turbine. The transfer function of the steam turbine, $((1+sFT_R)/(1+sT_R)$, is similar to the transfer function of the transient droop compensation in a HPP. Accordingly, $R_{T,thermal}$ instead of $R_{T,hydro}$ (transient droop of hydro-governor) is defined in order to calculate time delay of the steam turbine. The derivation of $R_{T,thermal}$ is shown in Appendix.

As a result, the total delay of the TPP (t_{TPP}) in (1) is calculated as the addition of two delays given in (2) and (3). Furthermore, after the simulations with the average system frequency model in order to validate the t_{min} and Δf_{min} of a power system consisting only one type of TPP, an additional correction time delay ($t_0/2$) is added to t_{TPP}, and $t_{TPP,corr}$ is calculated. The difference between these two values is that t_{TPP} is associated with the estimate Δf_{min}, and $t_{TPP,corr}$ is used to estimate t_{min}. Therefore, the t_{TPP} and $t_{TPP,corr}$ are given in (1) and (4).

$$t_{TPP} = t_G + t_0/2 \tag{1}$$

1st assumption:

$$t_G = T_G + T_S + T_V \tag{2}$$

where T_G is governor time constant, T_S is servo time constant, and T_V is steam valve bowl time constant.

TABLE II
COMPARISON OF THE SIMULATION RESULTS AND DELAY MODEL

$t_{min,eq,corr}$ (s) (Estimated)	$t_{min,eq,corr}$ (s) (Simulated)	$\Delta f_{min,eq}$ (Hz) (Estimated)	$\Delta f_{min,eq}$ (Hz) (Simulated)
4.81	4.79	-1.44	-1.1

2nd assumption:

$$t_0/2 = H_{eq} R_{T,thermal} \left(1 - D_{eq} \Big/ \left(\frac{1}{R_p} + D_{eq}\right)\right) \tag{3}$$

where R_p is permanent droop.

$$t_{TPP,corr} = t_G + t_0 \tag{4}$$

A realistic power system model comprises different types of generation with different types of governor and turbine parameters (e.g. 3 TPPs and 1 HPP in the generic 12-bus system). Therefore, the delay model of a generic power system with different generation mixes is developed considering the response of each CPP independently based on the time delay calculation of HPPs [17] and TPPs (1)-(4). The calculation is based on the weighted average of time delay values of each CPP (t_{CPP}) according to their power ratings (n_{CPP}). The estimation of the time to reach the minimum frequency ($t_{min,eq}$) and maximum frequency deviation ($\Delta f_{min,eq}$) are defined as follows:

$$t_{\min,eq} = \sum n_{CPP} t_{CPP} \Big/ \sum n_{CPP} \tag{5}$$

where n_{CPP} is power rating of the CPP in system MVA base.

$$t_{CPP} = t_{G,CPP} + t_{0,CPP}/2 \tag{6}$$

where $t_{G,CPP}$ is for a HPP, and for a TPP.

$$t_{0,CPP}/2 = H_{eq} \frac{R_{T,CPP}}{r_{CPP}} \left(1 - D_{eq} \Big/ \left(\frac{1}{R_{p,CPP}} + D_{eq}\right)\right) \tag{7}$$

where $R_{T,CPP}$ is $R_{T,hydro}$ for a HPP or $R_{T,thermal}$ for a TPP.

$$r_{CPP} = \sum R_{p,CPP} / R_{p,CPP} \tag{8}$$

$$\Delta f_{\min,eq} = \Delta P_L \frac{1}{D_{eq}} \left(e^{-t_{\min,eq} D_{eq}/2H_{eq}} - 1\right) \tag{9}$$

Similar to the above calculation for the TPP (4), $t_{min,eq}$ is amended by adding $t_{0,CPP}/2$ for TPPs in (6) in order to estimate the $t_{min,eq,corr}$ consistently with the simulation results. The comparison of the simulation results and the delay model calculations for the generic power system are presented in Table II.

The tuning methodology of T_{Droop} and K_{Droop} is designed in order not to cause possible frequency instability by interacting with the primary frequency control of CPPs. Thus, $t_{min,eq,corr}$ and $\Delta f_{min,eq}$ values from the developed delay model are used for the T_{Droop} and K_{Droop}. $t_{min,eq,corr}$ defines the duration of the variable-droop control, and $\Delta f_{min,eq}$ determines how much additional power is released in order to increase frequency ($\Delta f_{increase}$) as demanded. Response of the variable- droop control is illustrated in Fig. 6, and the parameters are calculated as follows:

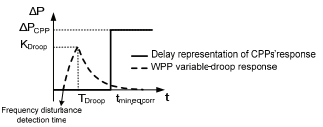

Fig. 6. Illustration of the tuning methodology of the variable-droop control

$$T_{Droop} = t_{\min,eq,err}/2 \tag{10}$$

$$K_{Droop} = \frac{-H_{eq}\left(R_T^* D_{eq} + \Delta f^*\right) - T_d D_{eq}}{\Delta f^* + R_T^* D_{eq}} \tag{11}$$

where

$$R_T^* = \sum n_{CPP} \frac{R_{T,CPP}}{r_{CPP}} \left(1 - D_{eq} \Big/ \left(\frac{1}{R_{p,CPP}} + D_{eq}\right)\right) \Big/ \sum n_{CPP} \tag{12}$$

$$\Delta f^* = 2\ln\left(\left(\Delta f_{\min,eq} + \Delta f_{increase}\right)\frac{D_{eq}}{\Delta P_L} + 1\right) \tag{13}$$

$$T_d = \sum n_{CPP} t_{G,CPP} / \sum n_{CPP} \tag{14}$$

According to the formulations above for the generic 12-bus system with 50% wind penetration scenario, the T_{Droop} value is calculated as 2.5 s (i.e. $t_{min,eq,corr}/2 \approx 2.5$ s), and the K_{Droop} value is 15 pu in the installed capacity base of all WPPs (i.e. 850 MW) to increase the minimum frequency point by 250 mHz (i.e. $\Delta f_{increase}$=0.25/50 pu).

VI. Simulation Results

In the simulations, the largest infeed from G2 is tripped to demonstrate the performance of the proposed inertial response control and to compare it with the existing control concepts. The advantages of the proposed control are presented in terms of the peak value of the additional active power and the released energy during the inertial response. The simulation results are shown in the following subsections; in the first subsection, all the aggregated WPPs are assumed to operate high wind speed (i.e. average wind speed (V_{wind}) =14m/s). In the second subsection, the WPP-2, which is connected at Bus 3 (Fig.1), operates at low wind speed (i.e. V_{wind}=10m/s) to assess the impact of the recovery period of the FC-VSWT on the power system frequency.

A. Simulation Results for High Wind Speed Operation

In Fig. 7, the minimum frequency point of the generic power system is compared for the proposed inertial response control and the existing control concepts. All three control concepts achieve the first operational metric 1 (Table I), however the temporary frequency control creates a double dip in the power system frequency due to the steep ramp-down rate of the released active power (Fig. 8). Additionally, the derivative control concept has the highest value for the time to reach the minimum frequency point. The reason is that in the derivative control more energy is released when the ramp-down rate equal to ROCOF compared to the proposed control. This can be seen in Fig. 8 which illustrates the active power output of the WPP-1 connected to Bus 5. For the operational

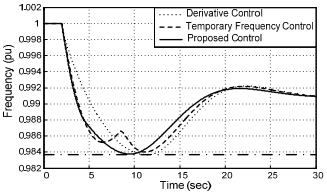

Fig. 7. Comparison of system frequency with the proposed and existing control concepts for high wind speed operation

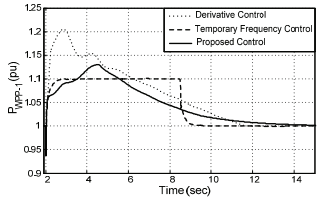

Fig. 8. Comparison of active power output of WPP-1 (connected to Bus 5 in Fig.1) with the proposed and existing control concepts for high wind speed operation

metric 2, all the control concepts provide sufficient active power within 200 ms after the detection of the disturbance. Only difference between the control concepts is the ramp-up rate of the released active power (Fig. 8), where the impact on the ROCOF is insignificant.

One of the advantages of the proposed control is to achieve operational metric 1 and 2 with releasing less than 15% additional active power. Accordingly, the total energy released during the inertial response for the proposed control is also less than the other control strategies. The released energy from the WPP-1 during the inertial response is compared for the control concepts in Fig. 9. Another advantage of the proposed control is that the dependency on the derivative component is limited selecting a small H_{WPP} value, which is implemented to achieve the operational metric 2. On the contrary, the derivative control does not have this flexibility due to the large H_{WPP} value and is only dependent on the df/dt signal. Furthermore, the temporary frequency control does not have the adaptive ramp-up and ramp-down rate for the released active power causing the frequency instability (e.g. double dip in Fig. 7).

B. Simulation Results for Low Wind Speed Operation

For low wind speed conditions, the recovery period occurs after boosting the active power by the inertial response control. The active power reduction due to the recovery period is highly dependent on the wind speed, released energy during the active power boost, and the duration of the active power boost [19], [28]. Considering the recovery period, the simulations are performed by taking the wind speed of the aggregated WPP-2 (200 MW) as 10m/s (WPP-1 and WPP-3 are operated at high wind speed conditions). Since the wind

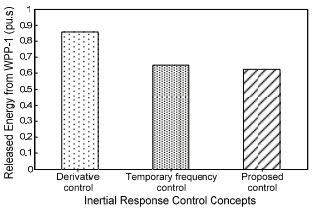

Fig. 9. Comparison of released energy from WPP-1 with the proposed and existing control concepts for high wind speed operation

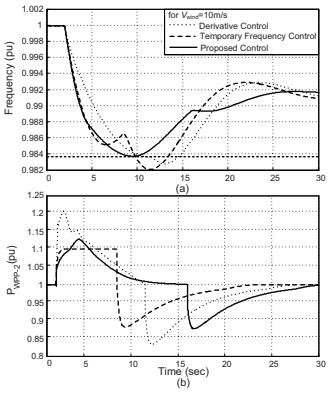

Fig. 10. Comparison of system frequency (a) and the active power output of WPP-2 (b) with the proposed and existing control concepts for low wind speed operation

speed has been modified in the simulations, the gain for the aggregated WPP-2 has increased not to change the load flow of the 50% wind power penetration scenario.

In Fig. 10, the impact of the recovery period on the system frequency is presented with the active power output of WPP-2. The double dip in the system frequency has become deeper for the temporary control due to the drop in the active power output of the WPP-2 in Fig. 10 (b). Both the temporary frequency control and the derivative control do not satisfy the operational metric 1 for the operation below rated wind speed of the WPP-2. Moreover, the proposed control has better performance than the other two control concepts in terms of the minimum frequency point, and the recovery period has a small impact when the system frequency tries to reach the quasi-steady state value. This is due to the low energy and peak value of the active power provided during the inertial response of the proposed control than the other control concepts.

For the generic power system, if the active power drop in the recovery period exceeds 0.25 pu (in 100 MW base), a double dip in the power system frequency will occur according to the simulation results. Also, the undelivered energy during the recovery period is calculated as 1.2 pu.s (in 100 MW base). Different average wind speeds cause different active power drop and undelivered energy assuming that the required energy is in Fig. 9 for the generic power system to achieve the operational metric 1. Thus, the impact on the frequency varies according to the average wind speed. The most severe double dip is observed when the wind speed is close to the rated wind speed. Considering different wind conditions for each WPP, WPPs can be coordinated to minimize the double dip in the power system frequency. In addition to these simulation results, the proposed control is less sensitive to the ROCOF measurement noise compared to the derivative control, also is more stable and flexible than the temporary frequency control.

VII. Conclusions

In this paper, a new inertial response control for WPPs is proposed and demonstrated considering the inertial response requirements of a generic power system. Additionally, the tuning methodology for the proposed control is described in detail taking into account the power system characteristics (i.e. inertia, governor response of the CPPs). Using the tuning methodology, the proposed control can be applied to any power system with high wind power penetration.

In order to assess the proposed inertial control and the existing control concepts (i.e. the derivative control and temporary frequency control), the generic power system with wind power penetration scenarios, and the aggregated WPP model are utilized with the operational metrics. According to these metrics, the simulation results are evaluated in terms of the power system requirements and the operational constraints of the FC-VSWT. The proposed controller provides less energy and peak active power compared to the existing control concepts while achieving the performance criteria. Another improvement has been made for the operation below rated wind speed where the impact of the recovery period has been reduced with the proposed inertial response control.

VIII. Appendix

1) Governor and prime mover block diagram [29] of CPPs in the generic 12-bus test system

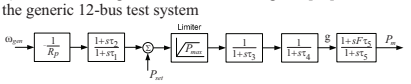

where R_p is permanent droop, τ_1 is governor response time, τ_2, is pilot valve time, τ_3 is servo time constant, τ_4 is steam valve bowl time constant, τ_5 is steam reheat/hydro water starting time constant.

CPP Name/Type	(R_p, τ_1, τ_2, τ_3, τ_4, τ_5,F, H_{CPP})
G1/Steam	0.05, 0.15, 0, 0.1, 0.3, 10, 0.237, 10
G2/Steam	0.05, 0.15, 0, 0.1, 0.3, 10, 0.237, 8.32
G3/Steam	0.05, 0.15, 0, 0.1, 0.3, 10, 0.237, 6.93
G4/Hydro	0.05, 124.47, 8.59, 0.25, 0, 0.74, -2, 6.67

2) The derivative control and the temporary frequency control parameters utilized in the simulations

Control Type	Parameters
Derivative Control	T_{filter}=20ms, H_{WPP}=28 pu
Temporary Frequency Control	T_{filter}=20ms, ΔP_{temp}=0.1 pu, t_{temp}=6.5 s

3) For the delay model, the second assumption is employed to calculate the derivative of the change in the turbine valve position ($d\Delta g/dt$) [17]. To calculate this change, $R_{t,hydro}$ is taken into account for HPPs from the following block diagram:

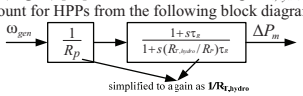

Considering the simplification of $R_{t,hydro}$, in the following block diagram of the thermal turbine, $R_{t,thermal}$ can be assumed as R_p/F. Then it can be treated as the second assumption of the HPP delay model.

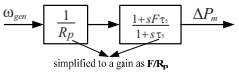

IX. Acknowledgement

This work was supported by Aalborg University-Vestas Wind Systems A/S partnership under Vestas Power Program. Any opinions, findings, and conclusions or recommendations expressed in this material are those of the authors and do not necessarily reflect those of Vestas Wind Systems A/S.

X. References

[1] Z. Chen, J. M. Guerrero, and F. Blaabjerg, "A review of the state of the art of power electronics for wind turbines," *IEEE Trans. Power Electron.*,vol. 24, no. 8, pp. 1859–1875, Aug. 2009.

[2] J. B. Ekanayake, L. Holdsworth, Wu XueGuang , N. Jenkins, "Dynamic Modeling of Doubly Fed Induction Generator Wind Turbines," *IEEE Transactions on Power Systems*, vol.18, no.2, pp. 803- 809, May 2003.

[3] A.D. Hansen, G. Michalke, "Multi-pole permanent magnet synchronous generator wind turbines' grid support capability in uninterrupted operation during grid faults," *IET Renewable Power Generation*, vol.3, no.3, pp.333-348, Sept. 2009.

[4] National Grid UK, "National Electricity Transmission System Seven Year Statement," May 2011.

[5] J. Bömer, K. Burges, C. Nabe, and M. Pöller, "All Island TSO Facilitation of Renewables Studies", Final Report for Work Package 3, [Online]. Available: http://www.uwig.org/Faciltiation_of_Renwables_WP3_Final_Report.pdf

[6] P. W. Christensen, G. C. Tarnowski, "Inertia for Wind Power Plants-State of the Art Review Year - 2011 ", in Proc. *10th International Workshop on Large-Scale Integration of Wind Power into Power Systems as well as on Transmission Networks for Offshore Wind Power Plants*, pp. 457-463, Oct. 2011.

[7] ENTSO-E, "Network Code for Requirements for Grid Connection Applicable to all Generators," June 2012.

[8] National Grid Code Frequency Response Working Group, "Requirements for System Inertia," UK, July 2010.

[9] G. Lalor, A. Mullane, and M. O'Malley, "Frequency Control and Wind Turbine Technologies," *IEEE Trans. Power Systems,* vol. 20, no. 4, pp. 1905-1913, Nov. 2005.

[10] M. Kayikci and J. V. Milanovic, "Dynamic Contribution of DFIG-Based Wind Plants to System Frequency Disturbances," *IEEE Trans. Power Systems,* vol. 24, no. 2, pp. 859-867, May. 2009.

[11] J. Morren, S. W. H. de Haan, W L. Kling, and J. A. Ferreira, "Wind turbine emulating inertia and supporting primary frequency control," *IEEE Trans. Power Systems,* vol. 21, no. 1, pp. 433-434, Feb. 2006.

[12] J. F. Conroy and R. Watson, "Frequency response capability of full converter Wind turbine generators in comparison to conventional generation," *IEEE Trans. Power Systems,* vol. 23, no. 2, pp. 649-656, May 2008.

[13] J. Morren, J. Pierik, and S. W. H. de Haan, "Inertial response of variable speed wind turbines," *Electric Power Systems Research,* vol. 76, no. 11, pp. 980-987, Jul. 2006.

[14] O. Anaya-Lara, F. Hughes, N. Jenkins, and G. Strbac, "Contribution of DFIG-based wind farms to power system short-term frequency regulation," in *Proc. IEE Generation, Transmission and Distribution,* vol. 153, no. 2, pp. 164-170, Mar. 2006.

[15] J. M. Mauricio, A. Marano, A. Gomez-Exposito, and J. L. Martinez Ramos, "Frequency Regulation Contribution Through Variable-Speed Wind Energy Conversion Systems," *IEEE Trans. Power Systems*, vol. 24, no. 1, pp. 173–180, Feb. 2009.

[16] S. Wachtel and A. Beekmann, "Contribution of wind energy converters with inertia emulation to frequency control and frequency stability in power systems," in *Proc. 8th Workshop on Large-Scale Integration of Wind Power into Power Systems,* pp. 460-465, Oct 2009.

[17] N. R. Ullah and T. Thiringer, "Temporary primary frequency control support by variable speed wind turbines-potential and applications," *IEEE Trans. Power Systems,* vol.23, no.2, pp.601-612, May 2008.

[18] K. Ping-Kwan, L. Pei, H, Banakar, B. T. Ooi, "Kinetic Energy of Wind-Turbine Generators for System Frequency Support," *IEEE Trans. Power Systems,* vo1.24, no.1 , pp.279-287, Feb. 2009.

[19] G. C. Tarnowski, P C. Kjaer, P. E. Sorensen, and J. Ostergaard, "Variable speed wind turbines capability for temporary over-production," in *IEEE Power & Energy Society General Meeting,* pp. 1-7, Calgary, USA, July 2009.

[20] A. Adamczyk, M. Altin, Ö. Göksu, R. Teodorescu, F. Iov, "Generic 12-Bus Test System for Wind Power Integration Studies," *EPE Joint Wind Energy and T&D Chapters Seminar*, Aalborg, Denmark, Jun. 2012.

[21] *Electrical simulation models for wind power generation*, IEC 61400-27, 2012

[22] M. Asmine, J. Brochu, J. Fortmann, R. Gagnon, Y. Kazachkov, C.-E. Langlois, C. Larose, E. Muljadi, J. MacDowell, P. Pourbeik, S. A. Seman, and K. Wiens, "Model Validation for Wind Turbine Generator Models," *IEEE Trans. Power Systems*, vol. 26, no. 3, pp. 1769–1782, Aug. 2011.

[23] J. Jonkman, S. Butterfield, W. Musial, and G. Scott, "Definition of a 5-MW reference wind turbine for offshore system development," National Renewable Energy Laboratory (NREL), 2007.

[24] M. Soltani, T. Knudsen, J.D. Grunnet, and T. Bak, "AEOLUS Toolbox for Dynamic Wind Farm Model, Simulation, and Control," *European Wind Energy Conference*, Warsaw, Poland, Apr. 2010.

[25] M. Altin, R. Teodorescu, B.-Bak Jensen, U. D. Annakage, F. Iov, P.C. Kjaer, "Methodology for Assessment of Inertial Response from Wind Power Plants", *IEEE Power & Energy Society General Meeting,* San Diego, USA, July 2012.

[26] P. Kundur, *Power System Stability and Control*, 1993, McGraw-Hill.

[27] M. Chan, R. Dunlop, and F. Schweppe, "Dynamic Equivalents for Average System Frequency Behavior Following Major Disturbances," *IEEE Trans. Power Apparatus and Systems*, vol. PAS-91, no. 4, pp. 1637–1642, Jul. 1972.

[28] G. C. Tarnowski, "Coordinated Frequency Control of Wind Turbines in Power Systems with High Wind Power Penetration," Ph.D. dissertation, Dept. Elect. Eng., Technical University of Denmark, Copenhagen, Denmark, 2012

[29] P. M. Anderson and A. A. Fouad, *Power System Control and Stability*, 2nd ed. Wiley-IEEE Press, Oct. 2002.

XI. Biographies